NEUROBIOLOGY OF OLIGODENDROCYTES IN THE PLP MUTANT RUMPSHAKER

by

Mónica López Fanarraga
Licenciada en Veterinaria

Submitted for the degree of Doctor of Philosophy in the Faculty of Veterinary Medicine, University of Glasgow, Scotland, U.K.

Applied Neurobiology Group,
Department of Veterinary Surgery,
University of Glasgow
March, 1993

ProQuest LLC.
789 East Eisenhower Parkway
P.O. Box 1346
Ann Arbor, MI 48106 – 1346

To my happy family

Thank you for your love and sympathy,
especially to my mother for her unconditional encouragement, support and friendship throughout my career.

(Spanish)

A mi familia felíz

En agradecimiento por vuestro cariño y comprensión,
especialmente a mi madre por sus ánimos, apoyo y amistad incondicional a lo largo de toda mi carrera.

II. ABSTRACT

The *jp^{rsh}* is a murine recessive X-linked point mutation of the PLP gene characterised by a single amino-acid substitution (Ile^{186} →Thr). Affected hemizygous males and homozygous females showed tremor and ataxia of the hindlimbs. No seizures, infertility or premature death of the animals occurred. Morphological examination of the *jp^{rsh}* mutant CNS tissue revealed a noticeable hypomyelination which included abnormally thin and vacuolated myelin sheaths, intermingled with unmyelinated axons. There were appropriate oligodendrocytes numbers at the time of myelination, in fact, cell counts were higher than for the wild type in the spinal cord and were increasing progressively with age. Older mice demonstrated a gradual myelin production the spinal cord.

Immunocytochemistry of *jp^{rsh}* CNS tissue revealed a defect in the production of PLP while myelin sheaths immunostained intensely for DM-20. Quantification of the PLP/DM-20 mRNA levels indicated that the PLP expression in individual cells was decreased, particularly in younger mutants. However, the total number of PLP/DM-20 expressing cells was higher than for age-matched wild type mice. PLP/DM-20 mRNA levels did not correlate with the final low amounts of protein. The ability of *jp^{rsh}* oligodendrocytes to differentiate was assessed by staining cell dissociations from the optic nerves and spinal cord taken from mice at different ages and cultured for variable lengths of time with specific antigenic markers. Mutant oligodendrocytes differentiated normally to the GalC stage. The number of MBP immunostained cells was decreased, particularly when mutant oligodendrocytes developed *in vitro* although the expression in individual cells was normal. The immunoreactivity against the C-terminal antibody recognizing both PLP and DM-20 was also decreased. However, PLP/DM-20+ mutant cells immunostained at the appropriate time. O10, PLP and O11 indicative of the most mature stages in wild type oligodendrocytes, were virtually absent. Finally, ^{3}H-thymidine labelling in the spinal cord revealed that *jp^{rsh}* oligodendrocytes, identified by morphological and PLP expression, divide well into adulthood probably contributing to the delayed myelination of the spinal cord.

Asymptomatic heterozygote *jp^{rsh}* females did not reveal the predictable histological mosaic myelination pattern observed for other PLP mutant heterozygotes.

LIST OF CONTENTS

LIST OF TABLES

LIST OF FIGURES

END MATTER

III. ACKNOWLEDGEMENTS

To all those people who have in any way been influential in my own development and learning and who have contributed to my education I owe my gratitude.

My special thanks are due to my supervisor Professor Ian Griffiths for giving me this unique opportunity to develop my career, for his encouragement and his confidence in me and my work and for having made an effort with my broken English. I would also like to thank to all members of the neurobiology group with whom I have maintained an affectionate friendship over these years; for their efficiency I thank Nan, Jennifer, Mailis, Angelo, Sylvia, Sheelah, Kathy and Douggie. I specially thank Christine and Paul for their comments on the thesis.

My sincere thanks to Ilse for her advise, help and for having taught me various techniques. I would also like to thank everybody else working at the Institute of Neurological Sciences.

I am very grateful to the Basque Government for supporting me all throughout these studies and the Multiple Sclerosis Society in Scotland which financially supported the research. I also thank Professor N. T. Gorman and Professor P.G.E. Kennedy for allowing me to use the facilities of their departments. My sincere thanks to Alan May for all the photography.

Finally, for their patient and tireless, practical moral support I would like to thank all my friends Alfonso, Aurelia, Begoña, Cris, Juan, Jenny, Kate, Lina, Martin, Mounia, Myriam and Suly.

I. DECLARATION

The contents of this thesis are the work of the author. The thesis has not been previously submitted for the award of a degree to any other university.

Mónica López Fanarraga.

CHAPTER 1: INTRODUCTION

A. CNS

1. THE AREAS OF STUDY

The two areas of the central nervous system (CNS) on which studies in *jp^{rsh}* have been focused were the spinal cord and the optic nerve. The study of these tracts has several advantages. First, these areas of the CNS have been previously investigated in detail, accordingly, their embryological and cellular development, microscopic anatomy, ultrastructure, etc, are reasonably well documented. They are also areas that have been chosen for most of the work in other proteolipid protein (PLP) mutations. Second, the spinal cord and the optic nerve differ in their embryology, cell development, myelination time, fibre sizes and distribution and cellular content. The spinal cord represents a more complex structure than the optic nerve. It contains a number of different axon tracts in the peripheral white matter as well as a neuron cell bodies in the centrally located grey matter. On the other hand, the cell population of the optic nerve is comprised of only glial cell bodies and blood vessels, and a homogeneous axonal population. Recent studies in the spinal cord suggest that the developing spinal cord is considerably more complex, in terms of gliogenesis, than the developing optic nerve. Finally, these structures are easily localized and dissected in mice at all ages which allows more accuracy in the work.

2. DEVELOPMENT IN THE CNS

a) Introduction

The nervous system is one of the most complex structures known to man, and certainly the most complex organ system in the body. This is due in part to its large number of cells (about 10^{12} neurons in man and many more glial cells) and in part to the precise patterns of connections that neurons make onto other neurons. Not surprisingly, many features of the development of the nervous system are poorly understood. Although the gross embryological neural development has been accurately documented, the complexity of the massive increase in cell numbers and further cellular arrangements that take place as the structures develop are obscure and poorly defined. In fact, there is very little literature combining the embryological origin and cellular development of the different CNS structures.

b) Embryology and myelination of the CNS

The CNS is derived from the ectoderm. This structure begins as the neural plate closes to produce at tubular formation known as the central canal (Climent and Bascuas, 1982). The cranial portion of the canal, which is the broadest portion, develops three encephalic vesicles of which the prosencephalon is the most cranial. This dilatation of the neural tube generates the cerebral hemispheres and the diencephalon.

(1) Spinal cord embryogenesis

The caudal portion of the neural tube will develop the spinal cord. The neural tube shows a pseudostratified arrangement of neuroepithelial cells. The cells of the ependymal layer divide and accumulate giving rise to the neuroblast and spongioblasts, eventually developing into the grey matter of the spinal cord. The outer layer of the neural tube containing the elongated cell processes of the neuroblasts constitutes the future white matter (Climent and Bascuas, 1982). In the old animal the neuroepithelial cells will constitute the ependymal cells of the adult.

The cellular development of the spinal cord is very complex. The origin, migration patterns, division and differentiation of the progenitor cells are poorly documented in the spinal cord (Fok-Seang and Miller, 1992). Distinct hypotheses have been proposed to explain the spinal cord origin of the macroglia which comprises the oligodendrocytes and the astrocytes. It has been suggested that glioblasts, initially located in the region of the central canal, subsequently migrate to the peripheral white matter, proliferate and differentiate into astrocytes and oligodendrocytes (Gilmore, 1971). Another hypothesis contemplates the possibility of macroglial cells originating directly from the spinal cord radial glia (Hirano and Goldman, 1988). It has also been proposed that the precursors of the macroglia are produced locally by the division of the multipotential neuroepithelial cells after the production of the neuroblasts (Skoff, 1975; Skoff *et al.*, 1976a).

Recent investigations have shown that the migration and differentiation of oligodendrocyte precursors in the spinal cord follows a rostral-caudal and ventral-dorsal sequence of differentiation during embryonic development (Warf *et al.*, 1991). It is also known that there are oligodendrocyte-type-2 astrocyte (O-2A) progenitor cells, similar to those described for the optic nerve, but that these represent a small number of the A2B5+ cells (Fok-Seang and Miller, 1992) (see section 2.c) (figure 1).

(2) Myelination in the spinal cord

The spinal cord begins myelinating during the later stages of embryonic development. Before myelination commences, the histological appearance of the spinal cord reveals small unmyelinated axons, subdivided into bundles by radial glial processes which contain filaments and extend towards the pia (Remahl and Hildebrand, 1990). Among the axons, a few scattered undifferentiated glioblasts can be seen, but cells with ultrastructural features typical for the astroglial and oligodendroglial lineages are not yet present. At this stage microglial cells are not identifiable (Remahl and Hildebrand, 1990).

The ensheathment of the axons by oligodendrocytic processes, which was always thought to be a stereotyped process, has been recently re-described in the feline spinal cord white matter. Here, during the very early stages of myelination many oligodendrocytes appear to interact with axons in a manner similar to that adopted by Schwann cells in the peripheral nervous system (PNS) (Remahl and Hildebrand, 1990) (figure 2). These oligodendrocytes connected to a single axon, generally of large calibre, exhibited the most mature cytology. Glioblast-like cells co-exist with these mature forms of oligodendrocytes until later periods, which will subsequently differentiate and myelinate the remainder of the axons (Remahl and Hildebrand, 1990). Therefore, a two stage myelin sheath production by oligodendrocytes has been described. At stage one, only large fibres are myelinated in a Schwann cell-like fashion and in stage two all smaller calibre axons progressively acquire a myelin sheath. However, this finding has not been verified in other species so far. Hahn *et al.* (Hahn *et al.*, 1987) have reported a similar sequence of events in the myelination of the PNS where larger fibres are myelinated prior to smaller ones. Del Rio Hortega's classification of oligodendrocytes also describes a similar type of Schwann-cell-like myelinating oligodendrocyte in various species (see section 3.a.).

(3) Optic nerve embryogenesis

The optic vesicles are derived from the diencephalon and remain connected to this structure by the optic stalk which is composed of a small marginal zone containing the axons of retinal cells and a ventricular cell layer surrounding the optic canal (Skoff *et al.*, 1976a). Morphological studies in the developing rat optic nerve suggest that the invasion of axons into the optic stalk induces the differentiation of the ventricular cells from the optic stalk into type-1 astrocytes at approximately embryonic day 16 (Skoff *et al.*, 1976b; Skoff *et al.*, 1976a; Miller *et al.*, 1985). On the other hand, *in vitro* studies propose the neuroepithelial cells as possible type-1 astrocyte precursors (Small *et al.*, 1987; Richardson *et al.*, 1990).

(4) Myelination in the optic nerve

Myelination in the optic nerve has been described in detail in the rat. At birth (embryonic day 21), the optic nerve is composed entirely of 200 to 400 nm non-myelinated axons remaining so up until day two (Black *et al.*, 1982; Meier and Bischoff, 1975). The axons contain microtubules, small mitochondria and small vesicles. In transverse section, groups of axons are separated by radially oriented astrocytic processes which often contain round homogeneous fat droplets and glycogen granules. Between the axons, longitudinallyarranged glial cell processes are frequently found which exhibit a granular matrix and, rarely mitochondria or dense bodies (Meier and Bischoff, 1975). Myelination starts around 6 days after birth, proceeding rapidly. By 8 days of age, most fibres are not yet associated with oligodendrocytic processes although axons in varying stages of wrapping are present (Black *et al.*, 1982). The morphology of axons at 8 days of age is similar to those from the 2 day-old optic nerves, although at this stage the axonal diameters have increased by around 50% i.e. up to 500-600 nm in diameter (Meier and Bischoff, 1975; Black *et al.*, 1982). There is no critical axonal diameter for myelination although axons of ≥ 1 μm diameter are preferably myelinated. However fibres of less of 0.5 μm in diameter are also myelinated while much larger neighbouring axons remain unmyelinated. Axonal diameter parameter continuously increases during the ensheathment until the adult size is reached (Black *et al.*, 1982). The association of the axon with oligodendrocytes seems to be an important factor for the axonal development as axons not associated with oligodendrocytic processes do not exceed 0.2-0.3 μm diameter until intimate association is made (Black *et al.*, 1982). Frequently, myelinated axons appear in clusters, often in relationship with an active oligodendrocyte (Meier and Bischoff, 1975). A representative field of a section of a 16 day-old optic nerve shows profiles of fibres not yet associated with glial processes, fibres in which ensheathment has just begun, fibres in which the myelin sheath has not yet been compacted, and fibres with compact myelin. Glial proliferation is reported to slow dramatically after 19 days postnatal in the rat optic nerve (Skoff, 1990). Optic nerves at 28 days contain approximately 85% of the axons ensheathed (Black *et al.*, 1982) and by 30 days they are composed primarily of myelinated fibres with only a few unmyelinated axons that show oligodendroglial processes in their vicinity (Black *et al.*, 1982). Once several wraps of myelin have been laid down, the *g* ratio remains fairly constant (around 0.75) throughout development (Black *et al.*, 1982: *g* is defined as the ratio of axon diameter to that of the axon plus myelin sheath; an increased *g* ratio indicates that the sheath is disproportionately thin for the axonal size).

Myelination of the optic pathway exhibits a general rostral-caudal gradient extending from the eye to the lateral geniculate nucleus (Skoff *et al.*, 1976b; Skoff, 1990).

c) Glial cell development

The cellular origin of the oligodendrocytes and astrocytes in the CNS remains controversial. There are two approaches to the study of glial cell development in the CNS: the histological approach, based on the study of the morphological and, to some degree, the antigenic characteristics of the macroglial cells *in vivo*, and the tissue culture approach, where the cells are dissociated, allowed to differentiate *in vitro* and are then immunologically identified.

While the traditional histological description of the developing CNS identified astroblasts, oligodendroblasts as well as very few undifferentiated glioblasts, tissue culture experiments have revealed several macroglial cell types (Skoff *et al.*, 1976a). At present, the O-2A progenitors identified in tissue culture have not been directly identified *in vivo* (section 2) (Skoff and Knapp, 1991). More than 80% of the dividing cells in the optic nerve can be classified histologicaly as either oligodendroblasts or astroblasts rather than undifferentiated glioblasts (Skoff *et al.*, 1976a). In fact, histological autoradiographic investigations demonstrate that oligodendrocytes attached to myelin sheaths can divide (Skoff, 1990; Arenella and Herndon, 1984; Skoff *et al.*, 1976a). Thus, some authors (Skoff and Knapp, 1991; Skoff *et al.*, 1976a) argue the possibility of differentiated macroglia cells to vacillate in their selection of a specific lineage demonstrating developmental plasticity and the ability of glia to adapt to an altered environment (Skoff and Knapp, 1991; Raff *et al.*, 1984b).

(1) Histological appearance of the developing glia

The development of the glial population has been precisely described in the optic nerve as it is a well defined structure with a relatively homogeneous fibre population where gliogenesis is unencumbered by neurons. It also myelinates postnatally, thus being particularly suitable to study this process.

The glial cell population in the premyelinated optic nerve (1-6 days of age) consists mainly of astrocytes in varying developmental stages (Skoff *et al.*, 1976a). These are the first morphologically-identifiable macroglial cells. Ultrastructurally they present a moderately stained and loosely packed stellate cytoplasm which forms several processes radiating from the perikaryon to interdigitate with other astrocytic processes. Although these immature astrocytes have very few, if any, filaments they exhibit other features characteristic for astrocytes such as glycogen granules, *puncta*

adherentia and wide cisternae of endoplasmic reticulum which are always filled with a flocculent material. Polysomes, lipid droplets and mitochondria are also present. Their nucleus, which is often irregularly shaped, contains dispersed chromatin with a rim of condensed chromatin along the nuclear envelope and frequently a nucleolus (Skoff *et al.*, 1976a).

Later-proliferating astroblasts resemble mature fibrous astrocytes with a more electrolucent cytoplasm and nucleus with evenly dispersed chromatin, although still showing immature features like the larger number of organelles and fewer bundles of filaments (Skoff *et al.*, 1976a). While the perikarya and processes of these developing astrocytes contain large numbers of filaments, they also have many more microtubules and other organelles than the fully differentiated fibrous astrocytes (Vaughn and Peters, 1967; Meier and Bischoff, 1975). The transition of early postnatal astrocytes to fully differentiated astrocytes is gradual. By 21 days after birth, there are many astrocytes which are almost identical in every respect with mature fibrous astrocytes, but alongside are other astrocytes whose cytoplasmic features are intermediate between those of mature and early postnatal astrocytes. Astrocytic processes are found beneath the meninges and around vessels, as well as grouping the axons in fascicular bundles throughout the optic nerve (Meier and Bischoff, 1975; Vaughn and Peters, 1967). This distribution of astrocytes corresponds best to the *in vitro* type-1 astrocytes (Miller *et al.*, 1989) which are the first to differentiate *in situ*, approximately at embryonic day 16, probably from the neuroepithelial cells from the optic stalk (Skoff *et al.*, 1976a; Small *et al.*, 1987; Richardson *et al.*, 1990; Sturrock, 1976). The second type of astrocyte identified *in vitro*, termed type-2, begins to differentiate during the second postnatal week from a bipotential O-2A progenitor cell after generating the oligodendrocytes (Raff *et al.*, 1983).

Some authors have also identified glioblasts in the newborn mouse optic nerve (Meier and Bischoff, 1975). These cells exhibited pronounced chromatin aggregates close to the nuclear envelope (Meier and Bischoff, 1975). The cytoplasm showed many free ribosomes which were often arranged as rosettes; the rough endoplasmic reticulum appeared as a sheet-like cisterna or as few short cisternae and the Golgi apparatus was poorly developed and situated in a perinuclear position. Mitochondria contained both light and dense matrices. The cytoplasm was confined to a more or less narrow zone around the nucleus and processes were seldom encountered (Meier and Bischoff, 1975). Oligodendroblasts were also observed in newborn mouse optic nerve. These cells were intermediate forms of developed glioblasts (Meier and Bischoff, 1975; Skoff and Knapp, 1991) comprising postmitotic cells which were larger with a rounder nucleus containing more evenly dispersed chromatin, and some broad processes Skoff *et al.*, 1976a; Skoff *et al.*, 1976b). A characteristic of these

cells was a well developed Golgi apparatus which often reached into the cytoplasmic extensions, and microtubules. Some cells contained lamellar inclusions and/or polymorphous fat droplets (Meier and Bischoff, 1975). The oligodendroblasts proliferated and differentiated into oligodendrocytes (Skoff *et al.*, 1976a; Skoff and Knapp, 1991; Skoff, 1990; Skoff *et al.*, 1976b) being very conspicuous at approximately five days postnatally, a day or two before the onset of myelination in the optic nerve (Skoff *et al.*, 1976a). More mature oligodendroblasts presented a cytoplasm of moderate to high electron-density packed with clusters of ribosomes, many small mitochondria and microtubules, thin cisternae of Golgi apparatus and endoplasmic reticulum often not stacked (Skoff *et al.*, 1976a; Skoff, 1990). The nucleus which was often larger than that of astrocytes (Skoff, 1990), was situated at one pole of the cell and showed small clumps of heterochromatin scattered throughout. Oligodendroblasts accounted for the majority of proliferating cells during the second postnatal week which is the period of myelin formation (Skoff *et al.*, 1976a; Skoff and Knapp, 1991; Skoff, 1990; Skoff *et al.*, 1976b). It has been suggested that occasional oligodendrocytes at various stages of development, including those of the "dark" variety described by Mori & Leblond (Mori and Leblond, 1970), can divide while connected to myelin sheaths (Skoff, 1990; Arenella and Herndon, 1984; Skoff *et al.*, 1976a). The ultrastructural appearance of dividing oligodendrocytes at five days of age corresponded to the oligodendroblasts present in 14 day-old nerves (Skoff *et al.*, 1976a; Skoff *et al.*, 1976b). Microglial cells are present at birth and increase progressively until the second and third postnatal week (Skoff *et al.*, 1976a; Sturrock, 1976).

Occasional necrotic cells have also been described during gliogenesis (Meier and Bischoff, 1975) although according a recent investigations (Barres *et al.*, 1992) more than 50% of the oligodendrocytes die in the optic nerve during development, mainly as a result of competition for survival factors such as platelet derived growth factor (PDGF) and insulin-like growth factor-1 (IGF-1) (figure 3). The growth factors appear to promote survival by suppressing an active death program in the glial cells (Barres *et al.*, 1992). These cells suffer a programmed self destructive phenomenon termed "apoptosis" involving RNA synthesis (Raff, 1992). The nucleus of these cells exhibits a highly condensed and sometimes fragmented chromatin which stains intensely with propidium iodide and the cytoplasm frequently contains multiple vacuoles (Barres *et al.*, 1992). Dead cells are rapidly removed from the tissue without inflammation (Raff, 1992).

(2) <u>In vitro</u> approach to glial cell development

Cell dissociations of rat optic nerve contain at least three different types of macroglial cells: oligodendrocytes and two types of astrocytes termed type-1 and type-

2, which differ in their morphology, antigenic phenotype, and timing of differentiation (Miller *et al.*, 1985; Raff, 1989) (table 1). These three types of macroglial cells in the optic nerve cultures develop from two different precursors. The type-1 astrocyte precursor cell has not been determined yet. Oligodendrocytes and type-2 astrocytes develop from highly motile (Small *et al.*, 1987) progenitor cell that labels with A2B5 but not Ran-2 antibodies (Raff *et al.*, 1983) (figure 1). This oligodendrocyte-type-2 astrocyte common precursor cell (O-2A) migrates, divides but differentiates into oligodendrocytes or type-2 astrocytes depending on different environmental signals (Small *et al.*, 1987; Raff, 1989). When dissociated from a perinatal optic nerve and cultured in the absence of foetal calf serum (FCS) O-2A progenitor cells give rise to oligodendrocytes, whereas cultured in 10% FCS they become type-2 astrocytes (Raff *et al.*, 1983; Raff, 1989). Type-1 astrocytes secrete PDGF which keeps O-2A progenitors dividing (Raff, 1989; Noble and Murray, 1984; Richardson *et al.*, 1990) preventing their premature differentiation into oligodendrocytes. It is believed that the O-2A progenitor cells start their migration when type-1 astrocytes stabilize at birth. These migrate from the brain along the nerve towards the eye guided by the axons (Small *et al.*, 1987).

Small numbers of proliferating O-2A progenitor cells are present in the nerve at embryonic day 15 (Small *et al.*, 1987). A week or so later, cells with the antigenic phenotype of type-2 astrocytes begin to appear. Some O-2A progenitors seem to undergo yet another developmental transition, not differentiating immediately and dividing to give rise to a different type of O-2A progenitor cell that persists in the adult nerve (Hardy and Reynolds, 1991) (see section 3). The O-2A progenitors are characterized in culture by a bipolar morphology and an undifferentiated and uncommitted antigenic profile A2B5+/vimentin+/galactocerebroside (GalC)-/glial fibrillary acidic protein (GFAP)- (Miller *et al.*, 1985; Berg and Schachner, 1982; Raff *et al.*, 1984b). Further differentiation towards more mature forms is recognised by reactivity with the mouse monoclonal O4 antibody (Sommer and Schachner, 1981), loss of A2B5 staining, as the GalC is acquired, and absence of vimentin (Raff *et al.*, 1984b). GalC is a marker for commitment of such cells to the oligodendrocyte lineage (Raff *et al.*, 1978) while GFAP is indicative of the astrocyte lineage (Bignami *et al.*, 1972). However, cultured O-2A progenitor cells are capable of reversing the differentiation process, even a couple of days after becoming GFAP+ type-2 astrocytes, to become oligodendrocytes GalC+/GFAP- (Raff *et al.*, 1984b).

Although cells with the antigenic phenotypes corresponding to type-1 astrocytes and O-2A progenitor have been described in cultures from developing cerebellum (Levi *et al.*, 1986b; Levi *et al.*, 1986a) and cerebrum (Ingraham and McCarthy, 1989), this simple classification does not correspond to the findings in

cultures from the newborn rat spinal cord as previously described or the olfactory bulb (Barnett *et al.*, 1993). Again this raises the argument of the validity of the tissue culture models for the study of developing glia cells. In fact, retroviral tracers have failed to demonstrate a common progenitor cell for both oligodendrocytes and astrocytes (Vaysse and Goldman, 1990). Other studies have also demonstrated several significant alterations in the timing of antigen expression in both O-2A progenitor cells and oligodendrocytes *in vivo* compared to the *in vitro* situation (Hardy and Reynolds, 1991). Therefore, there is no direct *in situ* evidence for the existence of a multipotential progenitor that is a major source of oligodendrocytes and some astrocytes (Skoff and Knapp, 1991). The developmental potential of cells may be altered when dissociated and cultured. Glial cell differentiation in culture may exhibit considerable plasticity, to the extent of actually switching lineages (Raff *et al.*, 1984b), although this plasticity should not be taken as their normal path of differentiation *in situ* (Skoff and Knapp, 1991).

d) Formation of the CNS myelin sheath

Myelinogenesis in the CNS is a complex process involving differentiated oligodendrocytes. The oligodendrocyte generally gives rise to thin processes, which associate with the surface of axons; then elongate and spirally wrap the axons in a clockwise or anti-clockwise direction (Skoff *et al.*, 1980). The free edges of lips will form the mesaxon which will elongate by growing of one of the lips over the other. It is unknown why oligodendrocytes choose a particular fibre after avoiding association with other much closer axons. The major dense line (MDL) results from the extrusion of the cytoplasm from the myelinating process and the apposition of the cytoplasmic membranes and the intra period line (IPL) forms as the mesaxon compacts by the apposition of the extracellular membrane face. Consequently the most mature sheaths will only show cytoplasm within the outer and inner ends of the spiralling process. The subsequent growth of the sheath is achieved by the addition of more turns to the spiral (Peters *et al.*, 1976). It has been postulated traditionally that the oligodendrocyte is situated some distance away from the sheath, the two being connected by a bridging process of cytoplasm. However, recent studies demonstrate that the oligodendrocyte/internode ratio is a flexible parameter as some large fibres internodes are ensheathed in a Schwann cell-like fashion, thus a 1:1 ratio (Remahl and Hildebrand, 1990). The myelin assembled and maintained by a single "Schwann-cell-like" oligodendrocyte is greater than that produced by an oligodendrocyte related to several sheaths (Remahl and Hildebrand, 1990). Other factors such as the CNS tract and the animal species also influence the number of internodes produced by a single oligodendrocyte.

The myelin deposition starts at several discrete sites along the entire length of an individual axon (Skoff *et al.*, 1980). The appearance of the sheath is a series of cuffs that form around the axon and later extend toward each other, eventually leaving only short intervening gaps, the nodes of Ranvier.

3. REVIEW CNS STRUCTURE

a) Cellular components of the CNS

(1) The oligodendrocyte

(a) Historical perspectives

The oligodendrocytes were first named and described by the Spanish histologist Del Rio Hortega (Del Rio Hortega, 1921; Del Rio Hortega, 1922; Del Rio Hortega, 1924). With Del Rio Hortega's silver carbonate stain, the cell was seen in profile, with little information regarding specific cytoplasmic components. It was named "the cell with few branches" the *oligodendrocyte*. In his extensive description of the oligodendrocyte, Del Rio Hortega classified these cells with regard to their position, as either perineuronal or interfascicular. A second classification derived from his analysis of the number and branching of the processes. Del Rio Hortega (Del Rio Hortega, 1922; Del Rio Hortega, 1924) found four patterns that he believed described the branching patterns of the processes of all oligodendrocytes whether perineuronal or interfascicular (figure 4). The first two types of oligodendrocytes had branches scattering in many directions; the other two forms dispatched processes parallel to adjacent myelin sheaths and therefore assumed a much more linear overall pattern. **Type I** oligodendrocytes possess a small soma with relatively numerous processes (5 to 10) which are long and very thin with periodic knot-like expansions of protoplasm and branching frequently occurring at obtuse angles. Type I is the most abundant of all the oligodendrocyte types. **Type II** are mostly found in the white matter, especially within fascicles of thinly myelinated axons, and in grey matter closely related to the cell bodies of neurons. Type II oligodendrocytes have a larger cell soma than type I but fewer primary processes (3 to 5). These are larger in diameter and divide at "T" or "Y" branches into smaller or secondary processes that are long and thin as in type I. This form is intermediate in frequency between type I and types III and IV. **Types III** and **IV** are more elongated than the other types and have only 1 or 2 processes. Both are prominent in the white matter in relation to the largest myelinated axons. They differ in that type III cells often have 2 processes, each reticulating over the surface of adjacent myelinated fibres. Type IV cells along with their processes, are flattened over the surface of a single large myelinated axon

such as for Schwann cells myelinating the PNS (Del Rio Hortega, 1921; Del Rio Hortega, 1922; Del Rio Hortega, 1924).

This classification of oligodendrocytes was supported by electron microscopical observations of neuroglia in the amphibian spinal cord (Stensaas and Stensaas, 1968). The authors confirmed that four basic types of oligodendrocytes could be identified in this tissue and supplemented the analysis by three-dimensional reconstructions of several oligodendrocyte soma from serial sections. Recently, a similar investigation of the feline spinal cord has lead to similar findings, as discussed below (Remahl and Hildebrand, 1990). Del Rio Hortega's silver carbonate stain of the white matter from young animals frequently demonstrated extensions from the oligodendrocyte somal regions that provided a spiral process around a forming myelin sheath. There seems little doubt that these processes were, in fact, the cytoplasm directly related to the myelin sheath in either the internal or the external aspect.

(b) Histological features of the developing oligodendrocyte

The oligodendroglial cells have been traditionally classified in three subpopulations according to their cytoplasmic density and state of differentiation (Mori and Leblond, 1970). The most immature form of oligodendrocyte is the **light oligodendrocyte** presenting a less organized arrangement of cytoplasmic organelles typical of actively proliferating oligodendroblasts (Mori and Leblond, 1970), these cells are characterised by a large pale cytoplasm which contains a light nucleus 6 to 8.5 μm in diameter with the chromatin slightly more clumped than in astrocytes; a smooth and regular nuclear envelope and a large and centrally located nucleolus. The cytoplasm is packed with organelles such as free ribosomes arranged as polysomes; a rather scanty rough endoplasmic reticulum for the size of the cell with non-prominent cisternae, usually not stacked; numerous microtubules and a variable Golgi apparatus. Centrioles are occasionally present. Mitochondria usually do not contain small dark granules. The cell membrane is not well defined. Occasional fine processes of a uniform diameter, measuring from 0.06 to 0.3 μm running fairly straight and unbranched, are characteristic of this variety of oligodendrocytes. While the processes include no ribosomes and only occasional mitochondria, they contain 1-20 microtubules which continue along their length (Mori and Leblond, 1970).

Medium oligodendrocytes are denser and smaller than light oligodendrocytes. They present an oval or irregularly rounded nucleus of 4-7μm in diameter with a few chromatin masses at the periphery and sometimes in the centre. Their cytoplasm is denser and usually less ample than those of light oligodendrocytes; the rough endoplasmic reticulum tends to have longer and more regularly stacked cisternae, and the free ribosomes, though still numerous are less abundant and less evenly

distributed. Golgi saccules are more prominent and distended, and finally the protoplasm between organelles is darker than in light cells. Microtubules are also present. Occasionally there are some lamellar bodies although these structures are more frequent in the dark type. Medium oligodendrocytes have fine processes containing microtubules similar to, but less numerous, than those of the light cells (Mori and Leblond, 1970).

When myelination is complete and the cell has fully matured, the cytoplasmic volume decreases and the nuclear chromatin becomes much more clumped (Skoff *et al.*, 1976a) constituting the typical **dark oligodendrocytes** whose dense cytoplasm and nucleus contrast strongly with nearby axons. Typically the nucleus is small and centrally located, more or less spherical with a diameter of 3.5 to 5.5 μm, although it may be flattened or crescent-shaped with chromatin masses attached along the inner nuclear membrane. The nucleolus is rather small and paracentrally located, often next to a peripheral chromatin mass (Mori and Leblond, 1970). There are only four or five short saccules of the Golgi apparatus which are distended by a light material and stand out in the dark surroundings. The membranes of the Golgi saccules are indistinct. The cisternae of the rough endoplasmic reticulum are rather long and often regularly stacked containing luminal material of a lesser density than the cytoplasm. A peculiar feature is the presence of the lamellar bodies. These structures consist of membranes which may be closely apposed or loosely arranged. Dark oligodendrocytes have only few processes, usually presenting the same density as the cytoplasm. They resemble those seen in the other two types of cell although shorter and darker.

The beginning of myelination coincides very closely in time with the termination of cell division for some oligodendrocytes, but there is very little evidence that oligodendrocytes begin synthesizing myelin proteins prior to their final cell division. The relationship among light, medium and dark oligodendrocytes was further investigated by autoradiographic techniques in two more detailed studies of the rat corpus callosum reported by Paterson *et al.* (Paterson *et al.*, 1973). The label appeared sequentially in the light, medium and dark oligodendrocytes, with kinetics that clearly supported the interpretation that the light oligodendrocytes were differentiating into the medium and subsequently into the dark form during variable lengths of time. The organelle content of either light or the medium oligodendrocytes could be said to be consistent with the myelinating activity. The profiles of oligodendrocytes during the peak period of myelination show an abundant cytoplasm containing numerous free ribosomes or polysomes, several moderate lengths of rough endoplasmic reticulum occasionally arranged in stacks, and several Golgi complexes. After myelination is completed, the morphology and the numbers of mature or dark oligodendrocytes change very little (Vaughn and Peters, 1974).

Fully mature oligodendrocytes are reported not to divide (Skoff *et al.*, 1976b) and to remain relatively indifferent to drastic changes in environment such as Wallerian degeneration as long as they themselves are not damaged (Skoff, 1975).

(c) In vitro morphology

The morphology of the oligodendrocyte *in vitro* represents a remarkable example of plasticity. My experiments in the mouse CNS (see chapter 3) demonstrate that freshly dissociated oligodendrocytes are capable of developing numerous processes in less than 2 hr after being plated on Poly-L-lysine-coated coverslips. These cells, when allowed to grow in culture, develop the various morphological forms previously described by Kuhlmann-Krieg *et al.* (Kuhlmann-Krieg *et al.*, 1988). Some of the morphological and ultrastructural characteristics found in the three varieties are described. **Type I oligodendrocytes** present a round or triangular cell body (approximately 10 μm in diameter) with few processes; an organelle-rich cytoplasm with scattered microtubules, narrow mitochondria, very prominent ribosomes and a nucleus with dispersed chromatin containing a small nucleolus. **Type II oligodendrocytes** usually display a larger cell body and a halo of highly branched processes which typically will develop large flattened membranous sheets containing myelin-specific antigens such as GalC, CNPase and MBP (Knapp *et al.*, 1987; Dyer and Benjamins, 1989; Konola *et al.*, 1991). Ultrastructurally they have a more homogeneous electrolucent cytoplasm with fewer organelles, mitochondria, numerous scattered microtubules and single ribosomes not organized in polysomes. A well developed Golgi apparatus; a smooth endoplasmic reticulum and a large number of coated vesicles are characteristic of these cells. The nucleus presents more condensed chromatin than in the previous category. **Type III oligodendrocytes** are less abundant than the other two categories. They express antigens indicative of the more mature forms of oligodendrocytes (Kuhlmann-Krieg *et al.*, 1988). These glial cells are usually very large and often display a bipolar shape with large extensions of flat membranes that can be connected to several processes. These oligodendrocytes are often characterised by numerous membranous whorls on cell bodies and processes. The main ultrastructural feature of type III is the more electron-dense matrix. Ribosomes and few polysomes are present as well as some dense lysosomal inclusions. The prominent rough endoplasmic reticulum often presents enlarged cisternae filled with an slightly electron-dense material. The nucleus is irregular in shape and often contains large amounts of condensed chromatin.

Oligodendrocytes maintained in culture for more than 3 weeks may exhibit the ultrastructural characteristics of the most mature cells corresponding with the dark-variety described *in vivo* by Mori and Leblond (Mori and Leblond, 1970; Kuhlmann-

Krieg *et al.*, 1988; Bradel and Prince, 1983). At this stage of differentiation, oligodendrocytes are capable of producing loose loops of myelin membranes, in the absence of neurones, which occasionally exhibit an ultrastructurally compacted appearance (Bradel and Prince, 1983).

(d) Immunological profile of the developing oligodendrocyte

The oligodendrocytes go through a complex differentiation pathway from O-2A progenitor cells to fully mature cells (Raff, 1989). Detection of a particular antigen serves as a means to identify the stage of differentiation. Progressive differentiation can be recognized by the expression of new molecules which can be detected immunologically (table 1). The O-2A progenitor cells have been traditionally identified by the A2B5 antibody (Raff *et al.*, 1983). However, this antibody, crucial to the identification of this cell lineage in the rat optic nerve, reacts with a subset of gangliosides on the cell's surface (Einsenbarth *et al.*, 1979). The study of other areas of the CNS has been confusing because these gangliosides are also expressed on neurons and astrocytes (Einsenbarth *et al.*, 1979; Schnitzer and Schachner, 1982) (table 1). The O4 antibody (Sommer and Schachner, 1981) is known also to react with the O-2A progenitor cells at a later stage of development before the expression of GalC, a marker for oligodendrocytes (see below) (Dubois-Dalcq, 1987). Very recently, the O4 immunoreactivity has been shown to coincide with a newly-described antibody AOO7 which also recognizes the, as yet undefined, proligodendroblast antigen (POA) that appears during the stage of progenitor development prior to the expression of sulfatide and GalC (Bansal *et al.*, 1992; Berry *et al.*, 1992). When O4 stains mature oligodendrocytes it recognizes different antigens such as sulfatide and seminolipids (table 2).

GalC is the first antigen indicating commitment of O-2A progenitor cells to the oligodendrocyte lineage (Raff *et al.*, 1978). It is known that CNPase and MBP follow in the development of cultured oligodendrocytes (Bologa-Sandru *et al.*, 1981; Konola *et al.*, 1991) closely followed by MAG and 1 or 2 days later by PLP/DM-20 (Dubois-Dalcq *et al.*, 1986; Knapp *et al.*, 1987; Konola *et al.*, 1991). MBP can first be detected diffusely throughout the cytoplasm of GalC+ cells (Dubois-Dalcq *et al.*, 1986; Konola *et al.*, 1991). Approximately a week later it is also detected as punctuate dots distributed along the edges of the processes (Dubois-Dalcq *et al.*, 1986; Konola *et al.*, 1991). Coarse grains of MBP staining are also detectable in sheets surrounded by loops of processes. MAG immunostaining is also confined to the cytoplasm until postnatal day 9 in the rat, presenting a higher intensity close to the nucleus (Dubois-Dalcq *et al.*, 1986). PLP and DM-20 are initially detectable only in the perinuclear region as granular shaped deposits (Dubois-Dalcq *et al.*, 1986; Konola *et al.*, 1991) and, as a result of the increase of the granules, it is detectable by 14

days in the processes (Dubois-Dalcq *et al.*, 1986; Konola *et al.*, 1991). MBP and PLP are differentially located in mature cultured oligodendrocytes as membranous sheets immunostained for MBP while PLP/DM-20 is detected mainly along the course of the cell processes (Konola *et al.*, 1991). CNPase is located mainly in the networks of processes and in the periphery of sheets (Knapp *et al.*, 1987; Konola *et al.*, 1991) (table 3).

The antigens defined by the O10 and O11 antibodies are the most mature antigens recognised by the "O" group of antibodies (Kuhlmann-Krieg *et al.*, 1988) (table 2). O10 defines a protein on the oligodendroglial surface, which has been detected in the mouse spinal cord at postnatal day 2 (Kuhlmann-Krieg *et al.*, 1988) whereas O11 recognises a surface lipid detectable after postnatal day 4. Both are indicative of mature stages of differentiation of the oligodendrocytes (Kuhlmann-Krieg *et al.*, 1988). Unfortunately, there is no evidence supporting the combined appearance of MBP, PLP and DM-20 with these two antigens. However our own studies suggest that O10 staining is expressed at about the same time as PLP/DM-20 and that O11 staining may be present slightly later than PLP.

(2) Other CNS cells

(a) The mature astrocyte

Astrocytes are star-shaped cells with a pale cytoplasm and nucleus whose processes extend into the surrounding neuropil forming glial sheets between fascicles of axons. In 1909, Cajal defined two astrocytic types, fibrous and protoplasmic, in the mammalian CNS. The majority of fibrous astrocytes are located in the CNS white matter and have a small cell body with cylindrical processes containing many intermediate filaments. Some of these terminate at the glia limitans, while others reach the surface of capillaries located within the tissue (Vaughn and Peters, 1967). By contrast, protoplasmic astrocytes are found mainly in grey matter and have broader processes containing fewer intermediate filaments. Fibrous astrocytes have numerous fibrils within their cytoplasm whereas protoplasmic astrocytes contain fewer glial filaments.

Ultrastructurally, the most distinctive feature of a mature astrocyte is the mass of glial filaments packing their cytoplasm. These are large polymers of GFAP (Raff *et al.*, 1983; Bignami *et al.*, 1972) arranged parallel to the long axis within the processes and forming bundles that extend through the perikaryon between the bases of the processes. This protein immunologically identifies astrocytes in tissue sections and cultures from the CNS. The external diameter of each filament is between 80 Å and 90 Å, and in cross sections they appear as electron-dense circles with clear centres (Vaughn and Peters, 1967). The astrocyte nucleus presents a homogeneous

distribution of the chromatin. In comparison with most other types of cells, the mitochondria, endoplasmic reticulum and Golgi apparatus are sparse within the cytoplasm of mature fibrous astrocytes. Microtubules are seldom observed within mature astrocytes but these cells contain glycogen particles, dense inclusion bodies and droplets that are probably of fatty nature (Meier and Bischoff, 1975; Vaughn and Peters, 1967).

The classification of astrocytes into fibrous and protoplasmic astrocytes according to their location in the CNS and morphological appearance may not be an accurate reflection of the extent of diversity within this family of cells. Two different types of GFAP+ cells have been detected in cultures of optic nerve of rats, on the basis of their morphology, growth characteristics and labelling with the monoclonal antibody A2B5 (Raff, 1989; Raff *et al.*, 1983). These may correspond to protoplasmic and fibrous astrocytes, respectively (Miller and Raff, 1984). Type-1 astrocytes have a flat, fibroblast-like morphology, proliferate in culture in the presence of FCS and do not bind detectable amounts of tetanus toxin or A2B5 antibody (Einsenbarth *et al.*, 1979; Raff *et al.*, 1983) although they bind Ran-2 (Raff *et al.*, 1984a; Bartlett *et al.*, 1981) (table 1). Type-2 astrocytes have a process-bearing morphology resembling neurons or oligodendrocytes and bind tetanus toxin and A2B5 antibody but not Ran-2 (Raff *et al.*, 1984a). These two phenotypes of astrocytes develop at different times and from different lineages, at least *in vitro* (Raff, 1989) (figure 1). It is believed that type-1 astrocytes develop before birth and are located at the periphery of the adult optic nerve where they form the glial limiting membrane, while type-2 astrocyte develop after the first week of postnatal life and are allocated in the interior of the adult optic nerve (Miller and Raff, 1984; Miller *et al.*, 1985). It has also been demonstrated that both type of astrocytes derive from different progenitors (Raff *et al.*, 1984a; Miller *et al.*, 1985; Miller and Raff, 1984; Raff *et al.*, 1983; Raff, 1989). Cells with characteristics similar to optic nerve type-1 and type-2 astrocytes have been described in cultures from other regions of the CNS including the cerebellum (Levi *et al.*, 1986b; Levi *et al.*, 1986a) and cerebral cortex (Ingraham and McCarthy, 1989), suggesting that they may be a common feature of the mammalian CNS. However, recent studies of neonatal spinal cord revealed at least five morphologically distinct classes of astrocytes (Miller and Szigeti, 1991) exhibiting different proliferative capacity as well as different Ran-2 and A2B5 immunoreactivity, suggesting that the spinal cord contains multiple classes of astrocytes which develop from distinct precursor cells (Miller and Szigeti, 1991).

(b) Microglial cells

Microglial cells have an electron-dense nucleus with large clumps of chromatin. Their cytoplasm is light to moderately stained containing long and

branching cisternae of granular endoplasmic reticulum (Skoff, 1990; Vaughn and Peters, 1967). Other distinguishing features include the dense core vesicles, no microtubules or filaments (Skoff *et al.*, 1976a) and large amounts of closely packed cisternae of the Golgi apparatus (Skoff, 1990). Microglial cells assume a variety of shapes. Like astrocytes, many have irregular outlines that conform to the contours of the surrounding neuropil. These cells have an ovoid appearance, with eccentrically located nuclei. Short stout protrusions sometimes extend from the perikarya. Nuclear profiles are rounded or elongated and contain clumps of chromatin which usually form broad irregular bands adjacent to the nuclear membranes.

The cytoplasmic density of these cells is greater than that of astrocytes, but less than the density shown by oligodendrocytes. Neither filaments, glycogen particles or microtubules occur in microglia. The rough endoplasmic reticulum of microglial cells is the most useful feature for distinguishing microglia from oligodendrocytes. It is generally absent in the narrow rim of cytoplasm that surrounds the nucleus, but is prominent where the cytoplasm is more voluminous at one pole of the perikarya and within the microglial processes. It consists of long narrow cisternae which characteristically have few ribosomes, and have a lumen of similar electron-density as the surrounding cytoplasm. Conversely, the Golgi apparatus has slender tightly-packed saccules and associated vesicles which frequently reveal electron-lucent contents. Dense lamellar bodies and homogeneous droplets, probably containing fat are frequent (Vaughn *et al.*, 1970; Vaughn and Peters, 1967).

(c) O-2A progenitor cells in the mature CNS

Recent studies based on tissue culture of the optic nerve of the rat have identified an adult progenitor cell (O-2A^{adult}) different from the one in perinatal animals (Wolswijk and Noble, 1989; Wren *et al.*, 1992) (figure 1). The O-2A^{adult} progenitors can be distinguished from the O-2A^{perinatal} progenitors by its morphology and antigenic phenotype. In contrast to the bipolar morphology of the A2B5+/O4- O-2A^{perinatal} progenitor cells (see section A.2.), most O-2A^{adult} progenitors isolated from the optic nerves of adult animals have one major branched process plus several smaller thinner processes (Wolswijk and Noble, 1989; Richardson *et al.*, 1990) (table 1). O-2A^{adult} progenitors are also labelled with A2B5, although not so heavily as the perinatal progenitors and they rapidly express the next antigen (Wolswijk and Noble, 1989). Furthermore, O-2A^{adult} progenitor cells do not label with antibodies to Vimentin, whereas O-2A^{perinatal} progenitors do (Wolswijk and Noble, 1989). In addition, O-2A^{adult} progenitors have a longer average cell-cycle time *in vitro* than O-2A^{perinatal} progenitors (65 hr versus 15 hr) (Small *et al.*, 1987; Wolswijk and Noble, 1989; Richardson *et al.*, 1990; ffrench-Constant *et al.*, 1988), migrate more slowly *in vitro* (Wolswijk and Noble, 1989;

Richardson *et al.*, 1990) and take longer to differentiate (5 days versus 2 days for 50% differentiation) (Wolswijk and Noble, 1989).

O-2A^{adult} progenitors first appear in the optic nerve in small numbers during the second postnatal week and replace the O-2A^{perinatal} progenitors as the dominant precursor population during the first postnatal month (Richardson *et al.*, 1990). Thus the O-2A^{adult} and the O-2A^{perinatal} progenitors seem to co-exist *in vivo* for several weeks. These cells are found in the adult rat optic nerve (ffrench-Constant and Raff, 1986; Wolswijk and Noble, 1989; Richardson *et al.*, 1990) and presumably provide a continuous source of new oligodendrocytes and type-2 astrocytes to replace those that die as a result of injury or normal cell turnover. It is not obvious, however, how these O-2A^{adult} progenitors manage to persist in the nerve beyond early postnatal development. O-2A^{adult} progenitors also differ from O-2A^{perinatal} progenitors in the rat optic nerve in the manner in which dividing cells generate oligodendrocytes (Wren *et al.*, 1992). O-2A^{perinatal} progenitors generally divide a limited number of times before all their daughter cells differentiate more or less synchronously into oligodendrocytes (Temple and Raff, 1986). In contrast, O-2A^{adult} progenitors appear to divide and differentiate asymmetrically, giving rise to mixed clones of cells containing both O-2A^{adult} progenitors and oligodendrocytes (Richardson *et al.*, 1990). Thus O-2A^{adult} progenitors may be capable of self renewal and their presence in the adult optic nerve may not require that they be continuously generated from a precursor cell (Richardson *et al.*, 1990). Recent investigations have reported that O-2A^{adult} progenitors modify their dividing characteristics towards a O-2A^{perinatal} progenitors fashion when cultured in the presence of PDGF and fibroblast growth factor (FGF) (Wolswijk and Noble, 1992). The characteristics of adult progenitor cells make these cells ideally suitable for the needs of the adult CNS (Wolswijk and Noble, 1989; ffrench-Constant *et al.*, 1988).

b) Biochemical composition of the CNS myelin sheath

(1) Introduction

Mature CNS myelin closely resembles PNS myelin by virtue of it having been formed by a cell process from a myelin-forming cell becoming wrapped spirally around the axon. However, several differences exist. The CNS myelin periodicity is somewhat smaller but the manner in which the myelin lamellae arise is identical (Peters *et al.*, 1976). CNS myelin is rarely directly attached to the soma of the myelin-forming cell although some Schwann cell-like oligodendrocytes occur in the developing spinal cord (Remahl and Hildebrand, 1990; Del Rio Hortega, 1922; Stensaas and Stensaas, 1968). In general, the cytoplasm of the oligodendrocyte in

the mature sheath is restricted to the inner and outer tongues. No basal lamina surrounds the CNS myelin sheath whose matrix is non-collagenated. The sheaths in the CNS never attain the same thickness as those around axons of similar diameter in the PNS, as has been demonstrated by studying the transition zone between CNS and PNS (Fraher, 1992).

Some morphological differences between mature CNS and PNS myelin reflect immunochemical and biochemical differences between the two. The PNS myelin, which is produced by Schwann cells which have a different embryological origin (see section A), has also evolved a quantitatively similar lipid composition and comparable protein content (Norton and Cammer, 1984). The CNS myelin composition is very similar for all the vertebrates. This biochemical composition of myelin reflects a precise evolution of the most appropriate membrane that would spiral wrap around the axon, thereby permitting fast saltatory conduction of nerve impulses. In the present review I describe only the characteristic of the CNS myelin (for a PNS review see: Norton and Cammer, 1984)).

(2) Lipids in myelin

Even though there are no lipids specific to myelin the high content of galactosphingolipids, cerebroside (galactosylceramide) and sulphatide are the distinguishing feature of myelin lipids (table 4). Cerebroside is the most "myelin typical" lipid and it is also an specific marker for oligodendrocytes (Raff *et al.*, 1978) as within the CNS it is restricted to those cells and myelin. The specificity of sulphatide for the myelin-oligodendroglial unit is less certain. In addition to cerebroside, myelin lipids are also enriched in cholesterol and ethanolamine phosphoglycerides relative to other membranes. These three lipids together comprise about 65% of the total lipid accounting for 45 to 50% of the total dry weight of myelin (Norton and Cammer, 1984).

Other lipids in myelin usually not included in routine analytical studies include di- and tri-phosphoinositide, a series of fatty acid esters of cerebroside, at least three galactosyldiglyceride derivatives, a series of gangliosides and some alkanes. Myelin contains only small amounts of phosphatidylinositol remaining tightly bound to myelin proteins. Beside the two main galactolipids, cerebroside and sulphatide, myelin has several minor galactolipids, half of which consists of several fatty acids esters of cerebroside, and the other half of two glycerol-based lipids, diacylglycerylgalactoside and monoacylmonoalkylglyceryl-galactoside, called collectively galactosyldiglyceride. A sulphate ester of these latter compounds also exists. The biosynthesis of these

glycerol derivatives appears to be closely associated with myelination (Norton and Cammer, 1984) (table 4).

(3) Myelin proteins

The most striking feature of CNS myelin proteins is their simplicity on SDS-PAGE as, in most species, they separate into only six prominent bands (Norton and Cammer, 1984).

(a) Myelin-associated Glycoprotein (MAG)

In the high-molecular-weight region of a typical SDS-polyacrylamide gel (>60,000), a number of minor, uncharacterised protein bands can be seen. These vary in amount, depending in the species and the degree of maturity. Although MAG is probably the major myelin glycoprotein characterised in this region, many other glycoproteins can be detected in most species (Norton and Cammer, 1984). MAG constitutes approximately 1% of the total CNS myelin protein and is also present in the PNS (Campagnoni and Macklin, 1988). It has an apparent molecular weight of 100 kDa, 30% of which is carbohydrate (Campagnoni and Macklin, 1988). This protein can exist in two isoforms with apparent molecular masses of 72 and 67 kDa. which are encoded by separate mRNAs (Lai *et al.*, 1987; Pedraza *et al.*, 1991) (table 3). Biochemical and immunological studies have demonstrated that it is most prominent in oligodendrocyte membranes in the periaxonal regions of the CNS myelin internodes but is absent from compact myelin (Sternberger *et al.*, 1979; Trapp *et al.*, 1989) Its presence has also been demonstrated in oligodendrocyte processes during initial ensheathment of CNS axons (Trapp *et al.*, 1989). The periaxonal localization together with the significant amino-acid sequence identity between the extracellular domain of MAG and other cell adhesion and ligand binding molecules supports a role for MAG in oligodendrocyte-axon interactions (Campagnoni and Macklin, 1988; Quarles *et al.*, 1984; Trapp *et al.*, 1989; Norton and Cammer, 1984).

MAG is a monotopic membrane protein and a large extracellular domain that contains five Ig-like regions, eight potential N-linked glycosylation sites and one of two possible cytoplasmic domains that contain putative phosphorylation sites (Arquint *et al.*, 1987; Campagnoni and Macklin, 1988). MAG mRNA has been detected at about a week after birth in rodents and increases until about 25-27 days postnatally after which it decreases (Campagnoni and Macklin, 1988). Thus, in spite of the popular notion that MAG may play an important role in the early interaction between the growing myelin sheath and the axon, the developmental data suggest that the protein is not expressed earlier than the major myelin proteins (MBP and PLP), and that the developmental peak of its synthesis is somewhat later than MBP (Campagnoni and Macklin, 1988).

(b) Wolfgram proteins

Three prominent bands are observed in stained gels in the molecular weight region of 43,000-60,000. These are the Wolfgram proteins W_1 & W_2 (Norton and Cammer, 1984). The amount of these proteins as well as their molecular weight varies among species and giving rise to some confusion in the literature. Recently, W_1 (molecular weight 42,000-50,000) has been shown to correspond in molecular weight, amino-acid composition and immunological properties to the previously purified myelin-specific enzyme CNPase (Campagnoni and Macklin, 1988; Norton and Cammer, 1984). Both W_{1a} and W_{1b} react with antiserum to CNPase, but the band at molecular weight 55,000 (W_2) does not.

(c) 2',3'-Cyclic Nucleotide 3'-Phosphodiesterase (CNPase)

The purified enzyme consists of two polypeptides (46 kDa and 48 kDa) that represent about 5% of the total protein in purified CNS myelin (Kurihara *et al.*, 1992; Sprinkle *et al.*, 1978; Sprinkle *et al.*, 1978). The two polypeptide forms of CNPase are encoded by separate mRNA (Bernier *et al.*, 1987) which are concentrated around oligodendrocyte perinuclear regions during active stages of myelination (Trapp *et al.*, 1987; Jordan *et al.*, 1989) (table 3). CNPase mRNA is translated on free polysomes and is actively retained within the perinuclear region of the oligodendrocytes becoming tightly associated with membrane shortly after synthesis (Bernier *et al.*, 1987).

CNPase has been detected immunologically within specific regions of the oligodendrocyte and myelin internode. These include the plasma membranes of oligodendrocytes and their processes, the paranodal loops, the periaxonal membrane and inner mesaxon, the outer tongue process and incisure-like membranes found in many larger CNS sheaths (Trapp *et al.*, 1988; Braun *et al.*, 1988). This wide distribution suggests that CNPase has a general function related to the maintenance of membranes that demarcate cytoplasmic channels within the myelin internode and plasma membranes of the oligodendrocytes. *In vitro* CNPase catalyses the hydrolysis of 2',3'-nucleotides into the corresponding 2'-nucleotide (Norton and Cammer, 1984). The *in vivo* function of CNPase is unknown as natural substrates for these enzymatic activities have not yet been found in brain. Since CNPase appears to be the first myelin-related protein detected during development, it may have a crucial role in early stages of myelination (Trapp, 1990).

(d) Proteolipid proteins (PLP/DM-20)

The proteolipid fraction comprises two proteins in the SDS gel with molecular weights of 25,000 and 20,500. These are PLP and its isoform DM-20, respectively.

The proteolipid proteins are highly hydrophobic intrinsic membrane proteins that represent about 50% of the total protein mass in isolated human CNS myelin (Nave and Milner, 1989). There is a controversy about the individual proportions of both of the proteolipid proteins (see below).

(a) Synthesis and trafficking of PLP and DM-20

Membrane-bound ribosomes are the main location for PLP synthesis (Hartman *et al.*, 1982; Colman *et al.*, 1982). The PLP polypeptide is synthesized and integrated into membranes of the rough endoplasmic reticulum (Colman *et al.*, 1982). The protein is acylated at a step following passage through the Golgi complex prior to its transport and insertion into compact myelin (Colman *et al.*, 1982; Trapp, 1990). Similar DM-20 protein trafficking has been observed in Hella cells transfected with DM-20 cDNA (Timsit *et al.*, 1992) (table 3). Antiserum directed against PLP/DM-20 stains compact CNS myelin intensely and produce particulate staining of perinuclear regions of actively myelinating oligodendrocytes (Hartman *et al.*, 1982; Colman *et al.*, 1982; Trapp, 1990). There is a substantial delay (30 minutes approximately) between synthesis of the polypeptide and its insertion into compact myelin (Colman *et al.*, 1982; Benjamins *et al.*, 1978).

(b) Protein structure and topological orientation

PLP is 276 amino acids long and has a molecular weight of exactly 30,000, which is considerably higher than the apparent molecular weight (approximately of 24,000-25,000) of the active protein on SDS polyacrylamide gel electrophoresis (Nave and Milner, 1989). It is highly hydrophobic and 75% of its amino acids appear to exist in an α-helical conformation (Stoffel *et al.*, 1984; Laursen *et al.*, 1984; Hudson *et al.*, 1989). SDS gel electrophoresis separates the major PLP from a related myelin protein with higher electrophoretic mobility (Nave and Milner, 1989). This protein, which co-purifies with PLP, was termed DM-20 from its apparent weight of approximately 20,000 on gels (molecular weight of 26,500). A close biochemical relatedness between DM-20 protein and PLP was revealed, including identical of amino-terminal and carboxy-terminal amino acid residues. The primary structure of DM-20 and its relationship to PLP was deduced from cloned cDNA sequences (Nave *et al.*, 1986) (figure 5.e). DM-20 differed from all known PLP cDNAs by lacking 105 nucleotides from the protein coding region (Nave and Milner, 1989) corresponding to a loss of amino acid residues 116 to 150 (Nave and Milner, 1989). Thus PLP and DM-20 differ by the internal deletion of 35 amino acid residues (from 116 to 150) (Nave *et al.*, 1987; Nave and Milner, 1989; Stoffel *et al.*, 1984; Trapp, 1990). DM-20 is present in almost the same quantity as PLP in adult bovine (Trapp *et al.*, 1983; Schindler *et al.*, 1990) and rat brains (Van Dorsselaer *et*

al., 1987) although it was previously believed that DM-20 was a minor component compared to PLP (Hudson *et al.*, 1987). DM-20 is detected earlier and in larger amounts than PLP at the beginning of myelination in the foetal bovine brain (Van Dorsselaer *et al.*, 1987; Schindler *et al.*, 1990). Just before birth PLP is less abundant than DM-20 in bovine brain (Schindler *et al.*, 1990). Similar results have been obtained in human spinal cord (Kronquist *et al.*, 1987) and mouse CNS (Gardinier and Macklin, 1988).

Rat, mouse, bovine and human PLP amino acid sequences are 99% identical, suggesting that their general three-dimensional structures are also virtually identical (Nave and Milner, 1989). PLP spans the lipid bilayer of myelin membranes; however, the precise orientation of the polypeptide within the membrane bilayer is unclear at present. PLP contains four stretches of hydrophobic amino acids, each of which is long enough to fully transverse the membrane bilayer (Milner *et al.*, 1985; Nave and Milner, 1989), hence the different models of insertion in the membrane proposed by different authors (figure 5.e). Hudson and co-workers suggest that PLP has only two transmembrane domains and that the great majority of the protein is located on the extracellular face of the oligodendrocyte plasma membrane (Hudson *et al.*, 1989). Laursen and co-workers, on the other hand, propose a model which has three putative transmembrane domains and some domains that may be exposed to each side of the bilayer (Laursen *et al.*, 1984). Finally, Stoffel's (Stoffel *et al.*, 1984; Trapp, 1990) model proposed that the major hydrophilic and positively charged domain of the protein is exposed at the extracellular surface of the myelin membrane. Most authors locate the orientation of the C-terminus at the cytoplasmic face of the oligodendrocyte membranes (Stoffel *et al.*, 1984; Laursen *et al.*, 1984; Konola *et al.*, 1992). However, the only established fact at present is that PLP is a polytopic membrane protein.

The region of PLP that is absent in DM-20 (residues 116-150) corresponds to the major hydrophilic and positively charged domain of the protein. This part of the sequence exactly precedes the putative third membrane embedded domain (Nave *et al.*, 1987; Houbre *et al.*, 1990) which is exposed at the extracellular surface of the myelin membrane in the model of Stoffel *et al.* (Stoffel *et al.*, 1984; Trapp, 1990) (figure 5). As DM-20 lacks most of these charged residues, it presumably contains its functional site in the second extracellular domain of the molecule as proposed by Laursen (Laursen *et al.*, 1984). This part of the molecule, which is identical in PLP and DM-20 is exposed to the cell surface and is acylated (Nave *et al.*, 1987).

Some other lower molecular weight proteolipid proteins, apparently related to the major myelin PLP, have been observed in proteolipid preparations isolated from brain (Chan and Lees, 1974; Macklin and Pfeiffer, 1983; Lepage *et al.*, 1986;

Schindler *et al.*, 1990) and translated *in vitro* from brain RNA (Sorg *et al.*, 1986). PIIß, an adult brain proteolipid (apparent Mr 24,000) (Helynck *et al.*, 1983) shares an identical N-terminal tripeptide (Mr24,000) with that of PLP as well as its amino acid composition (Schindler *et al.*, 1990). It reacts in immunoblot with the anti-tridecapeptide 117-129 antiserum. This proteolipid was never detected in foetal bovine cerebral hemispheres (Schindler *et al.*, 1990). Another uncharacterised proteolipid named PIIß', of approximately the same size as DM-20 (Mr 20,000) but different from PIIß (Schindler *et al.*, 1990), has also been described. Its amino acid composition differs from PIIß and DM-20 and in immunoblots did not react with the anti-tridecapeptide or anti-C-terminal PLP antibodies (Schindler *et al.*, 1990). PIIß' has been found to be the major proteolipid in foetal hemispheres before the appearance of white matter but was not detected in adult bovine brain (Schindler *et al.*, 1990).

(c) PLP gene localization and structure

The PLP gene locus has been located on the q-22 band of the X-chromosome (Mattei *et al.*, 1986) which is significant in the implication of this gene in a group of sex-linked myelin-deficiency disorders (see section B). The PLP gene was first isolated from a human genomic library (Diehl *et al.*, 1986) and further characterised in the mouse (Macklin *et al.*, 1987) and the rat (Boison and Stoffel, 1989). Its overall structure suggested a high degree of sequence similarities between the mouse and human gene and remarkably little change during evolution. The PLP gene in both species is approximately 17,000 base pairs in length and contains seven exons. Alternative RNA splicing of the primary PLP gene transcript generates either PLP or the 105-nucleotide shorter DM-20 mRNA.

(d) Transcription of the PLP gene

PLP specific mRNAs are highly abundant in the adult rodent brain (approximately 2% total mRNA) (Nave and Milner, 1989). The two major PLP mRNAs in rat brain are 3200 and 1600 nucleotides long, as shown by northern blot analysis (Nave and Milner, 1989; Campagnoni and Macklin, 1988). A third mRNA species of 2400 nucleotides is much less abundant (Nave and Milner, 1989). In mouse (Gardinier *et al.*, 1986; Nave *et al.*, 1986) and man (Kronquist *et al.*, 1987) the 3200-nucleotide PLP mRNA is the predominant form. The relative abundance of the family of mRNAs appears to be different from different species (Campagnoni and Macklin, 1988). The PLP gene expresses two families of mRNAs through alternative splicing (Nave *et al.*, 1987; Sorg *et al.*, 1986; Campagnoni *et al.*, 1992). The splicing of the PLP gene primary transcript in the brain appears to be developmentally regulated (Campagnoni *et al.*, 1992). During the early stages of

myelination the DM-20 mRNA is the predominant form and gradually declines with development (Schindler *et al.*, 1990; Campagnoni *et al.*, 1992). At later stages the PLP is the major form (Kronquist *et al.*, 1987; Gardinier and Macklin, 1988; Schindler *et al.*, 1990). PLP RNA levels are maximal at 18 days postnatally in brain (Campagnoni and Macklin, 1988). Recent application of polymerase chain reaction (PCR) technique demonstrated that DM-20 mRNA is detectable in embryonic mouse brain as early as embryonic day 11, showing a peak of expression at embryonic day 14, while PLP mRNA became detectable only at postnatal day 2 (Timsit *et al.*, 1992; Ikenaka *et al.*, 1992). Therefore, DM-20 mRNA is selectively spliced in a small amount from the very beginning of neural development (Ikenaka *et al.*, 1992). The formation of DM-20 mRNA involves the excision of intron III and a 105-nucleotides of the PLP gene (exon IIIB) (Nave *et al.*, 1987). The 5' end of the deleted sequence therefore constitutes an alternative 5' donor splice site, which is located within the open reading frame (exon IIIA) and is utilized with approximately 50% relative efficiency (Nave *et al.*, 1987). By standard SDS gel electrophoresis of the myelin proteolipid fraction, PLP appears two to ten-fold more abundant than DM-20. However, at the RNA level, PLP mRNA is only twice as abundant as DM-20 mRNA in rat brain indicating a slightly higher efficiency of PLP specific RNA translation (Nave *et al.*, 1986). Assuming that both mRNA forms are equally stable *in vivo*, PLP mRNA results from an about 2-fold higher splicing efficiency of the downstream splice site (Nave *et al.*, 1987).

Recent investigations have demonstrated that DM-20 expression is not restricted to oligodendrocytes. Astrocytes (Macklin, 1988; Ikenaka *et al.*, 1992), Schwann cells (Jordan *et al.*, 1990; McPhilemy *et al.*, 1989; Griffiths *et al.*, 1989; Kamholz *et al.*, 1992; Ikenaka *et al.*, 1992) and various other cell lines of neuronal and glial origin including C6 glioma, oligodendroglioma G-26, B104, PC12, NG108-15, N18-TG and Neuro 2A cells also produce DM-20 mRNA (Ikenaka *et al.*, 1992). DM-20 mRNA has also been detected in newborn mouse heart and, to a lesser degree, in spleen (Campagnoni *et al.*, 1992). The labelling was concentrated over the myocardial nuclei suggesting that substantial amounts of label were associated with the perinuclear, cytoplasmic regions of myocardial cells (Campagnoni *et al.*, 1992). Very recently I have also detected PLP mRNA expression in rat optic nerve A2B5+ cells.

(e) Function of the proteolipid proteins

The remarkable degree of evolutionary conservation of PLP among mammals (Nave and Milner, 1989) and the extraordinary susceptibility of this protein to mutations suggests that some functions of this protein are not yet known. PLP mutants display two seemingly unrelated phenotypic features associated with the loss

of function of PLP and DM-20. Firstly, the severe hypomyelination (see review in section B) together with an abnormally condensed IPL indicated that PLP/DM-20 must predominate in the IPL as predicted by studies of the topology of PLP/DM-20 in the oligodendrocyte plasma membrane (see below) (Hudson *et al.*, 1989). Secondly, striking phenotypic feature is the profound loss of oligodendrocytes in the CNS resulting in lethal mutations (see review in section B.3.). These features delineate two distinct roles for PLP and DM-20 in myelinating cells; one promoting oligodendrocyte survival and the other in providing stability at the IPL as a result of the homophilic interactions between PLP and/or the adjacent membrane (Schindler *et al.*, 1990). Some authors consider DM-20 as a more complex proteolipid which developed later in proteolipid evolution (Nave *et al.*, 1987). If DM-20 was inserted in the membrane following the PLP model, the major hydrophilic loop of PLP, which plays a key role in stabilization of the IPL, is almost entirely missing in DM-20 (Schindler *et al.*, 1990); thus, the homophilic interactions occurring between PLP molecules would not take place. However, as DM-20 is the only proteolipid detected in large amounts at the beginning of myelination, it is tempting to assume a particular role for DM-20 in the very early stages of the formation of the myelin sheath. Schindler *et al.* (Schindler *et al.*, 1990) proposed a two step myelination model where by the flattened oligodendrocyte process can spirally wrap around the enlarging axon as the different layers slip over one another. This can occur since the hydrophobic loop is missing in DM-20, which is the major proteolipid in early myelination. During the second step, PLP stabilizes the arrangement of the myelin sheath with its hydrophobic loop anchoring adjacent layers. This hypothesis is compatible with the fact that the IPL may be formed at later stages (Schindler *et al.*, 1990).

Recently, interest in the alternative roles for DM-20 in nervous tissue has increased. DM-20 mRNA has been detected in the embryonic mouse brain long before myelination occurs (Timsit *et al.*, 1992; Ikenaka *et al.*, 1992) and before PLP message is present (Van Dorsselaer *et al.*, 1987). DM-20 mRNA and protein production have also been described in astrocytes (Macklin, 1988; Ikenaka *et al.*, 1992) and Schwann cells (Jordan *et al.*, 1990; McPhilemy *et al.*, 1989; Griffiths *et al.*, 1989; Kamholz *et al.*, 1992; Ikenaka *et al.*, 1992; Puckett *et al.*, 1987). Additionally DM-20 mRNA has been found in various cell lines of neuronal and glial origin (Ikenaka *et al.*, 1992), as well as in non-related tissues such as cardiac muscle (Campagnoni *et al.*, 1992). Secondly, mutations within the PLP gene result in abnormal glial differentiation, such as degeneration of oligodendrocytes (Knapp *et al.*, 1986; Meier and Bischoff, 1975; Privat *et al.*, 1982; Skoff and Knapp, 1990; Boison and Stoffel, 1989; Jackson *et al.*, 1988; Jackson and Duncan, 1988; Nadon *et al.*, 1990; Fanarraga *et al.*, 1992b) and hypertrophy of astrocytes (Skoff, 1976). These findings strongly suggest that DM-20 plays additional roles beyond that of a structural

protein of myelin sheaths (Campagnoni *et al.*, 1992). These roles may include the compartmentalization and differentiation of the neural tube (Timsit *et al.*, 1992; Ikenaka *et al.*, 1992; Schindler *et al.*, 1990) or may even be involved in embryonic cell differentiation at all levels (Campagnoni *et al.*, 1992). A reduction in DM-20 mRNA occurred when PC12 cells were induced to differentiate into neuron-like cells by nerve growth factor (NGF) addition (Ikenaka *et al.*, 1992) which again supports the idea of DM-20 being necessary during the very early stages of cell differentiation.

Recently, the PMP-22 protein, in the PNS, has been found to be involved in Schwann cell growth-regulation (Snipes *et al.*, 1992) (see section B.2.b.). DM-20 could represent the CNS equivalent to this protein as the structural role of DM-20 has yet to be demonstrated.

(e) Myelin Basic Proteins (MBP)

The prominent band at 18,5000 kDa on SDS PAGE is MBP accounting for 30-35% of the total protein in purified CNS myelin. The myelin basic proteins consist of a family of low molecular weight product isoforms of a single gene by differential splicing (Ferra *et al.*, 1985; Campagnoni, 1988; Norton and Cammer, 1984). The complete amino-acid sequence of bovine and human MBP was published in 1971 (Norton and Cammer, 1984). Four major forms of MBP (21.5 kDa, 18.5 kDa, 17 kDa, 14 kDa) exist in rodents (Barbarese *et al.*, 1978). However, the basic proteins of all mammals are very similar (Norton and Cammer, 1984). They have isoelectric points greater than 10, are highly denatured in solution, and are very susceptible to proteolysis. They contain more than 50% polar amino-acids, have one tryptophan residue per molecule, and contain no cysteine. This is in contrast to PLP, which is rich in cysteine and tryptophan. The MBPs can be extracted from myelin by acid or salt solutions, but are also soluble in chloroform-methanol when myelin is treated with this mixture. When extracted from the membrane, they are very soluble in water (Norton and Cammer, 1984).

The basic proteins are extrinsic membrane proteins and located on the cytoplasmic side of myelin membranes (Omlin *et al.*, 1982) playing a structural role in maintaining the close apposition of the cytoplasmic leaflets of the MDL (Dupouey *et al.*, 1979; Privat *et al.*, 1979; Omlin *et al.*, 1982) as demonstrated immunocytochemically (table 3). Antibodies specific for MBP stain compact CNS myelin (Sternberger *et al.*, 1978a; Hartman *et al.*, 1982). Mutations in the MBP gene, such as *shiverer* (*shi*), correlate the absence of MBP with ultrastructural alterations in the MDL of the myelin membrane.

MBP mRNA is distributed diffusely over myelinated fibres within the adult CNS indicating that it is translated on free polysomes and transported to sites near

compact myelin during active stages of myelination (Trapp, 1990). MBP enters myelin within a few minutes after synthesis which may indicate that most of MBP synthesis occurs along the myelin internode on polysomes that are present in the outer tongue process. This site of MBP synthesis also explains the dramatic reduction of MBP immunoreactivity in perinuclear regions of oligodendrocytes during peak periods of myelination (Sternberger *et al.*, 1978b). Primary cultures of mouse brain oligodendrocytes show that MBP mRNAs activity is asymmetrical within the oligodendrocyte cell body, and then progressively label the cell processes (Amur-Umarjee *et al.*, 1990). Older cells have clumps of MBP mRNA at significant distances from the cell body (Amur-Umarjee *et al.*, 1990).

B. CNS MUTANTS

1. INTRODUCTION AND AIMS OF THE STUDY

Myelin mutants have significantly contributed towards our understanding of assembly and maintenance of myelin and its functional importance in the nervous system. The largest group of myelin mutations involve the PLP gene and are inherited in an X-linked recessive manner. The normal myelination process is impaired in these mutants leading to severe neurological dysfunctions such as tremor, ataxia and seizures, and, in most cases, the early death of the animal. Mutations of the PLP gene occur in several species including man, dog, pig, rat and mouse (table 5). In its most severe forms, dysmyelination results in only a few poorly compacted myelin sheaths, such as in the *md rat* (Duncan *et al.*, 1987b).

2. DYSMYELINATING MUTANTS

The dysmyelinating mutants are useful models for investigating the normal process of myelination. These animals provide a uniform system in which to study a specific defect in myelination and secondary effects resulting from that defect. Several of the mutant mice have been extensively characterised.

a) Shiverer mutant

The *shiverer (shi)* and its allele *myelin deficient* (shi^{mld}) exhibit tremors beginning approximately at postnatal day 12, becoming progressively worse until convulsions appear. These mice do no survive past 90-150 days (Chernoff, 1981; Hogan and Greenfield, 1984). Morphological analyses indicate that many axons are unmyelinated, and those that are myelinated have only low amounts of myelin. Immunological and ultrastructural observations of *shi* and shi^{mld} tissue indicates the total absence of MBP (Bourre *et al.*, 1980; Barbarese *et al.*, 1983; Hogan and Greenfield, 1984) reflected in the lack of the MDL of the myelin sheaths (Privat *et al.*, 1979; Dupouey *et al.*, 1979; Mikoshiba *et al.*, 1987). Recently, it has been established that the *sh* and shi^{mld} mutations map to the distal end of mouse chromosome 18 which contains the MBP gene (Okano *et al.*, 1988; Roach *et al.*, 1985). The *shi* mutation results from a deletion of exons 3-7 of the MBP gene (Roach *et al.*, 1985). In contrast, in shi^{mld} mice, there appears to be a duplication

of the MBP gene with the downstream gene inverted (Okano *et al.*, 1988; Popko *et al.*, 1987).

When *shi* oligodendrocytes are immunostained for carbonic anhydrase II (CAII) an early oligodendrocyte marker, there is elevated staining relative to normal animals (Cammer *et al.*, 1985). However, levels for both PLP and MAG are reduced, although significantly above MBP levels (Mikoshiba *et al.*, 1980). PLP mRNA levels in 21 day-old *shi* brain were at approximately 50% of normal, although the amount of PLP that accumulated in these brains was relatively less (Sorg *et al.*, 1986).

b) Trembler mutant

The autosomal dominant *trembler* mutation (*tr*) maps to the mouse chromosome 11 and manifests as a Schwann cell defect characterised by severe hypomyelination and continuing Schwann cell proliferation throughout life (Ayers and Anderson, 1973). Affected animals move clumsily and develop tremor and transient seizures at young age. Recently, the *tr* mutation has been identified in the peripheral myelin protein-22 (PMP-22) gene which encodes for a potentially growth-regulating myelin protein (Suter *et al.*, 1992).

c) Quaking mutant

The *quaking (qk)* mutation is autosomal recessively-inherited, and maps to the mouse chromosome 17 causing a disorder in both the CNS and PNS (Guenet, 1980). These mice exhibit tremors, which begins approximately at postnatal day 12 and continue throughout their lifetime. Tonic seizures occur in these animals, although they have a normal life-span. Affected females are fertile but affected males are sterile. Histological examination indicated grey translucent areas in the optic nerve and the myelinated tracts of the spinal cord and brain stem. There was a significant loss of CNS myelin, although PNS myelination was not severely defective at the light microscopic level. The density of oligodendrocyte cells was increased along fibre tracts (Friedrich, 1975), often with vacuoles in the cytoplasm suggesting a defective incorporation (Greenfield *et al.*, 1977) and a lysosomal degradation of myelin proteins (Watanabe and Bingle, 1972; Wisniewski and Morell, 1971).

No oligodendrocyte/myelin gene product has been clearly implicated as the primary site of the genetic lesion in *qk* mice. At present no myelin-specific gene has been mapped to the chromosome 17 in *qk*. It has been suggested that the defect in *qk*

is a maturation defect that results in an arrest in myelinogenesis (Wisniewski and Morell, 1971) due to the inability of the myelin membranes to assemble correctly, rather than in an inability of the cell to synthesize the proteins (Greenfield *et al.*, 1977).

3. REVIEW OF THE PHENOTYPE OF THE PLP MUTANTS

This group of myelin mutants comprises animals from different species such as *jimpy (jp)* mice and its alleles *jimpy synthesis deficient* (jp^{msd}) (Meier and MacPike, 1970) and jp^{rsh} (Cattanach and Beechey, 1991); the *md rats* (Boison and Stoffel, 1989) the *shaking pup (sh pup)* (Nadon *et al.*, 1990), the Type AIII pig (Harding *et al.*, 1973) and *Pelizaeus Merzbacher Disease (PMD)* in humans (table 5).

a) Clinical presentation

The first neurological abnormality seen in these mutants is usually a tremor, which is noted when they begin to ambulate at 10 to 12 days of age; however, a fine tremor may be seen in the *sh pup* as early as 7 days (Duncan, 1990). The tremor worsens with attempts to perform volitional movements and disappears when the animal rests or sleeps. In the *md rat* and *jp* mouse, seizures begin at 20 days of age and increasing in frequency and severity, resulting in death at about 25 to 30 days. A long lived "strain" of *md rats* has been noted in two different colonies with affected males living up to 85 days of age despite continued tremoring and seizure activity (Jackson *et al.*, 1988). In contrast to the murine mutants, *sh pup* hemizygotes can live for prolonged periods if hand-reared, but they have persistent neurologic deficits and may develop seizures after 3 to 4 months. The genetic heterogeneity of human *PMD*, with at least six known forms of the disease, results in a variable phenotype. The connatal form of *PMD* is the most severe, with affected children showing tremor, ataxia and athetosis; death occurs early in life, usually before the age of 10. Type AIII hypomyelinogenesis congenita described in the Landrace pig results in tremor and ataxia (Blakemore *et al.*, 1974).

b) Morphological characteristics

(1) Amount of myelin

Light microscopy of mutant CNS reveals a variable severity of hypomyelination for the different mutations. Later-myelinating structures in the brain, such as the corpus callosum, compared to the spinal cord (an earlier myelinating structure) seemed to be more affected (Duncan, 1990). Within one type of mutation some animals are more affected than others. In *jp*, clumps of myelinated fibres and occasional scattered myelinated fibres are seen. However, quantitation of the amount of myelin in the spinal cord of *jp* demonstrated only 1.6% of the amount in control animals (Duncan *et al.*, 1989). The allele of *jp*, the jp^{msd} (Billings-Gagliardi *et al.*, 1983) mouse has, in comparison, twice the amount of myelin as *jp* (Duncan *et al.*, 1989). Those mutants with the greatest amounts of myelin, that is the *sh pup*, Type AIII pig and jp^{rsh} live longer than those with little myelin. One exception, however, is the "older strain" of *md rats* which can live up to three times longer than the original mutant (Jackson *et al.*, 1988). As the increase in the amount of myelin in these older *md rats* is small, it is unlikely to be responsible for their longer survival.

(2) Myelin structure

There is also a great variation in the structure of the myelin formed in the X-linked mutants. In the *md rat* most of the myelin that is formed consists of loosely whorled layers of membrane. Similar, poorly compacted myelin is frequently seen in the other mutants. However, in both the *md rat* and *jp* mouse, occasional surprisingly thick and apparently well-compacted myelin sheaths with up to 20 lamellae can be seen (Duncan *et al.*, 1989; Duncan *et al.*, 1987b). In those mutants with more myelin the majority of myelin sheaths are thin (hypomyelination), even in mature *sh pups* at 2 years of age (Duncan, 1990). Certain smaller axons have thicker myelin sheaths, but examination of longitudinal sections of the spinal cord suggests that these are likely to have shorter internodes (Duncan, 1990). High power resolution of the myelin sheath of the *md rat* has shown an abnormality in the compacted myelin sheaths with fusion of the intraperiod line (Hudson, 1990a; Duncan *et al.*, 1989; Duncan *et al.*, 1987b; Rosenbluth, 1987). A similar abnormality can be seen in certain parts of the myelin sheaths found in *jp* (Duncan *et al.*, 1989). As PLP is thought to be localized predominantly at the intraperiod line (Hudson *et al.*, 1989), the previously noted lack of PLP in these mutants could result in this structural abnormality. Immunocytochemical staining of the myelin sheaths in the X-linked mutants has produced interesting but variable results. Myelin sheaths of the *md rat* and *jp* mice do not immunostain with the anti-C-terminal antibody (common for PLP and DM-20), which stains the myelin found in the *sh pup* and type AIII pig (Duncan, 1990). In PMD, PLP is not detectable by immunostaining. In each mutant in which there is a lack of PLP staining, the myelin present is positive for MBP. Immunostaining of the same sheaths in serial sections of *md* and *jp* demonstrates that

they are MBP positive, yet PLP negative (Duncan *et al.*, 1989; Duncan *et al.*, 1987b). In the *sh pup*, although the myelin is PLP and MBP positive, the staining of myelin is poor when compared to controls (Yanagisawa *et al.*, 1987).

(3) Oligodendroglia in PLP mutants

The number of mature oligodendrocytes is reduced in the X-linked mutants as evaluated by both quantitative and qualitative microscopic studies of certain areas of the CNS (Duncan, 1990). Tissue culture studies of the optic nerve or brain of both *jp* and *md rat* confirm that fewer viable cells of the oligodendrocyte lineage are found in the mutants compared to controls (Zeller *et al.*, 1989). However, using anti-GalC antibodies as an oligodendrocyte-specific marker, *jp* oligodendrocytes have been seen to reach the GalC+ state of development (Ghandour and Skoff, 1988) and even to synthesize a fairly thick, though abnormally compacted, myelin sheath. These may represent the few oligodendrocytes capable of forming myelin (Duncan, 1990). Despite the apparent paucity of mature oligodendrocytes in these mutants cell kinetic studies in *jp*, *md rat* and *sh pup* (Jackson and Duncan, 1988; Knapp *et al.*, 1986; Duncan, 1990) have shown an increased glial cell proliferation, most probably of oligodendrocytes. However it has also been documented that the premature death of these cells occurred especially in *jp* (Meier and Bischoff, 1975; Knapp *et al.*, 1986; Knapp *et al.*, 1990; Privat *et al.*, 1982; Skoff and Knapp, 1990; Vermeesch *et al.*, 1990), and *md rat* (Boison and Stoffel, 1989; Jackson and Duncan, 1988).

A unique cellular abnormality of oligodendrocytes noted in the *md rat* and *sh pup* is distension of the rough endoplasmic reticulum and nuclear envelope (Jackson and Duncan, 1988;Dentinger *et al.*, 1982; Duncan *et al.*, 1983). In the *sh pup* these distensions contain a floccular material, whereas in the *md rat* the rough endoplasmic reticulum swellings are often larger in size but appear more vacuolar. A mild swelling of the rough endoplasmic reticulum in oligodendrocytes has been reported in jp^{msd} (Billings-Gagliardi *et al.*, 1983) whereas in *jp*, dying oligodendrocytes are present but the only consistent cytoplasmic abnormality is the presence of abnormal membranous profiles (Meier and Bischoff, 1975). Distension of the rough endoplasmic reticulum in the *sh pup* and the *md rat* may be the key to the underlying biochemical defect in these mutants. These two mutations are located in exons 2 and 3 respectively resulting in the insertion of a proline residue (Nadon *et al.*, 1990; Boison and Stoffel, 1989) (see below). The abnormal proteins may not be transported from the rough endoplasmic reticulum to the Golgi or if they are transported it is in an abnormal fashion resulting in their accumulation within the lumen or on the external luminal surface of the rough endoplasmic reticulum. In *jp*, distension of the rough endoplasmic reticulum does not occur. Immunocytochemical labelling of PLP in the rough endoplasmic reticulum, but not the Golgi apparatus

(Roussel *et al.*, 1987) of oligodendrocytes, suggests that PLP transport from rough endoplasmic reticulum to Golgi is blocked. In *jp* this protein may be so abnormal that it is rapidly degraded and hence distension of the rough endoplasmic reticulum does not occur.

c) Molecular genetics of the PLP mutations

The PLP protein has demonstrated to be intolerant to structural changes. Some of the described PLP mutations involve a proline introduction in the primary structure which is known to markedly affect protein structure (Hogan and Greenfield, 1984) (figure 5.e). However, other more conservative changes in the hydrophilic domains of the protein also provoke similar phenotypes, thus this demonstrates that it is not a proline phenomenon. Newly substituted residues may interfere with the pairing of hydrophobic regions, possibly in the formation of a functional oligomeric structure, thereby disrupting the normal folding of the molecule and subsequent transport to the sites of myelin assembly (Hudson, 1990a). The unusually high conservation of the PLP protein (100% between mouse, rat (Milner *et al.*, 1985) and human (Diehl *et al.*, 1986)) suggests multiple protein-protein interaction which do not take place in most PLP mutants (Schneider *et al.*, 1992).

4. AIM OF THE STUDY OF THE *jp^{rsh}* MUTATION

Previously-described mutations involving the PLP gene are lethal (Nave and Milner, 1989). The phenotype of these mutants includes degeneration and premature death of oligodendrocytes with associated hypomyelination. However, the recent discovery of *jp^{rsh}* reopened the discussion for the direct involvement of PLP mutations in the early death of these mutants. Even though *jp^{rsh}* is myelin-deficient it has normal longevity and a full complement of morphologically normal oligodendrocytes. Hypomyelination can thus be genetically separated from the PLP-dependent oligodendrocytic degeneration. Study of the *jp^{rsh}* mutation should hopefully contribute to our understanding of the complex role of proteolipid proteins, particularly DM-20 which is relatively abundant in *jp^{rsh}* CNS.

CHAPTER 2: MATERIALS AND METHODS

A. FIXATION

1. FIXATIVES

a) Paraformaldehyde (4%)

This fixative was used for tissues destined for *in situ* hybridization and immunocytochemistry on paraffin-embedded tissue sections. Each mouse required approximately 200 ml.

For 500 ml of fixative:

Add 20 g of paraformaldehyde to 500 ml of 0.1 M phosphate buffer.
Heat solution to 70° C;
Add 1 M NaOH until solution clears;
Cool solution to 4° C.

b) Karnovsky's modified fixative (Paraformaldehyde/Glutaraldehyde 2%/5%)

This fixative was used for tissues destined for light and electron microscopy as well as for immunocytochemistry on resin-embedded sections. The total volume required was calculated as before.

For 500 ml of fixative:

Prepare an 8% paraformaldehyde solution in ddH_2O as above;
(20 g of paraformaldehyde to 250 ml ddH_2O);
Add 100 ml of 25% glutaraldehyde;
Make up to 500 ml with 0.08 M caccodylate buffer;
Add 250 mg of $CaCl_2$;
Filter solution in a fume cupboard;
Adjust final pH to 7.2.

2. TECHNIQUES

a) Intra-cardiac perfusions.

(1) Technique

All perfusions took place in a fume cupboard.

Mice were killed by an overdose of halothane anaesthetic and immediately after death were pinned out in dorsal recumbency over a piece of cork, the skin of the thorax was removed; the sternum cut and the heart exposed. The perfusion was initiated through the left ventricle using a 21 x 1 or 25 x 5/8 gauge needle after a small cut had been made in the right atrium. The initial perfusate was 0.85% NaCl until most of the blood was flushed from the body (60 ml approximately), when it was changed to fixative. After the injection of about 60 ml, given over a period of

approximately 3 min, the degree of fixation was assessed by the rigidity of the animal. Some animals required up to 300 ml to achieve a good tissue fixation.

Fixed mice were kept in a moisturized container until the tissue dissection. After 1 hr at 4° C the desired tissue was removed and stored in the appropriate fixative.

(2) Dissection and storage of the samples

Microsurgical instruments and a low power microscope were used for the procedure.

The skin of the head and back was cut and the muscles were dissected longitudinally until the exposure of the skull and the spine. The removal of the bone started at the rostral end and continued with forceps until the brain and cerebellum were exposed. The vertebral arches were individually separated from the spine; the meninges and nerve roots were cut and spinal cord was then lifted from the canal by pulling from the caudal end. The brain and cerebellum were liberated from the skull by sectioning all the cranial nerves except the optic nerves, which were sectioned only for samples to be resin-embedded. Samples were stored at 4° C in universals with the same fixative used for the perfusion.

b) Tissue culture fixation.

Tissue culture coverslips were fixed by immersion in either 4% paraformaldehyde (cells destined for *in situ* hybridization), or methanol at -20° C (fixation and permeabilization for internal antigen staining) for 10 min.

B. PROCESSING OF THE TISSUE SPECIMENS

1. PARAFFIN ROUTINE PROCESSING

The following procedure is for processing tissue for embedding in paraffin wax:

Large tissue blocks (whole brains and, at least, 1 cm of length for the spinal cord) obtained from the perfused mice were placed in processing biopsy cassettes which were loaded in a basket of the *Shandon Elliot* automatic tissue processor (Histokinette) and processed through the following dehydrating solutions:

70% methylated spirit for 2 hr;
70% methylated spirit/5% phenol for hr;
90% methylated spirit/5% phenol for 2 hr;
Methylated spirit 2 hr;
Ethanol & 5% phenol for 1 hr;
1% celloidin in methyl benzoate for 4 hr;
3 x 1 hr Xylene;
Paraffin wax for 4 to 6 hr;
Tissues were blocked out in 60° C fresh paraffin wax.

NB: Celloidin was obtained from Merk "Necoloidine" (R) as a 8% solution, treated as a 100% solution when made up with methyl benzoate.

2. RESIN ROUTINE PROCESSING

The following procedure is for processing tissue for embedding in Araldite resin:

(Day 1)

Samples were placed inside glass bottles that fitted on a Taab rotator (2 rpm.) inside a fume cupboard and were rinsed with isotonic caccodylate buffer for 10-20 min.

The buffer was then replaced for a 1% osmium tetroxide in 0.1 M caccodylate buffer solution or 1% osmium tetroxide/1.5% potassium ferricyanide in 0.1 M caccodylate buffer (modified Karnovsky's fixation for myelin studies (Langford and Coggeshall, 1980)) for 2 hr and washed in the same buffer for 1 hr.

The tissue was dehydrated for 15 minutes in each of the following alcohols of increasing concentrations: 50%, 70%, 80% and 90% and rinsed twice in 100% ethanol for 20 min each.

The tissue samples were immersed twice in propylene oxide (1,2-epoxypropane) for 15 min and left overnight in the rotors immersed a 1:1 mixture of propylene oxide and resin mix.

(Day 2)

The 1:1 mixture of propylene oxide and resin was substituted for a 1:3 mixture of propylene oxide and resin and was left for 24 hr.

(Day 3)

The tops of the bijoux were removed to allow the propylene oxide to evaporate for 3 to 5 hr.

Processed samples were then embedded in rubber moulds filled with resin mix and were left to polymerize in a 60° C oven overnight.

NB: Resin composition: 30 g Araldite CY212 (resin), 25.2 g of D.D.S.A. (dodecenyl succinic anhydride) (hardener), 1.2 ml of D.M.P. 30 (2,4,6-tri-dimethylaminomethyl-phenol) (accelerator) and 1 ml of Di-butyl phthalate (plasticizer).

3. SECTIONS

a) Paraffin-embedded tissue sections

Paraffin-embedded tissue sections varied from 5 to 6 μm thick. The sections for immunocytochemistry were placed on Poly-L-lysine coated slides and then left overnight in a 60°C oven.

b) Resin sections

The resin blocks were loaded on a Reichert-Jung Ultracut E ultratome and cut at two different thickness 1 μm (thick sections) for light microscopy and 70 nm (ultra-thin sections) for electron microscopy (see below). The 1 μm sections were placed on either plain or gelatine coated slides (see section J.).

c) Ultra-thin sections

70 nm sections were cut with a diamond knife and mounted on 200 mesh-3.06 mm diameter copper grids. Occasionally, small sections were mounted on 50 or 100 mesh copper grids coated with 0.6% parlodion made up in amyl acetate.

4. STAINING TECHNIQUES

a) Light microscopy

(1) Haematoxylin and eosin stain for paraffin sections

The slides were dipped in fresh water; transferred to Mayer's haematoxylin for 30 sec; washed gently in running tap water for 2 min; transferred to Scott's tap water for 15 sec and washed in running tap water for 2 min.

The slides were counterstained by immersion in methylated spirits for 10 sec and then in a saturated alcoholic eosin solution for 25 sec.

The sections were dehydrated through methylated spirits and 2 x absolute ethanol, and then cleared in 2 x Xylene before mounting in DPX mountant.

NB: Mayer's haematoxylin was made up as follows: 1.0 g haematoxylin, 50.0 g potassium alum, and 0.2 g sodium iodate in 1 litre of water, brought to boiling point and left overnight before adding 1.0 g citric acid and 50.0 g chloral hydrate.

Scott's tap water substitute: 3.5 g sodium bicarbonate and 20.0 g magnesium sulphate in 1 litre of water.

(2) Methylene blue/azure II for resin sections

Methylene blue/azure II= 1.0% methylene blue, 1.0% azure II, 1.0% borax in distilled water.

The slides were placed on a 60°C hot plate flooded with stain for 10-30 sec and rinsed in running tap water.

b) Electron microscopy

Ultra-thin sections were stained by covering the grids with a saturated solution of uranyl acetate in 50% ethanol for 5 to 15 min at room temperature. The grids were then rinsed in 50% and 75% ethanol; twice in distilled water and air-dried.

Subsequently the grids were stained with Reynold's lead citrate for 5-10 min inside a NaOH moisturised chamber and washed in 1 M NaOH solution x 3 and in ddH_2O x 5.

NB: Reynold's lead citrate: 1.33 g $Pb(NO_3)_2$ (lead nitrate), 1.76 g $Na_3(C_6H_5O_7)_2H_2O$ (sodium citrate) each dissolved in 15 ml H_2O; mixed together and shaken vigorously for 1 min and then occasionally over a 30 min period. 8.0 ml 1.0 M NaOH was added to clear the solution and the volume made up to 50 ml with water; final pH 12.

C. MORPHOLOGICAL STUDIES

1. QUANTIFICATION OF GLIA AND CELL COUNTS

Quantification of glia and cell counts were performed on 1 μm Araldite sections of tissue post-fixed in osmic acid and stained with methylene blue/azure II. The area selected in the spinal cord was immediately adjacent to the ventromedian fissure and its continuation onto the ventral surface of the cord. With the aid of an eyepiece graticule and using a x 100 oil immersion objective, six fields were examined in each transverse section (three each side of the ventromedian fissure) and the glial nuclei counted. Endothelial nuclei were not counted. Whole sections of the mid-position optic nerve sections were counted because of the smaller size. A further section cut at least 10 μm from the first was treated in a similar manner for both spinal cord and optic nerve. Cells were categorized using their morphological characteristics (see chapter 1).

The diameter of glial cell nuclei was measured in longitudinal sections of the caudal segments of cervical cord using a calibrated eyepiece. The mean length of 50 nuclei (oligodendrocytes and astrocytes) was calculated.

Using a digitizer pad, Apple II computer and a computer pen, the areas of the optic nerve and spinal cord on light microscopy negatives were calculated and then incorporated in the correction of the total glial cell count using Abercrombie's formula as discussed by Sturrock (Sturrock, 1983).

2. MORPHOMETRIC STUDIES

Random fields of 70 nm sections of spinal cord and optic nerve post fixed in osmium ferricyanide, embedded in Araldite, placed onto parlodion-coated grids and double stained by lead citrate and uranyl acetate were photographed at an initial magnification of approximately 5000 for adult spinal cords and 7500 for optic nerves and young spinal cords and printed at approximately two times magnification. Calibration was achieved using a diffraction grating (2160 lines per mm) which was photographed and printed for each cord and optic nerve sample.

Fibres were classified as myelinated (when some turns of compacted myelin were present), ensheathed (when an uncompacted oligodendrocytic process surrounded the axon) or unmyelinated (naked fibres).

Using a digitizer pad, Apple II computer and a computer pen, 100 to 250 fibres were analysed by tracing around the axolemma and where appropriate the outer edge of the myelin sheath so allowing calculation of axonal and total area.

From this data the diameters of circles with equivalent areas were calculated allowing myelin thickness and *g* ratio to be derived: *g* is defined as the ratio of axon

diameter to that of the axon plus myelin sheath; an increased *g* ratio indicates that the sheath is disproportionately thin for the axonal size).

3. MYELIN DENSITY

These measurements were performed over the previously described electron-micrographs using the point counting method described by Williams (Williams, 1977).

Two different transparent ruled squares were used for this purpose due to the two different magnifications and axonal diameters. Areas of 2 and 5 cm^2 areas were chosen for the spinal cord and optic nerve electronmicrographs respectively. The total volume of myelin and cell cytoplasm was calculated by counting the number of intercepts (16 possible for the spinal cord and 36 for the optic nerve) making contact with the myelin or cell cytoplasm in each micrograph. Results are expressed as the ratio of actual contacts to possible contacts.

STATISTICAL METHODS:

Three animals of each type were analysed for all the studies unless otherwise stated. The *t* test (student *t* distribution) was applied and a *q* value of 0.995 was chosen.

D. IMMUNOCYTOCHEMISTRY

1. PEROXIDASE-ANTI-PEROXIDASE (PAP)

(Day 1)

Paraffin-embedded tissue sections:

Section were hydrated as follows:

Xylene 2 min;
Absolute alcohol 2 min;
Methylene 2 min;
Water 2 min;
Iodine 1 min;
Water 2 min;
5 % Sodium Thiosulphate 1 min;
Water 2 min.

Resin-embedded tissue sections:

The resin of the sections was removed by submerging the slides in sodium ethoxide solution using a basket rotor. After 30 min the removal was checked microscopically; the slides were washed 6 times in absolute alcohol and submerged in running water for 30 min.

The endogenous peroxidase activity of the tissue was then blocked by immersing the slides in a 3% hydrogen peroxide solution for 30 min (made up in absolute alcohol for the paraffin sections and in water for the plastic sections). The sections were washed in running water for 30 min

Non-specific binding sites were blocked with a 1:10 normal goat serum/PBS solution for 2 hr. The normal goat serum was then tapped off but the slides were not rinsed.

The sections were incubated at 4^{o} C with the primary antibody solution (made up in 1% normal goat serum/PBS) inside a moisture chamber overnight (antibody sources and dilutions see Table 6). The control sections had normal mouse or normal rabbit serum applied at the same dilutions as the control sections.

(Day 2)

The sections were allowed to warm to room temperature for over a 30 minute period.

The slides were then washed 6 times with PBS and the excess of liquid from around the specimen was wiped off. The link (secondary) antiserum was diluted to 1:10 with 1% normal goat serum/PBS was added to the sections and incubated for 1 hr.

The slides were then washed 6 times with PBS and the excess liquid was removed from around the specimen.

The sections were covered with PAP complex diluted with 1% normal goat serum/PBS for 30 min. The mouse complex was diluted 1:1000 and the rabbit complex 1:40.

The slides were washed with 6 changes of PBS and then with 0.2 M phosphate buffer (pH 7.3) for 2 min and then transferred for 20 min to filtered solution of 50 mg 3,4,3',4',-tetramino-biphenyl hydrochloride (DAB) in 50 ml distilled water which was then made up to 100 ml with the 0.1 M phosphate buffer.

330 μl of 30% aqueous hydrogen peroxide was added to the DAB solution and the colour allowed to develop for 5 min.

The sections were then washed in 0.2 M phosphate buffer for 2 min and running water for 5 min.

The sections were counterstained and mounted as follows.

Paraffin sections:

Haemalum 30 sec; running water 2 min and Scotts water 15 sec.

Sections were then dehydrated, cleared and mounted in DPX.

Resin sections:

1% osmium/caccodylate buffer 2 min and running water 15 min.

Sections were then cleared and mounted in DPX.

NB: Sodium ethoxide solution was made up from a 50% ripened sodium ethoxide solution in absolute alcohol. All incubations are carried out at room temperature in a moisture chamber unless otherwise indicated.

2. IMMUNOFLUORESCENCE

Immunofluorescence was performed only on cells cultured on coverslips.

40 μl of the primary antibodies diluted to the appropriate concentration in buffered staining solution (see below) were applied over the coverslips and incubated for 20 min (antibody sources and dilutions see Table 7).

The coverslips were then washed three times with staining solution before 40 μl of the secondary antibody were added and also incubated for 20 min.

The coverslips were washed three times with staining solution.

Cell permeabilization and internal immunostaining:

Cytoplasmic markers (MBP, PLP/DM-20, PLP and GFAP) required permeabilized cells prior to immunostaining. The cultures were permeabilized with methanol at -20^{o} C for 10 min.

The coverslips were washed with fresh staining solution and had the second primary antibody applied for the cytoplasmic antigen for 20 min. After incubation the cells were washed three times as before and 40 μl of the secondary antibody was

added for another 20 min before they were washed three times with staining solution and placed back onto the staining trays ready to be fixed.

NB: The coverslips where kept covered in fluid continuously. Buffered staining solution contained: 4% donor calf serum, 0.05% azide in HEPES buffer made up in Hanks buffered salt solution, Ca^{++} and Mg^{++} free (HBSS). All antibodies were diluted in this staining solution. All incubations were carried out at room temperature on closed staining trays.

Fixation:

Cells were fixed in cold methanol at -20° C for 10 min.

The coverslips were washed in ddH_2O; dried on a tissue; had their back cleaned; mounted in Cytifluor and were sealed with glyceel.

The slides were stored at 4° C.

NB: Cytifluor (glycerol/PBS mounting media containing an antifade agent).

E. *IN SITU* HYBRIDIZATION

1. PROBE DESCRIPTION

An ^{35}S-labelled cRNA probe for PLP (PLP1) which recognised the majority of the coding region and part of the 5' non-coding region (nucleotide 48-Bam-H1 site up to the Pst-1 site at nucleotide 867) was transcribed. The probe was made by Ms K. McPhilemy, Dr. L. Mitchell and Dr. C. Thomsom.

2. TECHNIQUE

The basic procedure was as described by Cox *et al.* (Cox *et al.*, 1984) and modified by Wilkinson *et al.* (Wilkinson *et al.*, 1987).

The *in situ* hybridization was performed on 6 μm paraffin-embedded tissue sections as well as on 4% paraformaldehyde-fixed oligodendrocyte cultures from wild type and *jp^{rsh}* mice at different ages.

The schedule for *in situ* hybridization has three phases. The first is a pre-treatment that renders the target (mRNA) accessible to the probe which preserving the morphology of the tissue. This stage included a proteinase K treatment of the sections and also an acetylation stage (Hayashi, 1978) aimed at decreasing non-specific binding by blocking basic groups of the proteins. The second phase is the hybridization of the riboprobe (0.1 ng/μl/kb) to the cellular mRNA which is performed under low stringency conditions that favour nucleic acid hybrid formation. The third phase consists of washing to remove unbound probe and produce an acceptable background. The sections are also treated with RNase to remove non-base-paired RNA from the tissue.

The technique was performed as follows:

(Day 1)

a) Tissue preparation

The sections were transferred through the following spirits and solutions:

Xylene for 10 min (paraffin-embedded sections only);
100% Ethanol for 5 min (paraffin-embedded sections only);
Methylated spirit for 5 min (paraffin-embedded sections only);
Saline for 5 min;
PBS for 5 min;
Fix with 4% paraformaldehyde for 20 min;
Fresh PBS for 5 min x 2.

b) Permeabilization

The sections were covered with freshly made proteinase K for 7 1/2 min at room temperature; then washed in PBS for 5 min and the proteinase K was inactivated by fixation in 4% paraformaldehyde for 5 min.

c) Prehybridization

The slide rack was taken to a fume cupboard were the sections were washed in a 11.1% triethanolamine solution for 10 min where 625 μl acetic anhydride were added twice (the second dose of 625 μl of acetic anhydride added 5 min after the initiation of the wash).

The slides were then transferred to PBS for 5 min; saline for 5 min; methylated spirit for 5 min; 100% ethanol for 5 min x 2 and were air dried at room temperature for 1 hr.

d) Hybridization

The total volume of the probe was calculated (brain sections x 6 μl; spinal cord sections x 3 μl) and adequately diluted with hybridization buffer (approximately 1:10 depending on the probe activity) having a 1:100 concentration of RNase free dithiothreitol (DTT) added to each vial. The vials had their lids perforated with a needle; were transferred to a 80°C water bath for 2 min and were cooled down on ice immediately after.

The probe was then applied to the sections and covered with a silicone-treated coverslip. The slides were placed horizontally inside a slide holding box which was sealed with tape, placed inside three vacuum sealed bags; immersed in a 50° C preheated water bath and left to hybridize at 50° C overnight.

NB: To produce an ideal moisturized environment for hybridization a tissue soaked in 2.5 ml formamide and 1.25 ml 20 x SSC in 1.25 ml ddH2O was placed inside the slide box.

(Day 2)

e) Post hybridization treatments

Solutions W1, W2, W3, W4 and W5 were degassed and preheated (see temperatures below) for at least 30 min.

Plastic bags were cut; the slide box opened and the slides were transferred through to the following washes:

W1 solution at 50° C for 30 min;
W2 at 65° C for 20 min;
W3 at 37° C for 10 min x 3;
Treat with 0.02 mg/ml RNase at 37° C for 30 min;
W3 at 37° C for 15 min;
W2 at 65° C for 20 min;
W4 at room temperature for 15 min;
W5 at room temperature for 15 min.

The sections were dehydrated through these solutions:

D1: 75 ml ethanol, 162.5 ml water, 12.5 ml 6 M ammonium acetate for 1 min;
D2: 150 ml ethanol, 87.5 ml water, 12.5 ml 6 M ammonium acetate for 1 min;

D3: 200 ml ethanol, 37.5 ml water, 12.5 ml 6 M ammonium acetate for 1 min;
D4: 237.5 ml ethanol, 12.5 ml 6 M ammonium acetate for 1 min; 100% ethanol for 2 min x 2.

Sections were then air dried at room temperature for at least 1 hr.

f) X Ray

The slides were exposed against Cronex (Dupont) medical screen radiograph film inside a radiographic cassette at room temperature overnight and developed as a normal X-ray-film. Image intensities on the developed films determined the length of exposure of the slides after dipping in the autoradiographic emulsion.

g) Solutions

(1) DEPC treated water

(Use ddH_2O)

1% DEPC of a 10% solution in ethanol at room temperature for 10 min. Autoclave and check smell (If DEPC is present heat at 90° C water bath until no smell).

(2) Proteinase K

(Use DEPC water)
0.002% proteinase K;
0.05 M TRIS-HCl; pH 7.6;
0.005 M EDTA.

(3) Dithiothreitol (DTT)

Prepare solution 1 M in DEPC water;
Do not autoclave.

(4) Hybridization mix

50% Formamide;
10% Dextran sulphate (50% solution);
20 mM TRIS-HCl, pH 8.0 (1 M solution);
0.3 M NaCl (5 M solution);
5 mM EDTA (0.1 M solution);
10 mM NaH_2PO_4, pH 8.0 (0.1 M solution);
0.5 mg/ml yeast tRNA (10 mg/ml);
Store at -20°C.
(Stock concentrations in brackets.)

(5) 20x Standard Sodium Citrate (20x SSC)

3 M NaCl;
0.3 M Trisodium Citrate;

(6) Wash Solutions

(a) Wash 1 (W1)

625 ml 20 x SSC;
185 ml dH_2O;
2.5 ml DTT just before use.

(b) Wash 2 (W2)

4 ml 20 x SSC;
12 ml dH_2O;
20 ml formamide;
8 ml DTT add just before use.

(c) Wash 3 (W3)

0.5 M NaCl;
10 mM TRIS-HCl, pH 7.5;
5 mM EDTA.

(d) Wash 4 (W4)

50 ml 20 x SSC;
450 ml dH_2O.

(e) Wash 5 (W5)

25 ml 20 x SSC;
475 ml dH_2O.

h) Glassware treatment

Soak in 6.0% sulphuric acid; 6.0% potassium dichromate solution overnight. Rinse for 2-4 hr in running tap water; then in deionised water 9 times and once in 0.01% DEPC water. Shake dry and wrap in aluminium foil. Bake in sterilising oven 180° C for 4 hr.

The slides were coated with Poly-L-lysine as for morphological studies but RNase-free slides were used as well as DEPC-treated water (see X.A.). The coverslips were siliconised to decrease probe binding. These were soaked in 1 M HCl for 30 min; washed in ddH_2O x 3 and air dried; siliconised by immersion in Repelcot(TM) for 20 min; rinsed in ddH2O and baked at 130° C for 90 min.

3. QUANTIFICATION OF AUTORADIOGRAMS

The average signal per cell was compared in enzymaticaly dissociated cells allowed to adhere to coverslips for 2 hr. Cells from both groups were processed in parallel to allow direct comparison. Following hybridization and development of the autoradiograms the integrated optical density of the signal from 150 cells of each group was measured using a Quantimet 970 (Cambridge Instruments) with a measuring frame to include the oligodendrocyte cell body area. The optical density of the background of a the same coverslip was subtracted from the antisense signal. The mean values were compared by grouped t test.

F. AUTORADIOGRAPHY

1. METHOD

a) Slide Dipping

Clean, dry slides were dipped a solution of Ilford emulsion K5 for [^{35}S] or K2 for [^{3}H] mixed in a 1:1 ratio with ddH2O containing 1.0% glycerol to provide a thin layer over the specimen. The emulsion was maintained at 42^{o} C in a water bath. After dipping, the slides had their backs cleaned and were air-dried in a plastic box together with silica gel for 4 to 6 hr. They were then stored in tape-sealed light-tight boxes containing a sachet of silica gel inside a black plastic bag, at 4^{o} C for the required exposure time as determined by the test exposure against the radiographic film (time could vary between 4 to 30 days depending in the isotope and emulsion used).

b) Developing

The autoradiograms were developed under safe light conditions by immersion in undiluted Kodak D 19 developer at 18^{o} C for 4 min. The action of the developer was stopped by immersing for 1 min in a 1% acetic acid/1% glycerol solution in water. The slides were fixed for 3 min in 30% sodium thiosulphate solution and then washed in water for 20-30 min in the dark before air drying.

c) Haematoxylin Counterstain

Autoradiographs were counterstained as follows:

ddH_2O for 2 min;
Haematoxylin for 30 sec;
ddH_2O for 2 min;
Scots water for 15 sec;
Dehydration and mount.

2. CELL COUNTS

The cell counts were performed on haematoxylin-counterstained autoradiograms. Up to 4 spinal cord sections were counted, 1 to 6 fields per section. One to 3 transverse sections of optic nerves were counted. The cells were then allocated as positive or negative depending on the degree of silver grains accumulation over the nucleus related to the background. The total glial cell count was corrected using Abercrombie's formula as described section C.1. of this chapter.

G. CELL CULTURE

1. TISSUE PREPARATION

a) Optic nerve dissection

About 10 to 20 mice were killed by an overdose with halothane in a closed chamber. The animals were sprayed with alcohol and decapitated. The skin of the head was removed; the skull cut and the brain exposed. This structure was then pulled backwards very slowly detaching the optic chiasm. Two small incisions were performed behind each eye ball releasing the optic nerves which were transferred to a 6 cm petri dish containing 6 ml of sterile HBSS (Ca^{++} and Mg^{++} free).

The connective tissue and the optic chiasm were removed from the optic nerve under a dissecting microscope, the nerves were immediately transferred to a fresh HBSS-filled petri dish which was removed to a laminar FLOW hood.

b) Spinal Cord Dissection

The skin and muscles from the neck and back were dissected and the dorsal arches of the cervical vertebrae removed to expose the cervical area of the spinal cord.

The meninges and dorsal columns of the spinal cord were cut longitudinally using a pair of sharp sterile forceps exposing the ventral columns which were then dissected free and placed in a sterile petri dish containing 6 ml of HBSS.

Under a dissecting microscope the grey matter was removed and the meningeal membranes were pulled out together with the ventral nerve roots. The clean tissue was immediately transferred to a fresh HBSS-filled petri dish inside a laminar FLOW hood.

c) Cell dissociation

The dissected tissue was collected on the inside of the lids of the petri dishes and minced with a scalpel blade (No. 10) and then transferred into a sterile centrifuge tube by adding and sucking back the 600 μl collagenase solution. This was incubated at 37° C for 30-45 min.

The tube was centrifuged at 1000 rpm. for 3 min and the supernatant was removed. 1 ml of 0.05% trypsin/0.02% EDTA solution was then added to the pellet and incubated at 37° C for 30 min after which 1 ml SD solution was added for 2 min to stop the enzymatic activity and prevent tissue clumping. The suspension was then centrifuged at 1000 rpm for 3 min and the supernatant removed.

The tissue was triturated in warm HBSS through needles of different gauges (21x1, 23x5/8, 25x5/8 and finally 27x1/2). The cell suspension was then centrifuged

at 1000 rpm for 10 min and resuspended in 200 μl of 50% HBSS, 50% Sato/0.1% FCS medium.

The cell density was calculated using a regular Levy counting chamber with a Neubauer ruling by counting the four large ruled squares in the corners (1 mm^2 = 16 squares) and the cell numbers were adjusted to 400.000-500.000 cells/ml with the same solution.

d) Plating

The cells were plated at 8.000-15.000 cells/coverslips (20 μl drops of the above cell suspension) onto 13 mm warm Poly-L-lysine-coated coverslips placed inside FLOW 24 well plates.

The culture plates were placed in the incubator at 37°C 5%, CO_2 until cells had attached (10 to 30 min).

The cultures were fed with 600 μl of Sato/0.1% heat inactivated FCS media.

The culture medium was changed after 24 hr to eliminate myelin and cell debris if this was present.

e) Culture conditions

The cultures were maintained at 37°C and 5% CO_2 in Sato/0.1% heat inactivated FCS media until immunofluorescence was performed.

2. SOLUTIONS

a) Hanks Balanced Salt Solution (HBSS)

Ca^{++} and Mg^{++} free solution.

(FLOW laboratories or SIGMA.)

b) Collagenase

50mg/ml stock solution of approximately 200 unit/mg collagenase (COUPER BIOMEDICAL) in HBSS (Ca^{++} and Mg^{++} free);

200 μl aliquotes were stored at -20° C and diluted 1:3 in L15 or HBSS (Ca^{++} and Mg^{++} free) for use.

c) Trypsin/EDTA

0.1% trypsin (FLOW laboratories) solution in HBSS (Ca^{++} and Mg^{++} free) in 0.5 ml aliquotes stored at -20° C.

0.04% dilution of EDTA (FLOW laboratories) in HBSS (Ca^{++} and Mg^{++} free).

A 1:1 mixture of both solutions was used.

d) SD Solution

0.52 mg/ml soybean trypsin inhibitor (SD);
0.04 mg/ml bovine pancreas DNase;
3mg/ml of factor V bovine serum albumin;
Made up in HBSS (Ca^{++} and Mg^{++} free) or L15.
1 ml aliquotes of SD solution were stored at -20° C until usage.

e) SATO media

Glucose 1 g/l;
Glutamine 2 mM;
Insulin (bovine) 10 μm/ml;
Transferrin (human) 100 μm/ml;
BSA-pathocyte 0.0286%;
Progesterone 0.2 μM;
Putrescine 0.1 μM;
Thyroxine 0.45 μM;
Selenite 0.224 μM;
Tri-iodo-thyronine 0.5 μM;
Made up in DMEM.
30 and 200 ml aliquotes were stored at -20° C.

NB: All these solutions used for the cell dissociation, plating and feeding are pre-warmed to 37°C before use.

3. CELL COUNTS IN CULTURE

Performed using a x50 oil objective for 2 hr cultures and at x40 for all the other cultures.

100 "healthy-looking" labelled cells (those that generally showed a bright even distribution of the immunofluorescent label as well as no signs of cell disintegration like the detachment of the cell processes from the cell body) were counted starting from a random field and scanning horizontally from that point.

The percentage of O4+ cells was taken as a 100%. The percentage of GalC+ cells of the O4+ was used to obtain the rest of the cell percentages. Therefore, cell percentages are expressed as the percentage of the O4+ population.

H. CELL MITOSIS STUDY

1. MATERIALS AND METHODS

a) Isotope preparation

The isotope was obtained from AMERSHAM as a 1.0 μCi/ml aqueous solution containing 2% ethanol of [methyl-^{3}H] thymidine (9.25 megaBq.).

In order to reduce the volumes to be injected in the animals, the isotope was evaporated to dryness in a stream of nitrogen and reconstituted at a concentration of 5 μCi/μl in 0.85% sterile saline.

b) [methyl-^{3}H]-thymidine labelling

Mice were injected 5 μCi per gram of body weight at the above concentration intra-peritoneally. The number of injections varied depending on the expected cell division rate.

Animals up to 50 days-old were injected once; 50 days-old were injected twice and 100 day-old mice were injected three times respectively. Repeated injections were given at 2 hr intervals.

Perfusion of the animals with Karnovsky's modified fixative (Paraformaldehyde/Glutaraldehyde) was performed two hr after the last isotope injection.

c) Samples, sections and autoradiography

1 μm thick tissue sections of araldite resin-embedded spinal cord samples were cut and placed onto gelatin-coated slides (see section J.).

The sections had the resin removed (see section A.IV.) before proceeding with autoradiography (see section F) to improve the counterstaining.

I. BUFFERS

1. PHOSPHATE BUFFER

Approximately 80% of 0.2 M Na_2HPO_4 in dH_2O plus
approximately 20% of 0.2 M KH_2PO_4 in dH_2O added to achieve a pH of 7.4.
Dilute 1:1 with ddH_2O to give final 0.1 M buffer.

2. PHOSPHATE BUFFERED SALINE (PBS)

8.006. g NaCl;
0.2012 g KCl;
0.2042 g KH_2PO_4;
1.1356 g Na_2HPO_4.
Buffer solution to achieve pH 7.3 in 1 litre of ddH_2O.

3. CACCODYLATE BUFFERS

The different caccodylate solutions were buffered to pH 7.2 to 7.3 with HCl.
The following caccodylate buffer solutions were used:

For fixative solutions:

A 0.08 M sodium caccodylate made up in ddH_2O.

Isotonic caccodylate buffer for routine electron microscopy processing:

16.05 g sodium caccodylate;
3.8 g NaCl;
0.055 g $CaCl_2$;
0.102 g $MgCl_2$;
made up to 1 l with ddH_2O.

Electron microscopy caccodylate buffer for modified Karnovsky's processing:

0.1 M sodium caccodylate in ddH_2O.

J. SLIDE AND COVERSLIP COATING

1. POLY-L LYSINE

Poly-L-lysine slides were prepared by covering clean glass slides with 0.01% Poly-L-lysine in ddH_2O at room temperature for 10 min. The excess Poly-L-lysine was then removed and the slides air-dried; rinsed in ddH_2O and air-dried again. They were kept at -70° C if not used immediately.

Coverslips were coated by immersion in a 1% solution of Poly-L-lysine in sterile ddH_2O for over 40 min. The coverslips were then washed twice in sterile ddH_2O for 40 min each time, air dried and freezed until usage.

2. GELATIN COATED SLIDES (SUBBED)

The gelatin solution was freshly made up for every experiment. Cleaned slides were dipped into a 1/1 gelatin emulsion in 1% glycerol at 43° C for 2 min. The slides were then oven dried until the emulsion gelled.

NB: Gelatin composition: 5.0 g gelatin made up in a 1 of boiling ddH_2O. After cooling down, 0.5 g. Chrome alum ($K_2SO_4Cr_2(SO_4)_324H_2O$) were added and the solution was filtered.

CHAPTER 3: *jprsh* NEUROBIOLOGY

A. INTRODUCTION TO THE *jp^{rsh}* STUDY

1. OBJECTIVES OF THE STUDY OF THE MUTANT *jp^{rsh}*

The description of the *jp^{rsh}* mutation is presented in the following sections. Firstly, an outline of the general phenotypic characteristics of the mutation including clinical signs, age of development, breeding characteristics and weight gain and tremor development studies will be given. In the next three sections the morphology of *jp^{rsh}* will be defined starting with the description of the immunochemical and morphological features on tissue sections of the mutant CNS completing the study with the investigation of the PLP mRNA expression. Finally, the last two sections of this chapter are focused on the development of cultured mutant oligodendrocytes and the *in vivo* cell division. The final chapter of the study concentrates in the description of the heterozygous female.

2. HISTORY OF THE MUTATION

The spontaneous "rumpshaker" (*jp^{rsh}*) mutation was first identified at the MRC Radiobiology Unit in 1988 and donated to Glasgow University Veterinary School for further investigation. Initial studies identified a generalized tremor associated with hypomyelination in the CNS (Griffiths *et al.*, 1990) and an X-linked inheritance pattern suggesting possible involvement of the PLP gene. Recent studies have characterised the *jp^{rsh}* as a recessive point mutation of the PLP gene involving a single amino-acid substitution ($Ile^{186} \rightarrow Thr$) (Schneider *et al.*, 1992).

The first mutant animals, which were characterized by the tremor were detected among the progeny of a single pair mating in a small stock of mice housed at the MRC Radiobiology Unit. These mice were homozygous for Robertsonian translocation Rb(1.3) IBnr. Evidence that the condition was inherited was provided by preliminary crosses using a distantly-related Rb(1.3) IBnr stock. The mode of inheritance was determined by breeding studies using the shaking or tremor as the phenotypic expression of the mutation. Routine histological and immunocytochemical experiments revealed that the *jp^{rsh}* mutation affected PLP production (Griffiths *et al.*, 1990). The other CNS proteins including DM-20 which is another product of the PLP gene were either unaffected or involved to a much lesser degree. *jp^{rsh}* had phenotypic differences from other PLP mutants suggesting that it would provide a useful model to study the PLP gene, its products, regulatory mechanisms and functions.

3. PHENOTYPICAL DESCRIPTION OF THE MUTANT

a) Clinical signs

The *jp^{rsh}* mutation is phenotypically recessive, which means that homozygous females and hemizygous males show clinical signs. Affected mice, both males and females, develop a generalized tremor at about 10 to 15 days of age which is activated by movement and disappears at rest. The tremor reaches its peak of expression at around 25 to 30 days being then detectable in inactive mice. After this age, the tremor is confined to the rear end during ambulation, generally persisting throughout the life of some of the oldest mutant animals (1 year old.). Mice remain agile and can climb cage bars. Viability, fertility and weight gain appear normal (see below).

b) Breeding and litter number studies

Hemizygous *jp* male (*jp*/Y) mice are sterile but the *jp^{rsh}* mutant do not show any sign of altered reproduction. The litter sizes were calculated by counting the number of pups per mutant and control litters one or two days after birth. No significant differences were found in the distributions of the number of pups per litter. The results are shown in figure 6.

c) Weight studies

Weight gain is one of the parameters indicating the degree of physical development. It can be affected by the mutation either directly or indirectly as a result of a deficient milking or feeding consequent of the excessive tremor of the pups.

Over a period of one year, 400 to 500 wild type and *jp^{rsh}* mice from our colonies were randomly picked and weighed inside a closed chamber as they were anaesthetised prior to euthanasia. There were no significant differences in weight at different ages between *jp^{rsh}* and control mice (figure 7) in contrast to *jp* mice which were abnormally small on visual inspection.

d) Tremor studies

The beginning of the tremor and its later progression in life was closely followed during the development of 24 *jp^{rsh}* litters. Four different degrees of tremor

were recorded: grade "0" for mice not showing the *jp^{rsh}* phenotype; grade "1" for animals with a certain degree of stiffness in the walk and/or occasional mild tremor; grade "2" for mice which showed tremor activated by movement and disappearing at rest; and finally, grade "3" for those mutants that showed tremor at rest. The commonest age of onset, of a grade "1" or "2" tremor was, generally, around 15 days. By 22 days of age all the pups used for this study showed either grade "2" or "3" tremor. The peak of expression was about 25-30 days of age.

The onset and degree of tremor showed by mutant mice was correlated to the physical development of the pups; the more developed the pups, the greater the signs. Grade "3" tremor was present only in young and physically well-developed mice, generally from small litters, and would last for approximately a week to then become grade "2". All mice reached at least grade "2" tremor persisting for a variable length of time; weeks, months or as long as a year. Eventually, the clinical signs declined until the tremor could be observed only when activated by movement while disappearing at rest. Slight clinical signs persisted in adult mice. These signs were confined to the rear end and included an abnormal gait or straight tail carriage. No obvious differences were found in the timing or the degree of the tremor between hemizygous males and homozygous females.

B. HISTOCHEMISTRY IN *jp^{rsh}*

1. INTRODUCTION AND AIMS OF THE STUDY

In previous studies, immunostaining for myelin proteins in spinal cord sections of *jp^{rsh}* mice identified virtually no reaction for PLP in the myelin sheaths (Griffiths *et al.*, 1990). The reduced, but definite, immunostaining with antiserum recognizing both PLP and DM-20 indicated a disproportionate expression of the two proteins as previously described in the *sh pup* and *jp^{msd}* mutants (Yanagisawa *et al.*, 1987; Gardinier and Macklin, 1988).

Quantitative immunoblotting studies of the spinal cord of *jp^{rsh}* showed a markedly reduced intensity of the PLP band at 10 and 40 days while the intensity of the DM-20 band relative to PLP was proportionately greater in the mutant (Griffiths *et al.*, 1990); staining for all four MBP isoforms was also reduced (Griffiths *et al.*, 1990). Other X-linked mutations such as the *md rat* (Yanagisawa *et al.*, 1986) and *jp* mouse (Sorg *et al.*, 1987) with undetectable PLP and DM-20 by immunoblotting, also exhibit a marked reduction of the other major myelin proteins. Immunocytochemistry was used to evaluate both the overall myelin proteins in paraffin sections as well as the composition of individual myelin sheaths in resin sections, so evaluating the quantity and quality of the myelin sheath produced. The relationship between the absence of PLP and abnormalities of the myelin sheath such as defects in the IPL can be investigated.

2. MATERIALS AND METHODS

The PAP technique was chosen for the detection of protein in paraffin and resin-embedded tissue sections of the CNS. The paraffin-embedded sections were used to assess the overall protein present. The resin-embedded sections allowed the identification of individual sheaths. The ages of the mice, dissection and processing procedures as well as the antibodies used for all the following experiments are fully described in chapter 2 and table 6.

3. RESULTS

a) Myelin proteins in jp^{rsh}

Paraffin sections of brain, optic nerve and spinal cord, as well as selected resin-embedded areas of the spinal cord stained intensely for MBP although the overall intensity was less in *jp^{rsh}* than age-matched controls due to the reduced quantity of myelin (figures 8, 9). Immunostaining for GFAP indicated that the number of astrocytic processes and intensity of staining increased moderately with age in *jp^{rsh}* compared to age-matched wild type. Early studies of the mutant tissue reported that the overall reactivity for MAG was decreased presumably due to the number of non-myelinating fibres. Those fibres with myelin sheaths immunostained normally for MAG (Griffiths *et al.*, 1990).

In control wild type mice both antiserum recognizing PLP and DM-20 (anti-C terminal antibody) stained myelin intensely (figures 8 to 10). In contrast *jp^{rsh}* myelin showed a marked reduction of PLP (anti-PLP-specific antibody) staining whereas the intensity of staining for PLP and DM-20 was only moderately decreased. No reaction was present in paraffin-embedded sections from the spinal cords of 20 day-old mutant mice immunostained with the anti-PLP-specific antiserum, while the anti-C-terminal staining was reduced (Griffiths *et al.*, 1990). When optic nerve sections from mutant and control mice between the ages of 20 and 90 days were processed in parallel, PLP/DM-20 and PLP staining seemed to increase with age (figure 8, 9, 11) in the mutants but was always less than in the age-matched normal mice. PLP immunoreactivity on resin-embedded sections of the *jp^{rsh}* spinal cord also increased with age. However, the PLP positive immunoreactivity was frequently localized in clumps generally at the periphery of the smaller sheaths increasing with age when the antibody was applied at a 1:250 concentration or higher (figure 10).

b) Serial section immunostaining

Immunostaining of serial resin-sections of the spinal cord revealed two main types of fibres MBP+/PLP/DM-20+/PLP- and MBP+/PLP/DM-20-/PLP-, very occasional MBP+/PLP/DM-20+/PLP+ fibres were also seen, generally presenting a focal staining of the outer edge of the sheath (figure 10d,10e,12).

c) Peripheral myelin assessment

Serial paraffin-embedded sections of the brain and resin-embedded sections from the spinal cord of 1 year-old mutant mice were immunostained for P_0, a major PNS protein, to assess for any possible Schwann cell invasion of the *jp^{rsh}* mutant CNS. No evidence of peripheral myelin was found (figure 13).

4. DISCUSSION

Immunocytochemical studies in *jp^{rsh}* revealed reduced levels of PLP staining particularly in compact myelin, with a relatively normal intensity of presumed DM-20 protein; thus, the PLP/DM-20 protein ratio was inverted even after the period of active myelination (Mitchell *et al.*, 1990). (The presence of DM-20 can be inferred only by immunostaining by using the two antibodies described). Previous studies on this mutation demonstrated that MBP and MAG proteins were also moderately decreased with respect to the wild type mice (Griffiths *et al.*, 1990). This is also the case for *jp* mice, the *md rat* and the *sh pup* (Quarles, 1990). Occasional PLP positive clumps of immunostaining were detected in *jp^{rsh}* spinal cord tissue. However, as the anti-PLP specific antibody recognizes a part of the PLP protein which should not be mutated in *jp^{rsh}*, there is a possibility that the antigen was recognizing an abnormal or an immature form of the PLP protein unsuitable for incorporating into the myelin sheath and so accumulating in the oligodendrocyte cytoplasm which surrounded the axons. The staining for both PLP/DM-20 and PLP increased with age although never achieving the same levels as in age-matched normal mice. The increased intensity of the PLP/DM-20 immunostain could be a consequence of the increased myelination of this tissue (see next section for more detail).

The disproportionate DM-20 expression seen in *jp^{rsh}* has previously been reported in other hypomyelinating mutants carrying a point mutations of the PLP gene which cause single amino acid substitutions in both PLP and DM-20 such as the *sh pup* and *jp^{msd}* mouse (Nadon *et al.*, 1990; Gencic and Hudson, 1990; Macklin *et al.*, 1991; Gardinier and Macklin, 1988; Yanagisawa *et al.*, 1987). However, the fact that these mutants produce some DM-20 in their myelin does not imply that the elevated DM-20 levels are necessarily functionally active. Recent studies have revealed that the *jp^{rsh}* mutation is the result of a single amino acid substitution (Ile^{186} →Thr) included in a putative membrane-embedded domain of the PLP/DM-20 molecule (Schneider *et al.*, 1992). Yet, compared to the other PLP mutants major differences in oligodendrocyte survival and development occur. Mutants with defects in other major myelin protein genes like *shi* (MBP gene (Roach *et al.*, 1985)) or those

of an unidentified nature (but not involving the PLP gene) like *qk* (Friedrich, 1974; Fujita *et al.*, 1990) do not exhibit increased glial cell death (Friedrich, 1975), while all PLP mutations affecting DM-20 are believed to be associated with increased oligodendrocyte death (Nave and Milner, 1989; Duncan, 1990). Comparing oligodendrocyte survival in jp^{rsh} with that in *jp*, jp^{msd} or *sh pup* suggests that a product of the PLP gene has a critical function in these cells before myelin assembly; this function, lost in most myelin mutants but sufficiently preserved in jp^{rsh}, enables most oligodendrocytes to survive, differentiate and produce myelin. The early expression of DM-20 and its relative abundance in jp^{rsh} suggests it as a candidate for this role.

Histochemical studies correlating protein composition with morphological appearance of myelin sheaths revealed that some myelin could be assembled even in the absence of PLP. However, both types of immunocytochemically defined myelin sheaths detected in jp^{rsh} (MBP+/PLP/DM-20+/PLP- and MBP+/PLP/DM-20-/PLP-) presented ultrastructural abnormalities of the IPL which is consistent with the structural function of PLP. Spinal cord sections from older jp^{rsh} mutants demonstrated a higher immunoreactivity against PLP. This could be the consequence of a slow but progressive PLP accumulation and insertion in the membrane as jp^{rsh} mutants have been reported to produce some detectable PLP in western blots (Griffiths *et al.*, 1990).

The possible presence of myelin repair by Schwann cells, as described for older strains of the *sh pup* (Duncan, personal communication), was assessed in 1 year-old mutant mice by immunostaining for P_0, a major peripheral myelin protein. Results indicated that no Schwann cell invasion was present in old mutant spinal cords. Further morphological examination of the PNS/CNS transition area also supported these findings.

C. MORPHOLOGICAL STUDIES

1. INTRODUCTION AND AIMS

The description of the pathological changes resulting from a mutation is an important step to define the role of a particular gene in the normal animal. The aim in this section was the description of morphology in the mutant tissue and possible repair of the lesion in order to overcome the deficiency.

2. MATERIALS AND METHODS

The tissue was prepared as described in chapter 2. Briefly, mice were anaesthetised until overdose and fixed by intracardiac perfusion with normal saline followed by a modified Karnovsky's paraformaldehyde/glutaraldehyde (2%/5%) fixative. Tissue was post-fixed in either 1% osmic acid or an osmic acid/potassium ferricyanide mixture. The blocks for the study were removed from C1-C2 segments of the spinal cord and mid portion of the optic nerves. The morphological studies were performed following the methods described in chapter 2.

3. DISTRIBUTION AND DEVELOPMENT OF THE LESION

The ventral spinal cord and the mid-optic nerve were chosen as representative areas of the diversity of the CNS. Although hypomyelination of the CNS was generalised, the pathological abnormalities were most marked in the spinal cord. Other CNS locations, although affected, did not show such a remarkable pathology. No abnormalities were seen in the PNS (figure 13c).

4. DESCRIPTION OF THE LESIONS

Myelination in *jp^{rsh}* commenced at the correct time in all the CNS locations examined when compared to the wild type mice.

a) Spinal Cord

(1) LM features

Light microscopic examination of methylene blue/azure II-stained resin-embedded sections of the spinal cord of *jp^{rsh}* mice revealed a reduction in the amount of white matter area at all ages (figure 14). There were no other overt changes up to the age of 16 days, although a reduced myelin content was noted in quantification studies performed on 10 day-old *jp^{rsh}* (Griffiths *et al.*, 1990) (figures 15, 16, 17). A characteristic increase in numbers of all glial cell types, particularly those of the oligodendrocyte lineage, was observed at all ages. Cell counts in older mutants revealed that the oligodendrocyte population increased progressively in the spinal cord.

Recent observations of spinal cord sections at various ages before and after myelination revealed occasional dying cells. These resembled the cells described by Raff (Raff, 1992) (figure 3, 17) as suffering apoptosis (see discussion). However, despite the occasional cell death in younger mutants, *jp^{rsh}* presented adequate numbers of "metabolically active" oligodendrocytes at the time of myelination displaying a large, pale and evenly stained cytoplasm, numerous processes many of which actively ensheathed unmyelinated or poorly myelinated axons. Oligodendrocytes embracing single large axons in a "Schwann-cell-like" fashion were a frequent finding in younger mutants (figure 15, 16). Astrocytes and microglial cells did not exhibit any abnormal appearance at the light microscopic level.

A marked myelin deficiency was noted in the ventral columns from *jp^{rsh}*. In the white matter large areas of tissue devoid of myelin sheaths were common. With increasing age there was an increased myelin staining mostly involving axons of with small diameters (figures 18, 19). The dorsal columns of the spinal cord were also morphologically examined. Cells resembling oligodendrocytes were obviously increased in number as the seen for the ventral columns. Although no fibre morphometry of the area has been performed, light microscopy revealed a moderate increase in the total amount of myelin with age. Vacuolation of some of the sheaths was occasionally present (figure 20).

(2) EM features

Electron microscopy of the spinal cord tissue confirmed the light microscopic observations. Mutant oligodendrocytes contained abundant rough endoplasmic reticulum, numerous free ribosomes and Golgi apparatus at all ages (figure 21). In very occasional cells the cisternae of the rough endoplasmic reticulum, but not the perinuclear cisternae, were slightly distended and many of the free ribosomes were monosomes rather than polysomes. Although oligodendrocyte processes were frequent and prominent during myelination they were often located adjacent to naked axons but did not myelinate them. Many oligodendrocytes embraced axons in a 1:1

ratio but frequently produced no compact myelin. This was a common finding in spinal cord sections from younger mutants (figure 21). Occasional oligodendrocytes contained dense inclusions with lamellar profiles similar to those illustrated by Lassman and co-workers in degenerating optic nerve (Lassmann *et al.*, 1978). Dying cells were conspicuous in the samples examined from mutant and wild type mice.

An atypical cell, not present in wild type mice, was also occasionally observed in spinal cords from older mutants (and some heterozygote females). These cells resembled those described in the monkey developing cord (Phillips, 1973) termed "primitive oligoblast". They were generally rod shaped and smaller than more mature oligodendroblasts and exhibited no apparent processes. Their nuclei were rod shaped or oval with an evenly contoured outline and contained very few, if any, chromatin clumps. Definitive nucleoli were not distinguishable. The cytoplasm was sparse and contained short straight cisternae of the rough endoplasmic reticulum with contents that resembled the cytoplasmic matrix. Vesicles resembling smooth endoplasmic reticulum were present, occasionally elongating resembling the Golgi apparatus. Mitochondria were conspicuous. Microtubules or centrioles were not encountered (figures 22, 23). These cells were easily overlooked at light microscopy because of their small size and indistinctive staining.

Astrocytes were similar to those in wild-type mice. There appeared to be a minimal increase in astrocytic processes in older mice but this was not uniform and varied between mice and within a given region of the spinal cord. Astrocytic processes were occasionally observed inserted between myelin lamellae or between axon and sheath as described in other myelin mutants (Griffiths *et al.*, 1981; Rosenbluth, 1987).

Hypomyelination of the spinal cord was probably the most characteristic finding in *jp^{rsh}* and became more obvious after 30 days of age. The majority of axons were either naked or, more commonly, surrounded by a disproportionately thin myelin sheath which was often irregular in outline. Occasional well compacted small myelin sheaths were present (figure 21). In many sheaths, one or several turns of uncompacted processes were interposed between compacted lamellae. Excessively prominent inner tongues were a frequent finding in younger mice. Redundant folds of myelin sheath were more common than in normal mice. Late-appearing myelin sheaths surrounding smaller fibres present in the older mutant spinal cord showed a reasonably thickness for the axonal diameter (figure 24). Some microglia containing myelin debris or membranous inclusions, either lamellar bodies as described below in oligodendrocytes or more wispy membranes, could be seen in younger mutants. The lesion did not reflect active demyelination as myelin debris was a relatively uncommon finding.

Myelin sheaths from *jp^{rsh}* mice displayed abnormalities of the IPL which was either absent, split, vacuolated or indistinguishable from the MDL (figure 25). The periodicity of *jp^{rsh}* and wild type myelin sheaths of fibres with a similar axonal diameter was mostly similar or identical, although in a significant minority of sheaths it was difficult to identify the MDL and IPL as separate entities. In some of these the periodicity of the putative MDL was normal and in others the distance was reduced (figure 25). The vast majority of the axons in the mutant were normal although occasional axons filled with swollen organelles were observed. No abnormalities were observed in sciatic nerves and nerve roots (Griffiths *et al.*, 1990).

b) Optic nerve

(1) LM features

No conspicuous abnormalities were recognised by light microscopy on resin-embedded sections of the mutant optic nerves. Necrotic cells were not detected at any age. Optic nerves from older mutant mice were reduced in calibre when compared to age-matched controls (figure 26). Total myelin detected by methylene blue/azure II staining was decreased indicating a smaller amount of myelin, yet individual fibres could not be analysed as the fibre diameters in the optic nerve were too small to enable axonal identification. Occasionally vacuolated sheaths were observed in the younger mice.

(2) EM features

Ultrastructural changes in the mutant optic nerves were not conspicuous until about 30 days of age at which time wild type nerves exhibited a homogeneously myelinated appearance (figure 27). As myelination progressed, many variably sized patches of amyelinated axons were observed adjacent to sheaths of normal compaction. The severity of this abnormality varied between animals with some showing considerably more myelinated fibres than others. A patchy appearance of the lesion could be seen sometimes in 90 day-old mutant optic nerves (figure 28). Variation in the thickness of the myelin sheath relative to axonal size was common. Occasional sheaths exhibited disproportionately thick myelin sheaths (figure 28b)

Glial cells appeared morphologically normal and cell death was not observed at any age. Oligodendrocytes did not contain abnormal inclusions. Astrocytic processes were slightly more prominent in older mutants. Undifferentiated cells such as those seen in the spinal cord, were not detected. Occasional degenerating axons were also seen in older wild type or *jp^{rsh}* mice.

5. MORPHOMETRIC ANALYSIS AND GLIAL CELL QUANTIFICATION

a) Materials and methods

The morphometric analyses of the axon size, myelin sheath thickness, *g* ratio and myelin density were performed on electron-micrographs of the C2 spinal cord segment as described in chapter 2. Earlier investigations on *jp^{rsh}* demonstrated that the results from cervical and thoracic spinal cord were virtually identical (Griffiths *et al.*, 1990).

b) Spinal cord

(1) Quantification of glia

Glial cell density, total glial cell numbers, and oligodendrocyte numbers were elevated in *jp^{rsh}* white matter in respect to wild type at all ages (figures 29, 30). Total astrocyte numbers were increased up to the age of 45 to 50 days following which values were similar to controls. Astrocytes represented a much smaller percentage of the total glia in the white matter as a consequence of the increased oligodendrocyte population (figure 31). Slightly higher numbers of microglial cells were present in mutants older than 40 days. Visual inspection of 1 year-old mutant spinal cord also revealed numerous glial cell bodies most of which resembled oligodendrocytes (figure 19).

Spinal cords of wild type and *jp^{rsh}* mice showed very occasional dying or apoptotic cells (figure 3, 17). Although these cells have not been quantified yet, the live/dying ratio seemed identical for both types of mice. Gross cell counts revealed 1 or 2 versus 1 to 3 dying cells per whole spinal cord section of wild type and *jp^{rsh}* cervical white matter. Dead cells were observed in wild type spinal cords up to 30 days-old, whereas they were still detected at 45 days in *jp^{rsh}* white matter. These cells were not detected at 60 days in the mutant tissue examined. Other cells which could not be catalogued as oligodendrocytes, astrocytes or microglial cells by their morphological appearance were labelled as unidentified cells. This group included glioblasts in neonatal mice, the previously mentioned "undifferentiated cells" seen in older mutant spinal cord sections and dying cells.

(2) Fibre morphometry

(a) Myelin thickness and g ratio

Significant differences from wild-type occurred in myelin thickness and *g* ratio from 10 days onwards (figure 32). Mean myelin sheath thickness and myelin volume increased as the *g* ratio decreased with age in normal mice (figure 32). However, mutant fibres presented a markedly elevated *g* ratio and a reduced myelin thickness and density suggesting the presence of thin myelin sheaths. Scatter graphs of myelin sheath thickness and axon diameter showed no correlation between the two parameters in mutant mice whereas a significant linear relationship was present in wild-type mice. The vast majority of points from jp^{rsh} ventral columns of the cervical cord were below the lower prediction band for the wild type (figure 33).

Significative axonal diameter differences were only detected at 45 days in the spinal cord (figure 34).

(b) Myelin density

Myelin density was markedly reduced at all ages in the spinal white matter of jp^{rsh} (figure 32).

c) Optic nerve

(1) Quantification of glia

Glial cell densities were reduced in jp^{rsh} during initial myelination, then recovered to be greater than in wild-type during and immediately following peak myelination, and were normal in animals over 50 days (figure 35). Total glial cell numbers in cross sections of the optic nerve of jp^{rsh} were also reduced initially then rose over normal levels between 20 and 45 days, and finally failed below normal in older animals (figure 36). Cell types were only classified from 50 days onwards as their morphological characteristics became patent (figure 36). At this stage, the oligodendrocyte numbers were reduced in mutant mice and remained so at all ages examined. Total astrocyte numbers were not significantly different from controls in the mutant optic nerve at 60 days, however, the astrocyte percentages were significantly increased in the mutant optic nerve at the age of 90 days (figure 37).

(2) Fibre morphometry

(a) Myelin thickness and g ratio

No difference was present in mean myelin thickness between wild-type and jp^{rsh} mice but the *g* ratio was slightly higher in mutant optic nerves at younger ages. This suggests that a small number of mutant sheaths were thinner than those in age

matched controls (figure 38). Scatter graphs of myelin thickness against axonal diameter showed that the vast majority of points for the two groups coincided (figure 39).

Mean axonal diameter and the axonal diameter frequency distributions were indistinguishable between wild-type and *jp^{rsh}* mice (figure 34).

(b) Myelin density

The total amount of myelin, as determined by point counting, was significantly reduced in the mutant mice (figure 38).

6. CHANGES IN ONE-YEAR OLD MICE

Light microscopic observations of *jp^{rsh}* tissue at 12 months of age revealed that the oligodendrocyte numbers in the spinal cord were still increased (figures 19, 20). Large fibres still demonstrated obvious hypomyelination while smaller fibres had acquired appropriate myelin sheaths. Microglial cells were more obvious than at younger ages in both *jp^{rsh}* and wild type.

No Schwann cell invasion was detected in semi-serial resin-embedded sections of the C1-C2 segments of the spinal cord stained with methylene blue/azure II or immunostained for P_0 (figure 13).

7. DISCUSSION

Quantification of the glial cell population in *jp^{rsh}* optic nerve and spinal cord revealed differences between these locations. Glial cell numbers in the mutant spinal cord remained elevated throughout life while, in the optic nerve following a peak at 20 days, numbers decreased to slightly below normal levels in the adult nerve. Both variations in cell numbers were due mainly to changes in the oligodendrocytes. Appropriate numbers of oligodendrocytes were present at myelination in *jp^{rsh}* . Therefore, we conclude that the hypomyelination present in *jp^{rsh}* CNS is not due to a lack of oligodendrocytes. Previously described X-linked mutations of myelination are associated with hypomyelination with varying degrees of oligodendrocyte loss (Skoff, 1976; Duncan *et al.*, 1983; Dentinger *et al.*, 1982). In the case of *jp*, premature cell death occurs prior to the time at which PLP is expressed (Vermeesch *et al.*, 1990; Ghandour and Skoff, 1988). A similar paucity of oligodendrocytes is not seen in non-X-linked mutations such as *shi* or *qk* (see previous discussion) and has

lead to the suggestion that a product of the PLP gene may be required for cell survival (Gencic and Hudson, 1990; Hudson, 1990b; Vermeesch *et al.*, 1990; Nadon *et al.*, 1990). Recently, *tr*, a peripheral dysmyelinating mutant has elucidated a peripheral protein termed PMP-22, involved in Schwann cell survival and proliferation (Suter *et al.*, 1992). Perhaps DM-20 represents the equivalent protein in the CNS. This hypothesis will be considered further over the next chapters.

The myelin deficiency exhibited in *jp^{rsh}* spinal cord was more marked at younger ages. Large axons were the first to be myelinated in the mutant ventral columns, although the myelin sheaths produced were abnormally thin and frequently vacuolated or uncompacted. Oligodendrocytes embracing single axons, and large patches of unmyelinated fibres, were a frequent finding in spinal cord sections from young mice. However, the initial *jp^{rsh}* myelination pattern evolved as the animal aged. Smaller fibres progressively acquired myelin sheaths of reasonably normal thickness, hence, by the age of 90 days most smaller axons were myelinated. Such fibres, despite being reasonably compacted, still exhibited abnormalities in the IPL and periodicity. This is to be expected as PLP is believed to be important in maintaining the close apposition of the extracellular face of the lipid bilayer to form the double intraperiod line (Duncan *et al.*, 1987b; Duncan *et al.*, 1989). Findings in *jp^{rsh}*, therefore, support the previous observations in other PLP mutants like the *jp* mouse and the *md rat* which are deficient in both PLP and DM-20 yet are able to produce compact myelin (with abnormal intraperiod lines). The production of extra sheaths was reflected in the slight increase in the spinal cord myelin density between 50 and 90 days in the mutant (figure 32). Abnormally myelinated large fibres demonstrated very little increase in myelin thickness during development. Age-related increments in myelin in the spinal cord have also been reported in other mutants such as the *md rat* and *sh pup* (Jackson *et al.*, 1988). Schwann cell invasion of the spinal cord as seen in a 22 month old *sh pup* (Duncan, personal communication) was not a feature in 1 year-old *jp^{rsh}* mice. The deficiency in the myelin content of the optic nerves was manifest as a lack of myelin sheaths rather than a reduction of the myelin per sheath as indicated by their *g* ratio (figure 38) and in the scattered graph of the myelin thickness against axonal diameter (figure 39). Although oligodendrocyte numbers in the optic nerve were slightly reduced in older mutants, this occurred much later than the period of myelination during which time cell numbers were actually higher (figure 35, 36). No noticeable recovery or evolution of any kind was seen for this structure. Differences in the severity of hypomyelination between early and later myelinating tracts have also been described for other PLP mutants (see review in: Duncan, 1990).

The optic nerve and spinal cord are known to differ in many aspects which may explain the disparity of findings between the two. First of all, both nervous

tracts have a very different embryological development and myelinate at different times (see introduction of the thesis for further details). Differences in the axonal populations (McQuarrie *et al.*, 1986), and more recently, in the glial cell lineages have also been reported (Fok-Seang and Miller, 1992). On the other hand, oligodendrocytes are known to be heterogeneous in terms of their myelination potential relative to axon size; the myelination unit has been seen to vary from a single axon of large diameter to many smaller axons myelinated by a single cell. One possible reason is that more myelin membrane is required for a single internode of a large axon than for multiple internodes of smaller axons (Blakemore, 1982; Remahl and Hildebrand, 1990). Consequently these facts may well underlie the presence of smaller fibres, either normally-myelinated or naked, and large fibres displaying a disproportionately thin myelin sheath often vacuolated or uncompacted. As the optic nerve is composed mainly of smaller axons, while the spinal cord comprises fibres of various diameters, the optic nerve would show either unmyelinated or normally myelinated fibres. However, the spinal cord would exhibit these two types plus a third variety of large hypomyelinated fibres.

The progressive increase in myelin seen in the ventral columns of the spinal cord could also be explained by examining the evolution of tissue myelination together with the oligodendrocyte population. Reports on early myelination in the developing feline spinal cord suggest a two step myelination process (see chapter I.) where large fibres myelinate earlier than smaller fibres (Remahl and Hildebrand, 1990). A similar myelination course has been reported for the PNS (Hahn *et al.*, 1987). Large fibres are myelinated by a different type of oligodendrocyte which produced a single internode in a Schwann-cell-like fashion; thus, an oligodendrocyte/internode ratio of 1:1 (Remahl and Hildebrand, 1990). These oligodendrocytes have also been reported to be morphologically more mature than the rest of the glial cells present in the spinal cord at the time (Remahl and Hildebrand, 1990). The second stage of myelination involves the differentiation of the oligodendroblasts which have been actively dividing and the production of myelin sheaths for the small calibre fibres with one oligodendrocyte myelinating several fibres (Remahl and Hildebrand, 1990). It is unknown if there is a feed-back signal from the unmyelinated tissue that would stimulate the division of these "later-myelinating" oligodendrocytes. But if this was the case, jp^{rsh} unmyelinated axons would promote myelination until all unmyelinated fibres were ensheathed. However, the optic nerve does not acquire detectable extra myelin sheaths. It is unknown yet why these separate tracts evolve differently in jp^{rsh} although most reasons point to the different nature of the axonal population in both structures. The presence of undifferentiated cells corresponding to those immature oligodendroblasts named "primitive oligoblasts" described in the developing monkey spinal cord (Phillips,

1973) may underlie the possible explanation of this phenomenon. This hypothesis will be considered further in section F after the presentation of more data.

In order to test the previous hypothesis the dorsal columns of the spinal cord were examined. These CNS tracts also present a homogeneous small diameter fibre distribution and myelinate after the ventral columns, closer to the myelination time of the optic nerve. Although no fibre morphometry of the area has been performed, light microscopy revealed a noticeable increase in the total numbers of myelinated fibres in older mutant mice (figure 20). Labelling of the dividing cells in these areas revealed an increased cell division at all ages as seen for the ventral columns of the spinal cord thus, differing from the optic nerve (see section F).

Therefore, there is a possibility that the oligodendrocyte population is divided into, at least two types of myelinating oligodendrocytes which have affinity for different diameter fibres. The two types would be present in the ventral columns of the spinal cord but only one type would occur in the optic nerve or dorsal columns of the spinal cord. Both types of oligodendrocytes, affected by the *jp*^{rsh} mutation, would exhibit a different programme of myelin production and turnover which is reflected in different patterns of myelination in the mutant CNS tissue (figure 20). Further investigation will be necessary to determine whether some oligodendrocytes are generally programmed to myelinate only certain types of fibres in the CNS. The *jp*^{rsh} mutation represents an example where the oligodendroglial diversity is separated by the mutational defect.

D. *IN SITU* HYBRIDIZATION STUDIES

1. INTRODUCTION

In situ hybridization (ISH) represents a valuable tool that enables the study of the expression of a particular gene. It offers the advantage of identification and location of the cells where that information is expressed. Thus, the developmental expression of PLP/DM-20 can be monitored in different anatomical regions of the CNS and mutational changes affecting the transcription of the gene can be detected.

2. AIMS OF THE STUDY

The aim was to quantify the numbers of PLP/DM-20-expressing cells and the intensity of the PLP/DM-20 signal in individual cells. It has been demonstrated for other mutations like *jp* and its allele jp^{msd} (Jordan *et al.*, 1989; Gardinier *et al.*, 1986; Gardinier and Macklin, 1988; Sorg *et al.*, 1987; Sorg *et al.*, 1986; Campagnoni and Macklin, 1988; Nave and Milner, 1989), *shi* and shi^{mld} (Popko *et al.*, 1987), *mld* (Tosic *et al.*, 1990; Fremeau and Popko, 1990), *md rat* (Kumar *et al.*, 1988; Boison and Stoffel, 1989; Gordon *et al.*, 1990), and *sh pups* (Nadon *et al.*, 1990) that the levels of mRNA frequently do not correlate with the final protein levels and that post-translational events were in many occasions involved in the low or null protein production in these mutants (Tosic *et al.*, 1990). The detection of oligodendrocytes using a cell-specific gene expression also complements identification based on cellular morphological characteristics.

3. MATERIALS AND METHODS

The basic procedure was as described by Cox *et al.* (Cox *et al.*, 1984) and modified by Wilkinson *et al.* (Wilkinson *et al.*, 1987). The method is fully described in chapter 2. A ^{35}S-labelled mRNA probe for PLP and DM-20 was hybridized to paraffin-embedded tissue sections of the spinal cord and brain of wild type and jp^{rsh} mice between 10 to 90 days of age.

The individual cell signal was identified on enzmatically dissociated cells. Oligodendrocytes obtained from the ventral columns of the spinal cord of 16 day-old mutant and wild type mice, were allowed to adhere to coverslips for 2 hr. These cells were then fixed and processed in parallel to allow direct comparison (see chapter

2 for more detail). Following development of autoradiograms the optical density of the signal from 150 cells of each group was measured and the mean values compared by t test. The average signal per cell for PLP/DM-20 mRNA was compared in both groups as described in chapter 2. Some dissociated cells from 7 day-old wild type and mutant mice spinal cords were cultured for a week, immunostained for GalC and hybridized over the same slide for visual inspection.

4. RESULTS

The cell density and total numbers of PLP/DM-20 mRNA-expressing oligodendrocytes were evaluated in paraffin-embedded sections. Positive oligodendrocytes were readily identifiable throughout the CNS of wild type and *jp^{rsh}* mice at all ages examined. The spinal cord of *jp^{rsh}* had increased PLP-expressing cell densities which continuously increasing with age (figures 40, 41). However, the percentage of PLP-expressing cells in the mutant, which was lower from 16 days of age, recovered by the age of approximately 80 days (figure 42). The optic nerve cell densities and numbers were slightly increased for both types of animals during early myelination, with a peak at 20 days. After the age of 40 days, numbers of PLP-expressing cells declined relative to wild type (figures 43, 44).

Visual inspection of the autoradiograms of tissue sections suggested that the signal intensity of PLP/DM-20 message per individual cell was less in *jp^{rsh}* at all ages in the spinal cord (figures 45, 46) becoming more conspicuous in 30 day old spinal cord (figure 47) and in the optic nerve (figure 48).

Quantification of individual cell expression was only performed at 16 days using freshly dissociated cells from the ventral columns of cervical spinal cord of wild type and *jp^{rsh}* mice (figure 49). The mean optical density of the signal from mutant cells was only 50% of that from the wild type (OD. Mean $\pm$ SEM; wild type 0.428 $\pm$ 0.029; mutant 0.211 $\pm$ 0.041; $p < 0.001$; 300 cells) examined. Dissociated spinal cord oligodendrocytes immunostained for GalC and hybridized for PLP demonstrated that morphologically mature oligodendrocytes which were GalC + did not achieve the same degree of PLP mRNA expression as wild type cells processed in parallel (figures 50 to 53).

5. DISCUSSION

As mentioned previously, *jp*^{rsh} nervous tissue contains adequate numbers of oligodendrocytes throughout myelination, and indeed the number in the spinal cord is elevated. This has been shown by two independent techniques, cell counts based on morphology and ISH which demonstrate that *jp*^{rsh} mutation is compatible with oligodendrocyte survival and their differentiation to the stage of expressing PLP/DM-20 mRNA. This contrasts with the *jp* mutant where the PLP/DM-20 expressing oligodendrocytes are reduced (Verity *et al.*, 1990) presumably as a result of the increased oligodendrocyte death (Knapp *et al.*, 1986; Knapp *et al.*, 1990; Meier and Bischoff, 1975; Privat *et al.*, 1982; Vermeesch *et al.*, 1990). The confirmation that cells of the oligodendrocyte lineage increase in numbers throughout life in *jp*^{rsh} spinal cord suggests that those previously described undifferentiated cells (figures 23, 24) in older mutants which morphologically resembled "primitive oligoblasts" (see section C.4.) were possibly a sort of oligodendrocyte progenitor cells or oligodendroblasts.

The average PLP/DM-20 message level per cell was reduced in *jp*^{rsh} when compared to the final protein levels were proportionately lower than the mRNA message. Similar findings have been reported for *jp* and *md rat* (Verity *et al.*, 1990; Sorg *et al.*, 1986; Hudson *et al.*, 1987; Kumar *et al.*, 1988). This suggests that the phenotypic effects of the mutation may be associated with reduced translation of major myelin proteins, in particular PLP causing a marked differential effect on the levels of PLP mRNA and protein (Mitchell *et al.*, 1992). However, it is unknown why there is a disproportionate expression of DM-20 protein in the mutant tissue.

E. CELL CULTURE

1. INTRODUCTION

Glial cell culture represents an excellent tool for the study of the plasticity of mutant cells as it enables the isolation and manipulation of individual oligodendrocytes from very early stages of differentiation to the most mature development.

Oligodendrocytes are known to undergo a complex differentiation pathway from progenitor cells to fully mature cells (Raff, 1989) involving the expression of different antigenic markers, of which, GalC is considered to indicate commitment to the oligodendrocyte lineage. The GalC antigen expression be followed by the synthesis of the myelin proteins and the expression of the antigens recognized by the antigens O10 and O11 (tables 1, 2). In recent years evidence has accumulated that a product of the PLP gene has some biological role other than as a structural component of myelin, possibly involved in the survival and perhaps differentiation of the oligodendrocytes. Cultures from PLP mutants have revealed the importance of the cell-cell interaction for the development of defective glial cells. *In vivo, jp* oligodendrocytes exhibit a cell cycle defect associated with the premature death of many cells as they begin to differentiate (Skoff and Knapp, 1990; Knapp *et al.*, 1986; Vermeesch *et al.*, 1990). *In vitro*, however, they are able to differentiate when cultured in medium conditioned by normal glial cells (Bartlett *et al.*, 1988). Oligodendrocytes in the *md rat* have also been seen to recover partially *in vitro* when cultured under regular conditions (Espinosa de los Monteros *et al.*, 1990). The jp^{rsh} mutation represents a model for the study of the influence of DM-20 and PLP on oligodendrocyte survival and differentiation as DM-20 is expressed disproportionately in respect to PLP. The appearance of DM-20 with respect to PLP also can be monitored in cultured jp^{rsh} oligodendrocytes.

2. AIMS

The purpose of these experiments was to study the influence of the jp^{rsh} mutation on oligodendrocyte survival and differentiation. The plan was to culture and compare cells from dissociated spinal cord and optic nerve and study their cellular morphology and antigenic profile as they developed in culture. The study was focused in the oligodendrocyte later stage of developmental markers such as O10, O11 and, of course, the products of the PLP gene.

3. MATERIALS AND METHODS

a) Oligodendrocyte development markers

The following antibodies were used for immunofluorescence. Mouse monoclonal antibodies O4, O10 and O11 (all IgM) and R-mAb (IgG_3) (see below) were all obtained as tissue culture supernatants, together with antiserum against MBP and two antisera for PLP; one directed against the PLP-specific region of the molecule and the other against the C-terminal common to PLP and DM-20 (PLP/DM-20) (Griffiths *et al.*, 1990; Fanarraga *et al.*, 1991; Fanarraga *et al.*, 1992a).

Secondary antibodies FITC, TRITC or Texas Red-labelled were used as appropriate (see table 7).

GalC has been detected with the R-mAb which recognizes GalC and Sulfatide. Results have been labelled as GalC.

b) Ages of mice and culture duration

(1) in vivo study

In order to investigate and compare the antigenic development of oligodendrocytes *in vivo*, cells were dissociated from spinal cords of both jp^{rsh} and wild type mice aged 3, 7, 10 and 16 days. Optic nerve cells were cultured from 7,10 and 16 day-old animals. The cells were allowed to adhere to the culture surface for 2 hr prior to the immunostaining with the above markers. This short duration in culture is insufficient for a significant differentiation of cells and the profile should indicate their *in vivo* status.

(2) in vitro development study

Oligodendrocytes from 3 and 7 day-old spinal cords and 7 and 10 day-old optic nerves were cultured in SATO/0.1% FCS medium up to 120 hr. The immunostaining was performed at 2, 24, 72 and 120 hr, after plating using the same markers as for the *in vivo* study (see above).

c) Method and percentage calculations

Double immunofluorescence labelling was performed at all time points as described in chapter 2. R-mAb immunostaining which was taken to indicate predominantly GalC, was the constant parameter in all double immunofluorescence experiments (GalC/O4; GalC/O10; GalC/O11; GalC/MBP; GalC/PLP/DM-20 and GalC/PLP-specific), being always detected with an anti-IgG_3 conjugated to TRITC. Taking the percentage of O4 positive cells as 100% for all cultures, the percentage of cells positive for the immunostaining with any of the mentioned antibodies was obtained from the double immunostaining using the percentage of GalC+ cells within the O4+ population. Results are expressed as the percentage of the O4 population.

The expression of A2B5 antigen was examined in some of the initial experiments but, as explained in the introduction of the thesis, the A2B5+ lineage is known to be different for various locations of the rat CNS as well as for different animal species (Schnitzer and Schachner, 1982; Fok-Seang and Miller, 1992). On the other hand, the A2B5 immunostain of mouse oligodendrocytes does not coincide with the rat (unpublished observations). Therefore, in order to simplify the situation, we used O4+ cells as the indicator of the least differentiated cells (Sommer and Schachner, 1981).

4. RESULTS

Cultured *jp^{rsh}* oligodendrocytes did not show obvious morphological differences from controls. Mutant cells produced a normal number of processes which, eventually, developed myelin sheets of comparable dimensions at the expected time in a similar manner to wild type cells (figure 54 to 56). Preparation of cultures from the mutant optic nerves required larger amounts of tissue than from wild type and the cell survival was possibly reduced, but no detailed investigations have yet been performed.

jp^{rsh} oligodendrocytes commenced their development by following the normal sequence of antigen expression. No difference in the number of O4 and GalC positive cells was detected in either the spinal cord or optic nerve cultures in *jp^{rsh}* versus wild type mice (figure 57). This indicated that mutant oligodendrocytes achieved the early stages of antigen expression, as shown in figures 58 to 63.

The first abnormalities were detected with the MBP immunostaining. Although *jp^{rsh}* oligodendrocytes started producing MBP simultaneously to wild type, the total number of cells expressing MBP was reduced in cultures from 3 and 7 day-

old spinal cords (figures 58, 59) as well as in 7 and 10 day-old optic nerve cultures (figures 61, 62). However, the expression in individual positive cells was identical to control wild type oligodendrocytes (figures 64 to 66). The MBP production in the 2 hr cultures, representing the *in vivo* situation, seemed to be less affected by the mutation (figures 66, 67). MBP positive cell counts reached values equivalent to wild type or even higher in 2 hr cultures from 10 and 16 day-old spinal cords (figure 60).

The most outstanding feature of the cultured jp^{rsh} oligodendrocytes compared to wild type cells was the *in vivo* and *in vitro* impaired expression of those antigens indicating mature cell differentiation (figures 58 to 63). PLP/DM-20 expression was reduced for all cultures at all ages and times examined. However, the onset of the immunoreactivity against this C-terminal antibody coincided with the wild type and occurred approximately 2 days prior the expression of the PLP-specific antigen in wild type cells. This indicates that those mutant oligodendrocytes capable of expressing PLP/DM-20 developed at the normal pace. The individual cell expression was variable but generally reduced when compared to controls (figures 68 to 70). PLP-specific immunoreactivity was virtually absent in most cultures. Those cells positive for PLP, which were found mainly in the optic nerve showed a very weak immunoreactivity when compared to wild type cells localized in small lumps in the processes (figures 71 to 73). Antibodies O10 and O11 antibodies which immunostain mature wild type oligodendrocytes, were negative in almost all jp^{rsh} cultures (figures 58 to 63). Very occasional O10+ or O11+ cells were detected although the immunostaining was very poor (figures 74, 75).

The comparison between *in vivo* and *in vitro* oligodendrocyte development revealed that although the main characteristics of the mutant cells were the same, the production of MBP was improved *in vivo* (figure 67). However, a similar phenomenon did not occur for PLP/DM-20, PLP, O10 and O11 expression (figures 76 to 79).

5. DISCUSSION

This study has examined the *in vivo* and *in vitro* differentiation of wild type and jp^{rsh} oligodendrocytes from the optic nerve and the spinal cord. The most important outcome was that jp^{rsh} oligodendrocytes were capable of developing in culture a considerable way to full maturity before further differentiation was blocked. Such cells when allowed to grow in culture were morphologically similar to those from wild type showing numerous processes that would develop membrane sheets of normal dimensions.

The A2B5 antibody was not used to recognize immature progenitor cells as previous investigations demonstrated that A2B5 does not consistently stain putative glial precursor cells in the mouse (Schnitzer and Schachner, 1982). It is also known to recognize several gangliosides present on neurons and astrocytes (Einsenbarth *et al.*, 1979; Schnitzer and Schachner, 1982; Berg and Schachner, 1981). Therefore, O4 was used to label O-2A progenitor cells instead. This antibody reacts with these cells at a later stage of development (Trotter and Schachner, 1989) recognizing a yet unknown antigen termed POA (Bansal *et al.*, 1992; Bansal *et al.*, 1989; Warrington and Pfeiffer, 1992) prior to the appearance of sulfatide and GalC (Bansal *et al.*, 1992). Antibodies against these two galactolipids have been pivotal in the study of oligodendrocyte development (tables 1, 2).

The GalC stage was achieved normally by *jp^{rsh}* oligodendrocytes, which is not surprising after examining the number of PLP/DM-20 mRNA expressing cells in *jp^{rsh}* CNS. However, the number of MBP expressing cells was reduced as much as 50% relative to the wild type although the expression in individual cells was not diminished. Immunostaining with the anti-C-terminal antibody recognizing PLP and DM-20 was also reduced both quantitatively and qualitatively, as individual mutant cells stained less intensively than wild type oligodendrocytes as expected according to previously dissociated spinal cord oligodendrocytes immunostained for GalC and showing a low PLP/DM-20 mRNA levels (see previous section). The immunoreactivity against the PLP-specific antibody was virtually absent, suggesting that DM-20 was being detected by the anti-C-terminal antibody. These results are supported by electrophoretic and immunoblotting data which show the virtual absence of PLP but presence of DM-20 (Mitchell *et al.*, 1990; Mitchell *et al.*, 1992). The *jp^{rsh}* reached the MBP and PLP/DM-20 positive stages at the same time as the wild type oligodendrocytes suggesting that those mutant oligodendrocytes persisted beyond early development following the normal timing of protein production. Those very few mutant oligodendrocytes that produced PLP stained very weakly when compared to positive cells from age-matched wild type cultures. However, the fact that some *jp^{rsh}* cells were positive for PLP does not imply that normal protein it has been detected, as we could be recognising abnormal products of the PLP gene.

O10 and O11 immunostain was also virtually absent in all cultures, although very occasionally positive cells were recognised in some cultures. As O10 and O11 have been poorly characterised, it is possible that abnormal proteins and lipids were recognised on the surface of the labelled mutant oligodendrocytes. Alternatively, all *jp^{rsh}* oligodendrocytes may not follow the regular differentiation pathway. A similar phenomenon also takes place in *jp* mutant oligodendrocytes which immunostain for O11 while being negative for O10 (Sommer and Schachner, 1984). As O10

recognizes a molecule defective in *jp* and *jp^{rsh}* which may be a product of the PLP gene. These conclusion would need further investigation.

The exact time at which normal oligodendrocytes express DM-20 is still uncertain. However, this protein is known to be present before PLP (Gardinier and Macklin, 1988; Van Dorsselaer *et al.*, 1987; Schindler *et al.*, 1990). According to the results from this present study, PLP/DM-20 antiserum immunostained cells which were already expressing MBP, while the PLP-specific antibody immunostained cells approximately 48 hr after detecting PLP/DM-20. Examination of the timing of the various antigenic markers in *jp^{rsh}* suggested the following antigenic profile sequence: O4, GalC, MBP, DM-20, PLP. O10 and O11 reactivities occur after the GalC stage (Kuhlmann-Krieg *et al.*, 1988), and approximately overlap with the DM-20 and PLP stages respectively.

Present results support our previous immunocytochemical and immunoblotting studies (Griffiths *et al.*, 1990; Fanarraga *et al.*, 1992a; Mitchell *et al.*, 1990; Mitchell *et al.*, 1992) which indicated that these mutants expressed MBP and DM-20 but virtually no PLP in their myelin. Although the major abnormality in the differentiation of the *jp^{rsh}* oligodendrocytes appeared between the stages of MBP and PLP expression, each antigenic step from MBP onwards was reached by a lower proportion of cells. Oligodendrocyte differentiation has been examined in other PLP gene mutants, principally *jp*. The data from *in vivo* and *in vitro* studies (Omlin and Anders, 1983; Ghandour and Skoff, 1988; Bartlett *et al.*, 1988) indicate that early differentiation of *jp* oligodendrocytes is relatively normal. The majority of cells express GalC and CNPase; some also produce MBP (Omlin and Anders, 1983) but reactivity for PLP (Ghandour and Skoff, 1988) or O10 (Sommer *et al.*, 1982; Sommer and Schachner, 1984) is rare or absent. Cultured oligodendrocytes from *md rat* also show retarded expression of both early and late differentiation markers, including MBP (Duncan *et al.*, 1987b), but some recovery occurs with prolonged culture particularly in the earlier-expressed antigens (Espinosa de los Monteros *et al.*, 1990). *jp* oligodendrocytes cultured in medium conditioned by normal glial cells have an improved survival and a more differentiated morphology (Bartlett *et al.*, 1988) suggesting that factors in the extracellular environment of mutant oligodendrocytes may partially inhibit their maturation.

An important question is why the phenotype of *jp^{rsh}*, particularly in relation to oligodendrocyte survival and maturation, is different from the other PLP mutations. DM-20 protein, a postulated factor in cell survival, is detectable in approximately 30 % of spinal cord oligodendrocytes of *jp^{rsh}* at 16 days of age and biochemical and immunocytochemical studies have also identified a relatively high level in myelin (Griffiths *et al.*, 1990; Mitchell *et al.*, 1990; Mitchell *et al.*, 1992). However, two

other mutants *sh pup* and *jp^{msd}* also have disproportionate expression of DM-20 (Yanagisawa *et al.*, 1987; Gardinier and Macklin, 1988), yet oligodendrocytes are depleted. In all three mutations the defect involves regions of the PLP gene encoding DM-20, so that this protein is defective. However, the resultant amino acid substitutions (*sh pup*, His^{36} →Pro; *jp^{msd}*, Ala^{242} →Val and *jp^{rsh}*, Ile^{186} →Thr) affect different regions of PLP/DM-20. It is quite possible that the survival of oligodendrocytes in the *jp^{rsh}* phenotype indicate that the mutation Ile^{186} affects a region of the PLP/DM-20 molecule which is not involved in vital membrane-related functions during cell development. Nevertheless, as the topography of PLP/DM-20 proteins in the cell membrane are still unknown the *jp^{rsh}* mutation could either affect an intramembrane domain or be exposed on the external or cytoplasmic surfaces depending on the model selected (see review in chapter 1, section A.3.).

An additional question is why normal or even increased numbers of oligodendrocytes survive in *jp^{rsh}* when only 30%, relative to wild type at 16 days of age, contain detectable DM-20 protein. It is possible that DM-20 is present in the remaining oligodendrocytes in amounts too low to be immunolabelled. Another explanation could be that DM-20 (or another minor proteolipid) is critical only at a specific stage of differentiation and that its absence at other times will not affect cell survival. A further possibility to consider is that due to the pleiotropic effects of mutations in the PLP gene the critical factor for cell survival is actually the product of a separate gene whose normal expression is dependent on some function of the PLP gene.

F. CELL DIVISION STUDY

1. INTRODUCTION AND AIMS

Many developmental studies have examined cell proliferation and turnover using tritiated thymidine labelling as an index of the DNA synthesis. [methyl-^{3}H] thymidine is a precursor of the DNA incorporated by a sequence of phosphorylation steps together with the other nucleoside triphosphates, into DNA during the S phase of the cell cycle (Knapp, 1992). Recently, the development of antibodies to the thymidine analogue 5-bromo-deoxyuridine (BrdU) has allowed the development of an immunocytochemical method analogous to the thymidine autoradiographic technique (Knapp, 1992). However, the inability of BrdU to cross the blood brain barrier in older animals and the fact that it labels more cells than [methyl-^{3}H] thymidine in culture (Knapp, 1992) lead our research to the use of the traditional radioactive method.

One of the most striking features of the *jp^{rsh}* phenotype is the increased oligodendrocyte population in the spinal cord which increases progressively and constantly from early myelination onwards. This project was commenced towards the end of my post-graduate study period; the results represent a preliminary examination of the problem which will require further studies. Similar studies have been started recently in the optic nerve but results are not yet available.

2. MATERIALS AND METHODS

Two *jp^{rsh}* and two wild type mice at 5, 10, 15, and 100 days-old and one at 50 days old were injected 5μCi/μl [methyl-^{3}H] thymidine in saline at a dose of 5μCi/g body weight as described in chapter 2. Two hours later mice were perfused with Karnovsky's modified fixative (Paraformaldehyde/Glutaraldehyde); their CNS tissue was dissected and processed following routine techniques for resin embedding. One μm thick tissue sections of spinal cord were cut, placed onto gelatine-coated slides, dipped in Ilford emulsion K2 and exposed for periods up to 4 weeks. Defaults of the methodology are given in chapter 2.

Cell counts were performed under regular light microscopical conditions. The nuclei of dividing cells which were evenly covered with silver grains, were counted. Only glial cell nuclei were counted, other dividing cells such as endothelial cells were not included in the cell counts.

3. RESULTS

The spinal cord of *jp^{rsh}* mutants demonstrated ^{3}H-thymidine labelled cells at all ages examined. The density of labelled cells and total numbers of labelled cells in the mutant spinal cord was slightly increased from the very early stages of development up to the latest ages examined (100 days of age) (figures 80, 81). The percentage of labelled cells relative to the total number of glial cells was also increased in the mutant spinal cord from 15 days of age onwards (figure 82).

Wild type spinal cord showed a peak of glial cell division between 10 and 20 days of age coinciding with the beginning of myelination in the ventral columns of the spinal cord. After the age of 20 days, about the end of the myelination in the spinal cord, glial cell mitosis declined substantially. This same peak of cell division also occurred in *jp^{rsh}* at that time (figure 80, 81), however, the density of labelled glial cells and total labelled glial cell counts remained high respect to controls, after the complete myelination of the spinal cord. Although these dividing cells have not been ultrastructurally classified yet, most of them resembled cells of a possible oligodendroglial origin (figure 83). Other labelled cells, such as endothelial cells from the blood vessels, were also present in some of the sections but were not included in the counts (figure 84). Occasional astrocytes were also labelled (figure 84).

4. DISCUSSION

The spinal cord of the mouse shows a peak of glial cell division between 10 and 20 days of age coinciding with the increased demand for oligodendrocytes at myelination. It is know that once myelination ends, glial cell mitosis declines substantially and is mainly restricted to microglial cells.

The most important feature in *jp^{rsh}* spinal cord when compared to other PLP mutations is the progressively increasing oligodendroglial population. Findings such as the ultrastructural presence of possible undifferentiated oligodendrocytes ("primitive oligoblasts": Phillips, 1973), together with the *in situ* hybridization studies, which demonstrated a progressive increase of PLP-expressing cells, suggested an increased oligodendroglial proliferation. [Methyl-^{3}H] thymidine, a well known precursor of DNA, was used to label the dividing cells in the tissue. The results indicated that the density of dividing cells, total labelled counts and percentages of dividing cells are all increased in *jp^{rsh}* at all ages after myelination. This could account for the continued supply of oligodendrocytes in the mutant cord. Other mutants such as *jp*, *md rat* and *sh pup* also exhibit an increased glial cell proliferation

rate in the spinal cord (Jackson and Duncan, 1988; Knapp *et al.*, 1986; Macklin *et al.*, 1991; Gencic and Hudson, 1990). However, it is accompanied of premature death of the oligodendrocytes especially in *jp* (Knapp *et al.*, 1986; Knapp *et al.*, 1990; Privat *et al.*, 1982; Skoff and Knapp, 1990; Vermeesch *et al.*, 1990) but also in *md rat* (Boison and Stoffel, 1989; Jackson and Duncan, 1988) thus there is no increase in the total glial cell population.

As it has been explained in the introduction of the thesis, there are some theories that differentiate the oligodendroglial population into "early" (Schwann cell-like) and "late" myelinating oligodendrocytes (Remahl and Hildebrand, 1990). The second type of oligodendrocytes proliferates actively later in myelination possibly commanded by a feed-back signal from the myelinated axons. Morphological findings together with a progressively increase of the PLP expressing cells, indicated an extra supply of oligodendrocytes or their progenitors in jp^{rsh} spinal cord. Although the thymidine labelled cells in the mutant cord have not been ultrastructurally identified yet, cells resembling very immature oligodendroblasts (such as those termed "primitive oligoblasts": Philips, 1973) were detected from 50 days onwards (figures 22, 23). These newly-produced cells would possibly correspond to the previously described second type of oligodendrocytes in charge of the myelination of the smaller fibres. Unmyelinated axons in the mutant cord might stimulate oligodendrocyte proliferation until complete myelination. As jp^{rsh} oligodendrocytes were not capable of myelinating the expected number of internodes the oligodendrocyte proliferation would continue until advanced ages.

A further question here will be to determine whether these cells are produced locally, as a consequence of a maintained basal division rate or if they are the result of the migration of oligodendroblasts from neighbouring areas, such as the grey matter or other regions along the spinal cord. The ultrastructrural presence of very immature glial progenitor cells suggests that these cells have been probably produced locally as O-2A progenitor cells are known to mature as they migrate while dividing (see chapter 1).

A remarkable finding in jp^{rsh} is that the percentage of dividing cells at a 100 days of age is greater than 0.8% over 6 hours, thus more than 3%/day. Although there is an obvious increment in the glial cell numbers in the mutant spinal cord this glia cell over-production never reaches the forecasted levels. Therefore, cell death, probably apoptosis is suspected as morphological examination of the tissue did not revealed conspicuous cell death (see chapter 1). Apoptosis would probably be the result of a competition for the insufficient supply of growth factors such as PDGF and FGF rather than a direct consequence of the mutation as jp^{rsh} oligodendrocytes seem

to survive well. Further work has been planed in order to identify the dividing cells ultrastructurally.

Optic nerve labelling is not yet concluded but preliminary results indicate that the cell division rate is not noticeably increased which is consistent with the glial cell counts in this tract (figures 35, 36). Findings suggest that the environment where the mutant oligodendrocytes develop may be also responsible for the cell proliferation. Environmental factors or feed-back signals from the tissue, other than DM-20, appear to be necessary for the oligodendrocyte proliferation, which occur in the spinal cord but not in the optic nerve. DM-20 would, therefore play the role of a survival factor involved in the oligodendrocyte development and differentiation, rather than affecting cell division. Recently similar roles have been attributed to the PNS protein PMP-22 mutated in *tr* mouse (Suter *et al.*, 1992) or to PDGF and IGFs in cultured O-2A (Barres *et al.*, 1992).

CHAPTER 4: *jprsh* HETEROZYGOTES

A. INTRODUCTION

1. X-CHROMOSOME INACTIVATION AND MOSAICISM

Lyon's hypothesis in 1972, (Lyon, 1972) supported by further studies in the mouse (Nesbitt, 1971), demonstrated X-chromosome inactivation during the early stages of the embryonic development as a regulatory mechanism to eliminate the aneploidy effects in female somatic tissue and still have a normal germinal function. The X-chromosome will remain inactivated through subsequent cell divisions and differentiation, thus many cell lines are established with each individual cell in the line having either the same maternal or the paternal active X-chromosome (Nesbitt, 1971). Hence heterozygotes for any X-linked genes would consist of two different clones of cells, consequently a mosaic (Nesbitt, 1971; Falconer and Avery, 1978; Nesbitt and Gartler, 1971) (figure 85).

As the PLP gene is known to be located on the X-chromosome (Mattei *et al.*, 1986), heterozygotes for PLP mutations such as *jp*, *md rat* and *sh pup* are, therefore, chimaeras for the oligodendrocyte population since two different clones of oligodendrocytes exhibiting different properties are generated after the inactivation. This results in the "wild type" clone, where the mutant X-chromosome has been inactivated, and the "mutant clone" where inactivation of the normal X-chromosome occurred (Lyon, 1972) (figure 85). Several PLP mutant heterozygotes have been studied for the presence of mosacism in the CNS (table 8) where patchy areas of hypomyelination/amyelination have been observed (see below).

2. REVIEW OF OTHER CNS X-LINKED MUTANT HETEROZYGOTES

Heterozygote females for X-linked mutations affecting myelination such as *jp* in mice, *md* in rat and *sh pup* in dogs, typically exhibit patches of hypomyelination/amyelination. These are most notable in the optic nerves and to lesser degrees in the ventral columns of the spinal cord of the female heterozygotes (Rosenfeld and Friedrich, 1984; Rosenfeld and Friedrich, 1986; Bartlett and Skoff, 1986; Hatfield and Skoff, 1982; Benjamins *et al.*, 1984; Skoff and Montgomery, 1981; Duncan *et al.*, 1987a).

Another interesting feature of some heterozygotes such as *jp*, is the capacity for restoration of the myelin deficient areas (table 8). Phenotypically-mutant cells seemed to be influenced by phenotypically-normal clones of oligodendrocytes and, in some instances, capable of normal myelination (Bartlett and Skoff, 1986; Rosenfeld

and Friedrich, 1984; Rosenfeld and Friedrich, 1986). This phenomenon has been observed at the hypomyelinated patches of the spinal cord and anterior commissure in *jp* heterozygotes where hypomyelination of the tissue is not associated with mosaic pattern (Rosenfeld and Friedrich, 1984; Bartlett and Skoff, 1986; Rosenfeld and Friedrich, 1986) (table 8).

The summary of the most important characteristics of all the previously mentioned heterozygotes for PLP mutations indicated in table 8.

3. AIMS OF THE STUDY

As previous heterozygotes for PLP mutations showed myelin mosaicism at different locations of the CNS ascribed to the X-chromosome inactivation (Skoff and Montgomery, 1981; Hatfield and Skoff, 1982; Duncan *et al.*, 1987a), we wished to determine if the heterozygotes for jp^{rsh} exhibited mosaic changes similar to heterozygotes for *jp*, *md rat* and *sh pup* and if so, whether the lesions recover with age.

4. MATERIALS AND METHODS

a) *Breeding of the crosses*

Several cages containing two wild type (+/+) females of the same genetic background to the *jp^{rsh}* animals and a single hemizygous *jp^{rsh}* (*jp^{rsh}*/Y) male were established. It was predicted that the matings would produce heterozygous (*jp^{rsh}*/+) females and wild type (+/Y) males, which could be used as controls. Other wild type female mice of another strain (BALB/D2Ma) were also mated with hemizygous *jp^{rsh}* (*jp^{rsh}*/Y) males at the same time to check the authenticity of the results.

Homozygous *jp^{rsh}* (*jp^{rsh}/jp^{rsh}*) females were also mated with wild type (+/Y) males to demonstrate that the progeny resulting from the reverse cross followed the X-linked mutation patterns and that the carrier females produced were phenotypically similar to those obtained above. Additional identical crosses were also established and checked with wild type male mice of another strain (BALB/D2Ma).

b) *Morphological specimens*

Glial cell and quantitative studies were performed using the progeny of the wild type (+/+) females mated to the hemizygous (jp^{rsh}/Y) males. Groups of three heterozygous females and three wild type males mice from the same litter were used at 16, 30, 50 and 90 days of age for morphological studies. Additional females and males at other ages were also examined but were not included in the quantitative studies.

The tissue was prepared as described in chapter 2. Briefly, mice were anaesthetised until overdosed and fixed by intracardiac perfusion with normal saline followed by a modified Karnovsky's Paraformaldehyde/Glutaraldehyde (2%/5%) fixative. Tissue was post-fixed in either 1% osmic acid or an osmic acid/potassium ferricyanide mixture. Additional mice were perfused with 4% paraformaldehyde and processed for paraffin embedding and serial-sectioning. The blocks for the study were removed from C1-C2 segments of the spinal cord and mid portion of the optic nerves. The morphological studies were performed following the methods described in chapter 2.

c) Immunological techniques

The PAP technique was chosen for the detection of protein in paraffin and resin-embedded tissue sections of 90 day-old jp^{rsh} heterozygote females and male litter-mates CNS. Paraffin-embedded sections were used to assesse for the overall protein present and resin-embedded sections allowed the individual sheath identification. The ages of the mice, dissection and processing procedures as well as the antibodies used for all the following experiments are fully described in chapter 2.

The myelin protein composition of the individual sheaths was evaluated by immunostaining adjacent serial resin sections for MBP and 2 peptide regions of the PLP/DM-20 molecule one being PLP-specific and the other recognising the C-terminal common to PLP/DM-20, referred to as PLP/DM-20. The antibodies used for the study are also described in the materials and methods chapter 2 (table 6).

The ISH technique was based on that described by Cox *et al.* (Cox *et al.*, 1984) and modified by Wilkinson and co-worker's (Wilkinson *et al.*, 1987). It was performed on 6μm paraffin-embedded tissue sections of cervical spinal cord of 20 and 30 day-old heterozygotes and controls as above. Sections of heterozygous and control spinal cords were cut and placed on the same slide. The probe recognizing the PLP/DM-20 mRNA and the technique used are described in chapter 2.

B. RESULTS

1. CLINICAL SIGNS AND PHENOTYPIC EXPRESSION

Twenty-one female and 17 male progeny of the wild type (+/+) females and the hemizygous (jp^{rsh}/Y) males mattings were examined. These progeny were heterozygous (jp^{rsh}/+) females and wild type (+/Y) males, generating asymptomatic carrier females. A different cross between homozygous jp^{rsh}(jp^{rsh}/jp^{rsh}) females with a wild type (+/Y) male demonstrated that the clinical phenotype of the progeny followed the X-linked mutation patterns producing tremor in the resulting (jp^{rsh}/Y) males and identical carrier females.

The conclusion of the mattings was that the jp^{rsh} mutation followed an X-linked pattern of inheritance. The jp^{rsh} hemizygous males resulting from crosses involving other strains were phenotypically identical to the jp^{rsh} mutant.

2. MORPHOLOGICAL STUDIES:

a) Description of lesions

No obvious patchy areas of hypomyelination/amyelination similar to those occurring in *jp* heterozygous (*jp*/+) females were seen in these (jp^{rsh}/+) animals. Abnormalities were detected in the spinal cord at all ages but were more conspicuous in older animals and most marked around the ventromedian fissure. These lesions were visible at light microscopy using resin sections whereas no definitive changes could be defined in paraffin sections of the brain and spinal cord. Optic nerve abnormalities were not noticeable though subtle defects were demonstrated by quantitative methods (see below).

(1) Spinal cord

Cross sectional areas from the whole spinal cord and white matter were the same in age-matched heterozygous female and normal male mice. The major abnormality in the spinal cord of heterozygous females was the presence of fibres with a disproportionately thin myelin sheath for the axon diameter (figures 86, 87). Such fibres were usually intermixed with those having a normal thickness of sheath; several such hypomyelinated fibres could be contiguous but large hypomyelinated patches were not found. Naked axons were present in the ventral columns of younger mice but were infrequent in older animals (figure 86). The majority of myelin sheaths,

both of normal thickness and hypomyelinated, were well compacted although sheaths with uncompacted myelin or intramyelinic vacuolation were also observed as seen for *jp^{rsh}* (figure 87). Folds of redundant myelin were present in the spinal cord sections at all ages at a higher frequency than seen in normal litter-mates (figure 86, 87). Glial cells appeared to be increased in number (see next section). No obvious ultrastructural degenerative changes in neither oligodendrocytes nor astrocytes were seen. Many oligodendrocytes appeared metabolically active with prominent rough endoplasmic reticulum and Golgi apparatus, even in older animals. Activated microglia/macrophages were a constant though not marked feature. Very occasionally macrophages were observed within the myelin sheaths. Also undifferentiated oligodendroblasts as those described in chapter 3 (section C.) were observed sometimes in 50 and 90 days old heterozygote spinal cords.

(2) Optic nerve

No major changes were expected in the optic nerve of these heterozygote females as some *jp^{rsh}* homozygous females (*jp^{rsh}/jp^{rsh}*) and hemizygous males (*jp^{rsh}*/Y) exhibited only small abnormalities in the optic nerves when compared to the spinal cord. Light microscopy revealed no evidence of hypomyelinated/amyelinated patches in optic nerve sections stained either with methylene blue/azure II or immunostained against MBP. Apart from this, only infrequently was a vacuolated myelin sheath noted in the nerves of animals older than thirty days. One of the females produced from the (+/+ x *jp^{rsh}*/Y) matings had no obvious abnormalities in the spinal cord although defects were detected in the optic nerve (see discussion).

Electron microscopical examination of the optic nerves of heterozygotes revealed reasonably well myelinated axons similar to those of the wild type (figures 88, 28) although on occasions small groups of thin calibre, unmyelinated axons were present distributed randomly through the area of the nerve in older mice (figure 28a). This feature, which could also be observed in control optic nerves until about the age of 30 days, (figure 88) represented the only evidence of a mosaic pattern in these heterozygotes. Astrocytic processes were not obviously increased.

b) Glial cell quantification

(1) Glial cell densities

Total cell densities in the ventral columns of the spinal cord and optic nerve were significantly increased in the female heterozygotes, presenting values over the control but below the full *jp^{rsh}* mutant (figures 29, 35).

(2) Total glial cell counts

These were greater in the spinal cords of heterozygotes from the ages of 50 and 90 days than in the wild type male litter-mate (figure 89, 90). The total numbers of oligodendrocytes, astrocytes and other cells (microglial and unidentified cells) were all higher in the female heterozygote for jp^{rsh} although the major change was in the oligodendrocyte counts which were increased by 30 to 40% (figure 91). Similar differences were present in the optic nerve particularly at 50 days and older except that the total number of astrocytes was not increased (figure 92).

c) Fibre morphometry

(1) Myelin thickness and g ratio

In the ventral columns of the spinal cord the mean myelin sheath thickness was reduced and the mean *g* ratio increased in heterozygous females (figure 93). The differences were significant at all ages except 30 days. Scatter graphs of myelin sheath thickness and axon diameter indicated that many fibres in the spinal cord were within the limits of the normal male litter-mates although at each age a small proportion fell below the lower prediction band indicating a disproportionately thin myelin sheath (figure 94).

The results in the optic nerve contrasted with those in the spinal cord as neither differences in the mean myelin thickness nor mean *g* ratio were present between the two groups at any age (figure 95). Scatter graphs of myelin thickness and axonal diameter indicated that the vast majority of values in the heterozygotes were within the same limits as the normal male siblings as seen for the fully jp^{rsh} mutant.

(2) Myelin density

The reduction in optic nerve myelin density in the heterozygote female was due to a decreased number of myelinated axons as well as a reduction of the myelin sheath thickness. Point counting of the myelin of both spinal cord and optic nerve showed a significant reduction in the myelin density in the female heterozygote (figures 93, 95).

Axonal density was not significant differences between the two groups in the cord and optic nerve.

d) Mosaicism study through serial sections

Myelin mosaicism present in the optic nerve is a feature of many X-linked myelin mutants. An optic nerve of a 30 day-old *jp^{rsh}* heterozygote was serially-sectioned along its entire length and stained with methylene blue/azure II. No evidence of mosaicism was found. Paraffin-embedded semi-serial-sections of brain were also examined by haematoxylin/eosin staining and MBP immunostain. In no instance mosaic hypomyelinated/amyelinated patches were detected.

e) Age-related development of the lesions

One year-old heterozygotes and wild type males were perfused and compared to controls in order to evaluate the repair capacity as seen for other heterozygotes like *jp* where complete morphological (Bartlett and Skoff, 1986) and biochemical (Kerner and Carson, 1984; Benjamins *et al.*, 1989) recovery is almost achievable.

Unexpectedly, the CNS lesions in *jp^{rsh}* heterozygotes, were still detectable in sections of 1 year-old spinal cord. The myelin deficit in the optic nerve and spinal cord was maintained through the life of the heterozygote. Scattered hypomyelinated fibres, characteristic of the younger heterozygotes were still present although most smaller axons, initially hypomyelinated, had acquired normal myelin sheaths (figures 19, 20). The oligodendrocyte numbers remain increased with respect to wild type males in the oldest mice examined (1 year-old). Microglial cells, as expected in old CNS normal tissue were seen to increase in the same manner for both types of mice.

3. DISCUSSION

The conclusion of all the previous findings was that the chimaeric state in *jp^{rsh}* did not involve a mosaic myelination pattern in the CNS. Heterozygotes for the majority of PLP, X-linked mutations like *jp* in the mouse, *md* in the rat and *sh* in the pup (Skoff and Montgomery, 1981; Duncan *et al.*, 1987a; Bartlett and Skoff, 1986) are characterised morphologically by patchy areas of hypomyelination/amyelination constituting a mosaic pattern as a consequence of the early inactivation of one X-chromosome (Lyon, 1972; Nesbitt, 1971). However, the presentation of this condition is not uniform. Generally the optic nerve is more affected than the spinal cord which could be the consequence of the different developmental patterns of these tissues. The glial cells in the optic nerve proliferate *in situ* after migration from the brain whereas, the origin of the glial cells in the spinal cord is still unknown (see chapter 1 section A.2.). Here, glial progenitors may have

different division or migrating patterns which may provide a considerable plasticity to the clone of oligodendrocytes expressing the non-mutant X-chromosome for the partial reparation of the deficiency (Rosenfeld and Friedrich, 1984; Bartlett and Skoff, 1986). On the other hand, individual variations can also be found within a mutation. For example, only 2/3 of heterozygous *jp* females may have amyelinated patches, exclusively in the optic nerves (Rosenfeld and Friedrich, 1984; Skoff and Montgomery, 1981). Other areas of the CNS, such as the anterior commissure, may show a reduced amount of myelin without evidence of patches (Rosenfeld and Friedrich, 1984). Also the spinal cord of *jp* presents normally and abnormally myelinated fibres without a mosaic pattern (Bartlett and Skoff, 1986). In the *md rat* the severity and position of the patches varies considerably along a single optic nerve (Duncan *et al.*, 1987a). In the *sh pup* the patches may be larger in the spinal cord than in the optic nerves (Skoff and Montgomery, 1981; Duncan *et al.*, 1987a). Thus, the pattern of the phenotypic expression for jp^{rsh} heterozygotes was unpredictable. But, since the mutation is less severe, not so obvious lesions are likely.

The results of the morphological study showed changes in the spinal cord of jp^{rsh} heterozygous females similar to those in *jp* heterozygotes (Bartlett and Skoff, 1986), particularly around the ventromedian fissure where normally- and abnormally-myelinated axons were present, although they were not grouped in patches but intermingled. Occasional aggregations of amyelinated small diameter fibres were present in younger heterozygotes. However, large diameter fibres, were more affected by hypomyelination/amyelination in older jp^{rsh} heterozygotes. Morphometric analysis of the cord supported the visual impression demonstrating a population of axons with disproportionately thin myelin sheaths. One of the females produced from the ($+/+ \times jp^{rsh}/Y$) matings demonstrated abnormalities in the optic nerves but not the spinal cord. It is possible that this female represented the extreme end of the X-inactivation distribution, with most spinal cord oligodendrocytes carrying the paternal jp^{rsh}-X-chromosome in the inactive condition, so allowing most myelin to be formed by functionally wild type cells.

The relatively minor changes in optic nerve myelination contrasted with both the spinal cord in the same mice and the optic nerve lesions in heterozygotes for *jp* in the mouse and *md* in the rat. Findings in the optic nerve of jp^{rsh} heterozygous females were minimal in most of the mice, being detected only by electron microscopy. No obvious amyelinated/hypomyelinated patches were observed but occasionally amyelinated-fibres, sometimes grouped in small bundles (two to four fibres), were identified, being the only indication of mosaicism. Morphometric analysis failed to show any difference in myelin sheath thickness relative to axon diameter confirming that most myelinated axons had a sheath of a normal thickness.

This result was supported by the findings in the optic nerves of jp^{rsh} hemizygous (jp^{rsh}/Y) male and homozygous (jp^{rsh}/jp^{rsh}) females where only myelinated fibres appeared normal and slight abnormalities were present when compared to the spinal cord (see chapter 3). Calculation of myelin density using the point counting method indicated that the total amount of myelin was reduced in heterozygote optic nerves, presumably correlating with the increased number of amyelinated axons. Similar myelin reduction in the absence of the mosaic distribution were seen in the anterior commissure (Rosenfeld and Friedrich, 1984) and in the myelinated patches of the optic nerve (Bartlett and Skoff, 1986) *jp* heterozygotes.

Total glial numbers and density were consistently higher in both spinal cord and optic nerves of the jp^{rsh} heterozygotes compared to their normal male siblings. The differences detected are ascribed to the heterozygous state and not to the different sex of the mice, as previous studies in wild type and jp^{rsh} animals demonstrated no differences between males and females (Griffiths *et al.*, 1990). The glial cell numbers in the heterozygote spinal cord were approximately intermediate of the wild type and full jp^{rsh} mutation. The absolute number of oligodendrocytes was elevated, although the proportions of cell types (oligodendrocytes, astrocytes, microglia and others) in the heterozygotes were similar. However, the increases were relatively small compared to the full jp^{rsh} phenotype, and were significant only in older animals. Cell death (Knapp *et al.*, 1990) or the presence of abnormal oligodendrocytes (Duncan *et al.*, 1987a), which are associated with the hypomyelinated patches in other mutants, was not a feature. Oligodendrocytes appeared to be metabolically active and "healthy". Occasionally immature oligodendroblasts as those previously described for the full jp^{rsh} mutant were seen possibly indicating some oligodendroglial replacement.

jp carrier females show a progressive repair of the myelin deficit in the brain anterior commissure (Rosenfeld and Friedrich, 1984) and in the spinal cord (Bartlett and Skoff, 1986), so that by adulthood full recovery has been achieved. However, poorly ensheathed areas of the optic nerve did not improve with age (Bartlett and Skoff, 1986). The reason(s) for recovery are not fully defined but several factors may operate. Although approximately 50% of oligodendrocytes should carry the mutation in the active condition due to random X-inactivation it may be that cell selection favours precursor cells carrying the wild type allele so that with time cells of this lineage will predominate. Additionally, there is evidence that *jp* cell survival is improved, cell death is decreased and functions of differentiated oligodendrocytes are enhanced when *jp* and "normal" oligodendrocytes are contiguous *in vivo* (Knapp *et al.*, 1990) or when *jp* cells are cultured in medium conditioned by normal glia (Bartlett *et al.*, 1988). It has also been reported that the oligodendrocyte cell division rate is increased during early adulthood suggesting that neuroglial cells in *jp*

heterozygote brain detect the myelin deficit and respond with a compensatory increase in the oligodendrocyte production (Rosenfeld and Friedrich, 1986). *jp^{rsh}* heterozygotes show an increased oligodendrocyte population in the optic nerve which do not occur in the full *jp^{rsh}* mutant where after 45 days of age the glial cell numbers drop below normal values (see chapter 3, section 5.C.). This phenomenon could signify that the presence of phenotypically-normal clones of oligodendrocytes may stimulate the oligodendrocyte cell division and/or the cell survival as it has been described for other mutants (Rosenfeld and Friedrich, 1986; Bartlett *et al.*, 1988; Knapp *et al.*, 1990). A similar phenomenon may take place in the spinal cord of the *jp^{rsh}* female heterozygote. However, as for yet unknown reasons, the spinal cord evolution in full *jp^{rsh}* involves an over-production of oligodendrocytes, this finding is not obvious.

The evolution of the lesions in the spinal cord of *jp^{rsh}* heterozygote seems to follow a similar pattern to *jp* heterozygotes where small diameter axons myelinate with age. A similar phenomenon has also been described for the full *jp^{rsh}* mutant (see chapter 3.C.) However *jp^{rsh}* heterozygote females never achieve full recovery as thinly sheathed fibres and were readily detectable in the spinal cord up to the age of 90 days. These fibres, presumably myelinated by oligodendrocytes carrying the *jp^{rsh}* mutation, behaved as expected for those previously described Schwann-cell-like oligodendrocytes in the mutant cord (see discussion on chapter 3.C.), thus they myelinated a single axon at early myelination.

Findings in *jp^{rsh}* heterozygotes could be explained, taking into account that as *jp^{rsh}* oligodendrocytes appear metabolically active (on morphological criteria) and survive well into adulthood (Griffiths *et al.*, 1990; Fanarraga *et al.*, 1992a; Fanarraga *et al.*, 1992b). Hemizygous *jp^{rsh}* males and homozygous *jp^{rsh}* females demonstrated that, altough the mutant spinal cord acquires extra myelin sheaths as the animal ages, large fibres, myelinated by Schwann-cell-like oligodendrocytes do not recover. In *jp^{rsh}* heterozygotes some of these cells will carry the *jp^{rsh}* allele in the active from and would successfully compete with those carrying the wild type allele in early myelination producing abnormal myelin sheaths thus, preventing subsequent myelination by the wild type clone of oligodendrocytes.

C. STUDY OF THE PROTEIN PRODUCTION IN *jp^{rsh}* HETEROZYGOTE

1. INTRODUCTION AND AIMS

This studies were performed in order to complete the description of the *jp^{rsh}* heterozygote female. Immunostaining for MBP and PLP/DM-20 would provide us of valuable information such as whether there is immunodetectable myelin in the area of study as well as the protein composition of the myelin sheaths present. ISH experiments would reveal the proportion of actively expressing oligodendrocytes. These findings could them be compared with the homozygous female and hemizygous male *jp^{rsh}* mutant and wild type.

2. PAP RESULTS

The majority of the myelin sheaths immunostained for both MBP and PLP. Occasionally MBP-positive sheaths failed to immunostain with PLP/DM-20 or sheaths reacting with the PLP/DM-20 antiserum were negative with the PLP-specific antiserum. Therefore at least three types of immunocytochemically-defined myelin sheaths were present in the heterozygotes which were MBP+/PLP/DM20+/PLP+; MBP+/PLP/DM20+/PLP- and MBP+/PLP/DM20-/PLP-.

Resin-embedded 1 μm semi-serial sections of the optic nerve and 5-6 μm paraffin-embedded semi-serial sections of the brain were immunostained against MBP to detect possible areas of focal hypomyelination/amyelination. No patches in the distribution of the myelin were detected.

3. *IN SITU* HYBRIDIZATION RESULTS

Visual inspection of autoradiograms from 20 and 30 day-old mice suggested no marked differences in either the number of PLP/DM-20 expressing cells or the intensity of signal per cell between normal male and heterozygous animals (figure 96). However, quantitative data identified an increase of 34 and 36% in the total numbers of expressing cells in white matter of the cervical cord of the 20 and 30 day-old heterozygote females, respectively.

These results indicate that there is no deficiency in the numbers of PLP/DM-20 mRNA-expressing cells in *jp^{rsh}* heterozygotes and suggest a slight increase in oligodendrocytes as deduced from the morphological studies. The individual cell

PLP expression was not analysed on dissociated cells as for the full *jp^{rsh}* mutant. However, visual inspection of the autoradiograms from the spinal cord of the heterozygote did not reveal an obviously decreased signal (figure 96).

4. DISCUSSION

Immunocytochemistry of the spinal cord revealed that all the sheaths, reacted with MBP antiserum. The majority of myelin sheaths reacted with the PLP-specific and PLP/DM-20 antiserum, contrasting with the findings for the homozygous *jp^{rsh}* female and hemizygous male mutants (Griffiths *et al.*, 1990) where reactivity for both, and in particular the PLP-specific antiserum, was severely reduced. Immunostaining against MBP in serial-sections of several locations of the CNS revealed no areas of amyelination/hypomyelination.

The *in situ* hybridization results indicate that there is no obvious defect in the number of PLP-expressing cells in *jp^{rsh}* heterozygotes. Oligodendrocytes in the amyelinated patches of the optic nerve of the *md rat* show an absence or severe reduction of PLP-expressing cells (Duncan, I.D., personal communication). As these patches were not detected in *jp^{rsh}* heterozygote females, the location of those oligodendrocytes expressing the *jp^{rsh}*-allele could not be determined, although, according to results for the full *jp^{rsh}* mutants, cells carrying the active *jp^{rsh}*-allele would express a lower signal than the oligodendrocytes from the wild type clone.

D. CONCLUDING REMARKS

Heterozygotes for mutations of the PLP gene represent an interesting target for the study of the interactions of mutant and wild type clones of oligodendrocytes generated after the inactivation of either X-chromosome thus producing a chimaera (Nesbitt, 1971; Falconer and Avery, 1978; Nesbitt and Gartler, 1971; Lyon, 1972). This heterozygote condition, which is reflected as a mosaic myelinating pattern for other PLP mutations such as *jp*, *md rat* and *sh pup*, did not affect jp^{rsh} heterozygote females in the same way.

The jp^{rsh} heterozygotes which are presumably, also chimaeras for the oligodendrocyte population did not show mosaic patches. None of the areas of the CNS that were studied demonstrated hypomyelinated/amyelinated areas despite showing histological abnormalities and an important myelin reduction which did not recover in time. In conclusion, the studies carried out on jp^{rsh} heterozygote have shown several major differences from other X-linked PLP mutants which may be attributed to the capability of jp^{rsh}-expressing oligodendrocytes to survive in time maintaining their abnormal activity, consequently not being replaced by wild type cells.

The elevated oligodendrocyte numbers in the optic nerve of the jp^{rsh} female heterozygotes, which does not take place in the homozygous (jp^{rsh}/jp^{rsh}) female or in the hemizygous (jp^{rsh}/Y) male, may represent an indication of the increased proliferation and/or the improved cell survival of the phenotypically-mutant clones of cells under the influence of phenotypically-normal oligodendrocytes as previously described for *jp* mutants (Rosenfeld and Friedrich, 1986; Bartlett *et al.*, 1988; Knapp *et al.*, 1990).

FINAL REMARKS

jp^{rsh} has proved to be a useful mutation of the PLP gene and provides compelling evidence for the uncoupling of hypomyelination and premature oligodendrocyte death. Other dysmyelinating non-X-linked mutations such as *shi* or *qk* do not exhibit a similar paucity of oligodendrocytes. Therefore, it has been suggested that a product of the PLP gene may be required for cell survival (Gencic and Hudson, 1990; Hudson, 1990b; Vermeesch *et al.*, 1990; Nadon *et al.*, 1990). Recent investigations have indicated that DM-20 may play additional role(s) involving cell survival and/or differentiation which might not be restricted to the oligodendrocytes. The expression of DM-20 is developmentally regulated, thus DM-20 levels which, in most species, constitute a minor proportion of the total CNS proteolipids, show an inverted ratio in embryonic CNS tissue (Schindler *et al.*, 1990; Campagnoni *et al.*, 1992). DM-20 mRNA has been detected in embryonic mouse brain long before differentiated oligodendrocytes appear in the tissue (Timsit *et al.*, 1992; Ikenaka *et al.*, 1992). All glial cells (Timsit *et al.*, 1992; Kamholz *et al.*, 1992) in addition to some neuronal cell lines, also express DM-20 (Ikenaka *et al.*, 1992). However in neuronal cell lines DM-20 mRNA activity dropped when the cells differentiated (Ikenaka *et al.*, 1992). Myocardial and spleen cells also express DM-20 mRNA (Campagnoni *et al.*, 1992).

These findings point to other possible functions of this protein which are absent in all PLP mutants, except *jp*^{rsh}, and result in the early oligodendrocyte death. We do not know why a point mutation in PLP^{Ile186} affecting the putative fourth membrane domain of the PLP and DM-20 molecules demonstrates this different phenotype. However, despite *jp*^{rsh} producing a mutated DM-20, this protein may be functional, allowing *jp*^{rsh} oligodendrocytes to survive well into adulthood. Other PLP mutants such as *sh pup* and *jp*^{msd} mice also produce detectable DM-20 (Gardinier and Macklin, 1988; Yanagisawa *et al.*, 1987) yet these point mutations may affect other more vital sequences of the protein, impeding its normal folding and/or insertion in the membrane. Nevertheless, it must be emphasised that this role for DM-20 is still hypothetical and as yet there is no direct proof of its direct involvement in cell survival or differentiation.

It is also unknown if DM-20 plays any structural role. It has been commonly accepted that PLP maintains the correct spacing between apposed bilayers as a result of the homophilic interactions involving the major hydrophilic loop of PLP (Schindler *et al.*, 1990). This highly charged sequence of the PLP molecule which plays a key

role in stabilization of the IPL, is almost entirely missing in DM-20 (Schindler *et al.*, 1990). Therefore, although DM-20 is inserted in the membrane and would, perhaps contribute to the stability of the IPL, it will never be as competent as PLP in maintaining this membrane arrangement. PLP-deficient mutants such as *jp^{rsh}*, that produce sufficient DM-20, may take advantage of this structural property. In fact, as *jp^{rsh}* produces very little PLP, the intermingling and interaction of both proteins in the myelin membrane may be responsible for the final compaction attained in some of the sheaths. On the other hand, as the hydrophobic interactions of DM-20 are not as suitable as those of PLP, this would be reflected ultrastructurally as an abnormal IPL which would be absent, split or vacuolated. The vacuolation observed in *jp^{rsh}* myelin sheaths might be the result of a poor anchoring of the IPL that would split either *in vivo* or perhaps as an artefact as a result of the fixation of the tissue and/or the histological processing of the specimen.

Another interesting conclusion derived from the study of *jp^{rsh}* mutation is the evidence of the heterogenicity of the oligodendroglial population. Del Rio Hortega silver carbonate stain of oligodendrocytes in 1923 revealed four classes of myelinating cells of which type IV would correspond with those recently described Schwann-cell-like oligodendrocytes seen in the embryonic feline cord (Remahl and Hildebrand, 1990). These cells responsible for the early myelination of the larger fibres would constitute an individual oligodendroglial population. Later in development there would be a second wave of myelination involving oligodendrocytes which at this stage are still undifferentiated and actively dividing. These cells would eventually complete ensheathment of the smaller fibres. Larger fibres in the *jp^{rsh}* spinal cord show an obvious hypomyelination and this is manifested by poor myelin deposition together with vacuolation of the sheath. However, smaller axons, which are initially unmyelinated, progressively acquire sheaths of a reasonably normal appearance. The possible explanation for this phenomenon, according to those previously-mentioned descriptions of oligodendrocytes in the developing CNS, suggests at least two sub-populations of oligodendrocytes. The early myelin sheaths therefore, correspond to oligodendrocytes myelinating in a Schwann-cell-like fashion, explaining the histological findings. These sheaths will still be detectable at older ages since *jp^{rsh}* oligodendrocytes survive into adulthood. The second type of oligodendrocyte that differentiates later in development and myelinates the smaller axons, displays its myelin deficiency by producing less myelin internodes per cell, rather than less myelin per internode as in the case of early oligodendrocytes. In this way, those myelin sheaths present exhibit normal thickness yet, many axons remain unmyelinated. Attending to these characteristics, the second type of oligodendrocyte could represent a more immature form than the early type. Thus, they may be capable of proliferating provided there are unmyelinated axons and/or the appropriate

tissue signals until complete myelination. This hypothesis has been partially supported by the increased ^{3}H-thymidine labelling of the spinal cord indicating an increased cell division rate. However, this contribution of extra oligodendrocytes does not seem to occur in the optic nerve where there are plenty of unmyelinated axons which do not acquire a myelin sheath. Findings in the dorsal columns of the spinal cord, where axons have a similar size as in the optic nerve and there is an increased oligodendrocyte proliferation, attain myelin sheaths. Findings indicate that the reason for the hypomyelination in the optic nerve is due to the decreased oligodendrocyte proliferation, perhaps involving a increased cell apoptosis, which may be a consequence of the individuality of these structures where the oligodendroglial precursor pool might be smaller and the axonal population completely different in origin and nature. These results lead to the conclusion that the CNS is very heterogeneous in nature and that each tract is capable of maintaining its own idiosyncrasy being particularly manifested in deficient situations.

Tissue culture experiments demonstrated that optic nerve and spinal cord oligodendrocytes developed in a similar fashion in terms of MBP and DM-20 production. However, the cell survival of the optic nerve cells seemed somewhat reduced when compared to cells cultured from the wild type optic nerve or the mutant spinal cord. Although this finding could be the result of deficient tissue manipulation or poor culture conditions, they point to the possibility of a decreased cell survival in the optic nerve as wild type oligodendrocytes developed normally under the same conditions. On the other hand oligodendrocyte numbers in the optic nerve, which are appropriate at myelination, seem to decline after 40-50 days in the mutant showing no signs of further replacement. Although cell death was not obvious in any of the nerves examined, apoptosis could have taken place with dead cells being cleared from the tissue in a very short time (Barres *et al.*, 1992; Raff, 1992), such reasoning could explain the findings. Although DM-20 may promote cell survival, it is more likely that other signals of unknown nature, present in the spinal cord but not in the optic nerve, are responsible for the increased cell division and later myelination, while DM-20 may be involved in further differentiation of the newly produced cells. The optic nerve in the female heterozygote ($jp^{rsh}/+$) showed an increased oligodendrocyte population. This may account for the possibility of mutant cell survival and/or proliferation being enhanced *in vivo* when influenced by phenotypically normal clones of oligodendrocytes. A similar phenomenon could also occur in the spinal cord. However, as the cell population is already increased in full jp^{rsh} mutants this could not be determined.

All the previously discussed topics indicate that the role of DM-20 in cell survival and development has probably been underestimated so far. Further

investigations will be necessary to clarify the involvement of this protein in embryogenesis and cell differentiation probably not only restricted to the CNS.

jp^{rsh} represents one system in which to carry out further studies as DM-20 production in the CNS is unencumbered by the usually more prominent PLP.

TABLES

MARKERS	O-2A PERINATAL	O-2A ADULT	OLIGODEN-DROBLAST	MATURE OLIGODENDROCYTE	TYPE-2 ASTROCYTE	TYPE-1 ASTROCYTE
A2B5	positive	positive	positive	negative	positive	negative
NSP-4	positive	positive	positive	positive	positive	negative
Vim	positive	negative	positive	positive->negative	positive	negative
O4	negative	positive	positive	positive	positive	negative
Transferrin	negative	negative	positive	positive	negative	negative
GalC	negative	negative	positive	positive	negative	negative
GFAP	negative	negative	negative	negative	positive	positive
Ran-2	negative		negative	negative		positive
CBAM	negative	positive	positive	positive	positive	
GPDH	negative	negative	negative	positive	negative	negative
CAII				positive	negative	negative

Table 1: Characteristics of some of the antigens that can be used to identify O-2A lineage glial cells and type-1 astrocytes.; (Noble *et al.*, 1989; Espinosa de los Monteros and Vellis, 1990; Pfeiffer *et al.*, 1990).

MONOCLONAL ANTIBODY	ANTIGEN	DETECTION IN SPINAL CORD
O3, O4, O5, O6	sulfatide	Postnatal day 0
O1, O2, O7	GalC	Postnatal day 0
O8	Lipid	Postnatal day 0
O9	Lipid	Postnatal day 0
O10	Protein	Postnatal day 2
O11	Lipid	Postnatal day 4
O12	Lipid	N.D.

Table 2: Properties of the antibodies O1 through O12 and time of detection in the mouse cervical spinal cord (Sommer and Schachner, 1981; Kuhlmann-Krieg *et al.*, 1988).

PROTEIN	SITE OF SYNTHESIS	LOCATION	% PROTEIN	FUNCTION	MODE OF TRANSPORT
MBP	Outer longue process. Free polysomes	Compact myelin	30%	Compaction of cytoplasmic leaflets	mRNA translocation
PLP/DM-20	Perinuclear cytoplasm. RER & Golgi apparatus	Compact myelin	50%	Compaction of extracellular leaflets	Vesicular. Microtubules.
CNP	Perinuclear cytoplasm. Free polysomes	All surface membranes except compact myelin	5%	Unknown	Vesicular? Soluble?.
MAG	Perinuclear cytoplasm. RER & Golgi apparatus	Periaxonal	1%	Axonal interactions	Anterograde: vesicular and microtubules. Retrograde: endosomes

Table 3: Table of the distribution of the myelin products in actively myelinating oligodendrocytes (Trapp, 1990).

SUBSTANCE	HUMAN	BOVINE	RAT
Total protein	30	24.7	29.5
Total lipd	70	75.3	70.5
Cholesterol	27.7	28.1	27.3
Total galactolipids	27.5	29.3	31.5
cerebroside	22.7	28.1	27.3
sulfatide	3.8	3.6	7.1
Total phospholipid	43.1	43	44
ethanolamine phophoglycerides	15.6	17.4	16.7
choline	27.7	28.1	27.3
serine	27.5	29.3	31.5
inositol	27.5	29.3	31.5
sphingomyelin	22.7	28.1	27.3
Plasmalogen	12.3	14.1	14.1

Table 4: Lipid distribution in human, bovine and rat CNS myelin (Norton and Cammer, 1984). Protein and lipid figures are expressed as percentage of dry weight; all others are expressed as percentage of total lipid weight. Plasmalogens are primarily ethanolamine phosphoglycerides.

DYSMYELINATING DISORDER	MUTATION	EXON/ INTRON	AMINO-ACID CHANGE
jp	splice site	Intron 4	exon 5 deleted &6 and 7 frame shifted
jpmsd	point mutation	exon 6	242 Ala->Val
md rat	point mutation	exon 3	74 Thr->Pro
sh pup	point mutation	exon 2	36 His->Pro
*PMD**			
type I classical	point mutation	exon 4	162 Trp->Arg
type I	point mutation	exon 5	215 Pro->Ser
type II connatal	point mutation	exon 2	14 Pro->Leu
jprsh	point mutation	exon 4	186 Ile->Thre

Table 5: Summary of the most characteristic point mutations in the PLP gene (adapted from (Hudson, 1990a)). All these alleles, except jp^{rsh}, are lethal disorders characterised by the degeneration and death of oligodendrocytes as the primary cause of hypomyelination. In contrast to *jp*, jp^{msd}, *md* rat, *sh* pup and *PMD* the jp^{rsh} mouse demonstrates that changes of PLP structure can cause severe hypomyelination not associated with cell death.

(*) There are other forms of *PMD* described including a total deletion of the PLP gene (Raskind *et al.*, 1991).

PRIMARY ANTIBODY	DILUTION	SOURCE	PAP COMPLEX	SOURCE	LINK
anti-GFAP	1:1000	Dakopatts	anti-Rabbit	ICN	goat-anti-rabbit (1:50)
anti-MBP	1:400	Dr. J.M. Mattieu, (Lausanne, Switzerland.)	anti-Rabbit	ICN	goat-anti-rabbit (1:50)
anti-MBP	1:1000	Dr. N.P. Groome, (Oxford,UK.)	anti-Rat	SEROTEC	goat-anti-rat (1:10)
anti-PLP/DM-20 (aminoacids 271-276)	1:500-750	Dr. J.C. Nussbaum, (Strasbourg, France)	anti-Rabbit	ICN	goat-anti-rabbit (1:50)
anti-PLP specific (aminoacids 117-129)	1:500-750	Dr. J.C. Nussbaum, (Strasbourg, France)	anti-Rabbit	ICN	goat-anti-rabbit (1:50)
anti-PLP specific (aminoacids 117-129)	1:125	Dr. N.P. Groome, (Oxford,UK.)	anti-Rabbit	ICN	goat-anti-rabbit (1:50)

Table 6: Antibodies, dilutions, sources and antibody links used for the PAP immunostaining.

PRIMARY ANTIBODY	DILUTION	SOURCE	SECONDARY ANTIBODY	DILUTION	SOURCE
anti-GFAP	1:1000	Dakopatts	anti-Rabbit-IgG TRITC or FITC	1:300	SIGMA
anti-MBP	1:400	Dr. J.M. Mattieu, (Lausanne, Switzerland.)	anti-Rabbit-IgG TRITC or FITC	1:300	SIGMA
anti-MBP	1:1000	Dr. N.P. Groome, (Oxford,UK.)	anti-Rat-IgG1 FITC	1:200	SEROTEC
anti-PLP/DM-20 (aminoacids 271-276)	1:500-750	Dr. J.C. Nussbaum, (Strasbourg, France)	anti-Rabbit-IgG TRITC or FITC	1:300	SIGMA
anti-PLP specific (aminoacids 117-129)	1:500-750	Dr. J.C. Nussbaum, (Strasbourg, France)	anti-Rabbit-IgG TRITC or FITC	1:300	SIGMA
anti-PLP specific (aminoacids 117-129)	1:125	Dr. N.P. Groome, (Oxford,UK.)	anti-Rabbit-IgG TRITC or FITC	1:200-300	SIGMA (TRITC); SEROTEC (FITC)
anti-A2B5; O4; O1; O10; O11	1;2-10	Dr. I. Sommer (Glasgow,UK.)	anti-Mouse-IgG1 TRITC or FITC	1:300	SIGMA
anti-GalC (R-mAB)	1;2-10	Dr. I. Sommer (Glasgow,UK.)	anti-Mouse-IgG3 TRITC or FITC	1:200	Jackson Laboratories

Table 7: Antibodies, dilutions, sources and secondary antibodies used for immunofluorescence.

MUTATION	SIGNS	MOSAIC CHANGES
jp	no clinical signs	Periphery of the optic nerve; Periphery of the ventral colums of the spina l cord adjacent to pia. Anterior commisure: myelin reduction in the absence of patches.
		Spinal cord and anterior commissure recover morphologically and biochemically
md rat	no clinical signs	Periphery and centre of the optic nerves. No mosaicism present in the spinal cord.
sh pup	some heterozygotes mild clinical signs	Periphery of the optic nerve altough less noticeable than in the spinal cord. Spinal cord showing patches at various levels

Table 8: Review of the main characteristics of the *jp*, *md* rat and *sh* pup heterozygotes (Kerner and Carson, 1984; Rosenfeld and Friedrich, 1984; Rosenfeld and Friedrich, 1986; Skoff and Montgomery, 1981; Bartlett and Skoff, 1986; Benjamins *et al.*, 1989; Duncan *et al.*, 1986; Duncan *et al.*, 1987a).

FIGURES

O-2A LINEAGE

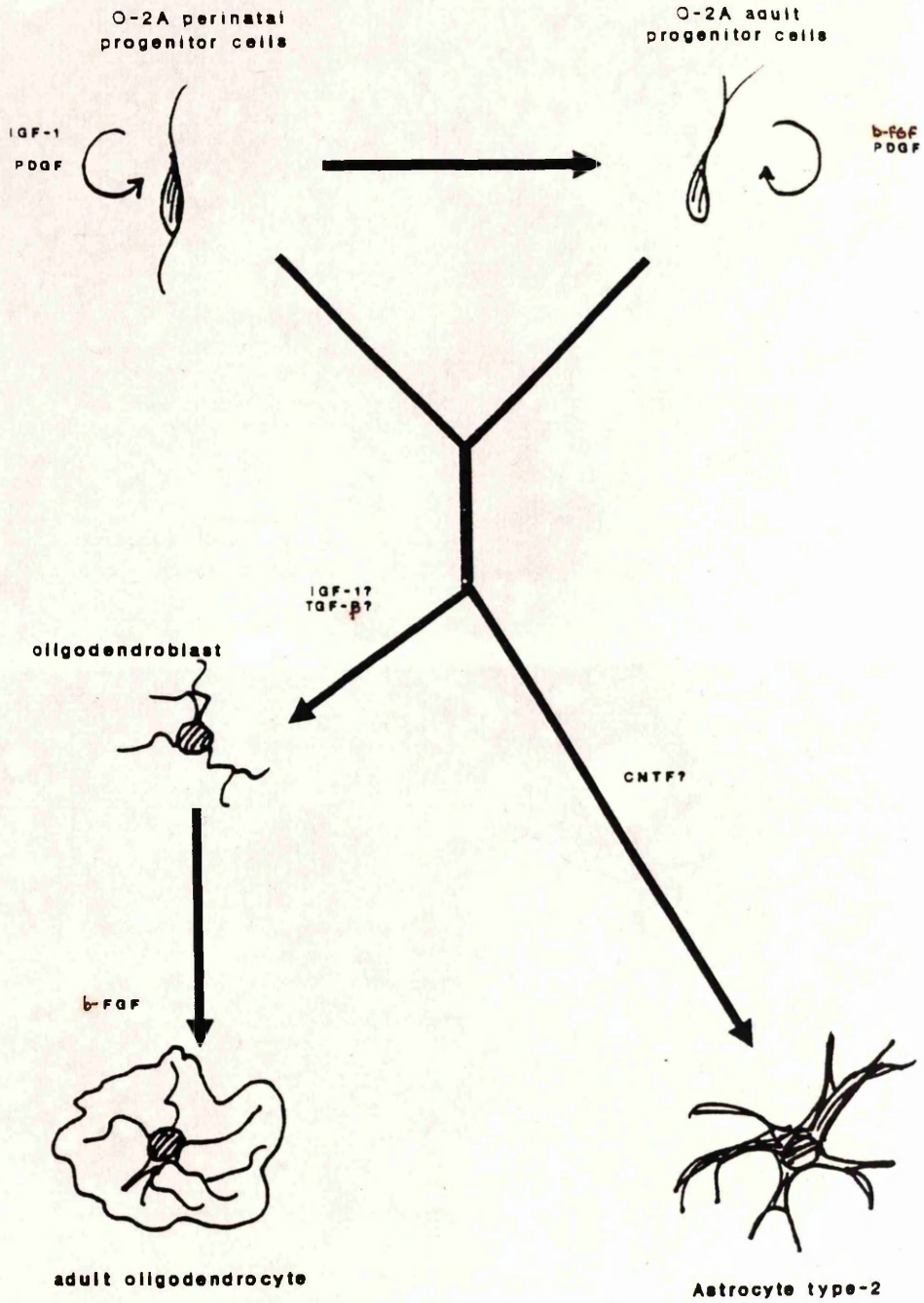

Figure 1: Proliferation characteristics of O-2A^{perinatal} and O-2A^{adult} progenitor cells and their derivatives (adapted from (Wolswijk and Noble, 1989; Noble *et al.*, 1989)). O-2A^{perinatal} are bipolar cells which divide symmetrically in the presence of type-I astrocytes which produce PDGF (Wolswijk *et al.*, 1991; Raff, 1989). O-2A^{adult} have a characteristic unipolar morphology and divide and differentiate asymmetrically such that a single clone of cell continues to generate more progenitors. Both O-2A^{perinatal} and O-2A^{adult} progenitors can differentiate into either oligodendrocytes or type-2 astrocytes. Astrocyte differentiation is induced by exposure to FCS or CNTF. Oligodendrocytes can be identified *in vitro* by their multipolar morphology, their antigenic expression and the lack of intermediate filaments which are present in type-2 astrocytes. The antigenic profiles of these cells are fully detailed in table 1.

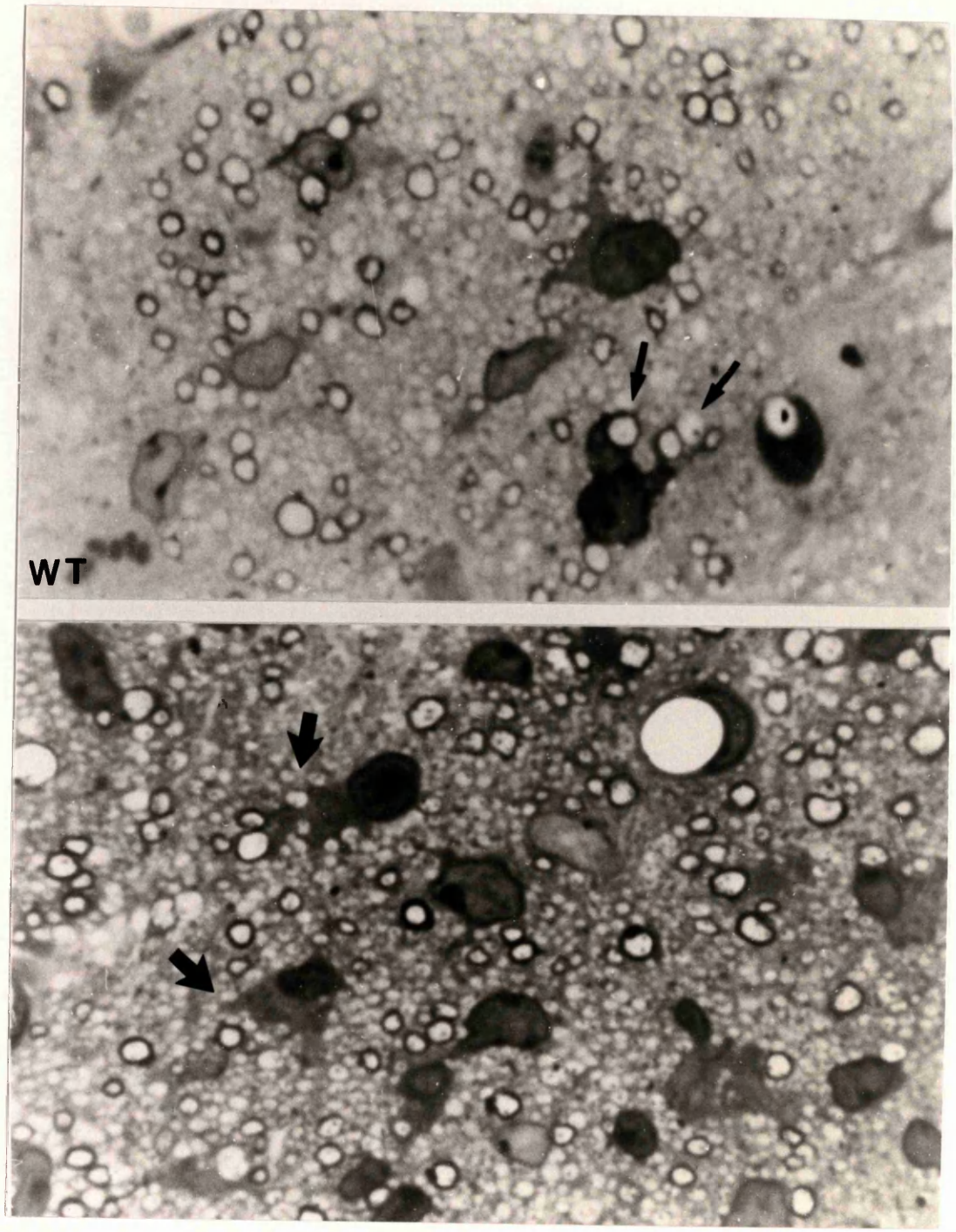

Figure 2: Light microscopic appearance of the developing spinal cord from 5-day-old wild type (WT) and 10-day-old *jp*^{rsh} mice (lower panel). Methylene blue/azure II stained resin sections from the C2 segment of the spinal cord. The myelination of the spinal cord commences with the ensheathment of the larger fibres as described by Remalh and Hildebrand (Remahl and Hildebrand, 1990). Processes of actively myelinating oligodendrocytes are seen ensheathing several large axons in both types of mice (arrows). Although the oligodendrocyte processes in the *jp*^{rsh} mutant contact nearby axons, many do not ensheath these fibres (thick arrows). (Approx. magnification: x 2000)

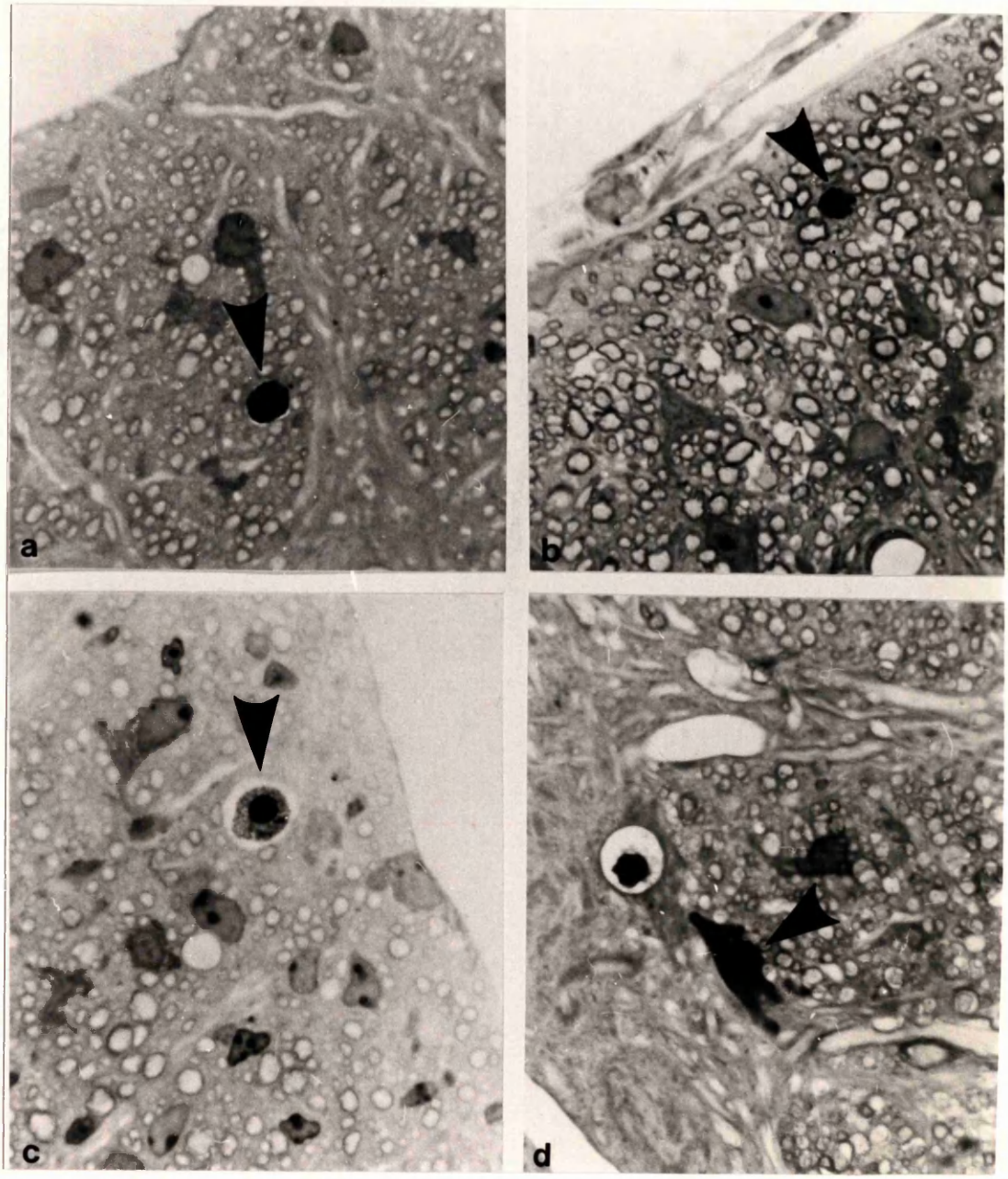

Figure 3: Light microscopic appearance of 10 and 16-day-old wild type (a, b) and *jp*^{rsh} mutant (c, d) spinal cord respectively. Methylene blue/azure II stained resin sections of the ventral white matter adjacent to the ventromedian fissure in the C2 segments. Examples of some glial cells which are probably suffering apoptosis (Raff, 1992) recognised by the condensed nuclear chromatin (arrow-heads). No significant increase in apoptotic cell numbers was seen in *jp*^{rsh}. (Approx. magnification: x 1000).

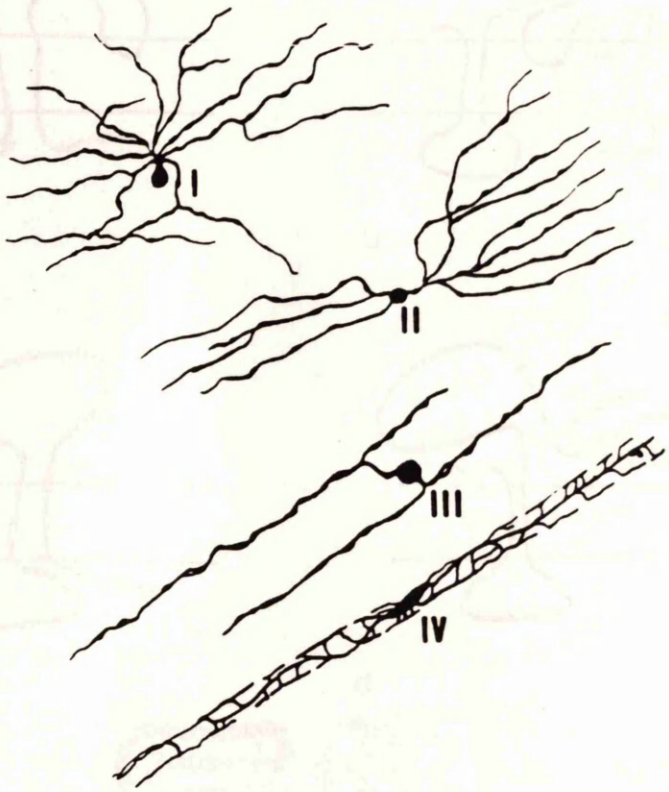

Figure 4: Representation of the four types of oligodendrocyte profile recognized by Del Rio Hortega in 1928 (Del Rio Hortega, 1922; Del Rio Hortega, 1924), and confirmed by Stensaas and Stensaas in 1968 (Stensaas and Stensaas, 1968). Type I is presumably related to many small myelin segments travelling through the tissue at many different angles. Type II is similar but related to segments of myelin within a fascicle containing many axons coursing in the same direction. Type III is related to two large segments of myelin and type IV to one large segment. Del Rio Hortega pointed at the similarity of the relationship between the type IV oligodendrocyte and the Schwann cell to the underlying myelin segments.

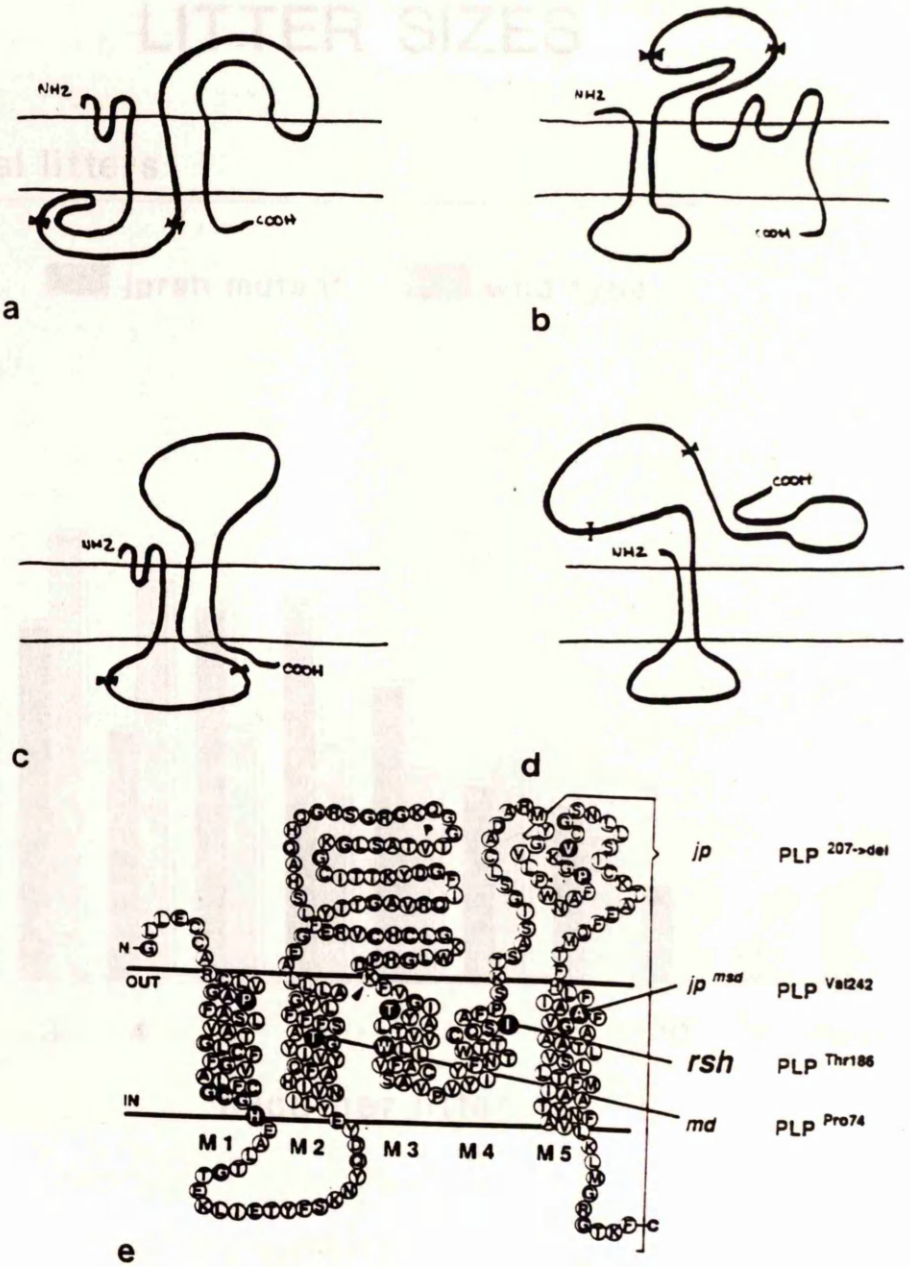

Figure 5: Schematic representation of the hypothetical models of PLP insertion in the myelin membrane and PLP mutations. a. (Laursen *et al.*, 1984); b. (Stoffel *et al.*, 1984); c. (Nave et al., 1987); d. (Hudson et al., 1989) and e. (Popot et al., 1991). PLP is the predominant integral membrane protein of the CNS and has multiple membrane spanning domains. DM-20 differs from PLP in the major hydrophilic domain of the 276-amino-acid. The position of the residues 116-150, absent in the DM-20 isoform, is indicated by arrowheads. The NH_2 end of the PLP molecule has been located at the extracellular side of the membrane for all the models. The model of PLP represented in figure 5.e. also shows the lethal mutations in the *jp* mouse (a deletion of the carboxy terminus), in the jp^{msd}, jp^{rsh} (rsh) and in the *md* rat. The position of other single-residue substitutions including several families with *PMD* are indicated by black circles. The wild type sequence (identical in rat, mouse and human) is shown. Putative alpha-helical membrane-associated domains of PLP are numbered M1 to M5.

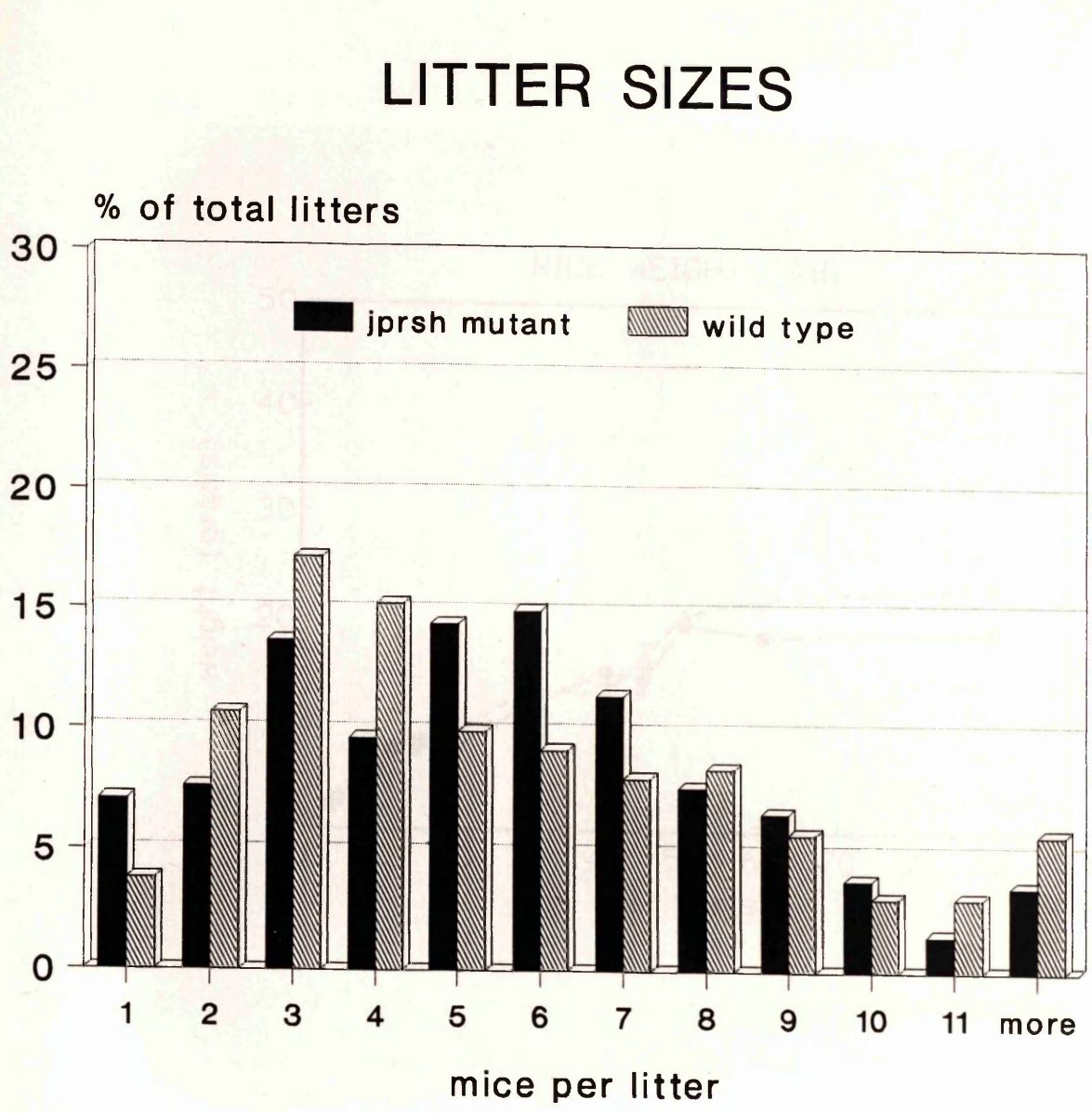

Figure 6: Results of the breeding studies. The data correspond to the percentage of the total litters studied, 394 for jp^{rsh} and 262 for the wild type.

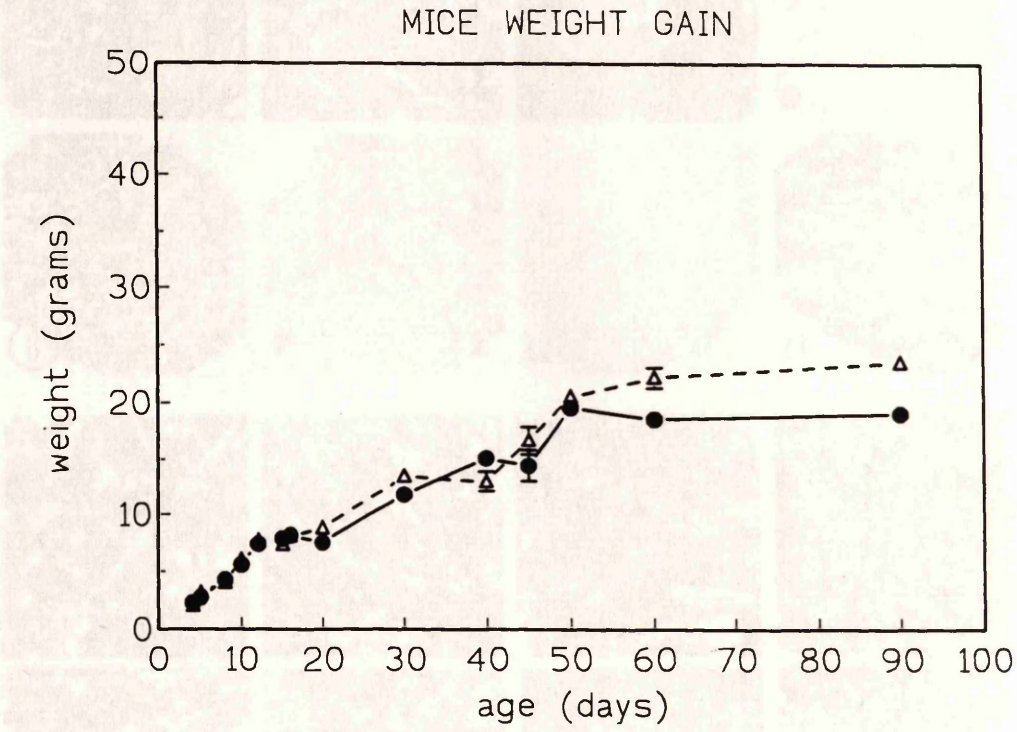

Figure 7: Age-related weight gains for both wild type (triangle) and jp^{rsh} mice (filled circle).

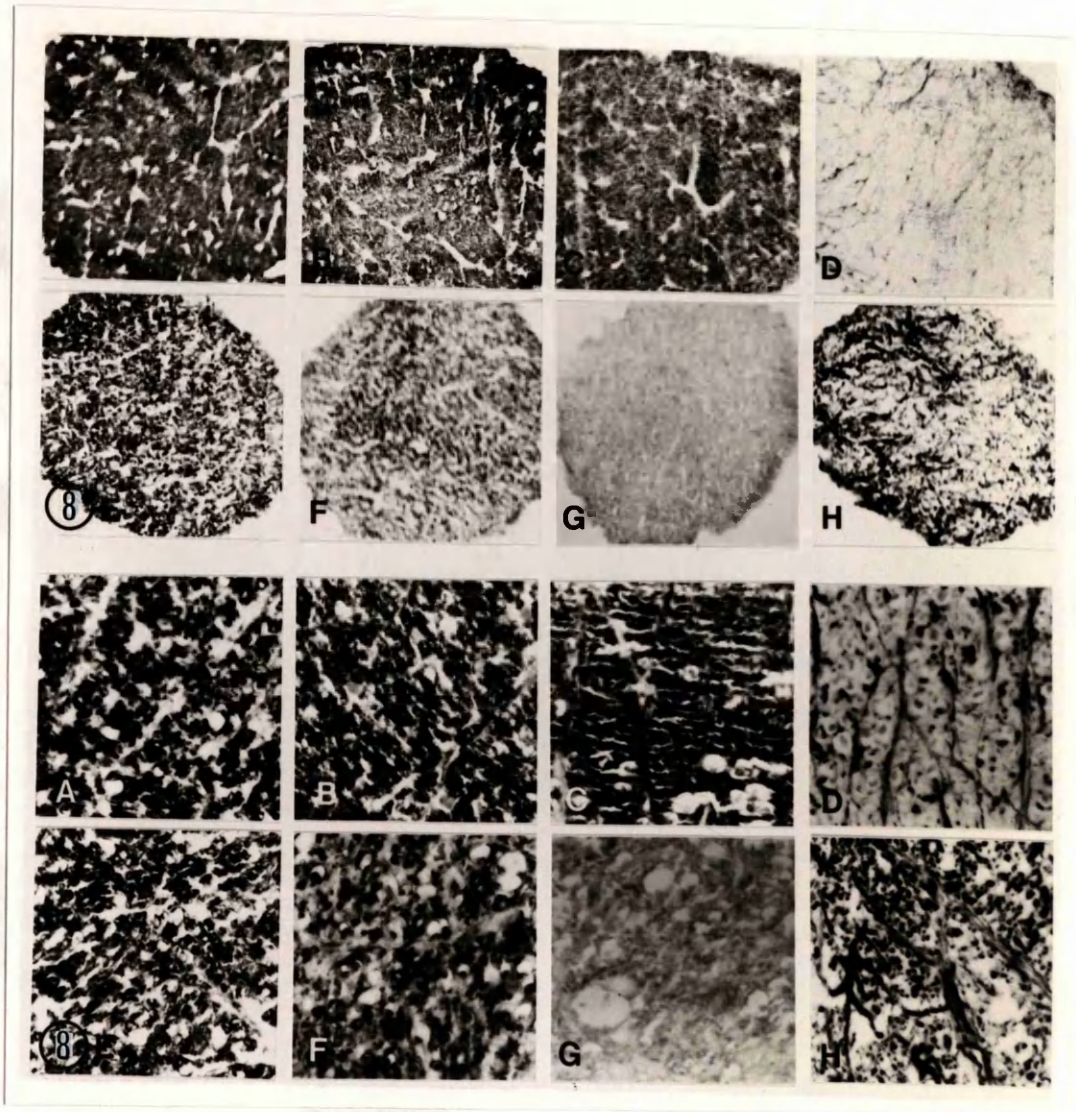

Figure 8: Immunostaining of optic nerves and ventral white matter of the spinal cord from 45-day-old mice. Upper panel: optic nerves from wild type and *jp*^{rsh} mice against MBP (A, E); PLP/DM-20 (B, F); PLP (C, G) and GFAP (D, H) using the PAP technique on paraffin-embedded sections. A-D are from wild type mice and E-H from *jp*^{rsh} mice. Lower panel: ventral white matter of the spinal cords from 45-day-old wild type and *jp*^{rsh} mice as before. Although all the myelin proteins are decreased in staining intensity in the *jp*^{rsh} the most profound reduction is seen with the PLP-specific antiserum. GFAP is increased in the mutants. (Approx. magnification: upper panel x 175, lower panel x 500).

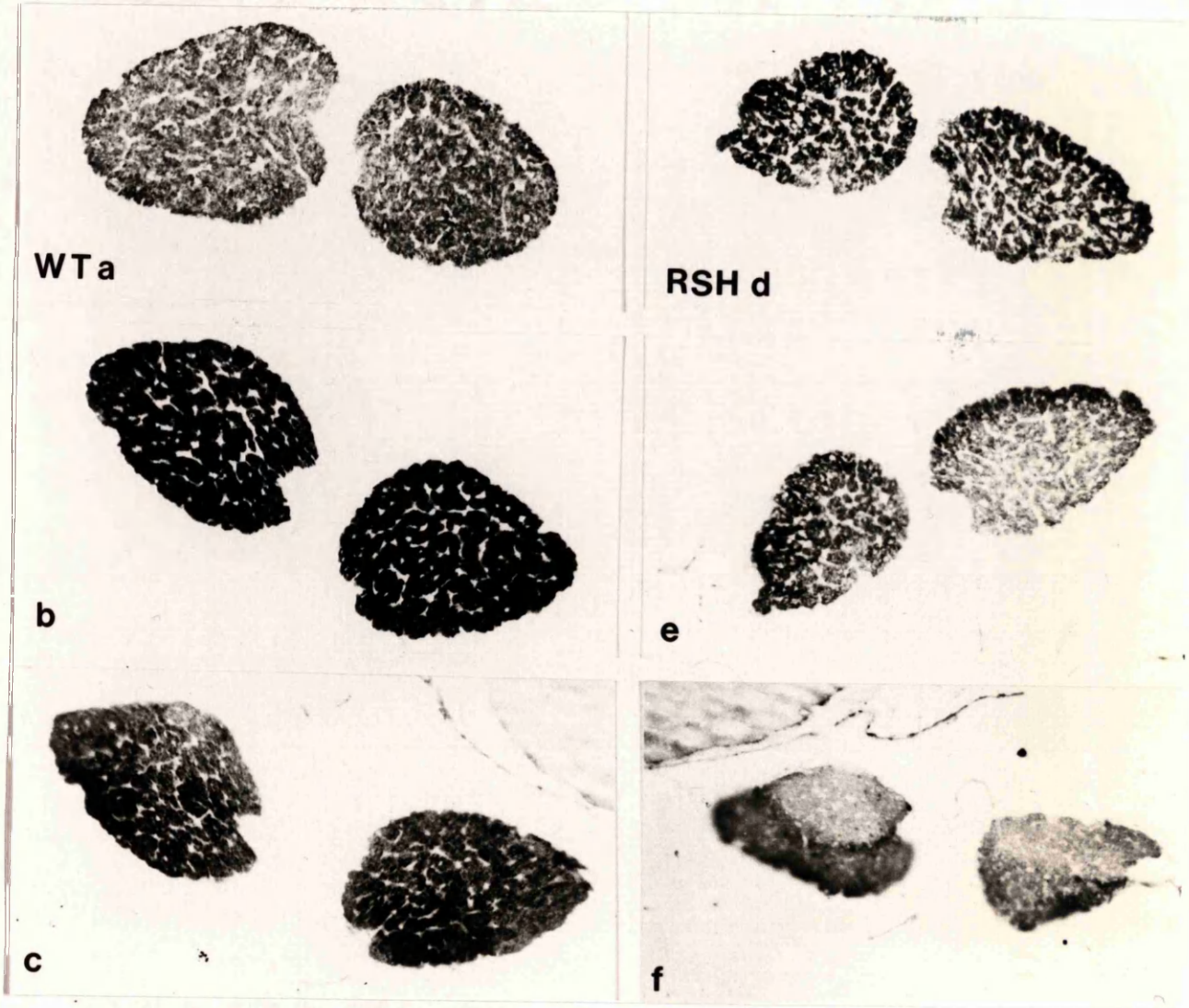

Figure 9: Immunostaining of optic nerves from 20-day-old from wild type (WT a, b, c) and *jp^{rsh}* mice (RSH d, e, f); MBP (a, d); PLP/DM-20 (b, e) and PLP (c, f) using the PAP technique on paraffin-embedded sections. At this age the amount of MBP in the mutant is slightly depleted. (Approx. magnification: x 90).

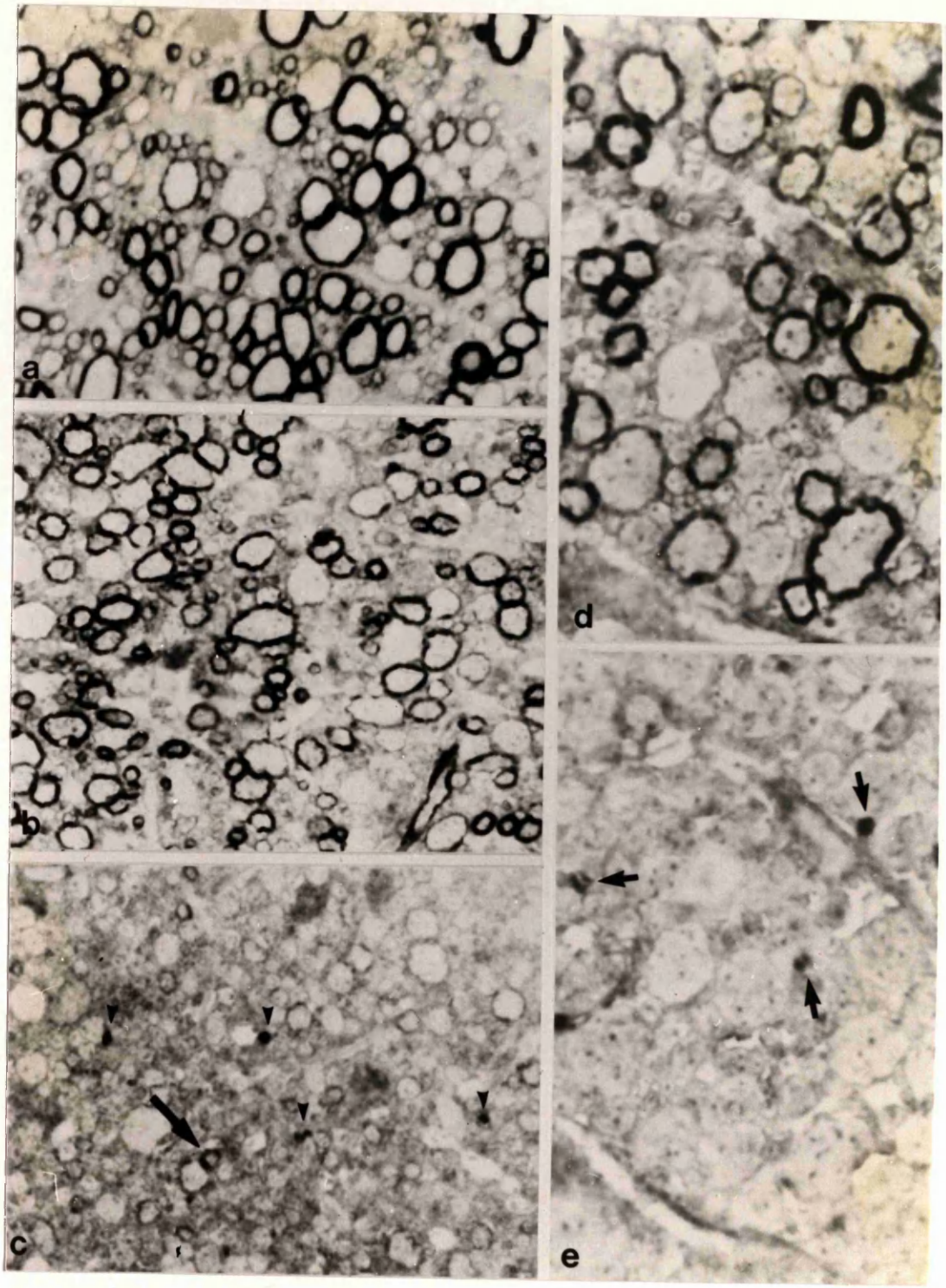

Figure 10: Spinal cord resin sections from 90-day-old jp^{rsh} mouse The sections are immunostained for MBP (a), PLP/DM-20 (b, d) and PLP (c, e). Numerous myelin sheaths are stained for MBP (a) and PLP/DM-20 (b). There is virtually no staining with the PLP specific antiserum except for a very occasional small sheaths (c,arrow-heads). Many axons lack a myelin sheath. Adjacent sections (d, e) show that the majority of sheaths present are immunostained by PLP/DM-20, whereas identical sheaths are not immunostained by the PLP-specific antiserum. The only PLP immunoreactivity present is frequently seen localised in clumps at the periphery of axons which may be included in the oligodendrocyte cytoplasm (c: arrowheads; e: small arrows). (Approx. magnification: a and c x 1000; d and e x 2000)

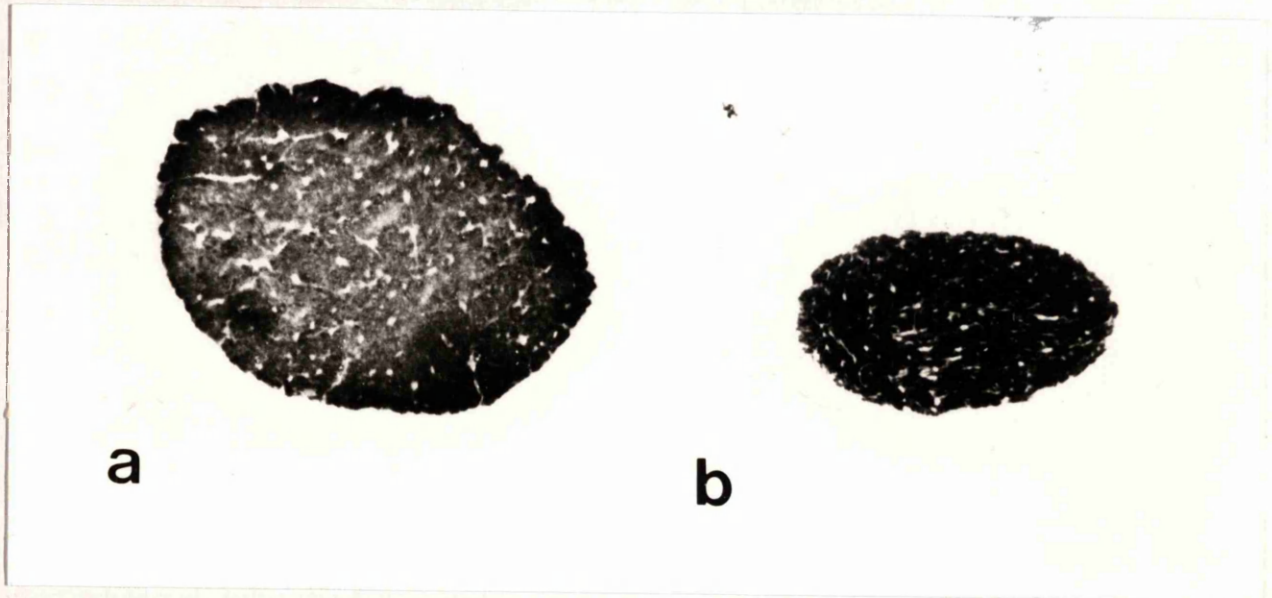

Figure 11: PLP/DM-20 immunostain of the optic nerves from 90-day-old wild type (a) and *jp*^{rsh} mice (b) using the PAP technique on paraffin-embedded sections. The PLP/DM-20 immunoreactivity at this age is similar to that detected in the wild type animals. There is an artefact present in the wild type optic nerve, the degree of staining should be as positive centrally as in the periphery of the section. (Approx. magnification: x 140).

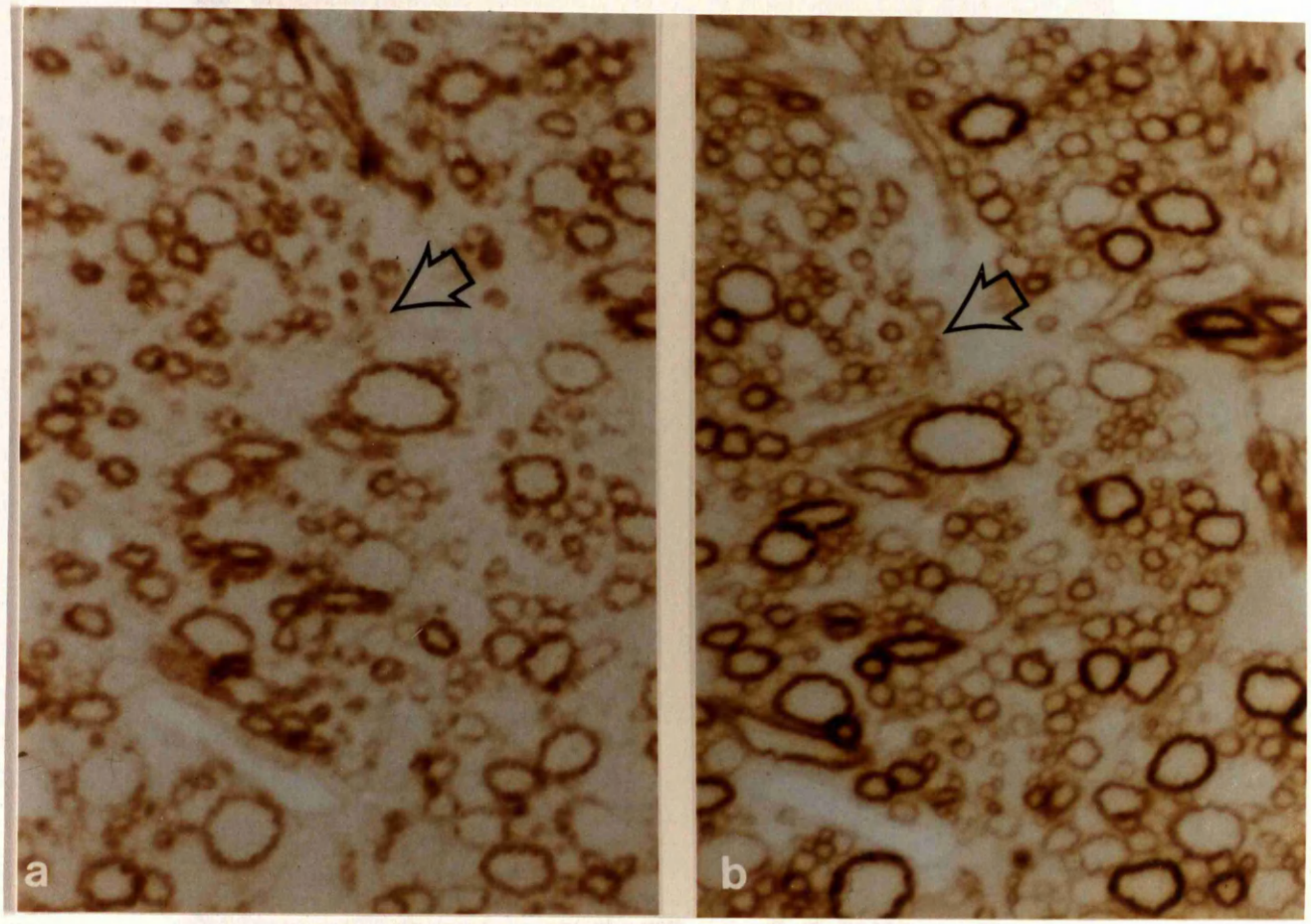

Figure 12: Adjacent sections of the spinal cord ventral columns from 90-day-old jp^{rsh} mutant immunostained by the PAP method against (a) PLP/DM-20 and (b) MBP. The majority of the sheaths immunostain for MBP and with a lower intensity for PLP/DM-20. The immunoreactivity is absent in occasional groups of smaller fibres (open arrow). (Approx. magnification: x 2000),

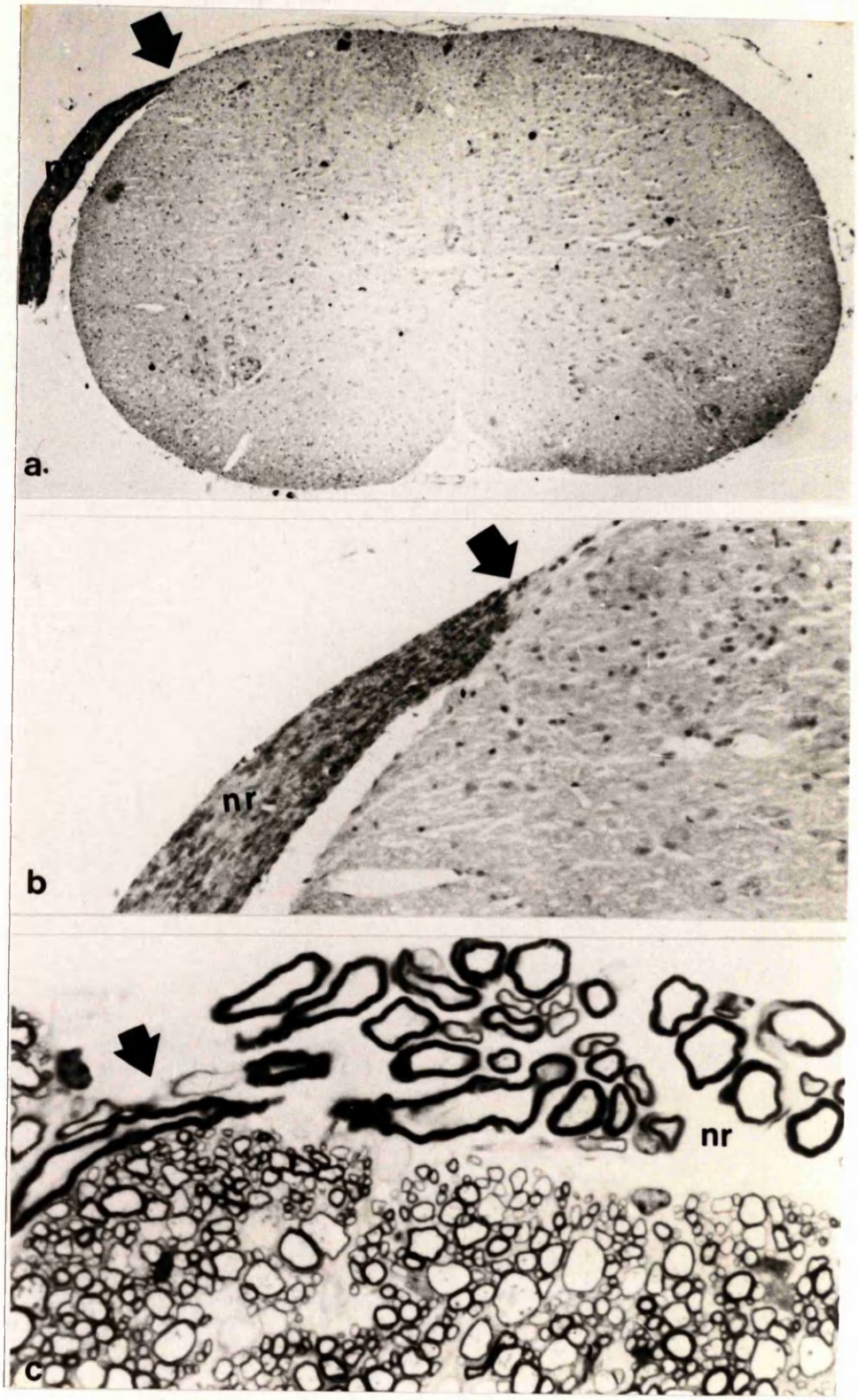

Figure 13: Paraffin-embedded sections of the spinal cord from a one year-old jp^{rsh} mice (a, b) immunostained for P_0 using the PAP technique. The immunostaining of the myelin sheaths in the PNS myelin of the nerve root (nr) is positive as expected. Immunoreactivity against the P_0 antibody was absent CNS myelin of the jp^{rsh} mice indicating no Schwann cell invasion of the CNS. The arrows point at the PNS/CNS transition zone. (c) Methylene blue/azure II stain of a resin-embedded section of the same area of the spinal cord as above. No evidence of PNS Schwann cell invasion or remyelination is detected. (Approx. magnification: a x 50; b x 200; c x 2000).

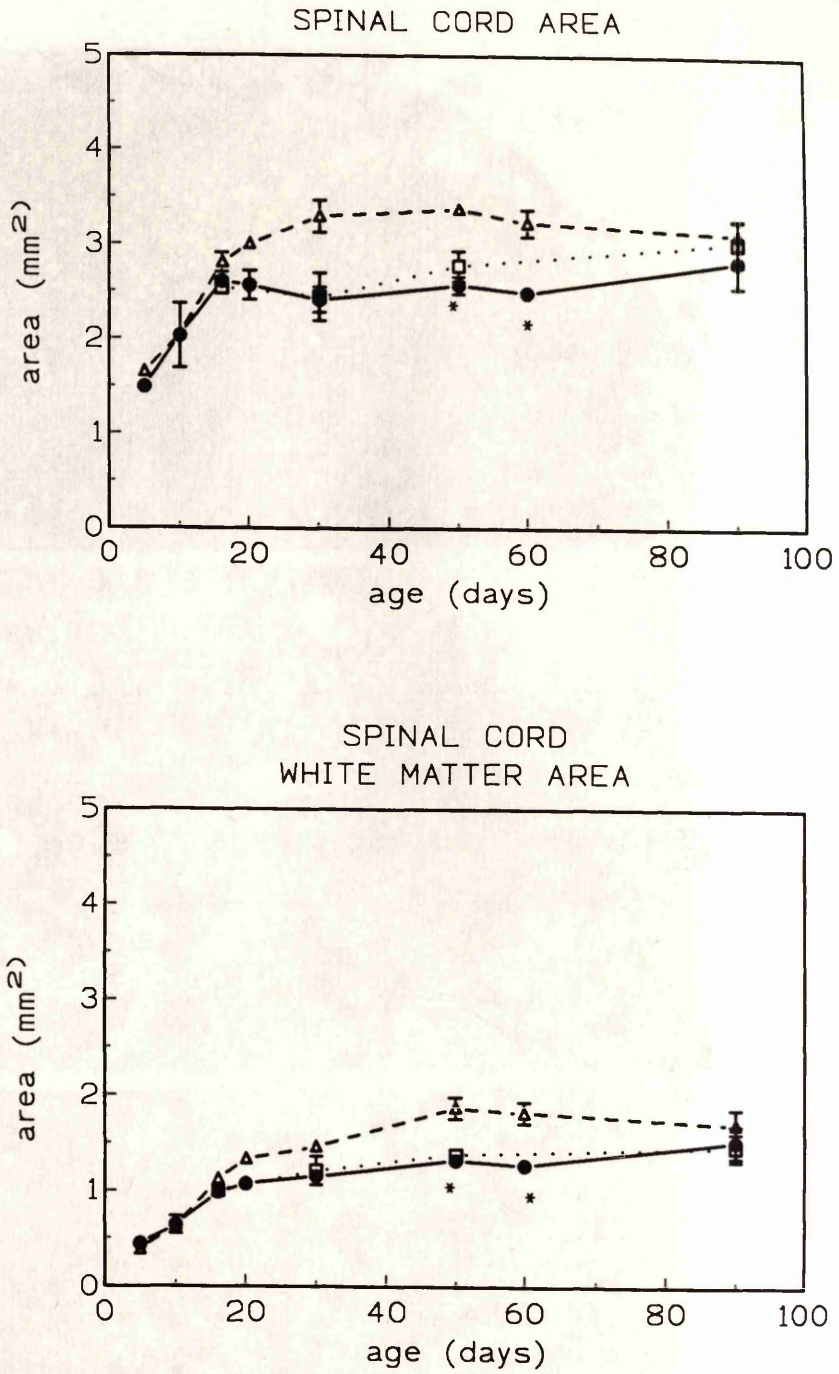

Figure 14: Spinal cord and white matter areas. Transverse areas of the C2 segment of the cervical spinal cord and white matter from the wild type (triangle), jp^{rsh} mice (filled circle) and jp^{rsh} heterozygotes (square). Both jp^{rsh} and jp^{rsh} heterozygotes show a marked reduction in the area from 20 days of age onwards which progressively diminishes. All data represent mean ± SEM; where error bars are not seen they fall within the symbol. Asterisks have been placed in values that differ significatively from the wild type.

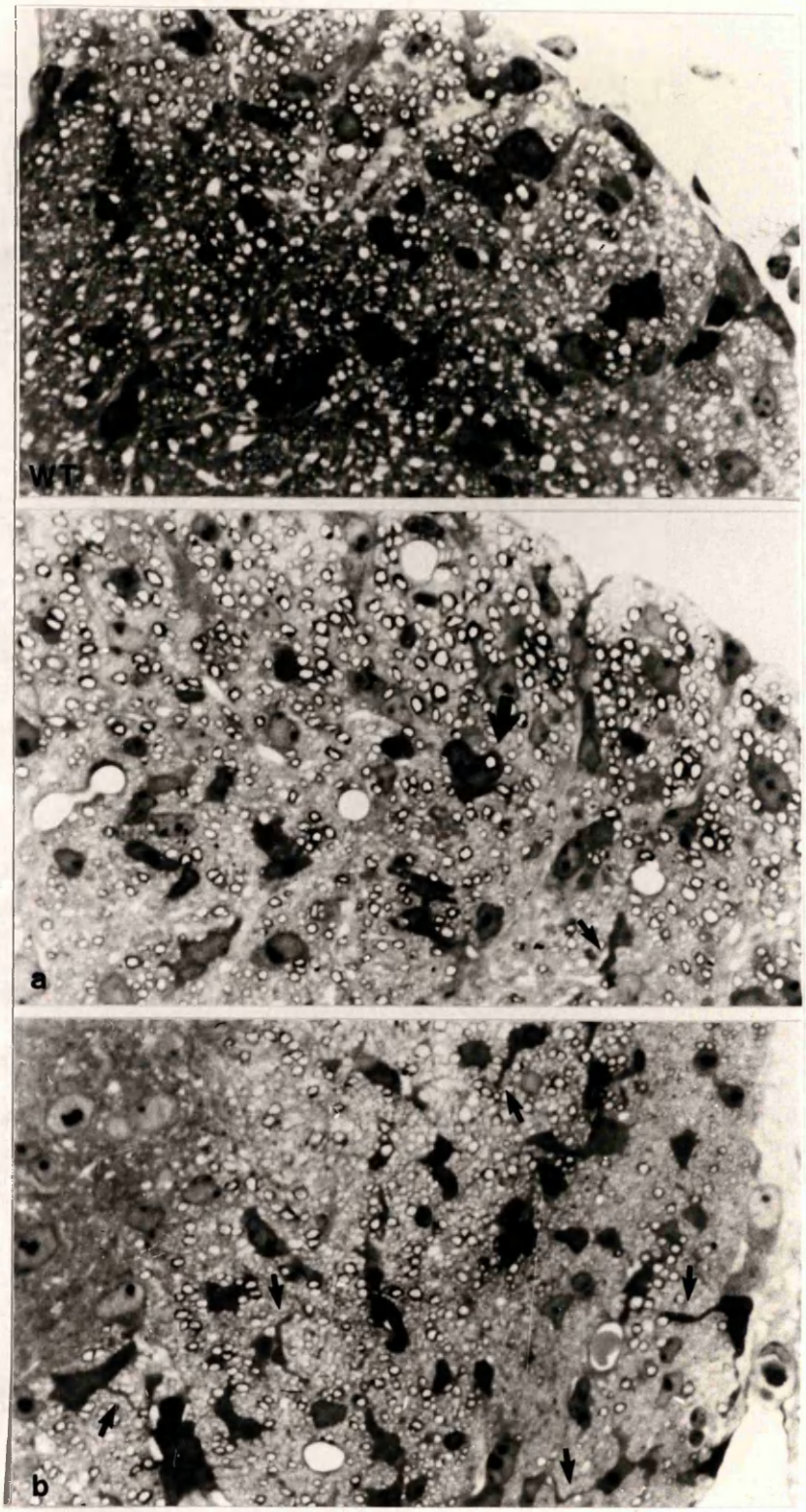

Figure 15: Light microscopic appearance of 5-day-old *jp*^{rsh} spinal cord. Ventral columns from the C2 segment of the spinal cord from wild type (WT) and *jp*^{rsh} (a). (b) Area adjacent to the ventromedial fissure in the mutant (the dorsal and lateral columns are also shown in the next figure). *jp*^{rsh} shows abundance of "healthy looking" oligodendrocytes actively producing processes that grow between the axons (arrow). Occasional oligodendrocytes are also seen embracing individual large calibre axons. At this age, the morphological appearance of the mutant resembles that of the age-matched wild type. (Approx. magnification: x 1000)

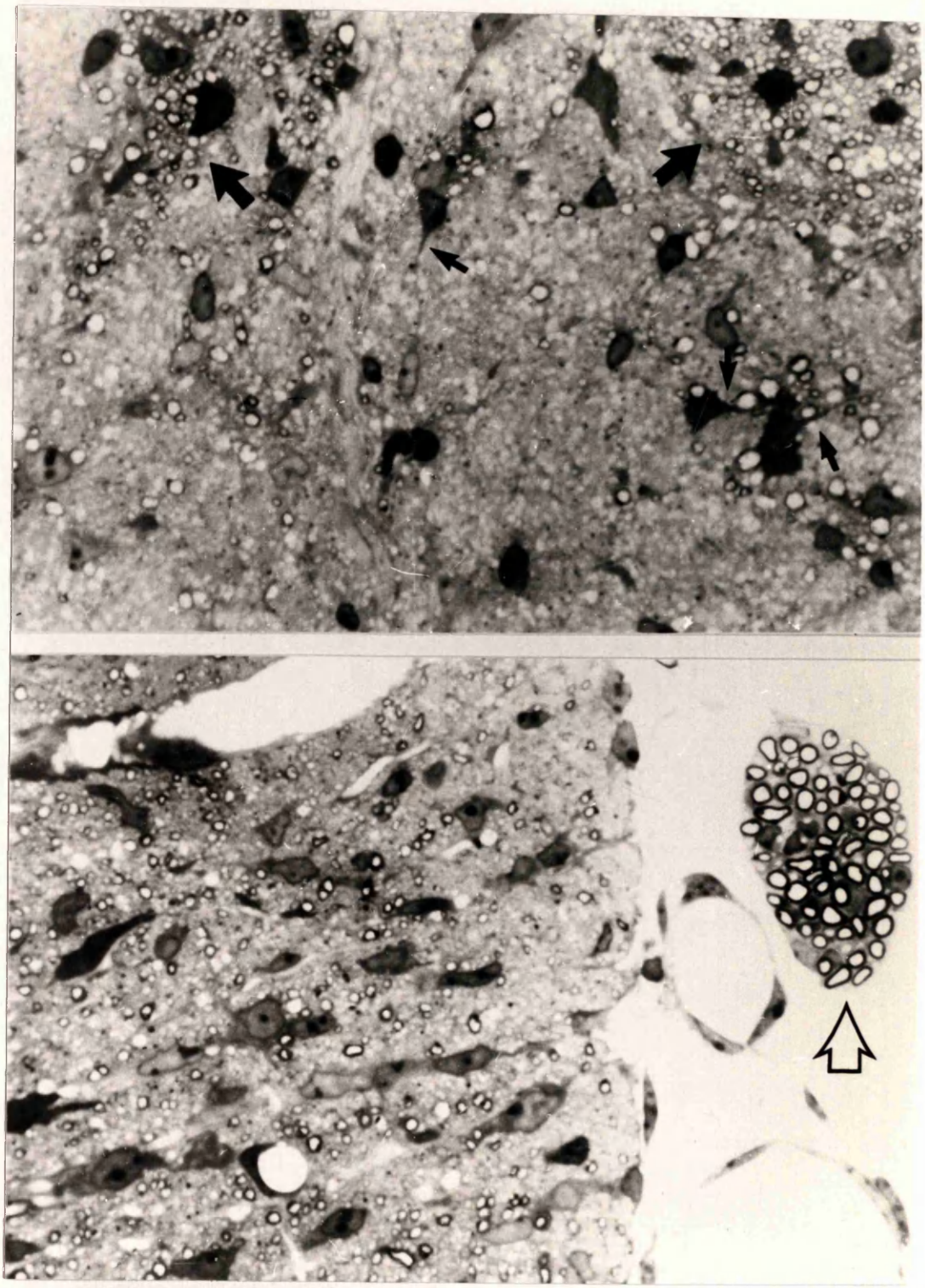

Figure 16: Light microscopic appearance of 5-day-old jp^{rsh} mutant spinal cord. Light microscopic photographs of the dorsal columns (upper panel) and lateral columns (lower panel) from the same jp^{rsh} cervical cord section as figure 15. The jp^{rsh} mutant oligodendrocytes produce abundant processes actively approaching naked axons (arrows). Myelination in the PNS is normal in the mutants (open arrow). (Approx. magnification: x 1000).

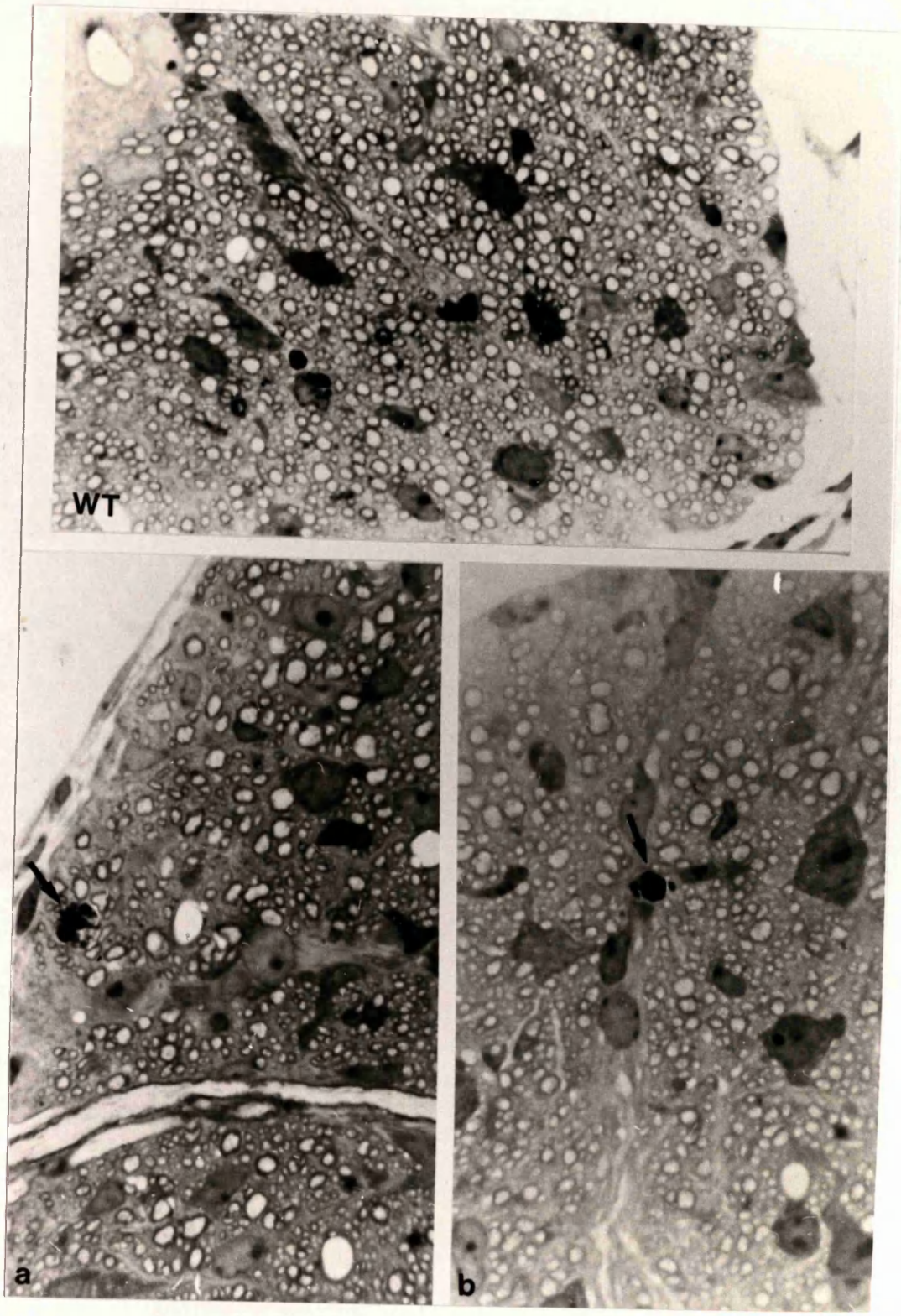

Figure 17: Light microscopic appearance of 10-day-old of wild type (WT) and *jp*^{rsh} (a, b) ventral columns from the C2 segment of the spinal cord. The abnormalities caused by the mutation start being evident around this age. The oligodendrocyte numbers are increased in respect to the wild type and there are some hypomyelinated areas. Some condensed nuclei, probably from cells ungoing programmed cell death, are an occasional finding (arrows). (Approx. magnification: x 1000)

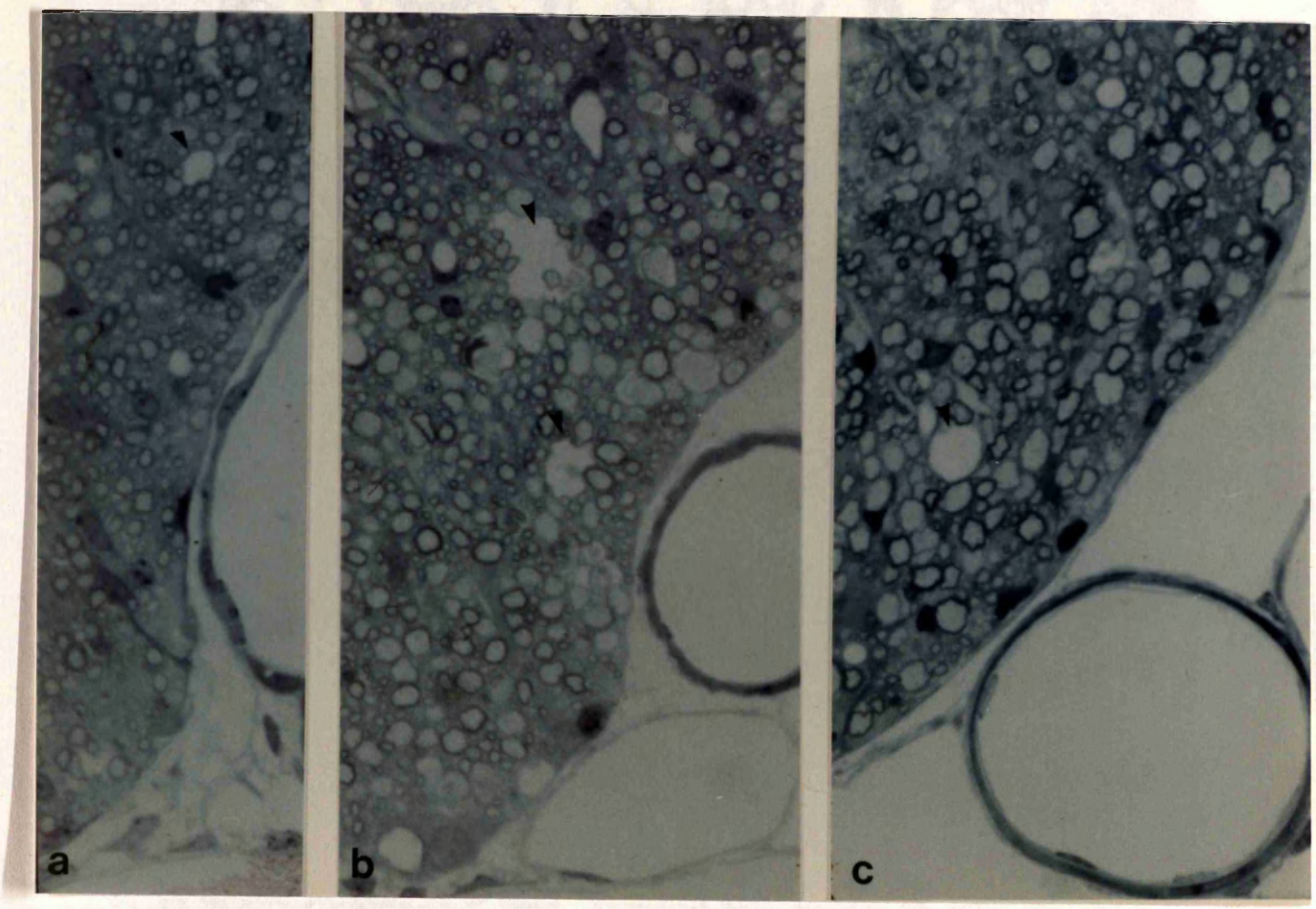

Figure 18: Light microscopic appearance of *jp*^{rsh} spinal cord at different ages. Methylene blue/azure II stained resin sections of the ventral white matter adjacent to the ventromedian fissure of the C2 segments of the spinal cord of *jp*^{rsh} at 16 (a), 30 (b) and 50 (c) days of age. Hypomyelination, intramyelinic splitting or vacuolation (arrow-heads) and increased cellularity are constant findings at all ages. (Approx. magnification: x 1000).

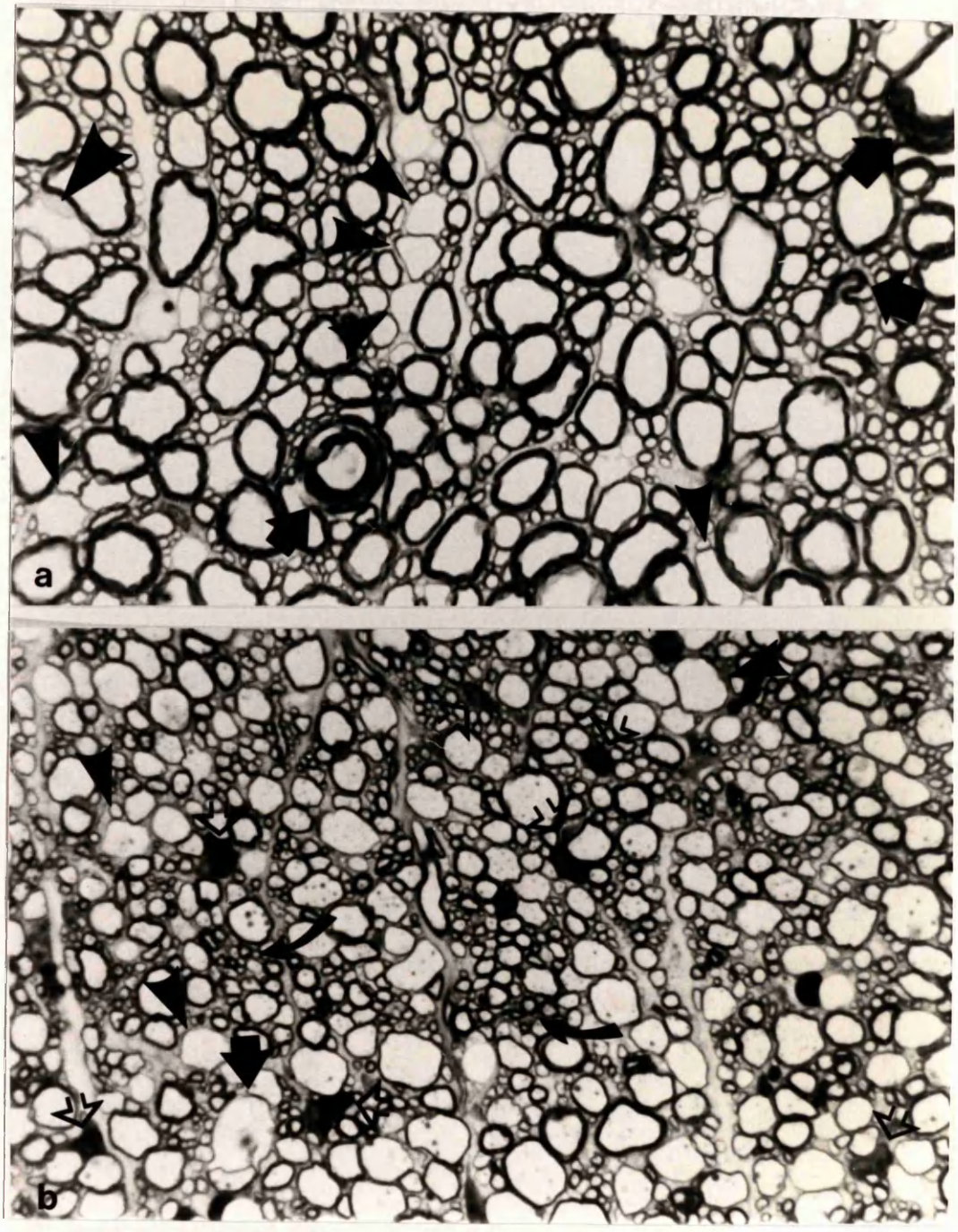

Figure 19: Methylene blue/azure II stained sections from the 1 year-old jp^{rsh} female heterozygote (a) and jp^{rsh} (b) ventral columns of the C2 segment of spinal cords. (a) The majority of axons are myelinated by sheaths of normal thickness in the female heterozygote. However, redundant folds of myelin (thick arrows) and scattered hypomyelinated/amyelinated axons (arrow-heads) are a common finding. (b) The morphological changes in the spinal cord of the 1 year-old full jp^{rsh} include an obviously increased oligodendrocyte population (open arrows) together with vacuolation of some of the sheaths (thick arrow) and hypomyelinated/amyelinated large axons. Most small axons are myelinated and present sheaths of normal thickness (curved arrows). Both types of mice demonstrate morphologically normal myelin sheath around smaller fibres, while large diameter fibres remain hypomyelinated or unmyelinated. (Approx. magnification: x 2000).

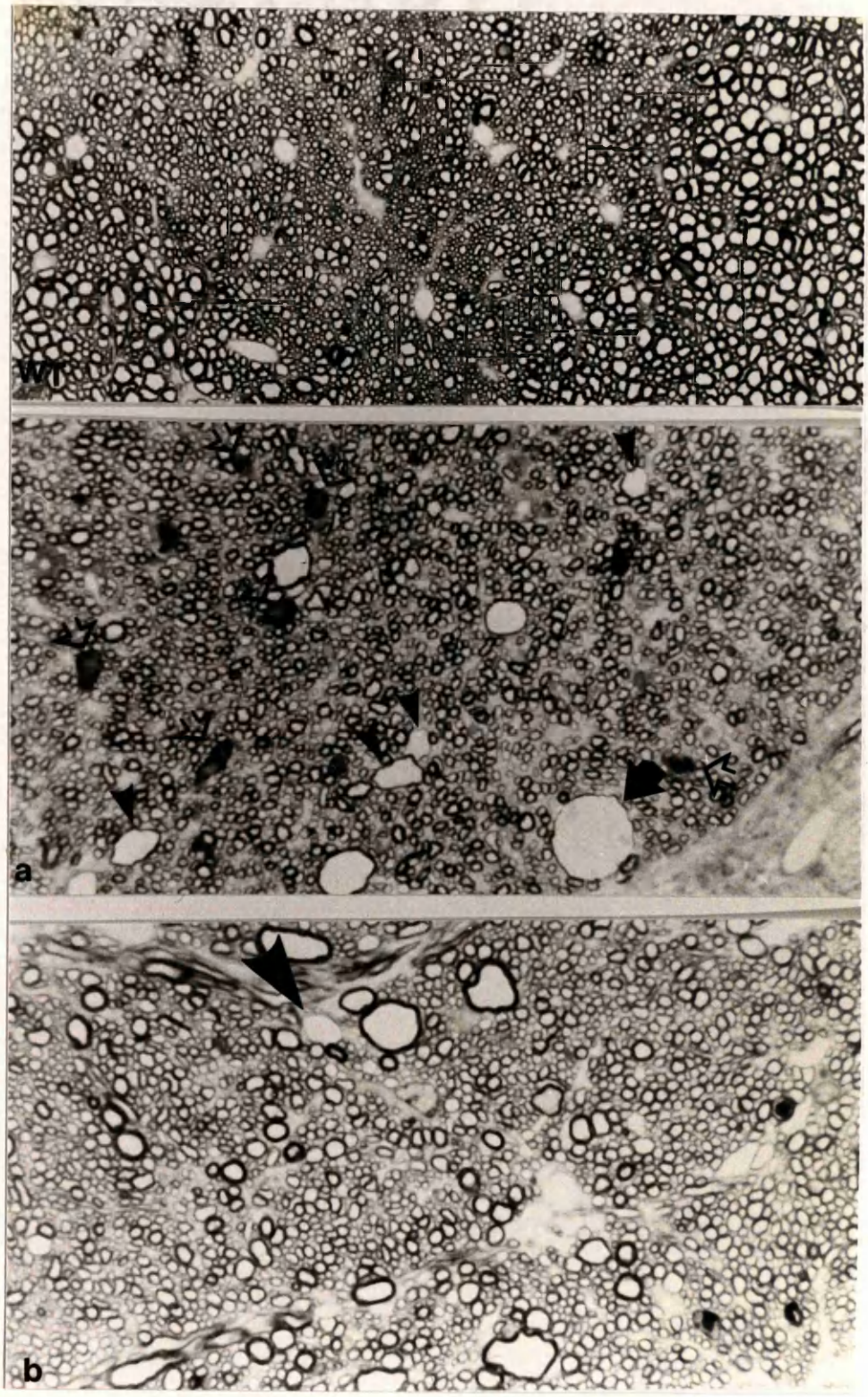

Figure 20: Light microscopic appearance of 1 year-old wild type (WT), jp^{rsh} (a) mouse and jp^{rsh} female heterozygote (b) methylene blue/azure II stained dorsal columns from the C2 segment of the spinal cord adjacent to the ventromedian fissure. (a) The dorsal columns of jp^{rsh} are well myelinated. Occasional large hypomyelinated (arrow-head) or vacuolated (thick arrow) fibres are present. Glial cell numbers in the dorsal columns of the spinal cord of jp^{rsh} are increased. (b) The dorsal columns in the jp^{rsh} female heterozygote present occasional hypomyelinated large axons (arrow-head). (Approx. magnification: x 2000).

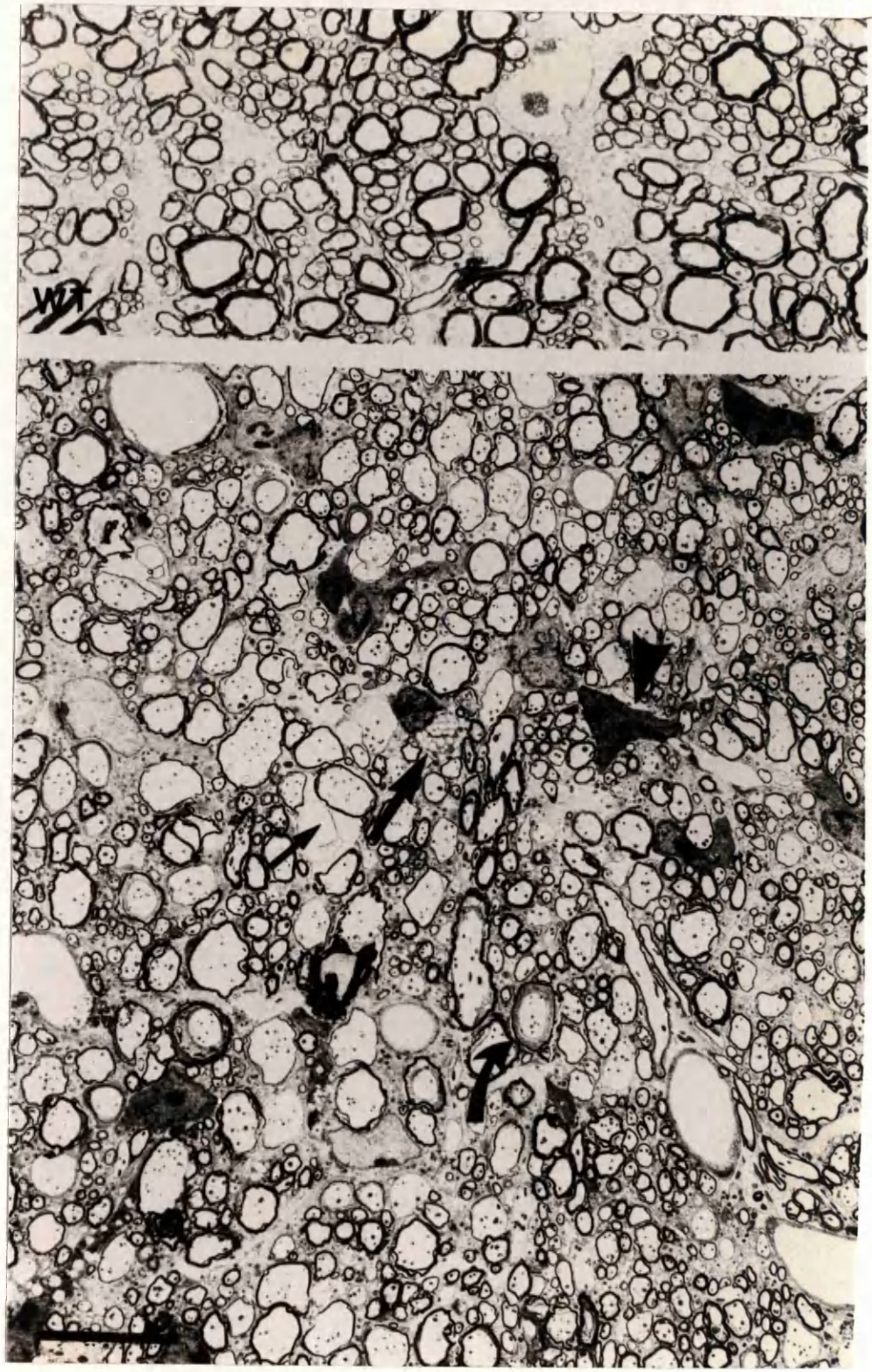

Figure 21: Ultrastructure of the ventral white matter from the spinal cord of 30-day-old wild type (WT) and jp^{rsh} mice (lower panel) The majority of the axons are surrounded by disproportionately thin myelin sheaths, some of which (curved arrow) contain uncompacted areas, and others (small arrow) have intramyelinic vacuolation. Oligodendrocytes (arrow heads) are increased in number. An occasional microglial cell containing membranous inclusions (large arrow) is also present. Scale bar 10 μm.

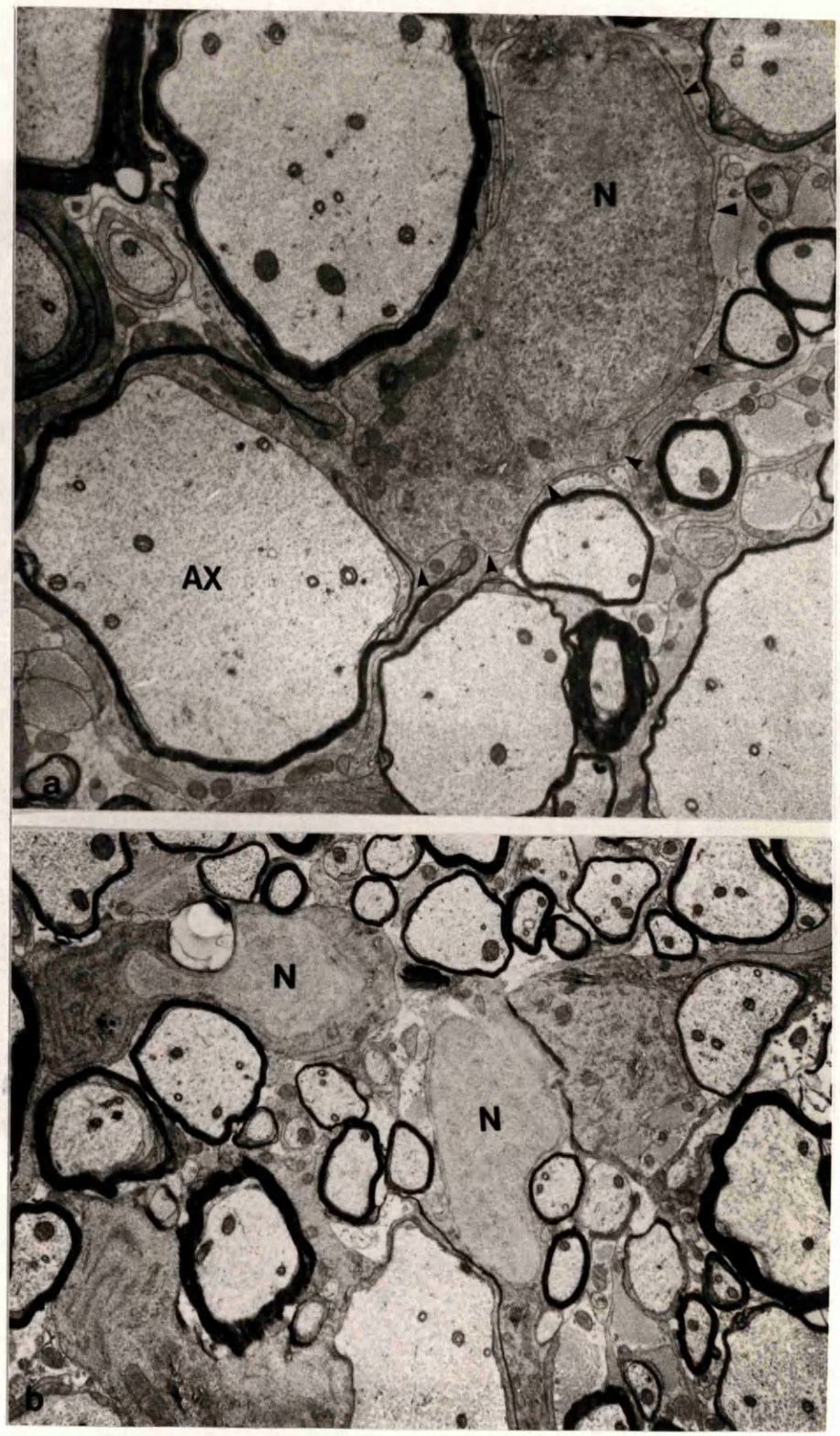

Figure 22: Electron-micrographs of atypical glial cells, possibly oligodendrocyte precursor cells observed in 50-day-old jp^{rsh} ventral columns. Similar cells were also occasionally seen in the female ($jp^{rsh}/+$) heterozygote but were never detected in the wild type mice. The contour of the cell in (a) is outlined with arrow-heads. Some of the characteristics of these cells include an undifferentiated appearance, a rounded nucleus (N) situated at one pole of the cell and a very sparse cytoplasm with very few organelles (see figure 23 for more details). Due to the small size of the cell, the low cytoplasmic density and the infrequent cell processes these cells are rarely detected at light microscopy. Some of these cells seem to be related to hypomyelinated axons although the cell contour becomes very indistinct. These cells resemble those termed as "primitive oligoblasts" described in the foetal monkey spinal cord (Phillips, 1973). (Approx. magnification: a x 15000; b x 10000).

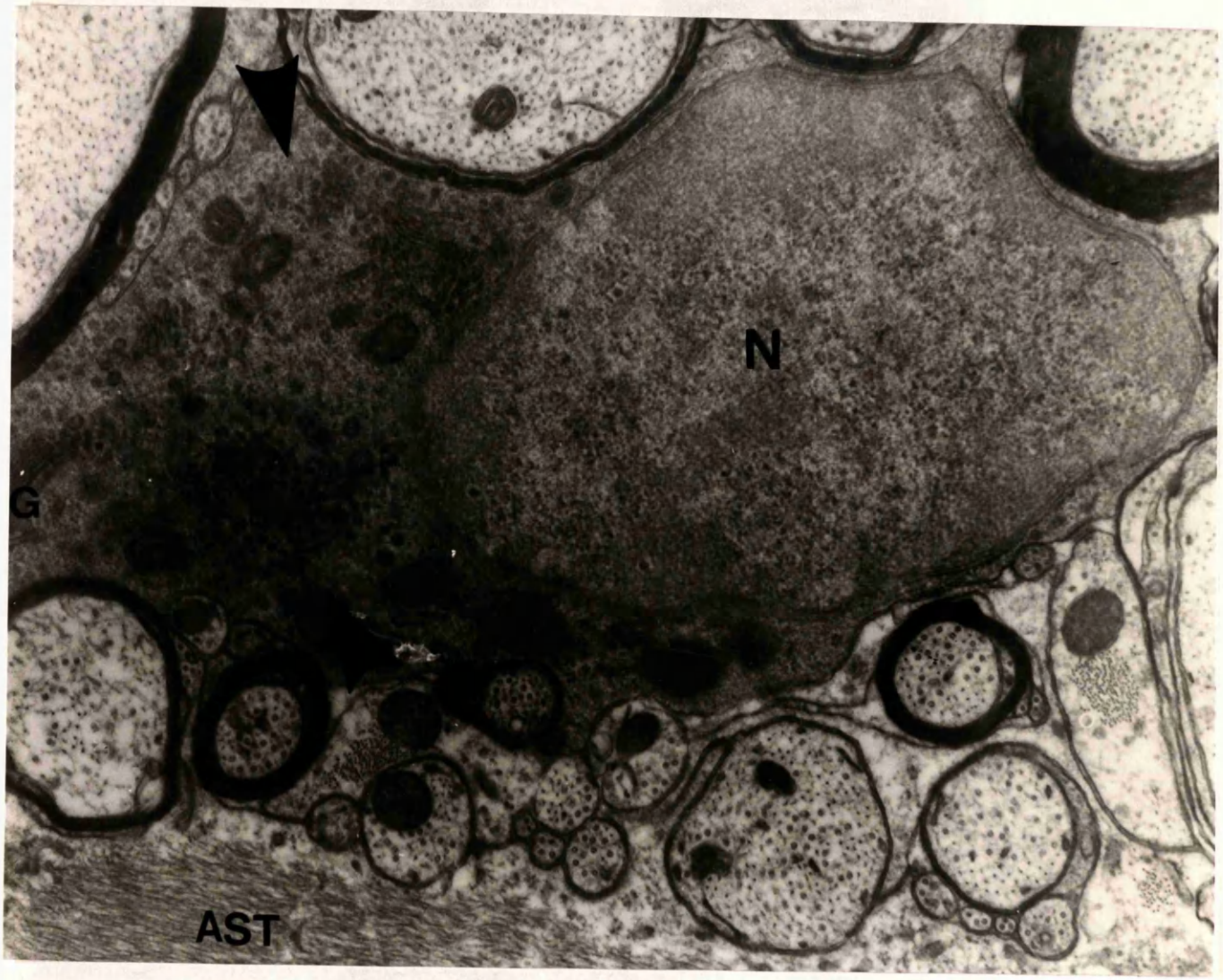

Figure 23: Electron-micrograph of an atypical glial cell, possibly an oligodendrocyte precursor, observed in 50-day-old jp^{rsh} ventral columns exhibiting a pale cytoplasm including mitochondria, Golgi apparatus (G), possibly some small filaments (arrow-head). The nucleus (N) contains dispersed chromatin. Cell processes are uncommon. These cells are seen frequently in the vicinity of naked or hypomyelinated axons which are usually surrounded by astrocytic processes (AST). The characteristics of this undifferentiated cell correspond to those termed "primitive oligoblasts" (Phillips, 1973). (Approx. magnification: x 30000).

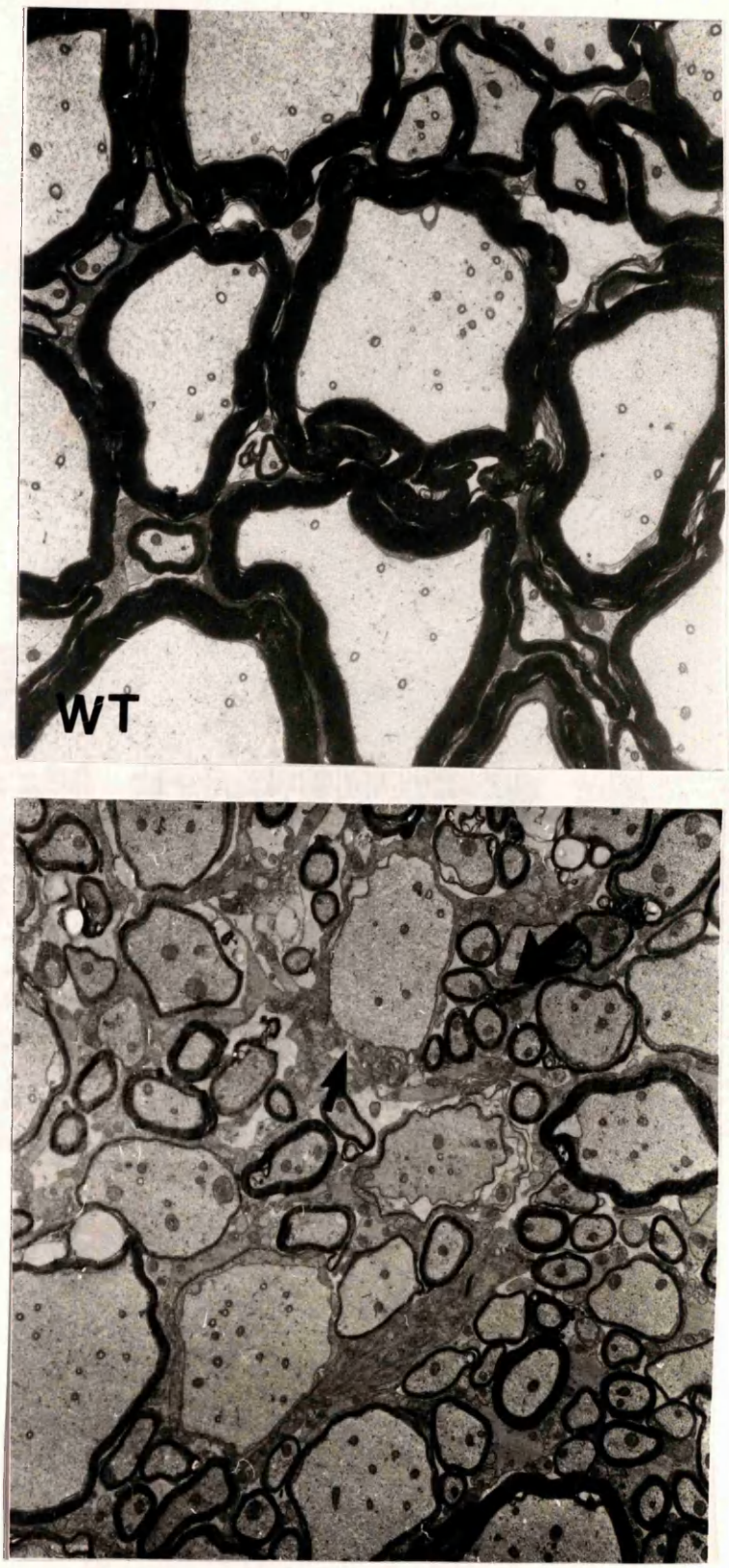

Figure 24: Ultrastructure of the ventral white matter of the C2 segment of the spinal cord from 90-day-old wild type (WT) and *jp*^{rsh} mice. Virtually all the smaller axons have acquired a myelin sheath of normal appearance (thick arrow). Larger axons remain hypomyelinated/amyelinated (small arrow). Vacuolation of some of the myelin sheaths is also a common finding at 90 days of age. (Approx. magnification: x 6000).

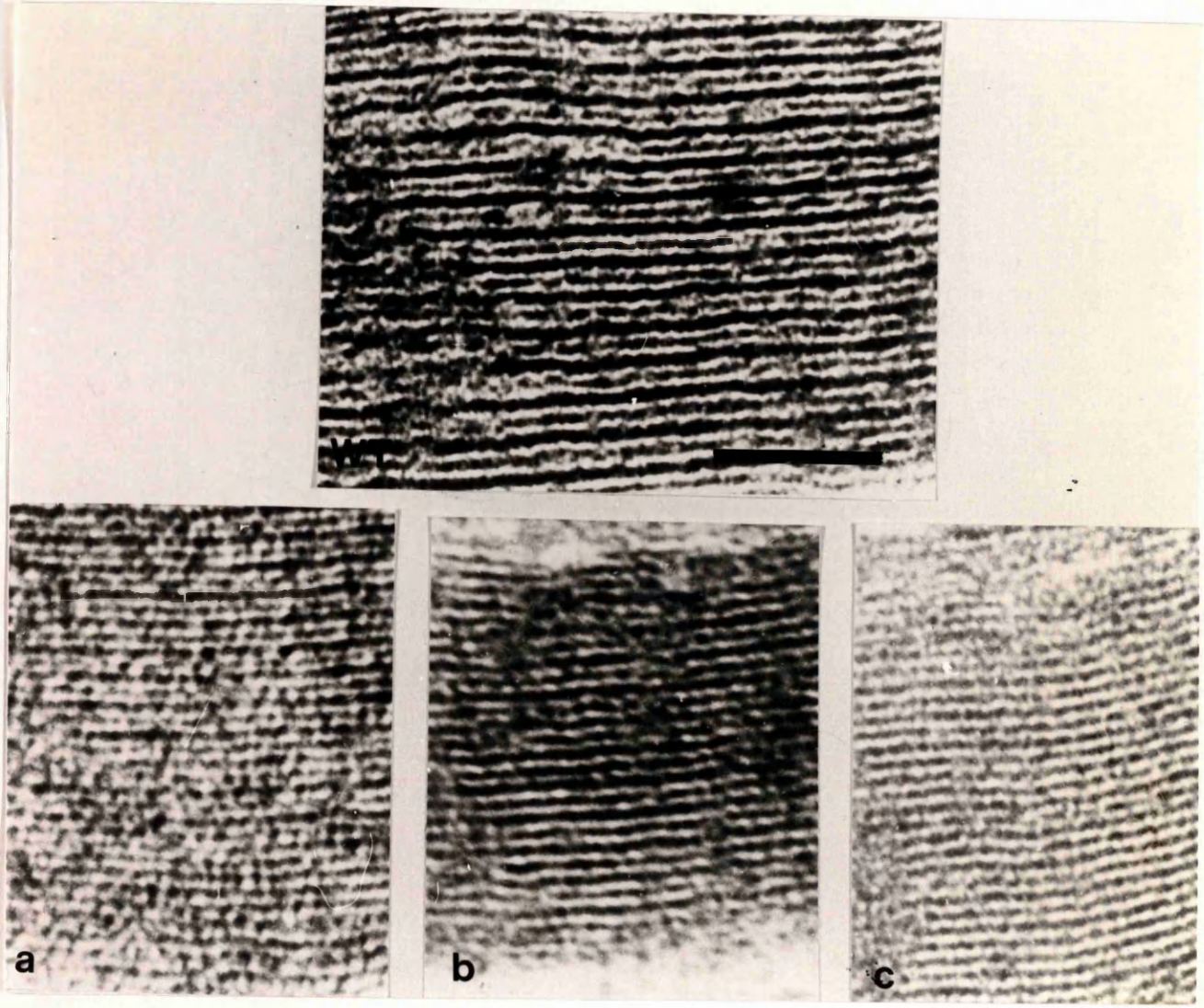

Figure 25: Ultrastructure of the myelin sheaths from 30-day-old wild type (a) and *jp*^{rsh} (b, c and d) mice. MDL and IPL lines are clearly distinguishable in the wild type myelin. The periodicity of the MDL in the mutant myelin is reduced when identifiable. The IPL of these compacted sheaths is very irregular. Scale bar 50 nm.

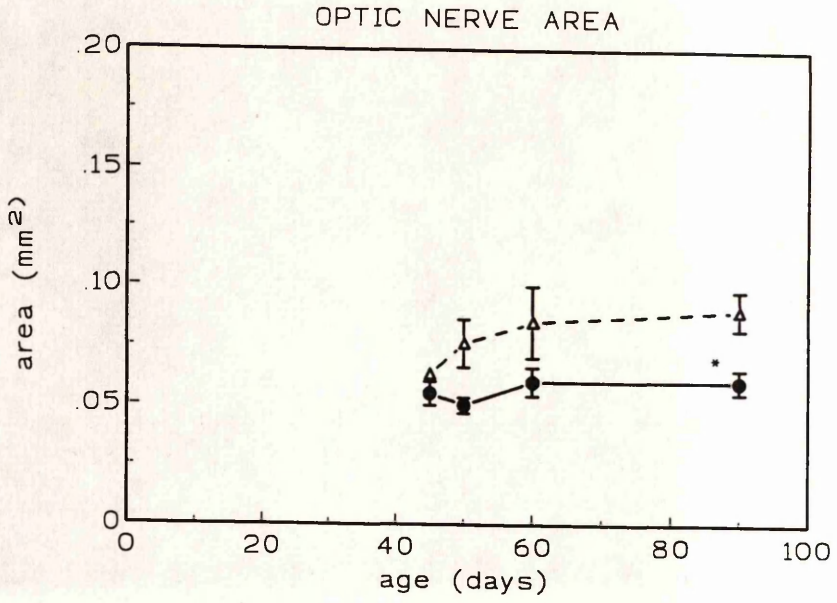

Figure 26: Optic nerve areas. Transverse areas of optic nerve sections from wild type (triangle) and jp^{rsh} mice (filled circle). Mutant nerves show a significant reduction in the area at all ages examined supporting the visual impression. All data represent mean ± SEM; where error bars are not seen they fall within the symbol. Asterisks have been placed in values that differ significatively from the wild type.

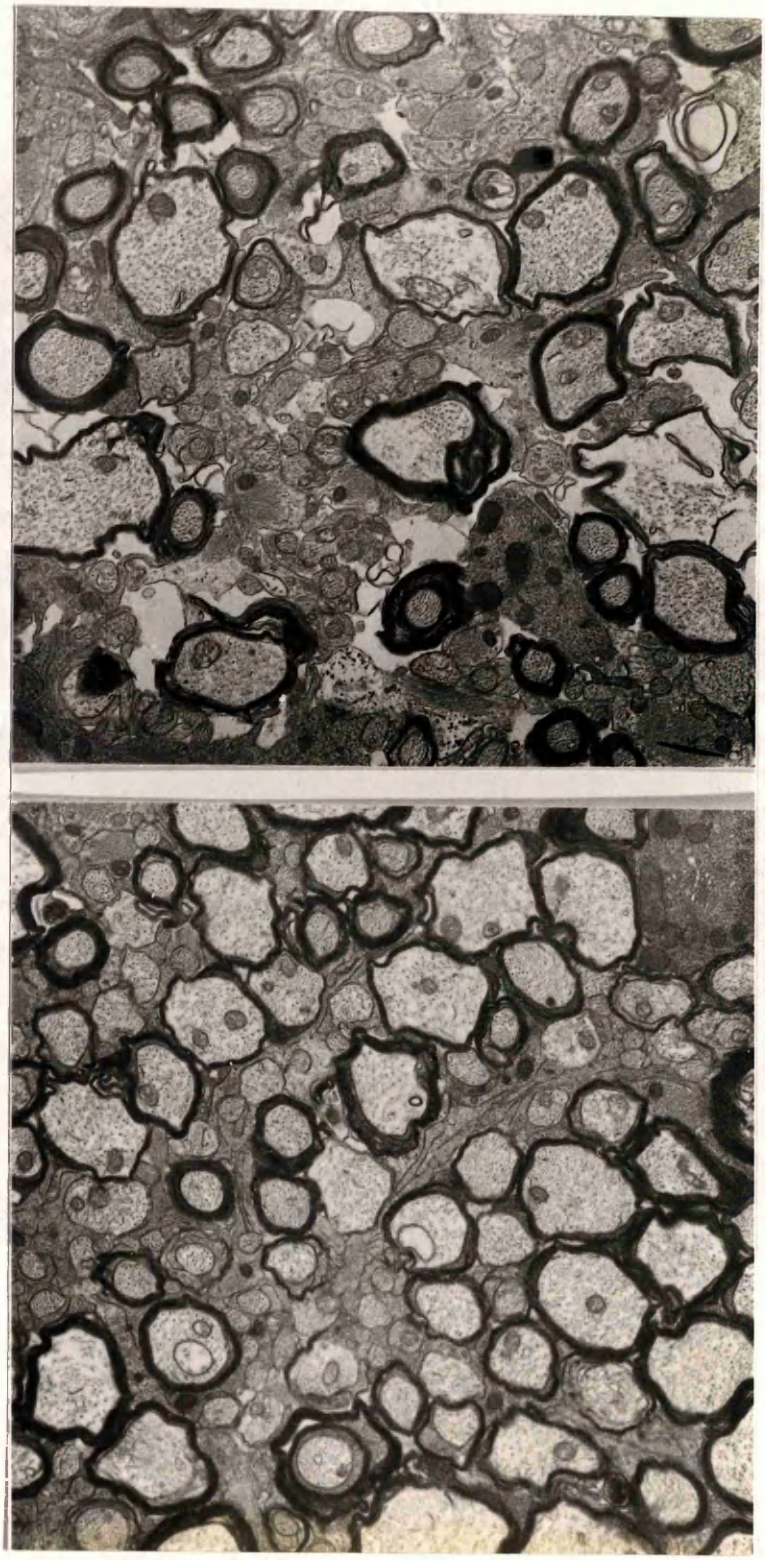

Figure 27: Ultrastructure of the optic nerves from 30-day-old *jp*^{rsh}. Nerves from two different mice are shown. Most myelinated axons have a larger calibre than the unmyelinated axons which tend to form bundles. Surprisingly, some 30-day-old mutant optic nerves present more myelin than some 90-day-old *jp*^{rsh} (figure 28). An equivalent wild type section is shown in figure 88 (WT). (Approx. magnification: x 9500).

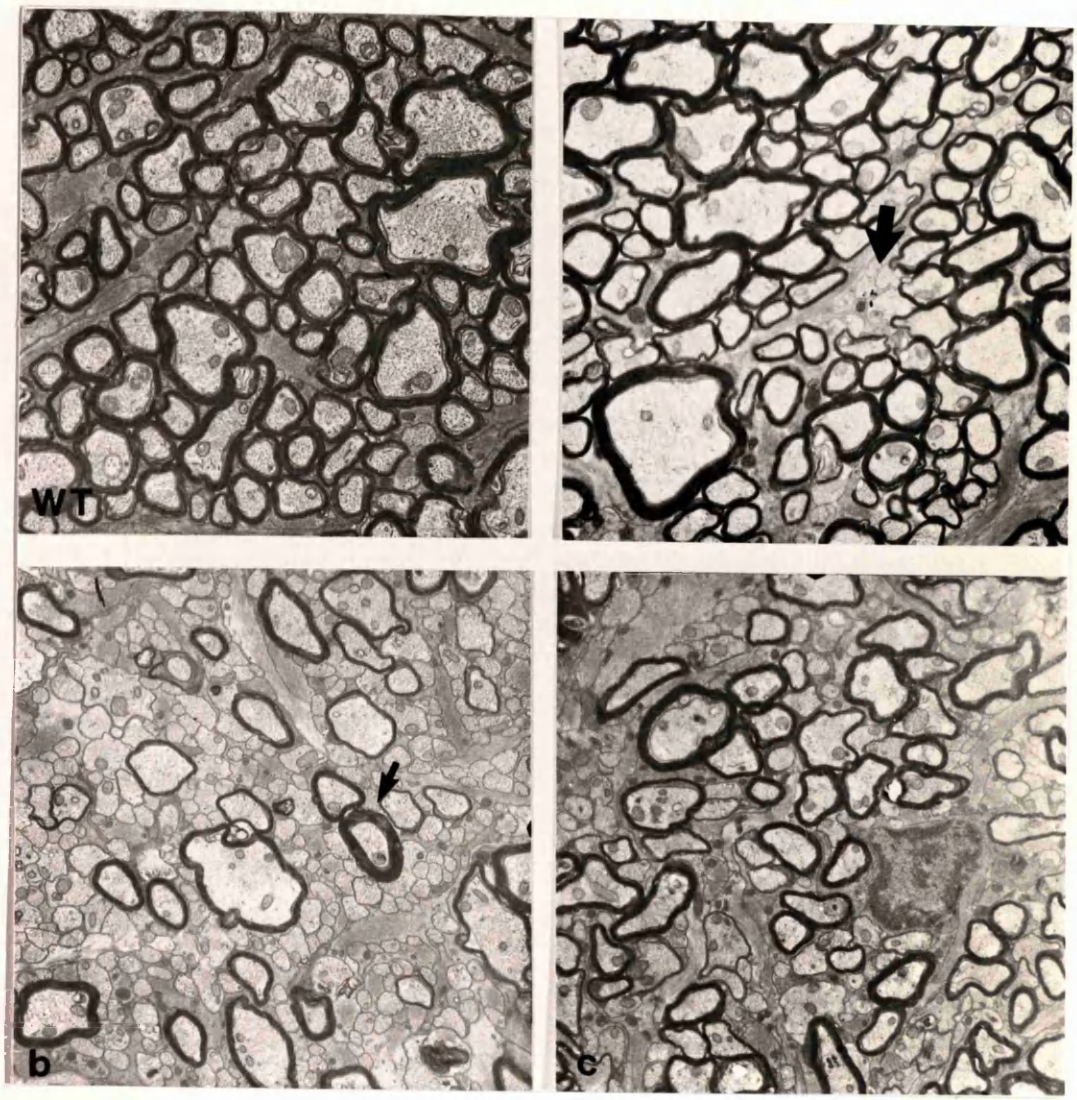

Figure 28: Ultrastructure of 90-day-old optic nerves from 90-day-old wild type (WT), female heterozygote (a) and *jp*^{rsh} mice (b, c). Heterozygotes do not show obvious mosaic changes in the optic nerves at 90 days, however, collections of small unmyelinated axons are detectable (thick arrow). The majority of mutant optic nerve axons are amyelinated (b, c). There is some variation in the thickness of myelin sheaths relative to axon size, for example one fibre (b, arrow) has a thicker sheath than expected. The presence of a thicker sheath is unusual, most being either normal or thinner. Astrocyte processes are moderately increased. (Approx. magnification: x 9000).

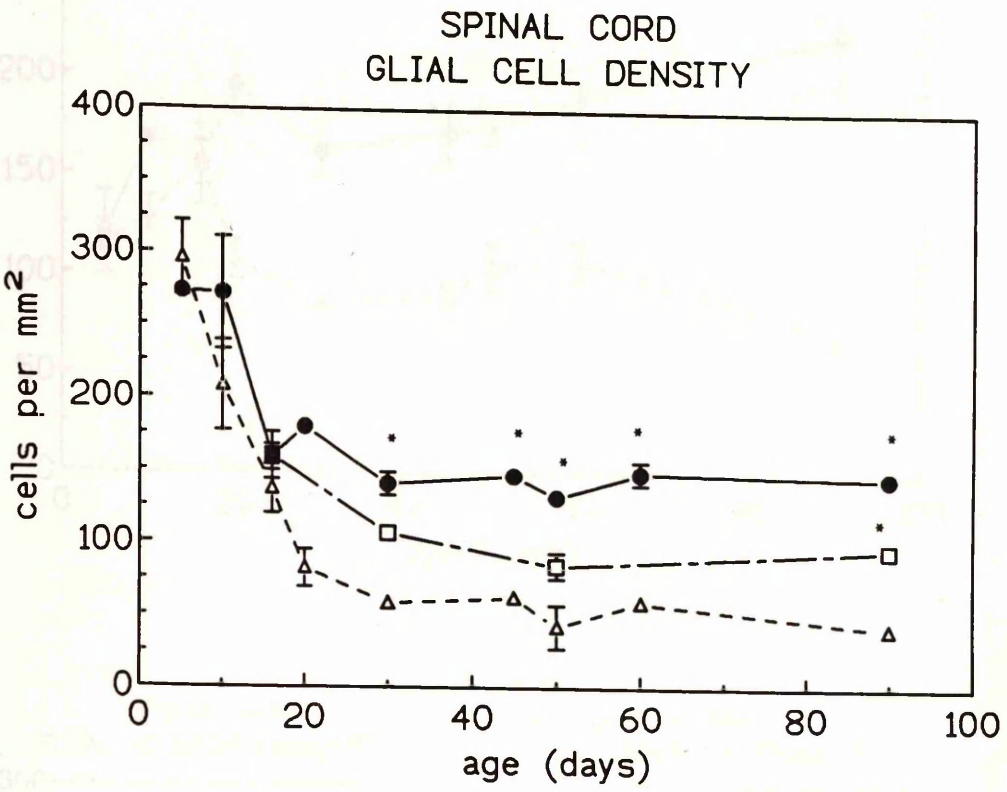

Figure 29: Glial cell density in the spinal cord. Values from wild type (triangle), jp^{rsh} (filled circle) and jp^{rsh} heterozygote (square). The values refer to cells in the white matter from the ventral columns of the C2 segment of the spinal cord. All data represent mean ± SEM; where error bars are not seen they fall within the symbol. The female heterozygote show a moderate increase in glial cell density the difference being more pronounced in older mice. However, it is never as marked as in jp^{rsh}. Asterisks have been placed in values that differ significatively from the wild type.

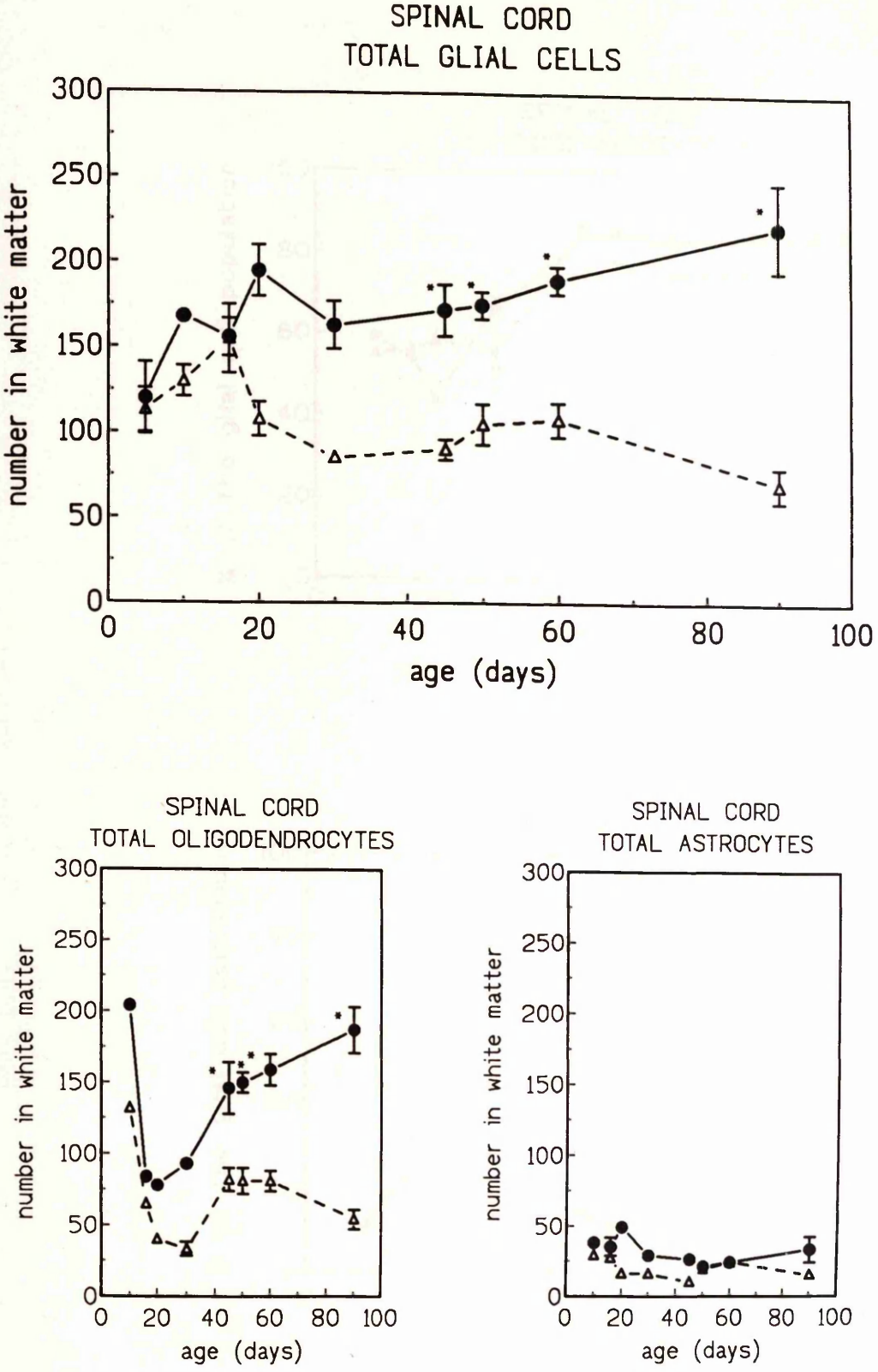

Figure 30: Total numbers of glial cells in the spinal cord. Values from wild type (triangle), and *jp*^{rsh} mice (filled circle). Total numbers of oligodendrocytes and astrocytes in white matter are also shown individually. Values refer to cells in the white matter from the ventral columns of the C2 segment of a transverse section from the spinal cord. All data represent mean ± SEM; where error bars are not seen they fall within the symbol. Asterisks have been placed in values that differ significatively from the wild type.

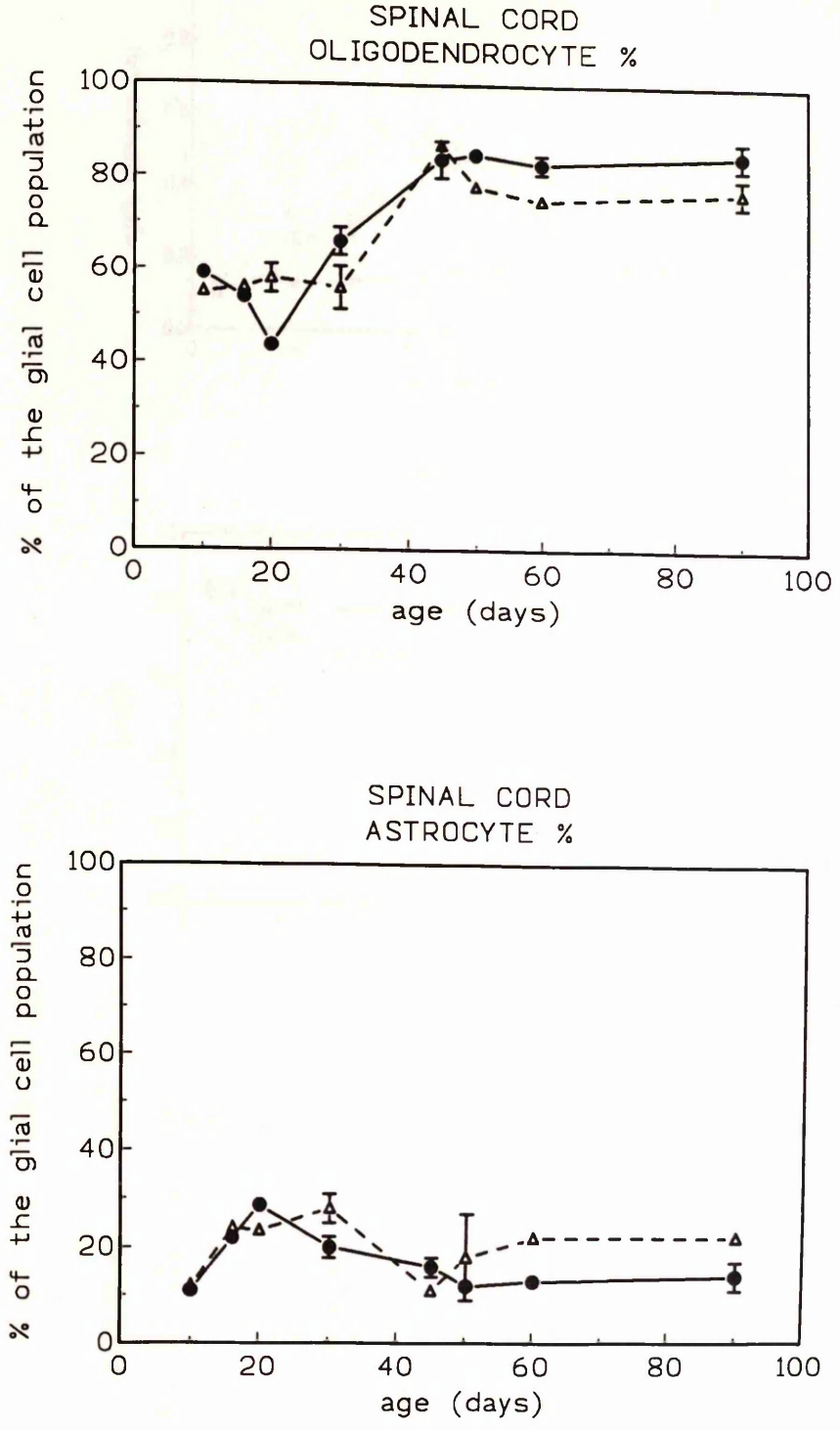

Figure 31: Percentages of oligodendrocytes and astrocytes in white matter of spinal cord. Percentages of the total numbers of glial cell population from wild type (triangle), and *jp*^{rsh} mice (filled circle). Total numbers of oligodendrocytes and astrocytes in white matter are shown. Mutants show an increased percentage of oligodendrocytes after the age of 30 days. Values refer to cells in a transverse section from the white matter from the ventral columns of the C2 segment of the spinal cord. All data represent mean ± SEM; where error bars are not seen they fall within the symbol.

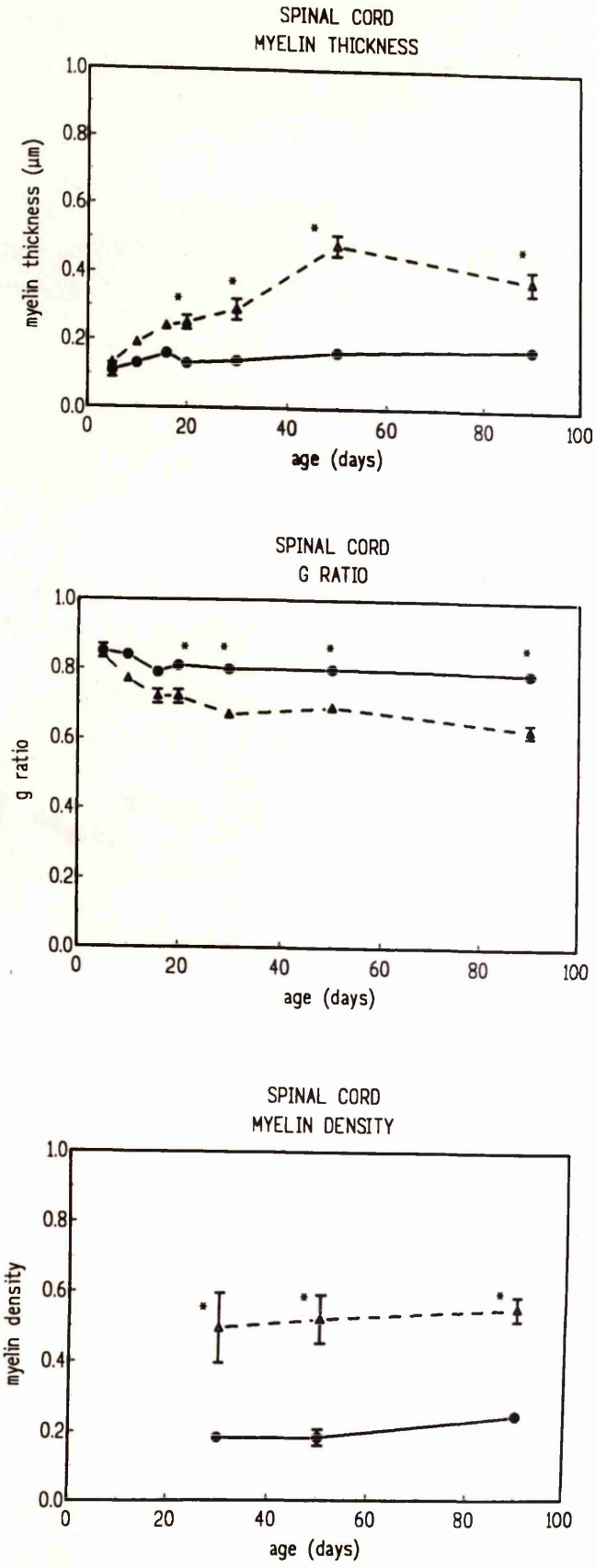

Figure 32: Morphometric analysis of the spinal cord. Values from wild type (triangle), and *jp*^{rsh} mice (filled circle). The values refer to the ventral columns of the C2 segment of the spinal cord. All data represent mean ± SEM; where error bars are not seen they fall within the symbol. Asterisks have been placed in values that differ significatively from the wild type. (upper panel) Myelin thickness; (centre) *g* ratio (*g* ratio defined as ratio of axon diameter to that of the axon plus myelin sheath); (lower panel) Myelin density (arbitrary units). These graphs evidence the profound hypomyelination in the mutant CNS.

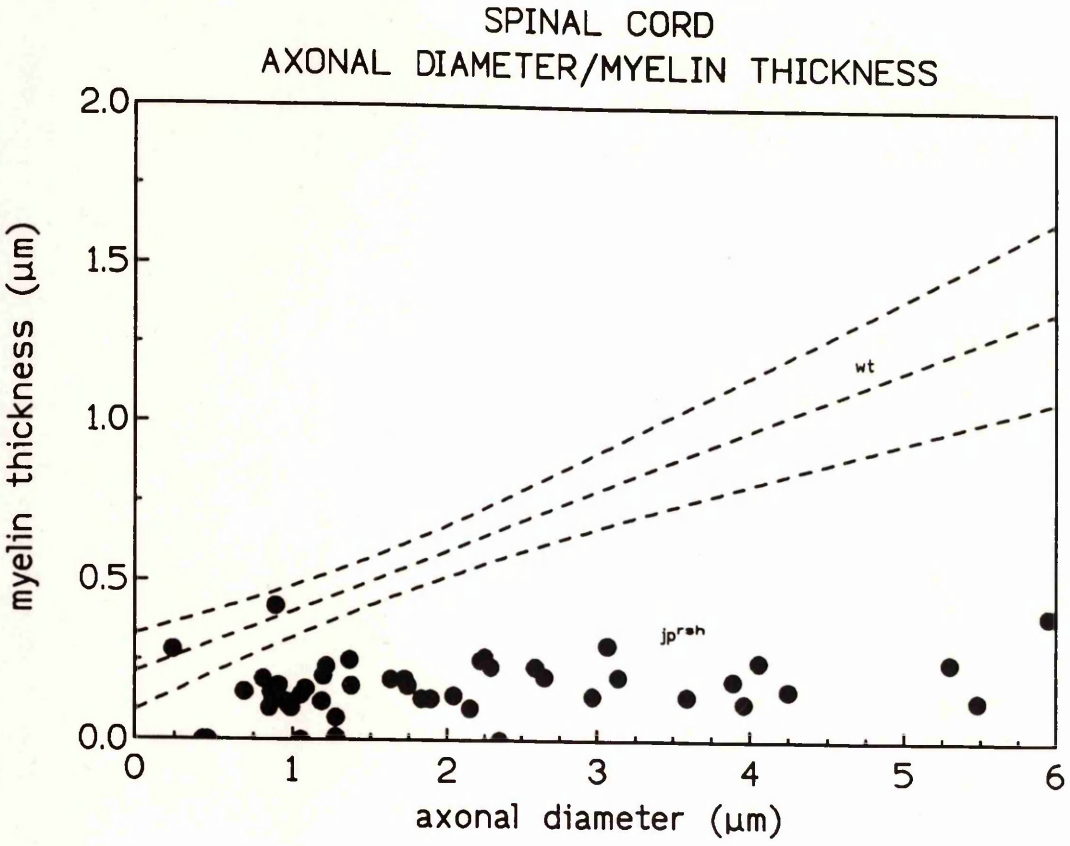

Figure 33: Scatter graph showing the relationship between axon diameter and myelin thickness in the white matter from the ventral columns of the spinal cord from 90-day-old jp^{rsh} mice (filled circles). The central line is the linear regression and the curved lines the prediction bands for similar data from 90-day-old wild type mice. The vast majority of values of jp^{rsh} are below the lower limits of the wild type mice. Only occasional smaller fibres are within the limits for the wild type.

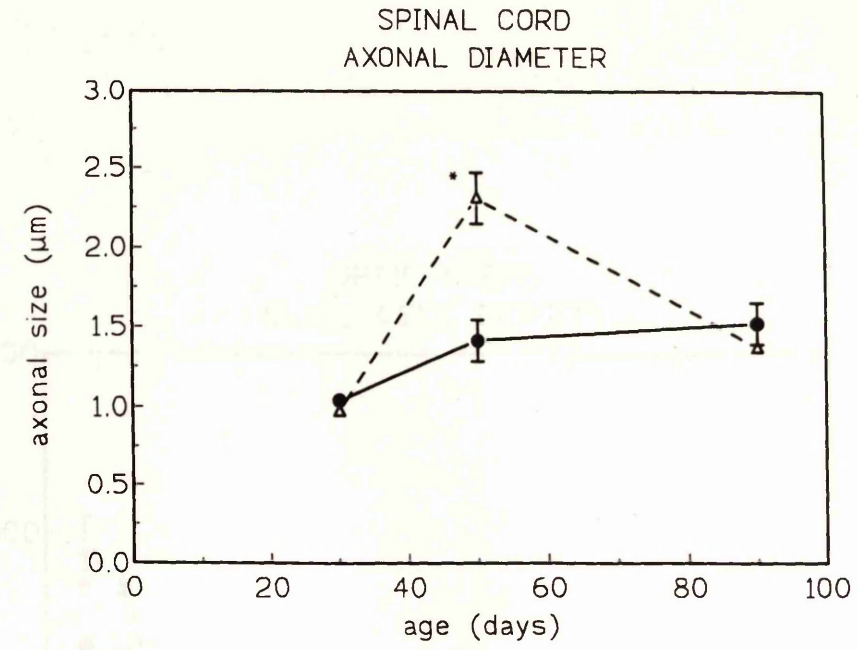

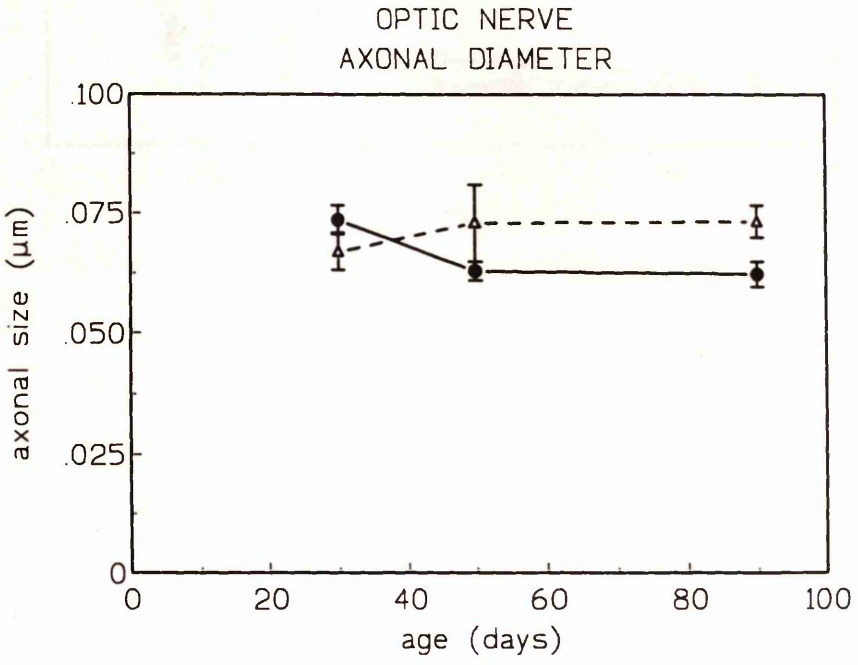

Figure 34: Spinal cord and optic nerve mean axonal diameters from wild type (triangle) and *jp*^{rsh} mice (filled circle). The values refer to axons in the white matter from the ventral columns of the C2 segment of the spinal cord and mid-point optic nerve. All data represent mean ± SEM; where error bars are not seen they fall within the symbol. An asterisk has been placed beside the value that differs significatively from the wild type.

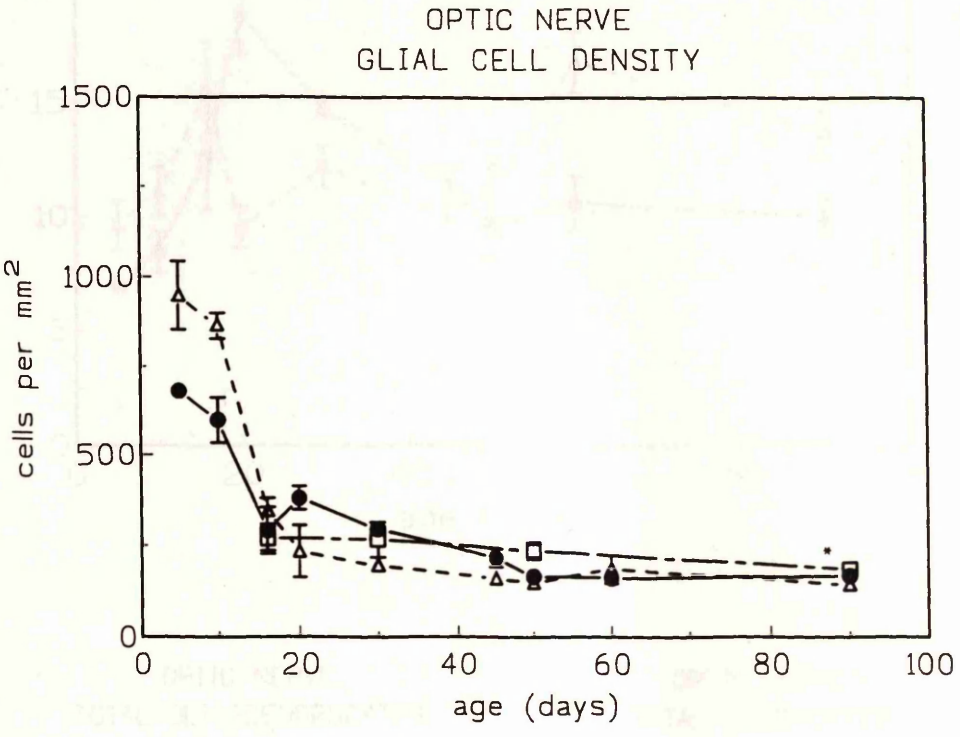

Figure 35: Optic nerve glial cell density. Values from wild type (triangle), jp^{rsh} (filled circle) and jp^{rsh} heterozygote (square) mice mid-optic nerve. The glial cell density parameter is quite similar in the three types of mice. jp^{rsh} mice initially show a lower glial cell density that is compensated after 20 days to became normal at around 45 days of age. Heterozygote glial cell density remained slightly higher than the wild type for all the ages examined. All data represent mean ± SEM; where error bars are not seen they fall within the symbol.

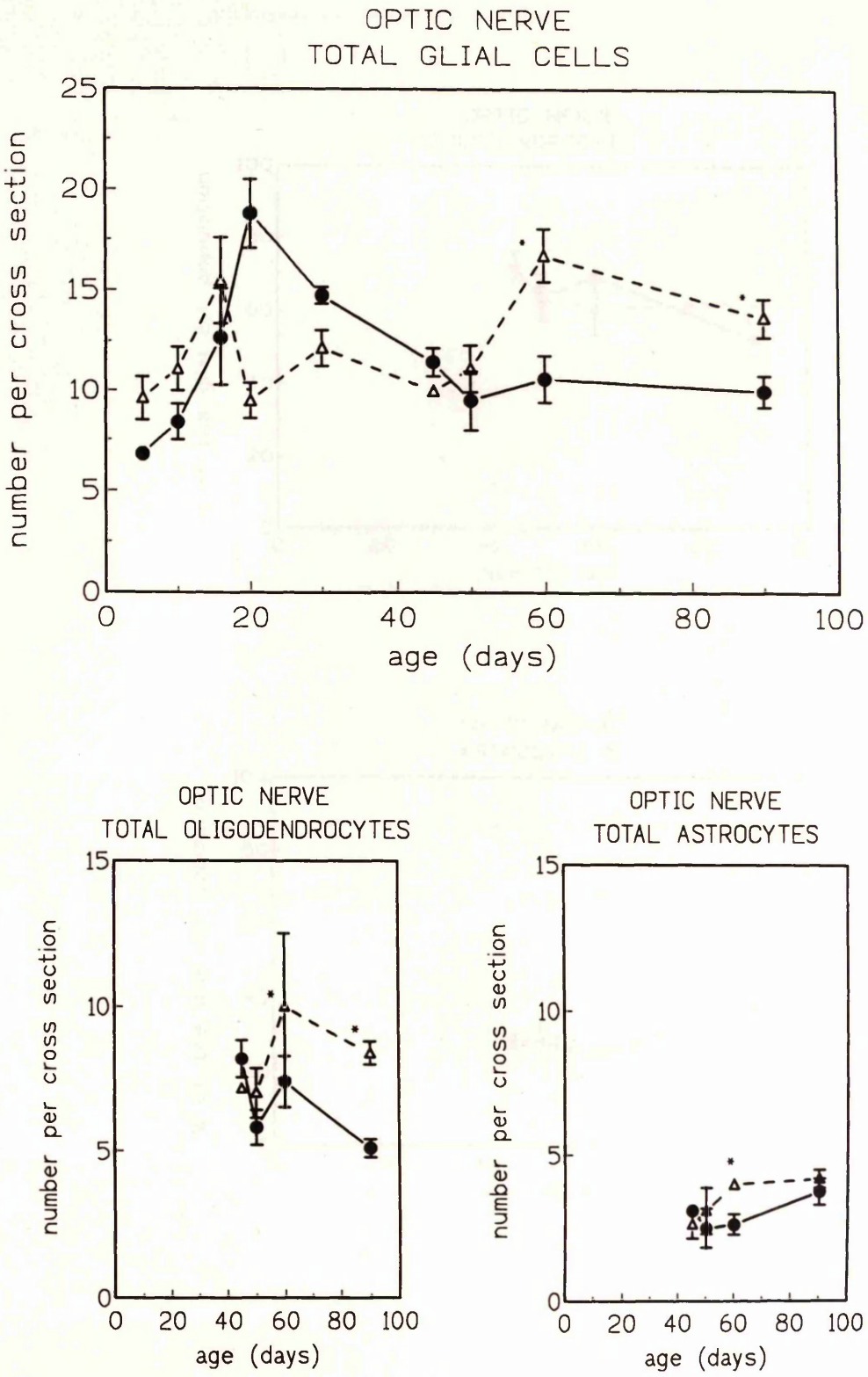

Figure 36: Total numbers of glial cells in the optic nerve. Values from wild type (triangle) and *jp*^{rsh} (filled circle) mice mid-optic nerves. Total numbers of oligodendrocytes and astrocytes are also shown individually. The total numbers of oligodendrocyte numbers in the optic nerve of the mutant, which are initially below the wild type values, became adequate at myelination, then dropping below the wild type values at the age of 45 days. Morphological examination of the optic nerve at this age did not reveal an increased cell death. Cell density in *jp*^{rsh} indicates that these results are the consequence of the smaller total volume of the mutant nerve and that cell numbers stabilize at normal levels after this age. All data represent mean ± SEM; where error bars are not seen they fall within the symbol.

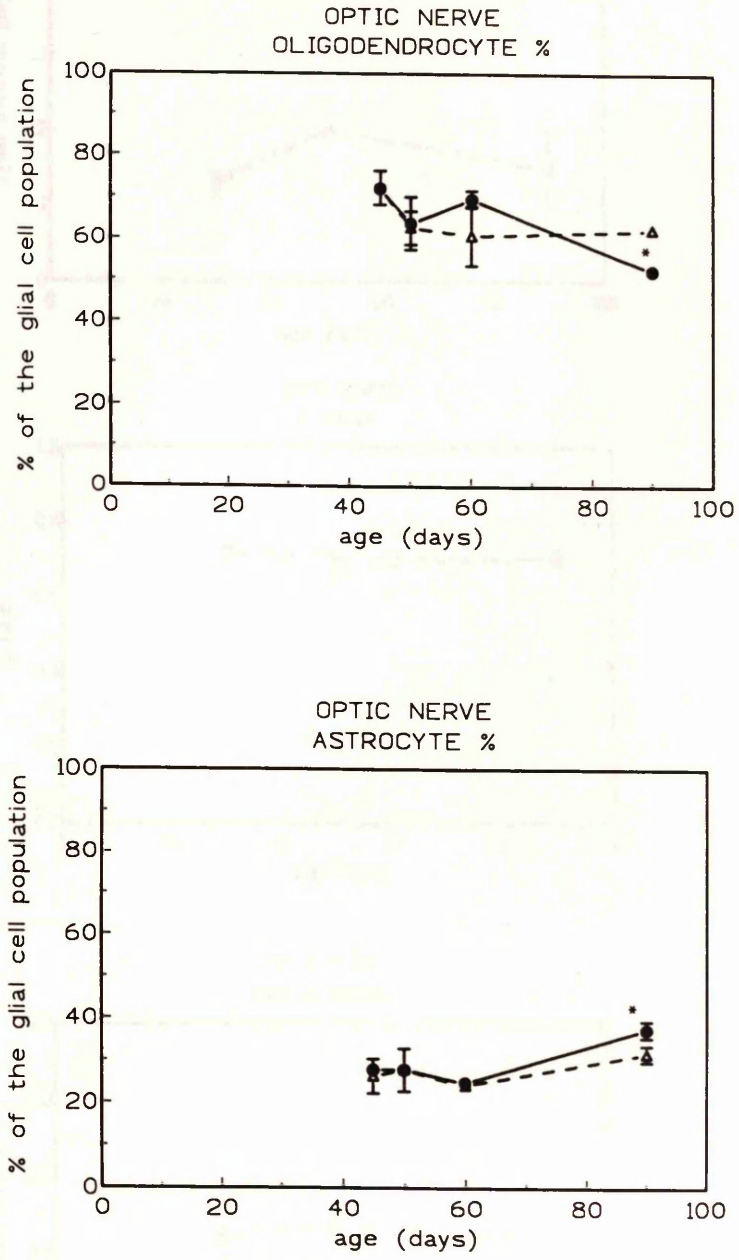

Figure 37: Percentages of oligodendrocytes and astrocytes in the optic nerve. Percentages from the total numbers of glial cell population from wild type (triangle) and jp^{rsh} (filled circle) optic nerve. jp^{rsh} shows a normal oligodendrocyte percentage until the age of 60 days when it increases over wild type, being followed by a later drop in the oligodendrocyte percentage accompanied of an increase of the astrocyte percentage. All data represent mean ± SEM; where error bars are not seen they fall within the symbol. An asterisk has been placed beside the value that differs significatively from the wild type.

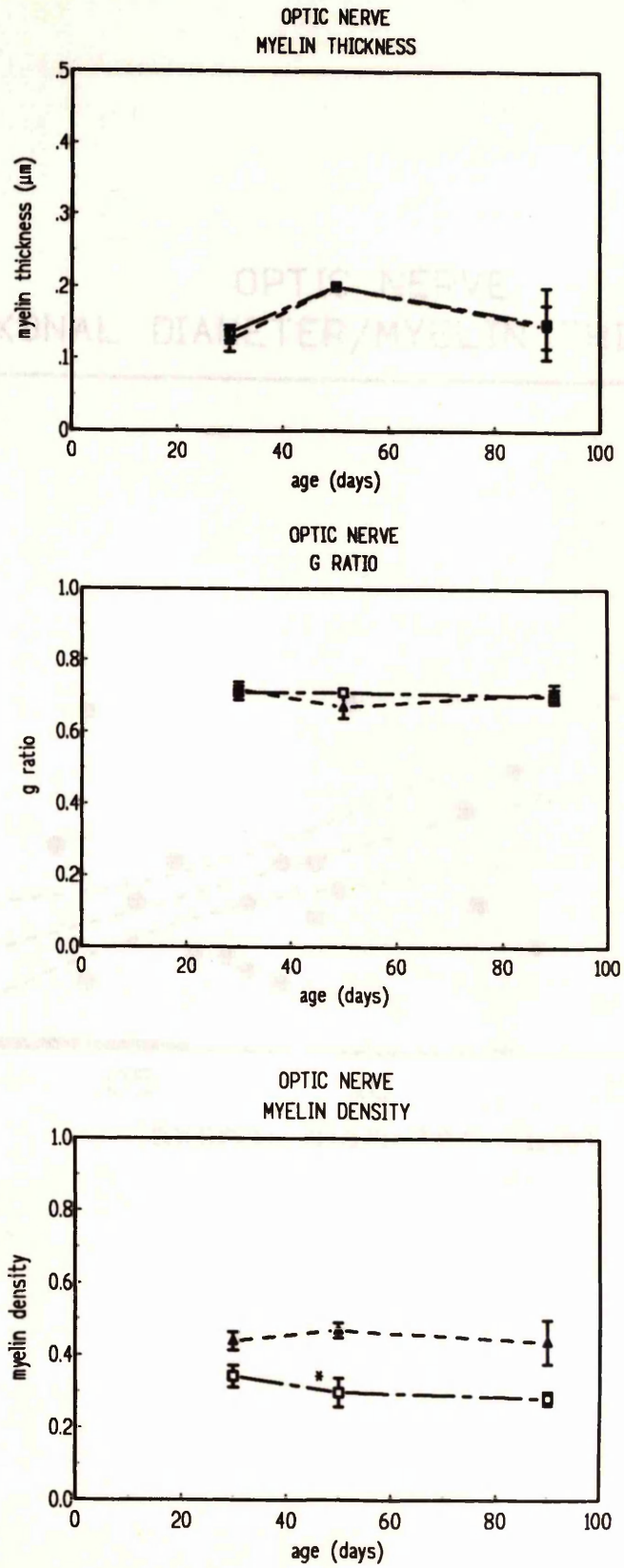

Figure 38: Morphometric analysis of the optic nerve from wild type (triangle) and jp^{rsh} mice (filled circle). The values refer to cells in a cross section of the optic nerve mid-way between the globe and chiasm. All data represent mean ± SEM; where error bars are not seen they fall within the symbol. Asterisks have been placed in values that differ significatively from the wild type. (upper panel) Myelin thickness. (centre) *g* ratio (*g* ratio defined as ratio of axon diameter to that of the axon plus myelin sheath). (lower panel) Myelin density (arbitrary units). The values of the myelin thickness and *g* ratio reveal that most mutant myelin sheaths produced in this area of the CNS are only slightly thinner than age matched wild type fibres. However, myelin density values demonstrate a noticeable myelin deficiency in jp^{rsh} tissue as it includes the amyelinated fibres not included for the myelin thickness and *g* ratio studies.

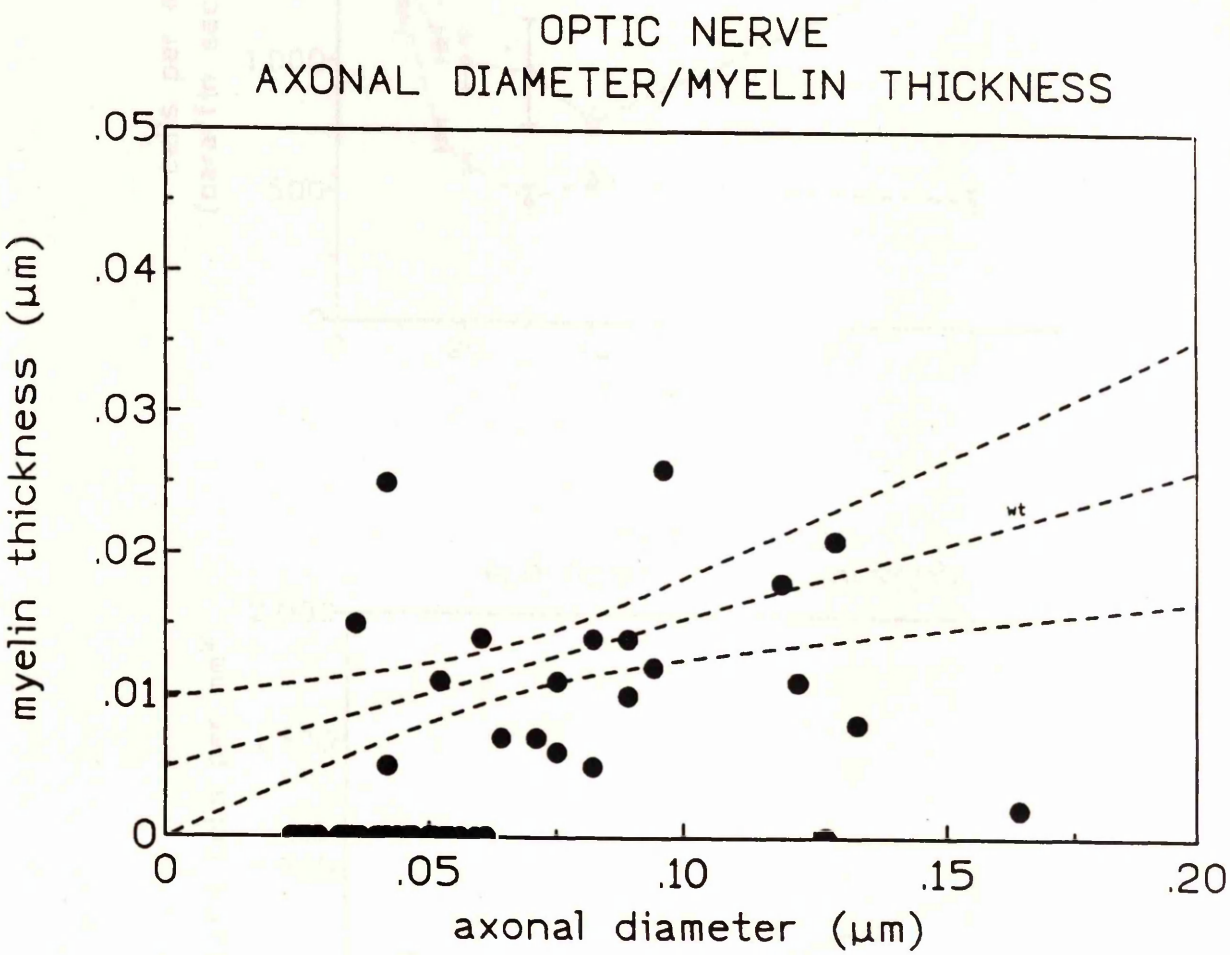

Figure 39: Scatter graph showing the relationship between axon diameter and myelin thickness in the optic nerve from 90-day-old jp^{rsh} mice (filled circle). The central line is the linear regression and the curved lines the prediction bands for similar data from 90-day-old wild type mice. The vast majority of the data from jp^{rsh} mice are within the wild type prediction bands. However, a large numbers of completely unmyelinated fibres are also present in jp^{rsh} mice. The resulting data distribution supports the morphological impression (see figure 28b, 28c) demonstrating that myelin sheaths produced in the optic nerve resemble those of the wild type, although unmyelinated fibres are abundant. This graph can be compared with the equivalent for the spinal cord shown in figure 33.

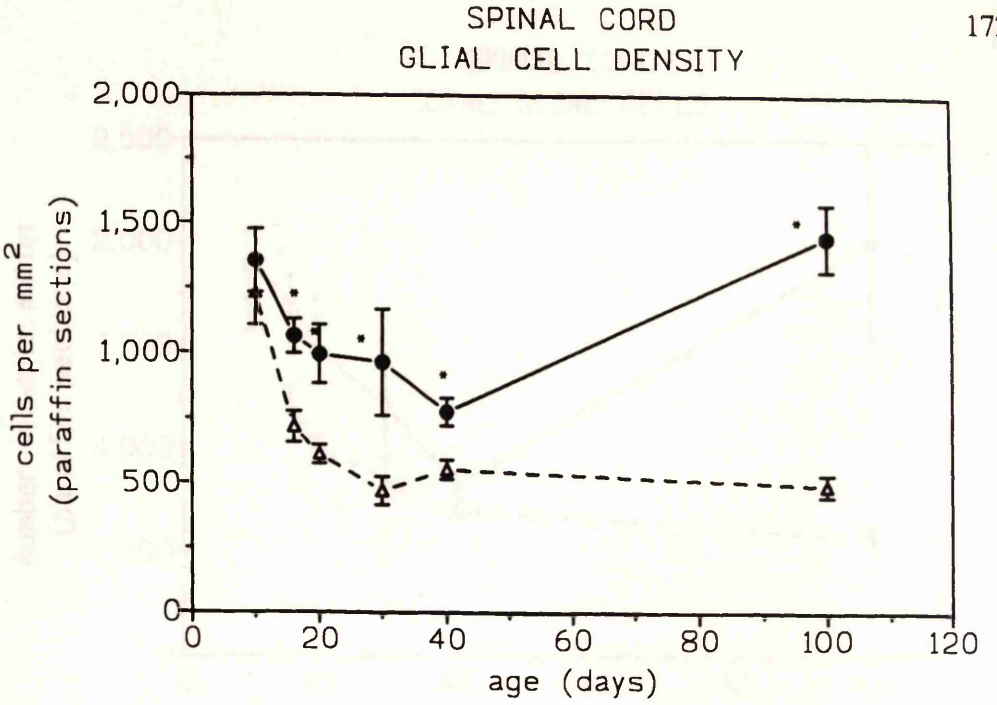

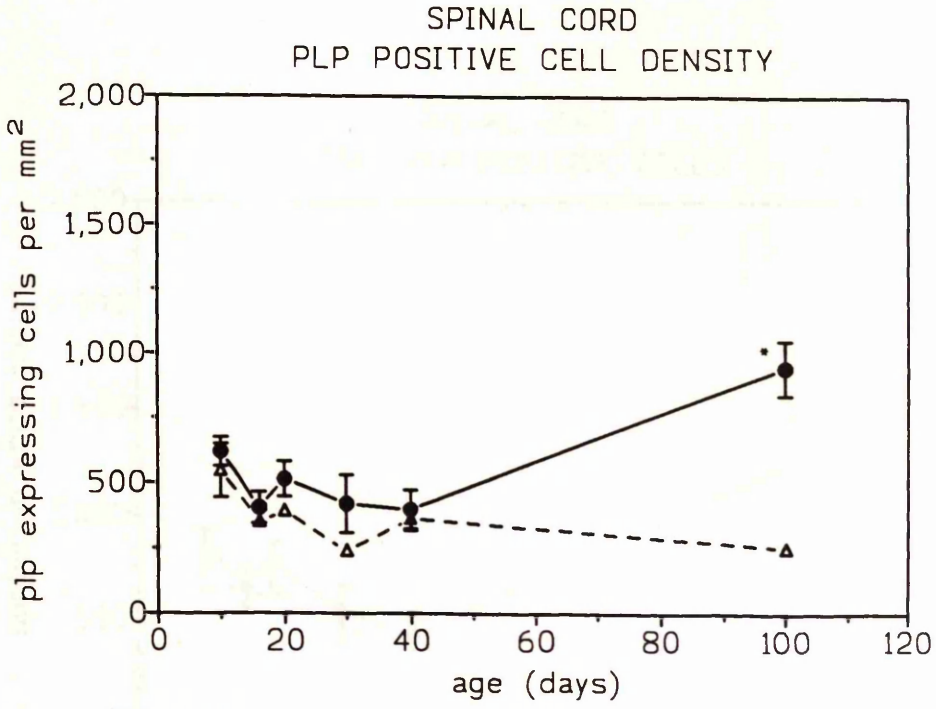

Figure 40: Density of PLP-expressing cells in the ventral columns of the C2 segment of the spinal cord in wild type (triangle) and *jp*^{rsh} mice (filled circle). Paraffin sections were hybridized to a ^{35}S-labelled riboprobe recognising both PLP and DM-20 transcripts. *jp*^{rsh} mice show a progressive increase in PLP-expressing cells. This finding supports morphological observations as well as indicating that the progressive increment of the glial cell population is due to an over-production of oligodendrocytes and/or oligodendroblast (see figure 84). As cell counts are influenced by any change in volume, (which is lower in *jp*^{rsh} due to the decreased amount of myelin) the glial cell density is also presented. All data represent mean ± SEM; where error bars are not seen they fall within the symbol.

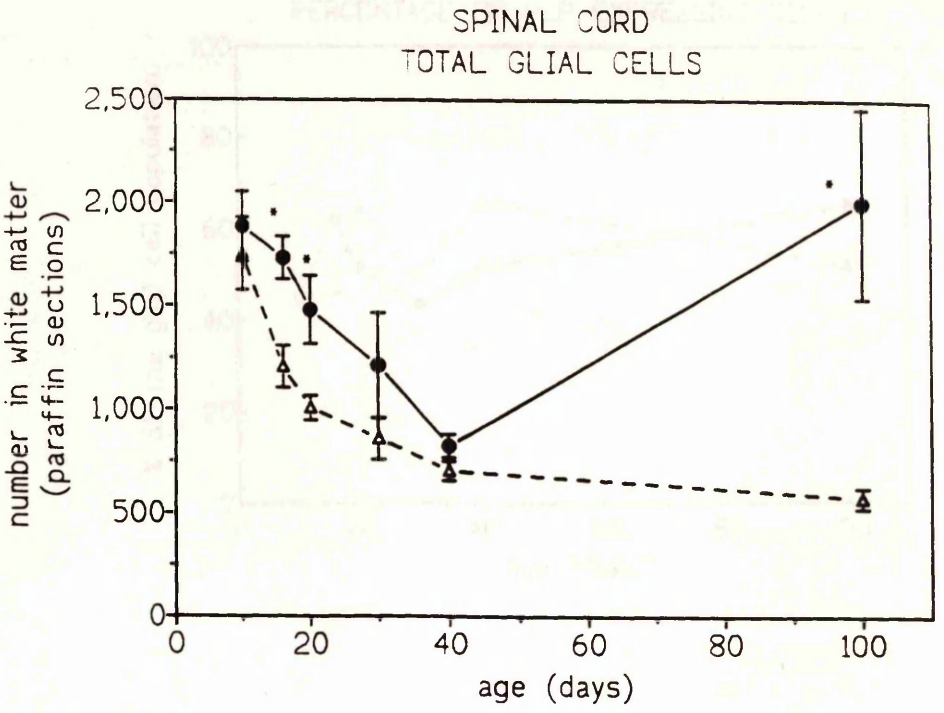

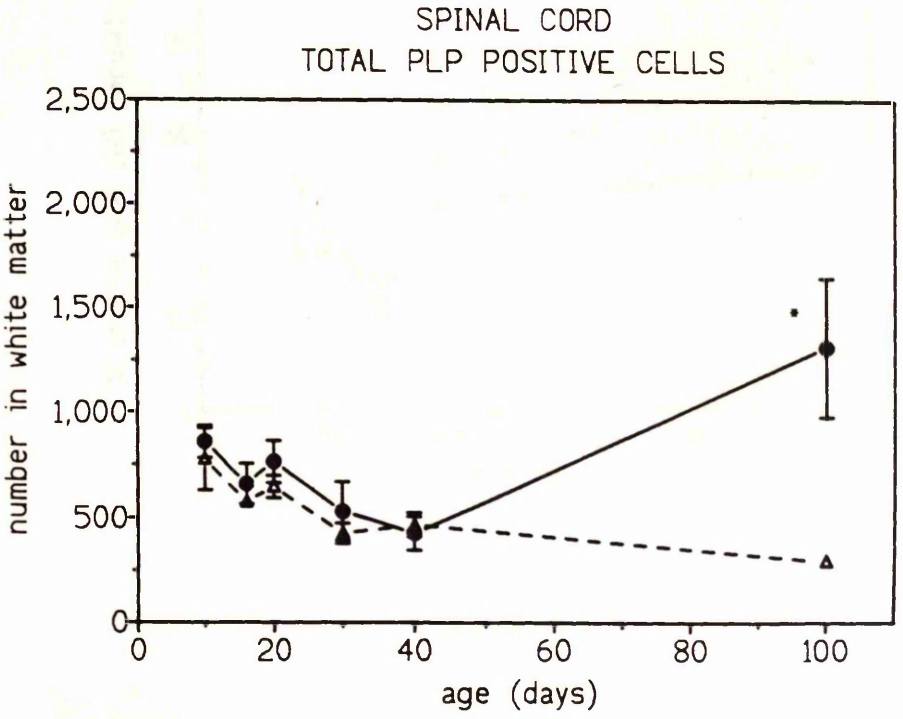

Figure 41: Total numbers of PLP-expressing cells in the wild type (triangle) and jp^{rsh} mice (filled circle) spinal cord. Total glial cell numbers in the white matter of jp^{rsh} increase dramatically after 40 days as a consequence of the increase of the PLP-expressing cells. Total numbers of glial cells in the spinal cord are also shown as cell counts are influenced by any change in volume. All data represent mean ± SEM; where error bars are not seen they fall within the symbol. Asterisks have been placed in values that differ significatively from the wild type.

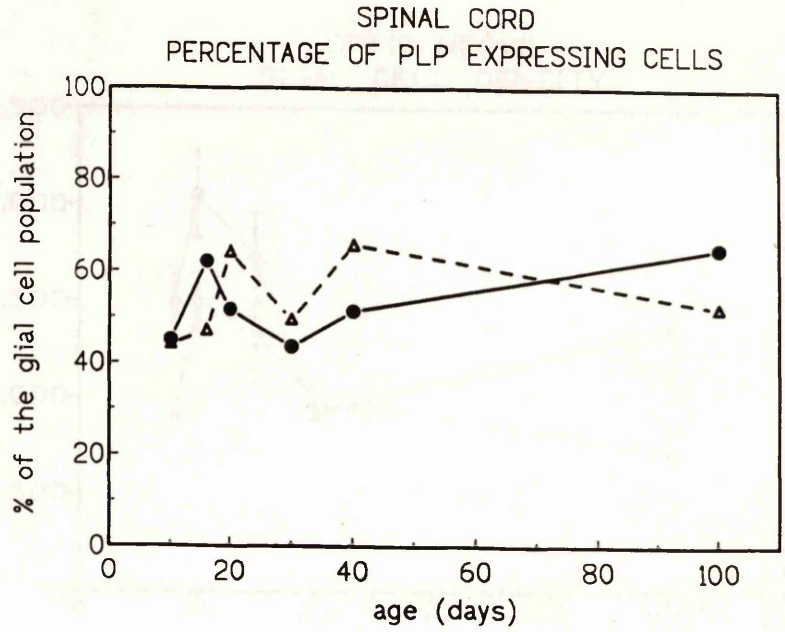

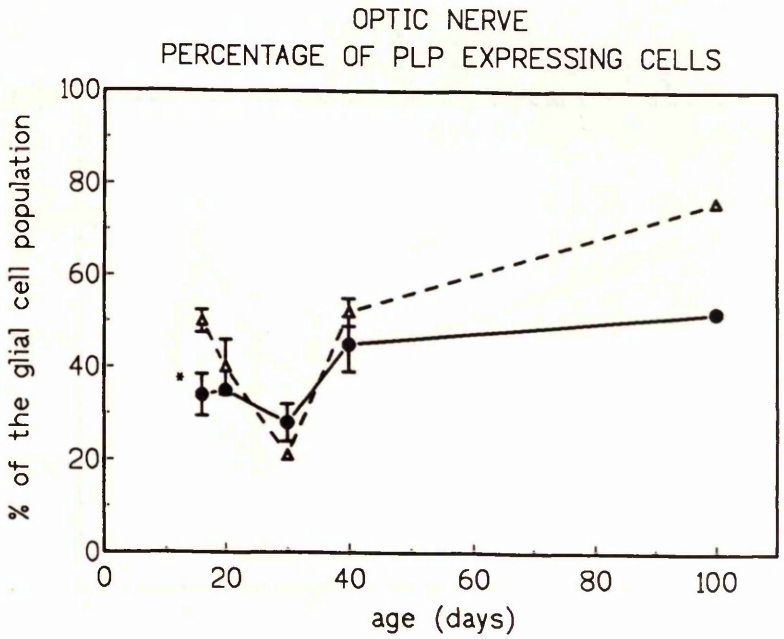

Figure 42: Percentages of PLP-expressing cells in the wild type (triangle) and *jp*^{rsh} mice (filled circle) spinal cord and optic nerve. All data represent mean ± SEM; where error bars are not seen they fall within the symbol. An asterisk has been placed beside the value that differs significatively from the wild type. The percentage of PLP-expressing cells in the spinal cord demonstrates that not all the cells morphologically resembling oligodendrocytes were actively expressing PLP in the mutant. However, by the age of 100 days, the percentages of expressing oligodendrocytes increase according to the morphological findings (figure 84.b).

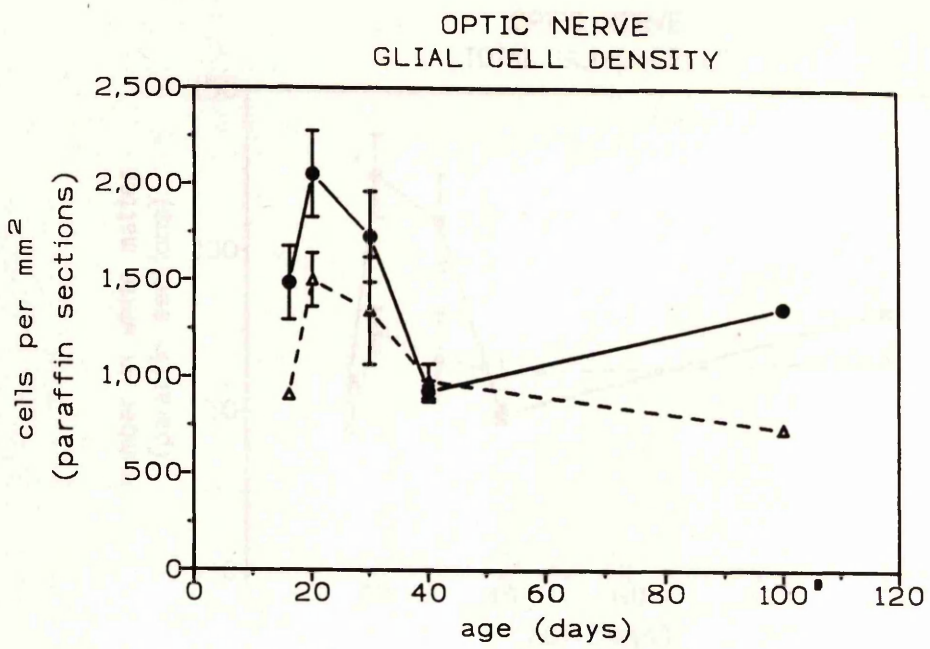

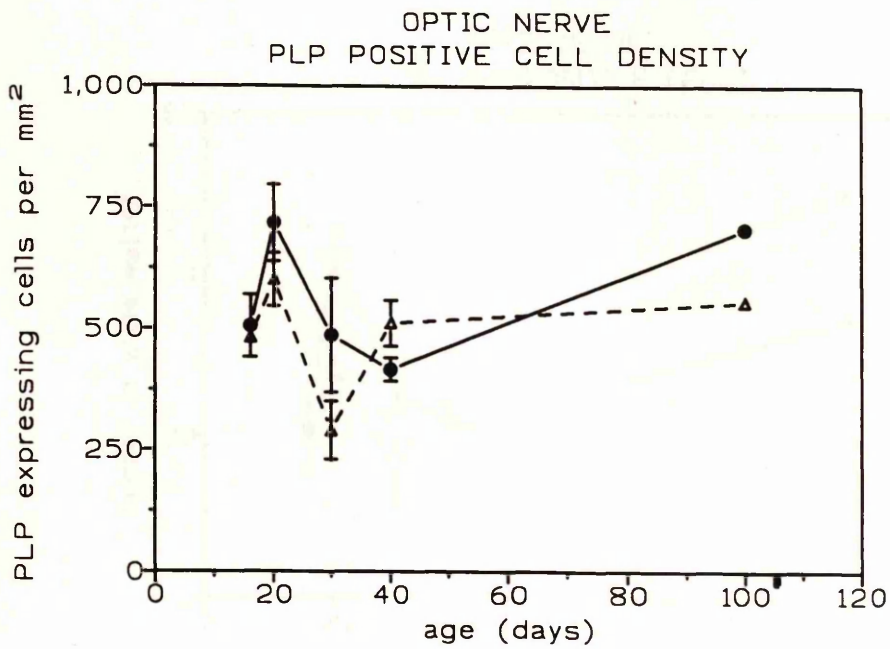

Figure 43: Density of PLP-expressing cells in the wild type (triangle) and *jp*^{rsh} mice (filled circle) optic nerve. The values refer to cells in a cross section of the optic nerve mid-way between the globe and chiasm. Glial cell density drops at 40 days of age in the mutant, recovering by the age of 100 days as a result of an increase in the PLP-expressing cells. All data represent mean ± SEM; where error bars are not seen they fall within the symbol. As cell counts are influenced by any change in volume, (which is lower in *jp*^{rsh} optic nerve) the glial cell density is also presented. (@) Shows the result obtained from a single experiment.

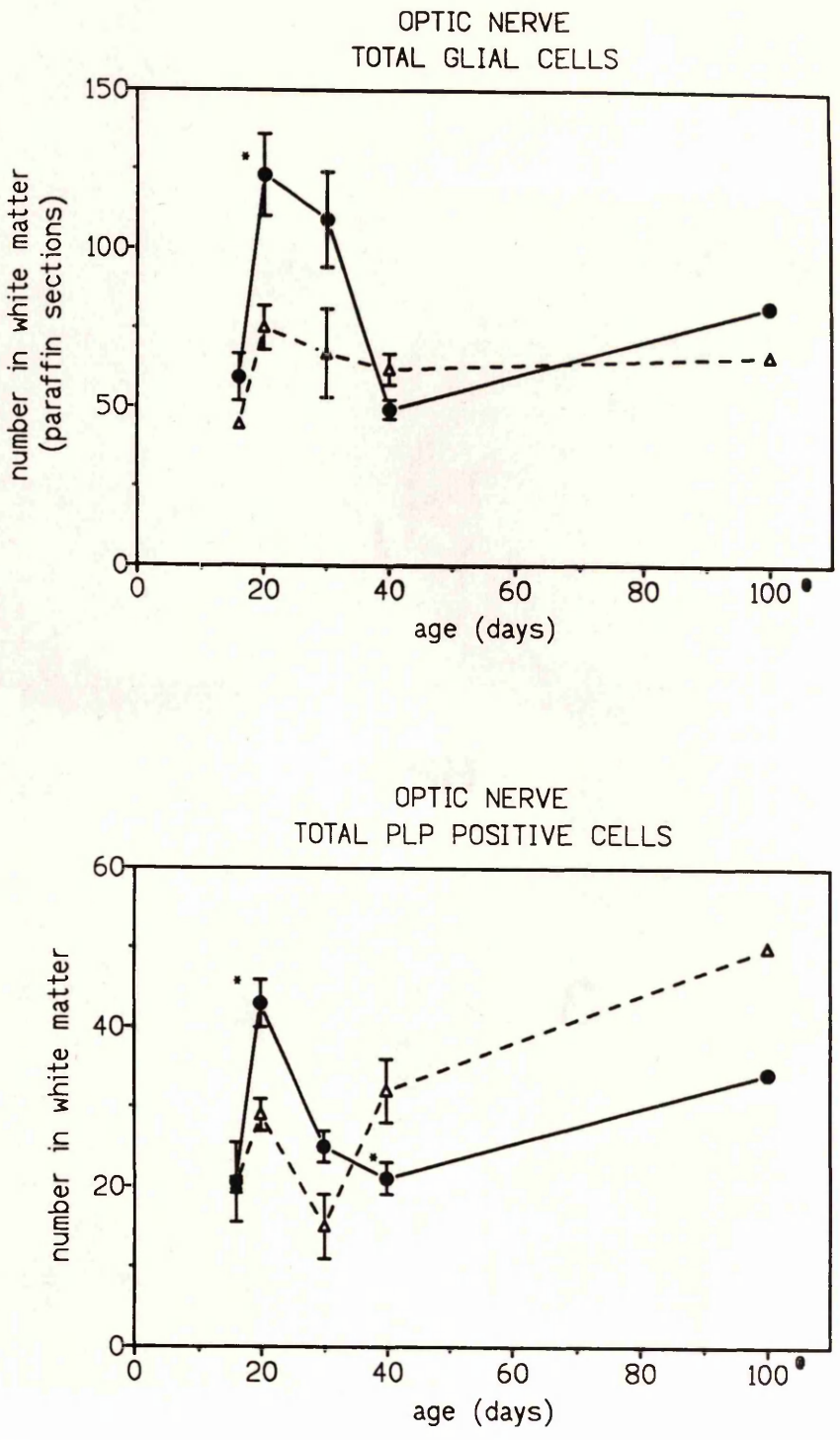

Figure 44: Total numbers of PLP-expressing cells in the wild type (triangle) and jp^{rsh} mice (filled circle) optic nerve. Values from the wild type and jp^{rsh} mice from the same experiment as in the previous figure. Total numbers of glial cells in the mutant drop below wild type numbers after 40 days of age mainly as a result of a decrease in the PLP-expressing cells. All data represent mean ± SEM; where error bars are not seen they fall within the symbol. Morphological data also indicate that the oligodendrocyte numbers in the optic nerve drop below normal counts around 40 days of age and that there is a increase in the astrocyte numbers (figure 35). Total numbers of glial cells in the paraffin-embedded of the optic nerves are also presented as cell counts are influenced by any change in volume. All data represent mean ± SEM; where error bars are not seen they fall within the symbol. An asterisk has been placed beside the value that differs significatively from the wild type. (@) Shows the result obtained from a single experiment.

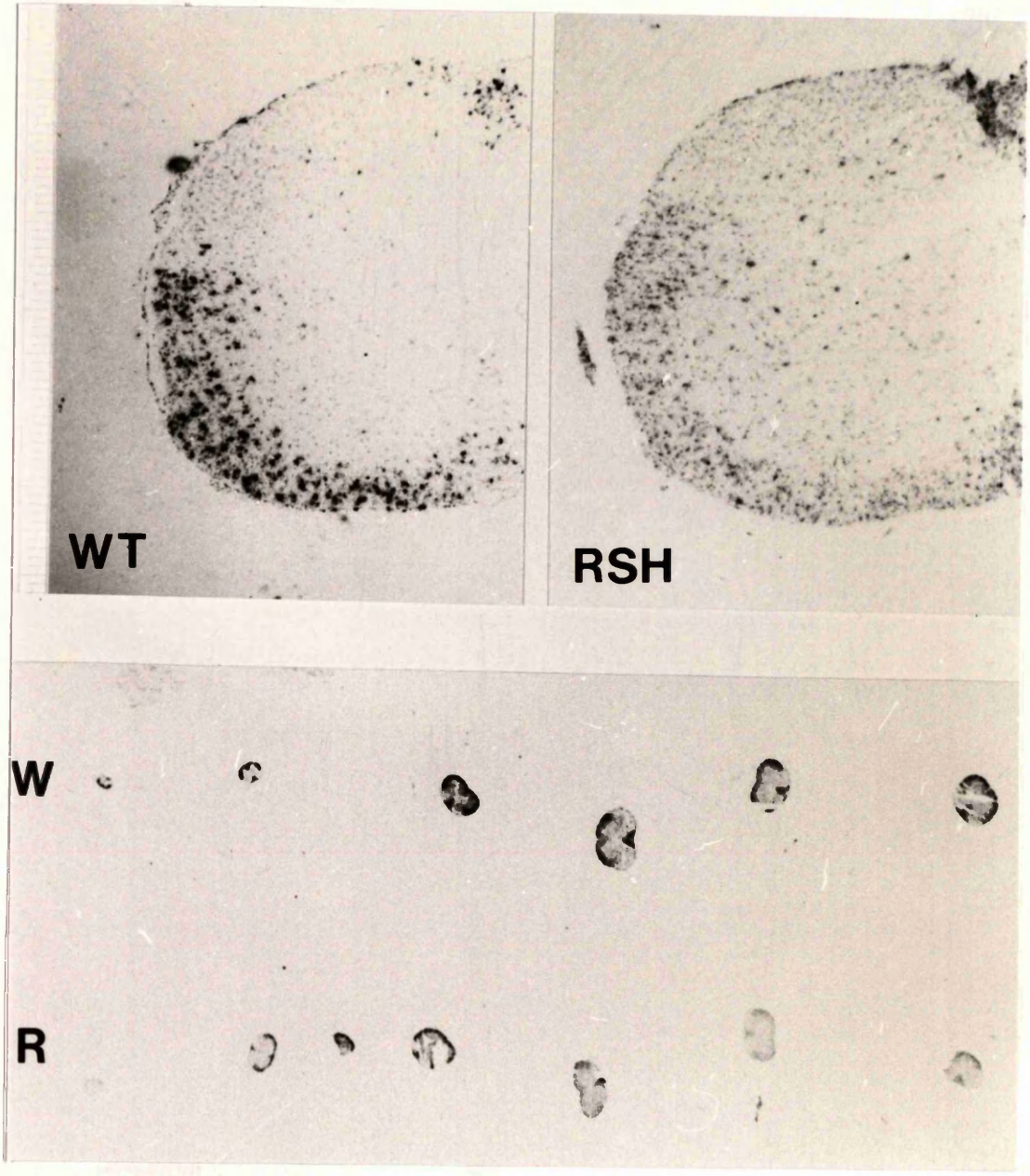

Figure 45: Autoradiograms of the spinal cord from 5, 10, 16, 20, 30, 40 and 90-day-old mice. *In situ* hybridization for PLP/DM-20 mRNA on paraffin sections from wild type (W) and jp^{rsh} (R) mice at the mentioned ages hybridized and incubated on the same slide and counterstained with haematoxilin (some spinal cord sections are missing). Upper panel show details of the 10-day-old wild type (WT) and mutant (RSH) mice spinal cords. The intensity of signal per cell as well as the overall expression of PLP/DM-20 are decreased in jp^{rsh} (see figures 46 and 47 for more detail). (Approx. magnification: upper panel x 53, lower panel x 2).

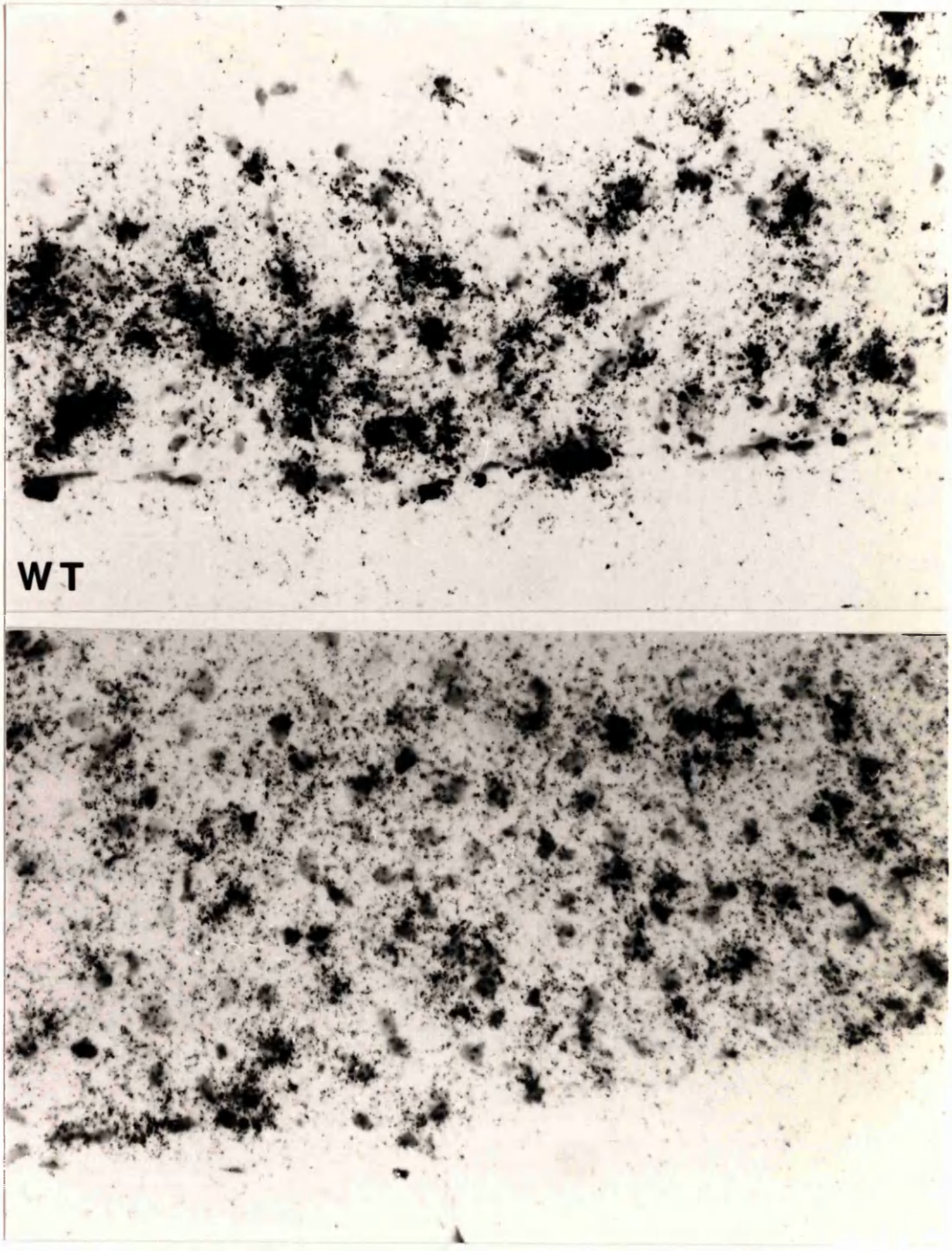

Figure 46: Autoradiograms of the *in situ* hybridization for PLP/DM-20 mRNA of the white matter from the ventral columns of the spinal cords from 10-day-old wild type (WT) and mutant mice (lower panel). Foci of silver grains signifying expressing oligodendrocytes are present in each, but the intensity of the signal is less in the mutant. Nuclei of non-expressing cells are also present. (Approx. magnification: x 500).

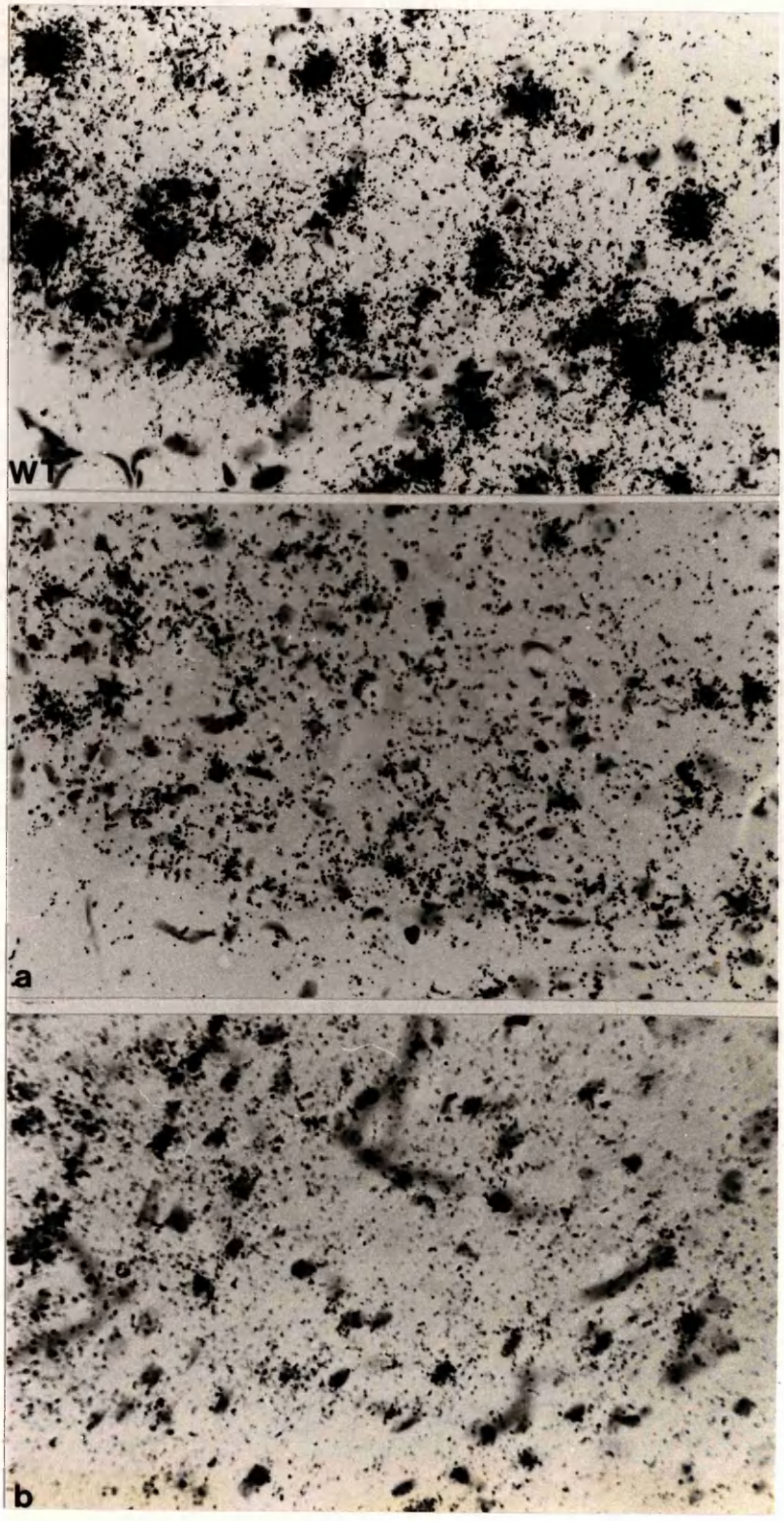

Figure 47: Autoradiograms of the *in situ* hybridization for PLP/DM-20 mRNA of white matter from the ventral columns of the spinal cords from 30-day-old wild type (WT) and mutant (a, b) mice. The individual cell expression of PLP/DM-20 in jp^{rsh} is more decreased than in 10-day-old spinal cord samples (figure 46). There is an evidence of an increased cellularity in the mutant as demonstrated by the amount of counterstained glial nuclei. (Approx. magnification: x 400).

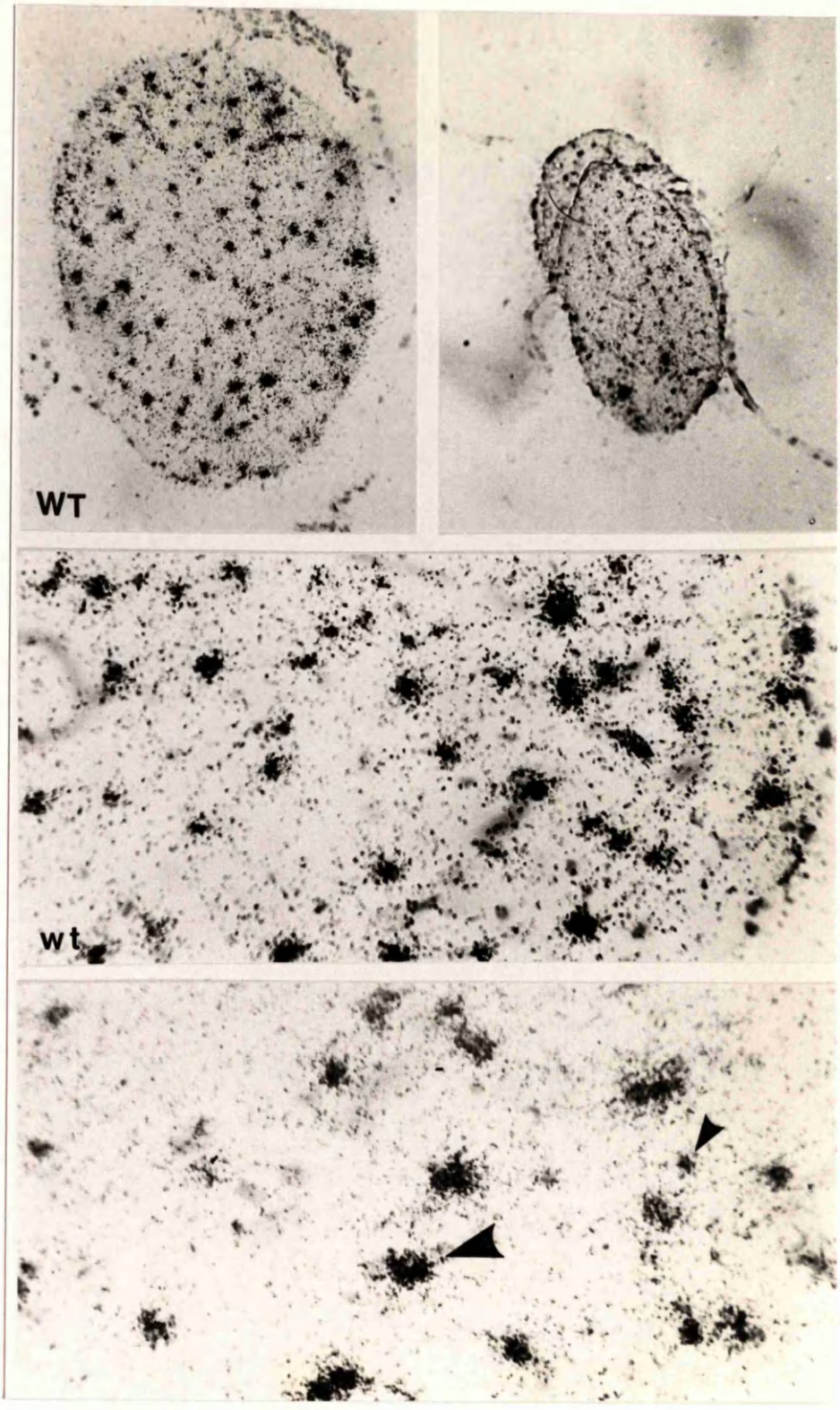

Figure 48: *In situ* hybridization for PLP/DM-20 mRNA in 100-day-old wild type (WT, wt) and jp^{rsh} mice optic nerves. Upper panel shows a general view of the hybridized section of both types of optic nerves at the same magnification. Silver grains over the nuclei signify the individual PLP/DM-20 cell expression. The individual cell expression as well as the total number of expressing oligodendrocytes is decreased in jp^{rsh} optic nerve in respect to wild type age-matched controls (see figures 43 and 44 for quantified data). Cell expression is variable in jp^{rsh} mice although most cells express very little PLP/DM-20 (small arrow-head). Occasional oligodendrocytes show a normal labelling (large arrow-head). Nuclei of non expressing cells counterstained with haematoxilin are also present in the autoradiogram. (Approx. magnification: upper panel x 142, lower panel x 500)

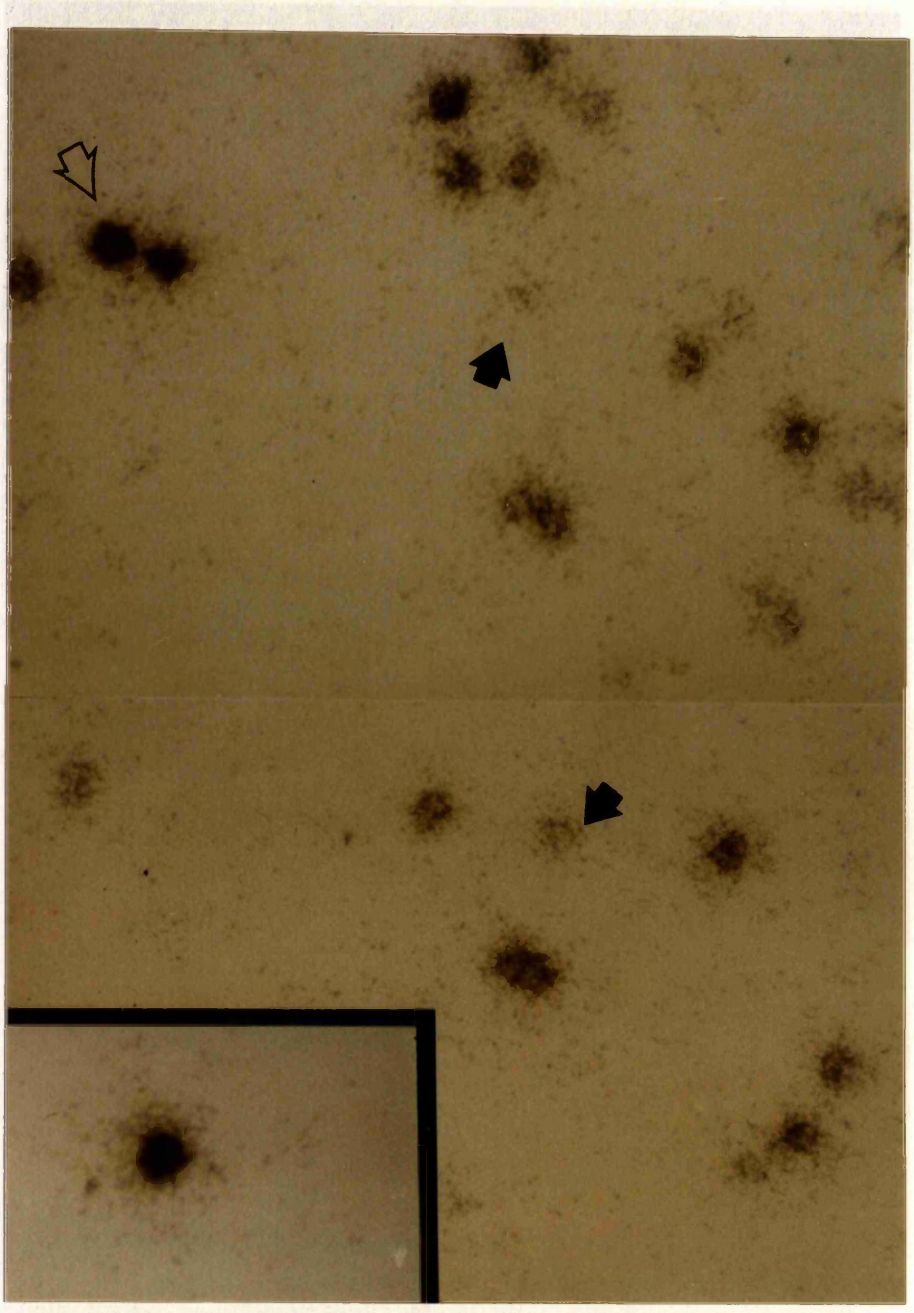

Figure 49: Autoradiograms of dissociated oligodendrocytes from the ventral columns of the spinal cords from 16-day-old mutant mice. Cell were dissociated and were allowed to adhere to the coverslip for two hours before hybridization for PLP/DM-20 mRNA. Cells were not counterstained, showing only expressing oligodendrocytes. The signal of individual cells was measured by densiometry and the average message level per cell was significantly reduced. *jp*^{rsh} dissociated oligodendrocytes expressed variable levels of PLP/DM-20. Although some cells labelled as wild type cells (open arrow), others showed a significantly reduced mRNA message (thick arrows). The inset shows a control wild type expressing oligodendrocyte. (Approx. magnification: x 450).

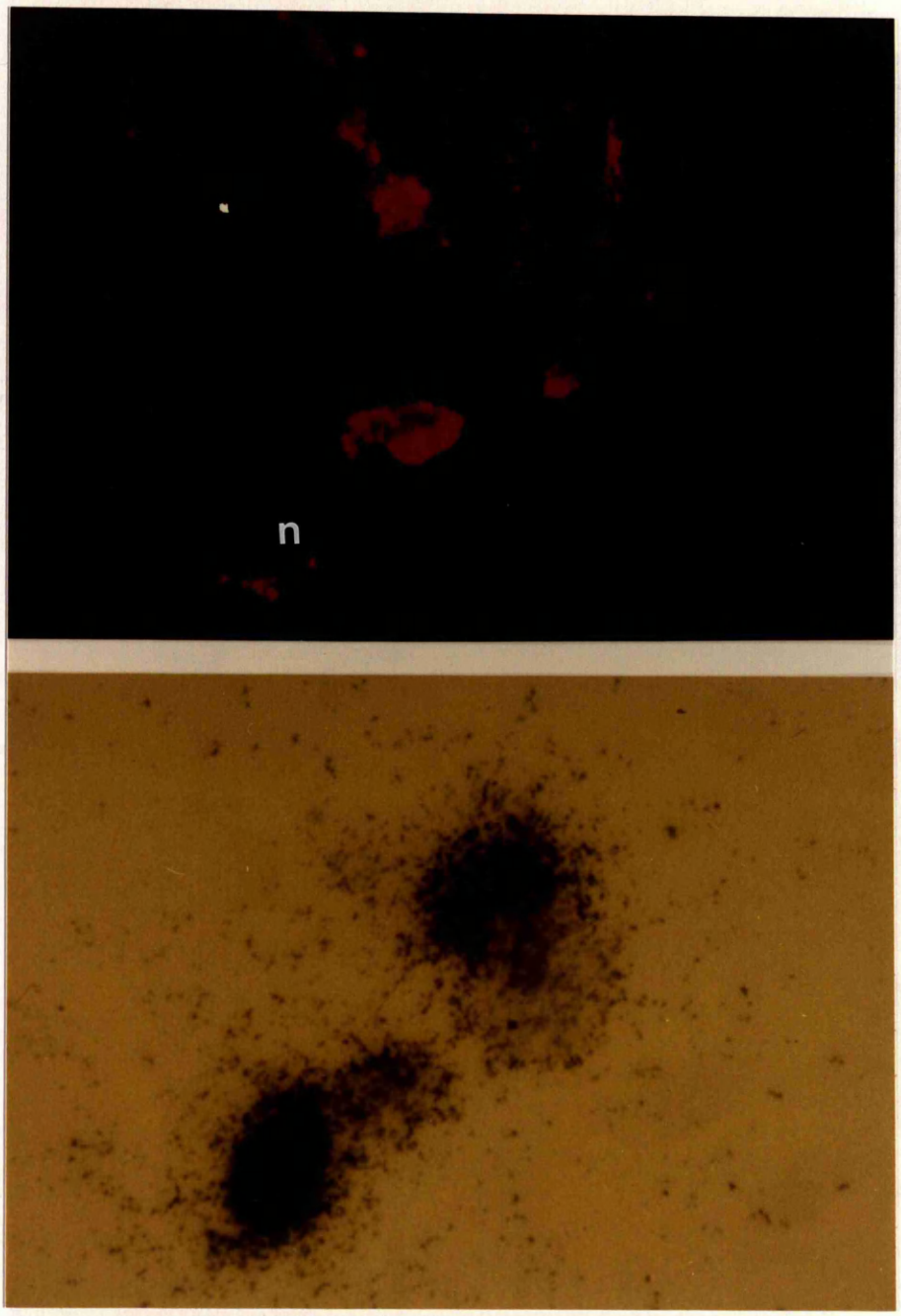

Figure 50: Autoradiogram of two wild type immunostained oligodendrocytes from dissociated ventral columns of the spinal cord of 7-day-old mice cultured for 7 days and immunostained with GalC. Same experiment as figures 51, 52 and 53. (upper panel) GalC immunostained oligodendrocytes. (lower panel) Autoradiogram of the same cells. The accumulation of silver grains over the nuclei of the cells signifies the PLP/DM-20 expression. In this case the abundance of silver grains blackens the GalC immunofluorescence over one of the nucleus (n). (Approx. magnification: x 450).

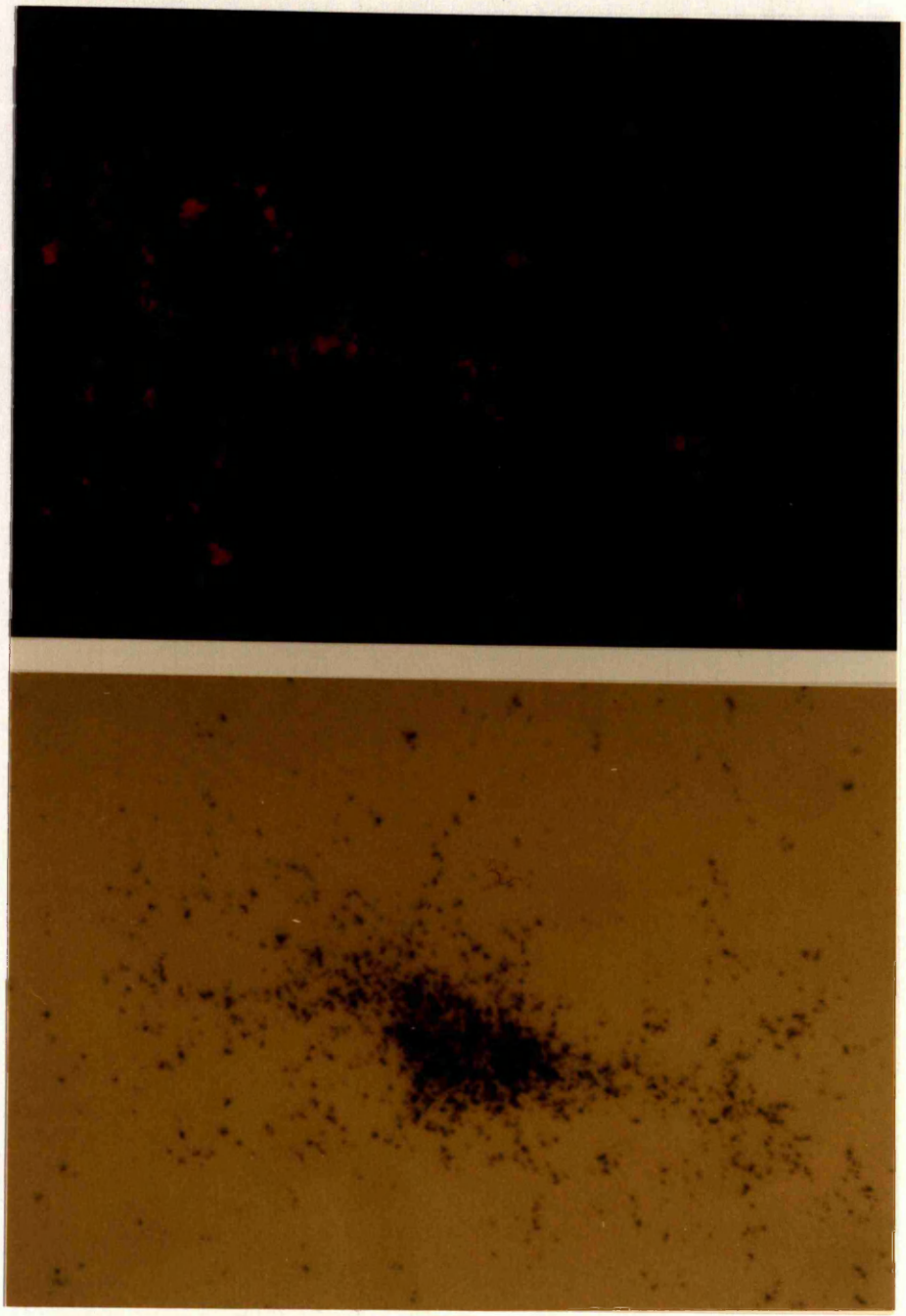

Figure 51: Autoradiogram of a wild type immunostained oligodendrocyte. Cell from dissociated ventral columns of the spinal cord of 7-day-old mice cultured for 7 days and immunostained with GalC. Same experiment as figures 50, 52 and 53. (upper panel) GalC immunostained oligodendrocyte. (lower panel) Autoradiogram of the same cell. The accumulation of silver grains over the nuclei of the cells signifies the PLP/DM-20 expression. (Approx. magnification: x 450).

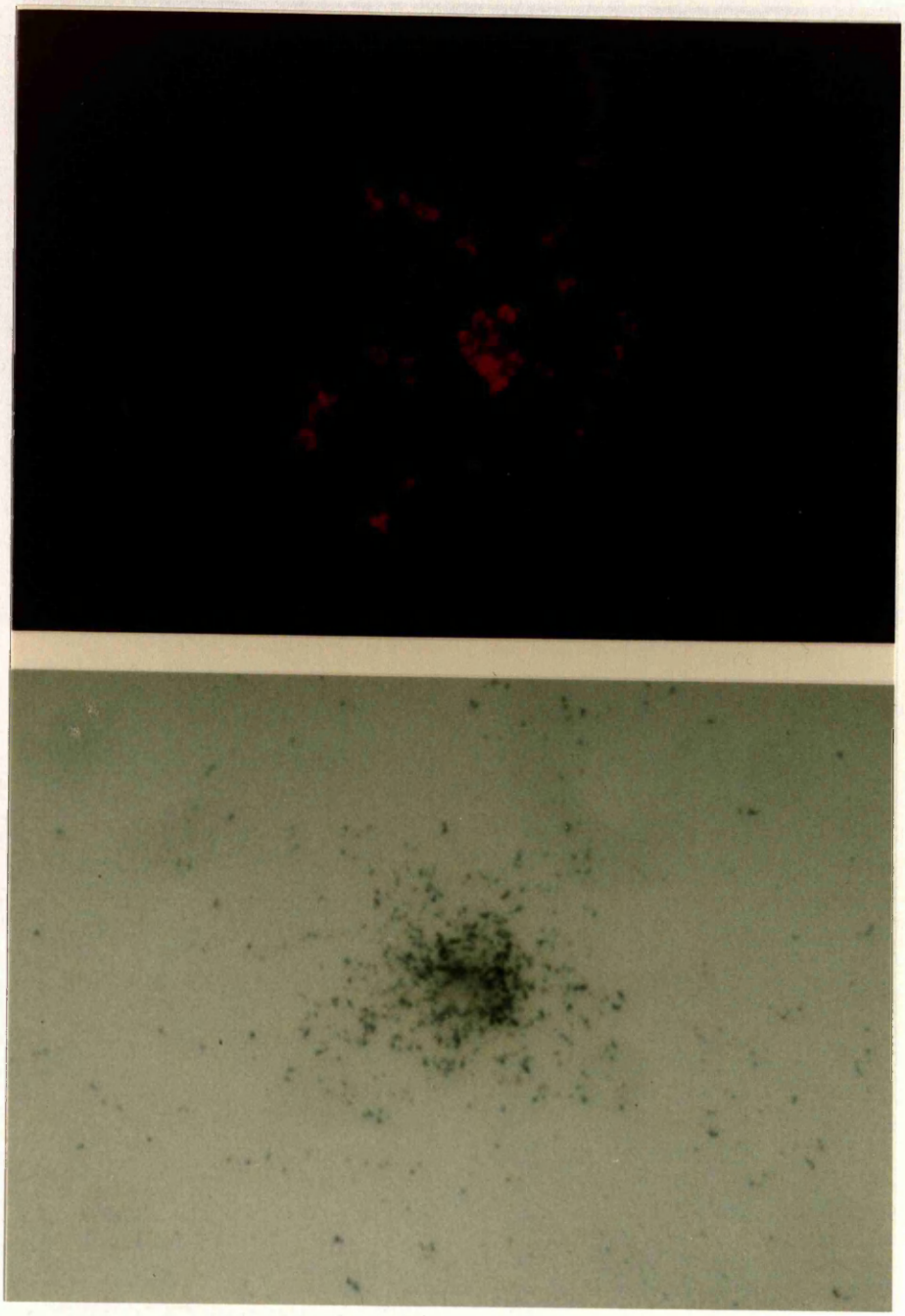

Figure 52: Autoradiogram of a jp^{rsh} immunostained oligodendrocyte. Cell from dissociated ventral columns of the spinal cord of 7-day-old mice cultured for 7 days and immunostained with GalC. Same experiment as figures 50, 51 and 54. (upper panel) GalC immunostained oligodendrocyte. (lower panel) Autoradiogram of the same cell. The accumulation of silver grains over the nuclei of the cells signifies the PLP/DM-20 expression. (Approx. magnification: x 450). The mutant individual cell expression is significantly reduced when compared to controls (figures 50 and 51).

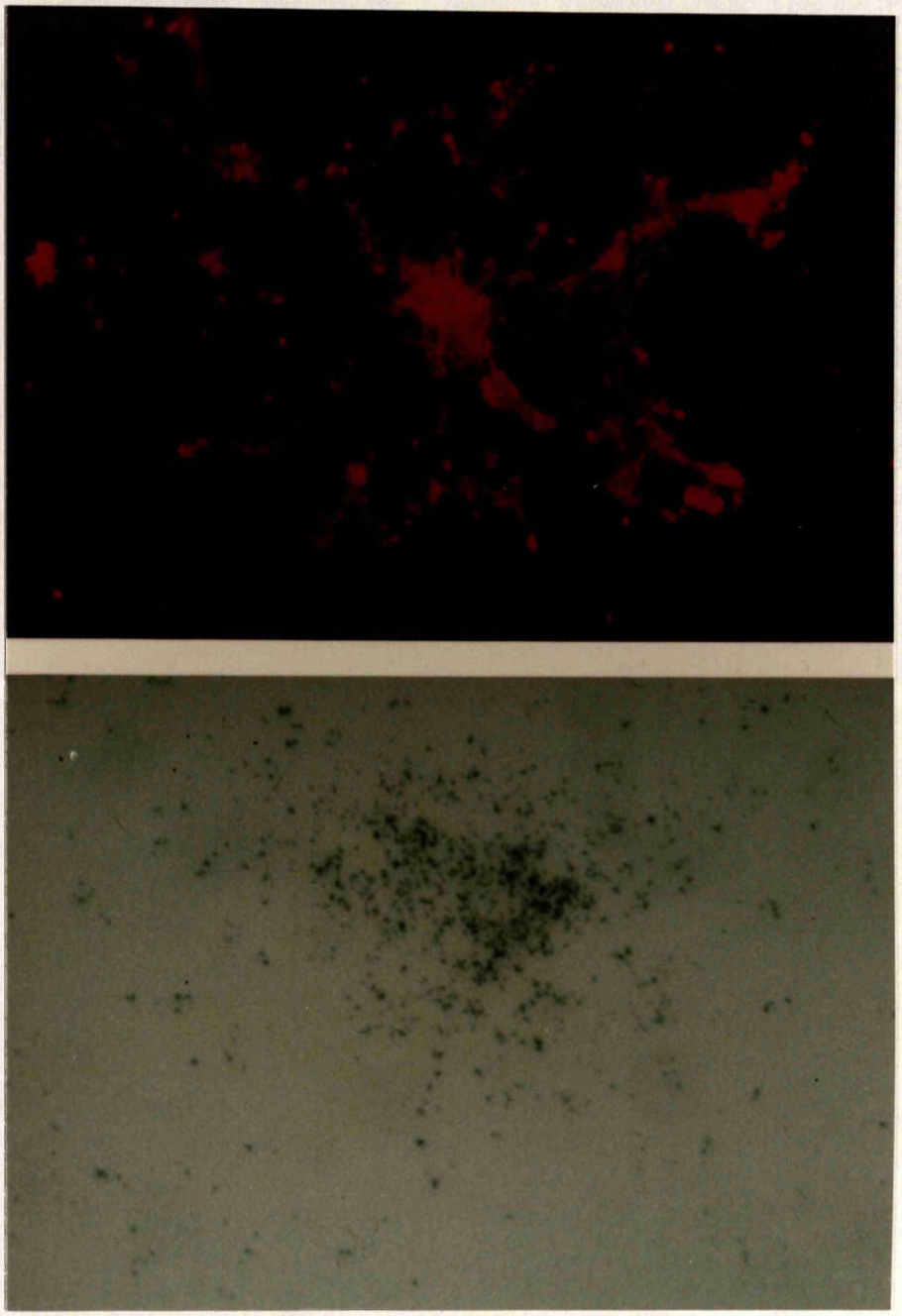

Figure 53: Autoradiogram of a jp^{rsh} immunostained oligodendrocyte. Cell from dissociated ventral columns of the spinal cord of 7-day-old mice, cultured for 7 days and immunostained with GalC. Same experiment as figures 50, 51 and 53. (upper panel) GalC immunostained oligodendrocyte. (lower panel) Autoradiogram of the same cell. The accumulation of silver grains over the nuclei of the cells signifies the PLP/DM-20 expression. (Approx. magnification: x 450). Although GalC reveals the morphological profile of a mature mutant oligodendrocyte, this cells expresses low amounts of PLP/DM-20 when compared to wild type controls hybridized under the same conditions (figures 50, 51).

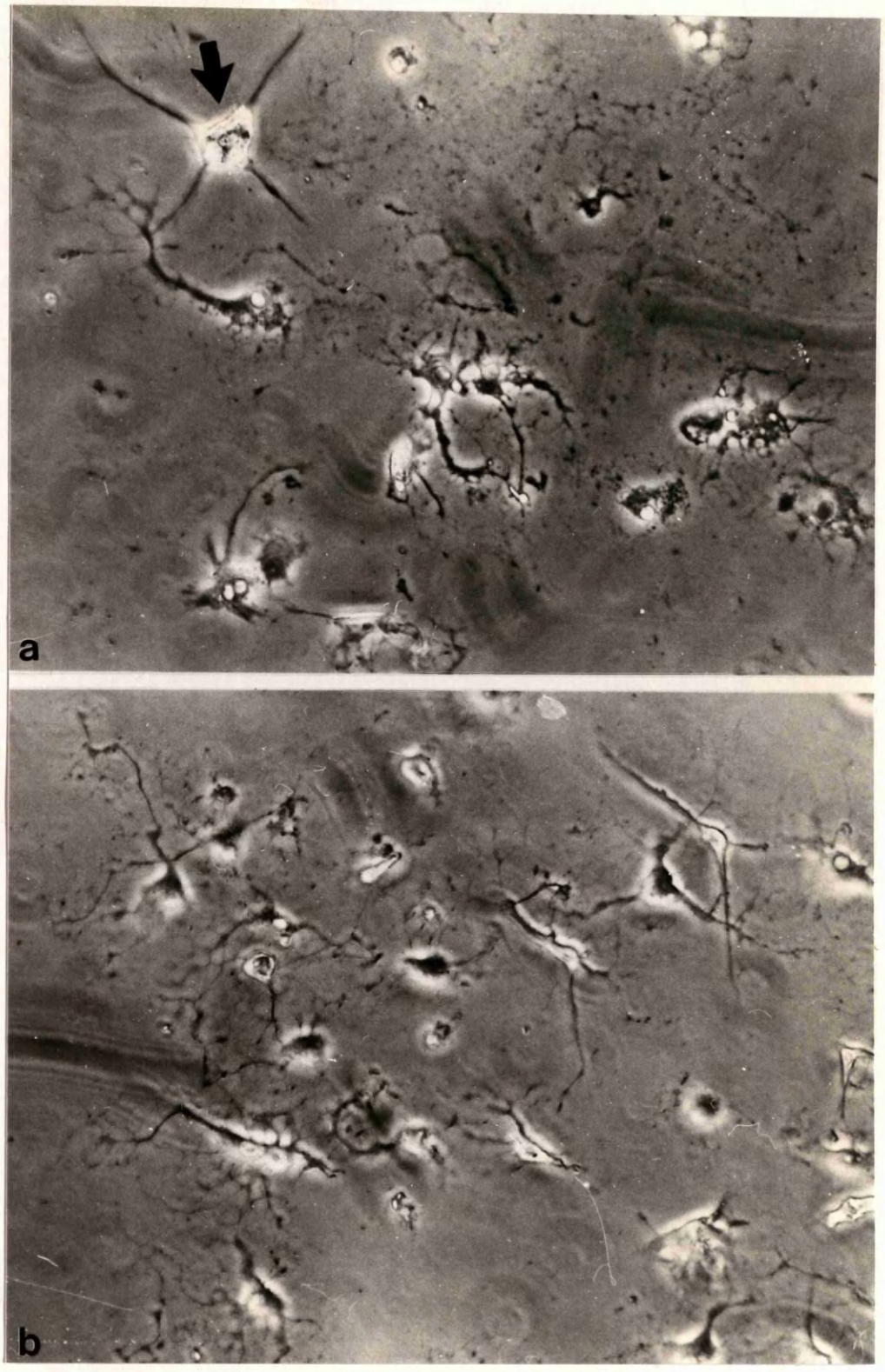

Figure 54: *In vitro* morphological appearance of live jp^{rsh} oligodendrocytes taken from optic nerves of 16-day-old and cultured for 7 days. Mutant cells show no major changes in morphology with processes and membranes of normal dimensions being produced at the expected time in a similar manner to wild type cells. (a) Astrocytes are occasionally present in the culture dishes (arrow). (Approx. magnification: x 450)

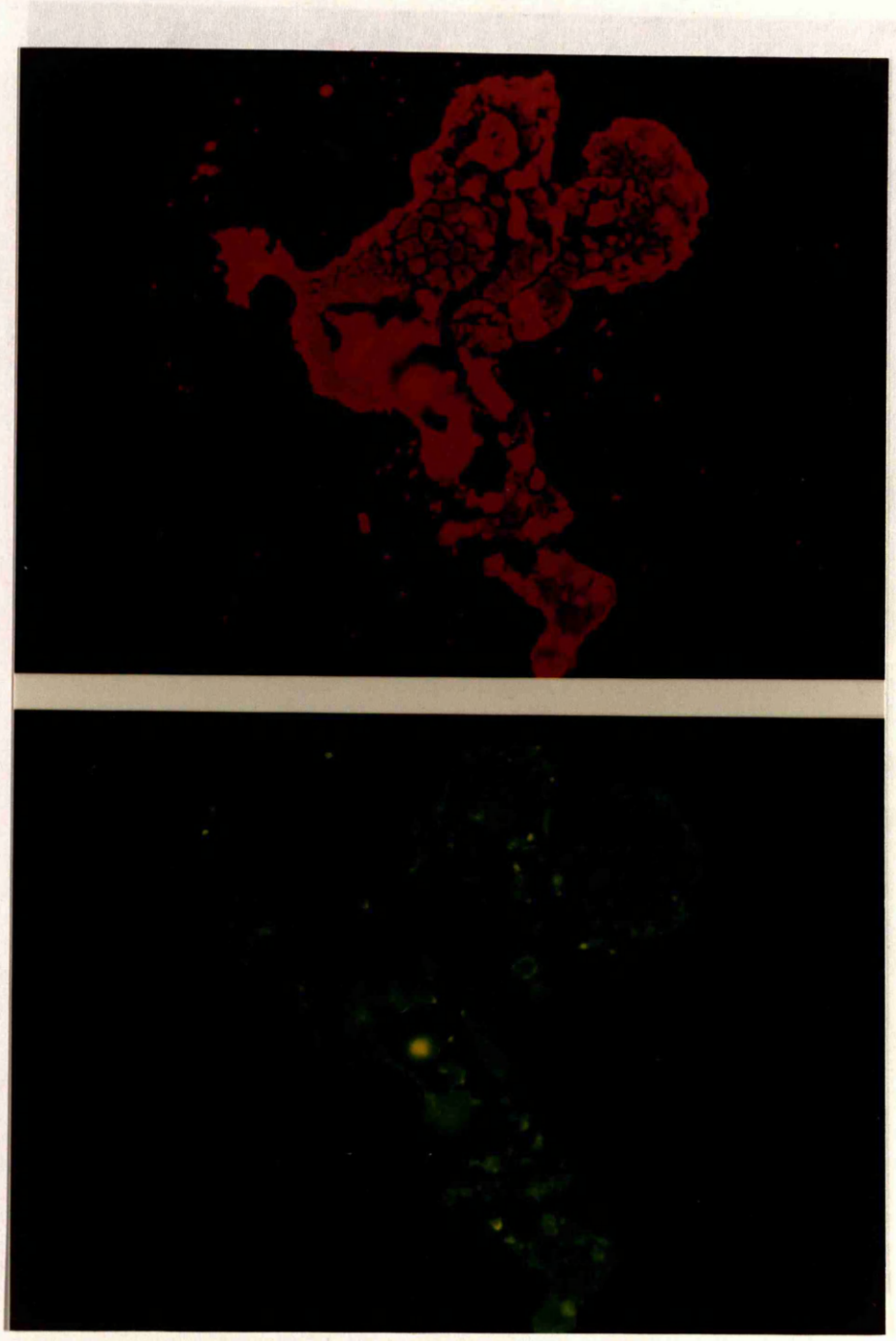

Figure 55: Double immunolabelling for GalC and O4 antigens in 120 hour-old cultures of spinal cord from 3-day-old *jp*^{rsh} mouse from the same experiment as figure 56. GalC (upper panel) is visualized by rhodamine (goat-anti-mouse IgG_3 TRITC) and O4 (lower panel) by fluorescein (goat-anti-mouse IgM FITC) labels. Both antibodies were applied to live unfixed cultures. This mutant oligodendrocyte exhibits myelin membranes of normal appearance. (Approx. magnification: x 450)

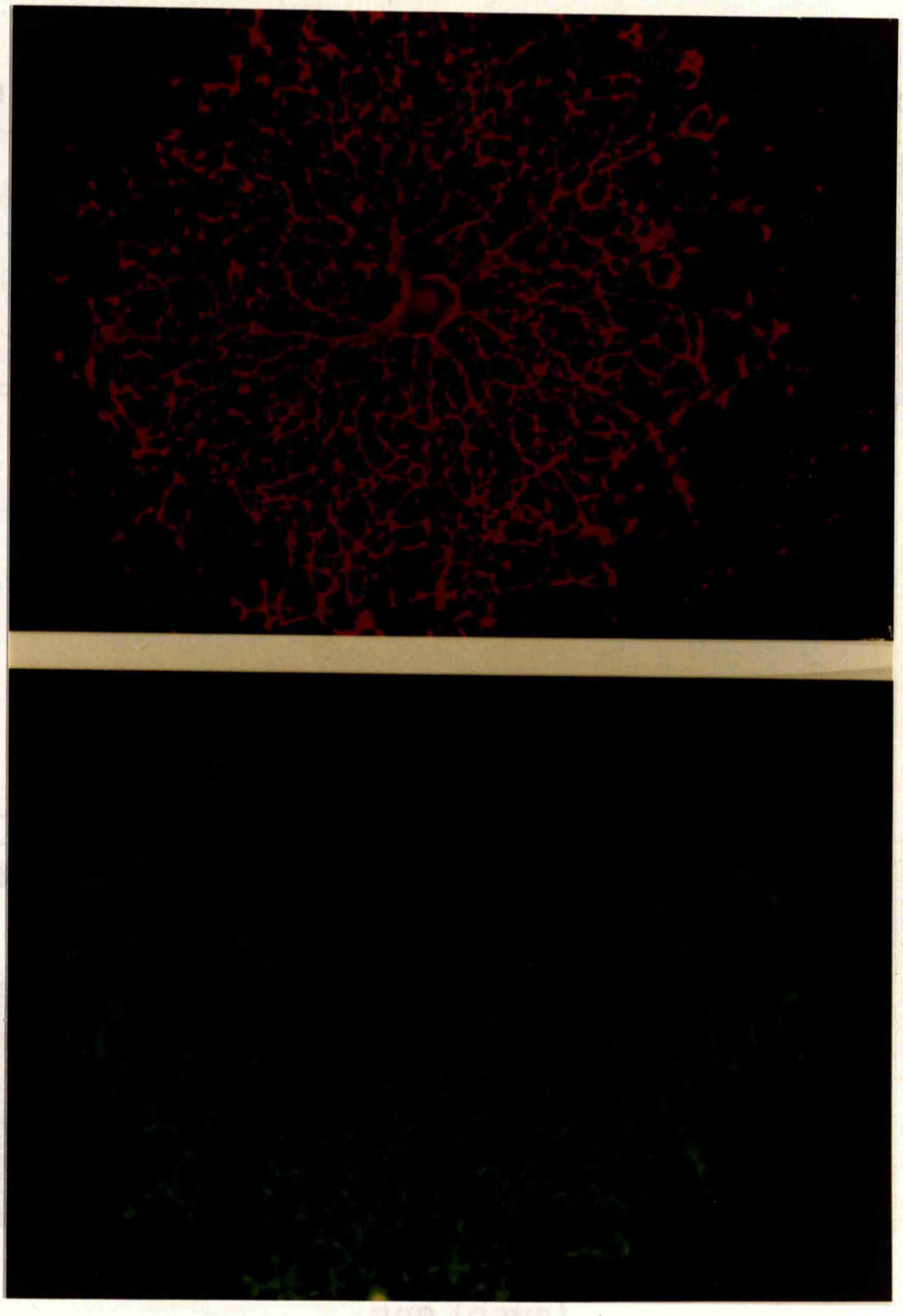

Figure 56: Double immunolabelling for GalC and O4 antigens in 120 hour-old cultures of spinal cord from 3-day-old jp^{rsh} mouse from the same experiment as in the previous figure. GalC (upper panel) is visualized by rhodamine and O4 (lower panel) by fluorescein labels. Both antibodies were applied to live unfixed cultures. Mutant oligodendrocytes produce abundant processes in culture. (Approx. magnification: x 450).

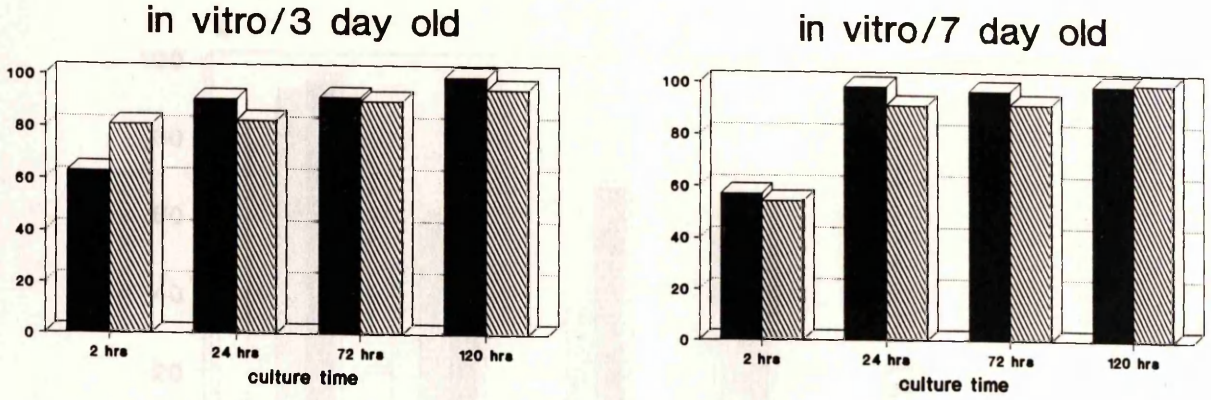

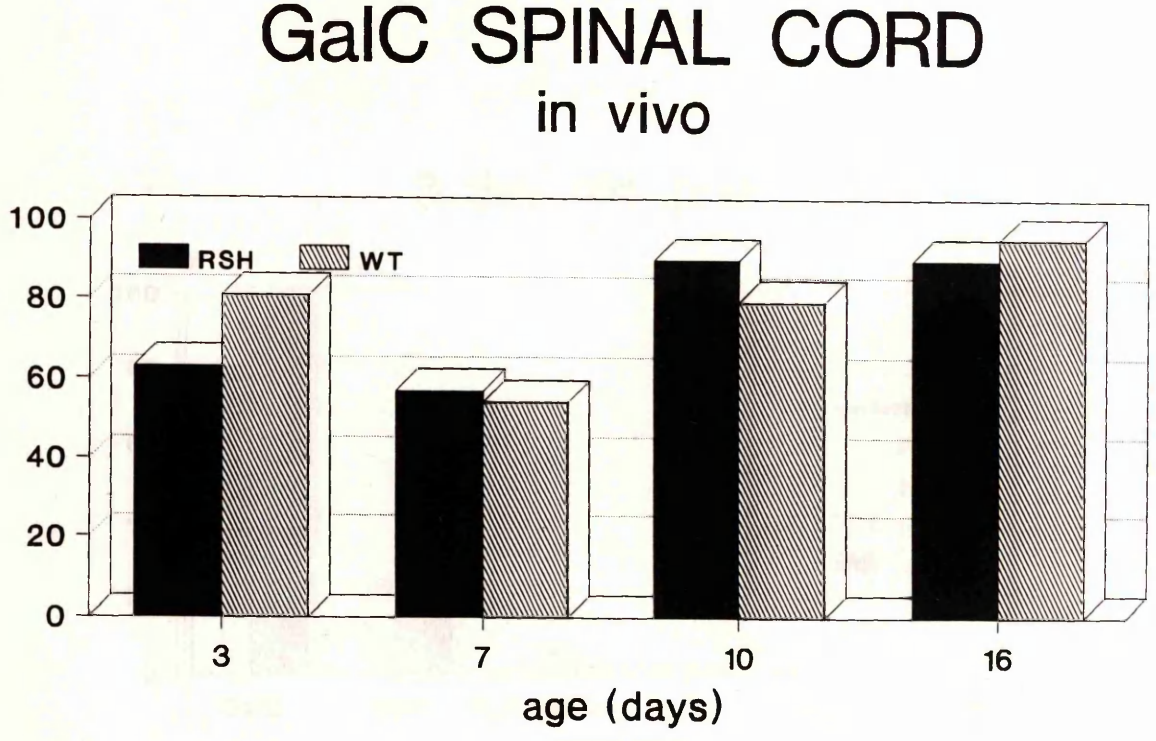

Figure 57: GalC *in vivo* and *in vitro* labelling on spinal cord cell dissociations from wild type and jp^{rsh} mice at different ages cultured for different times (as indicated). Comparison between the *in vivo* and the *in vitro* development. The development of cultures from 3 and 7-day-old mice are presented. Mutant oligodendrocytes are capable of achieving the GalC+ stage in a similar manner to wild type cells.

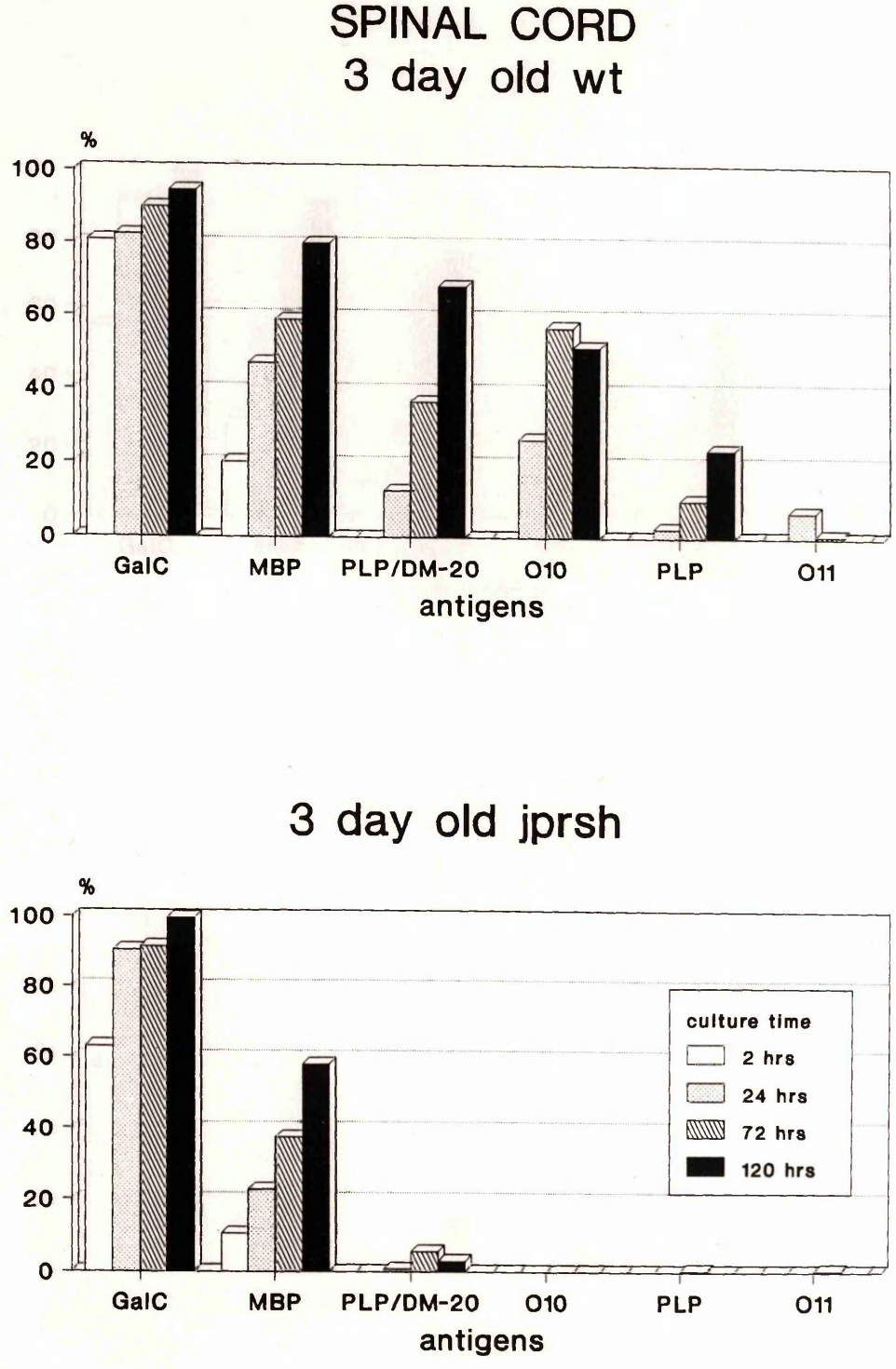

Figure 58: *In vitro* development of the antigenic profile of the oligodendrocytes obtained from 3-day-old wild type (WT) and jp^{rsh} mice spinal cords. Values are the mean of a minimum of 2 experiments and refer to the percentage of the O4+ population expressing the represented antigens. The tissue was obtained from the ventral columns of the cervical cord, dissociated and left in culture for the indicated times.

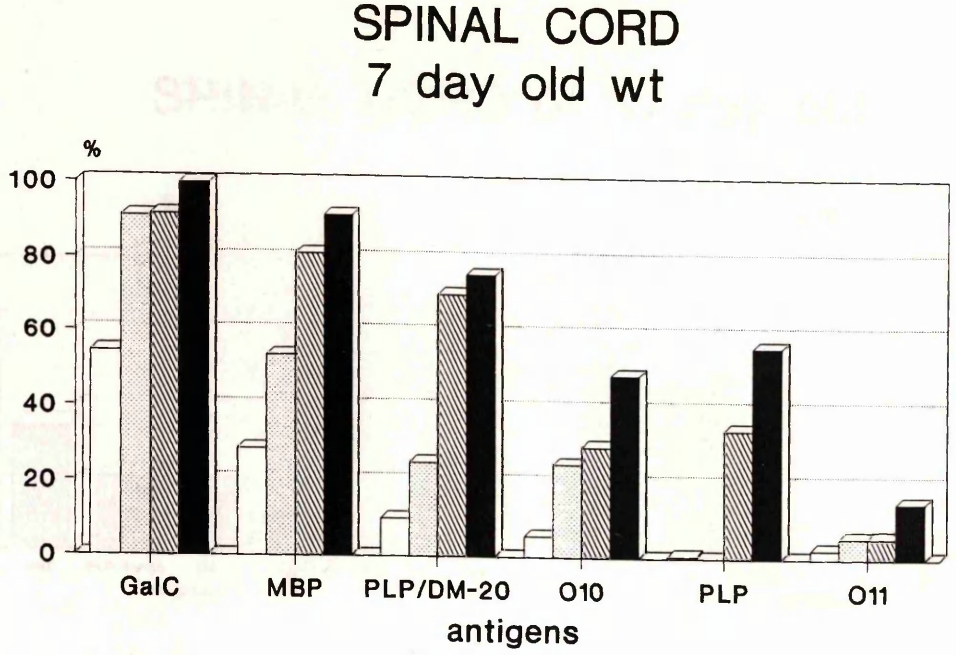

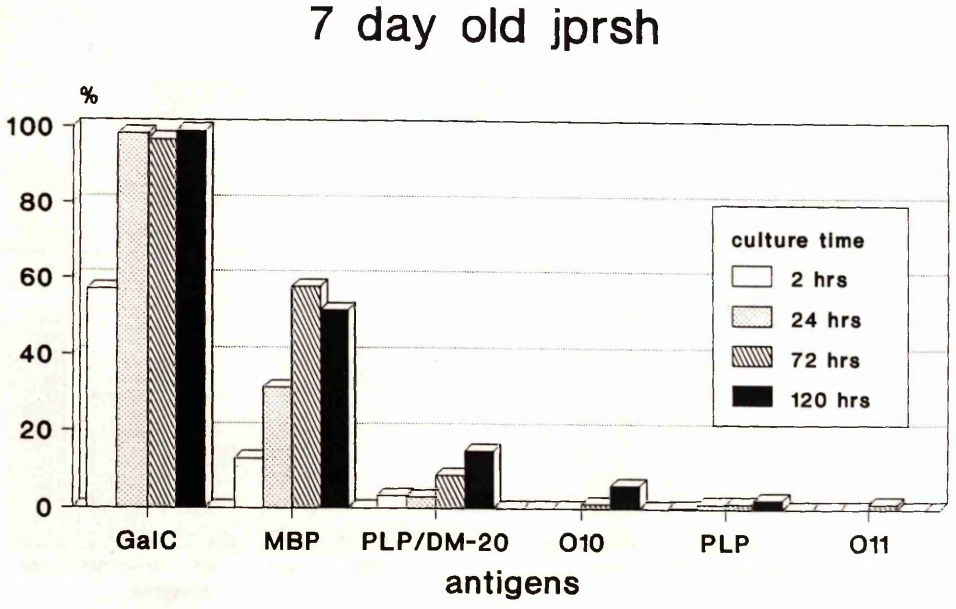

Figure 59: *In vitro* development of the antigenic profile of the oligodendrocytes obtained from 7-day-old wild type (WT) and *jp*^{rsh} mice spinal cords. Values are the mean of a minimum of 2 experiments and refer to the percentage of the O4+ population expressing the represented antigens. The tissue was obtained from the ventral columns of the cervical cord, dissociated and left in culture for the indicated times.

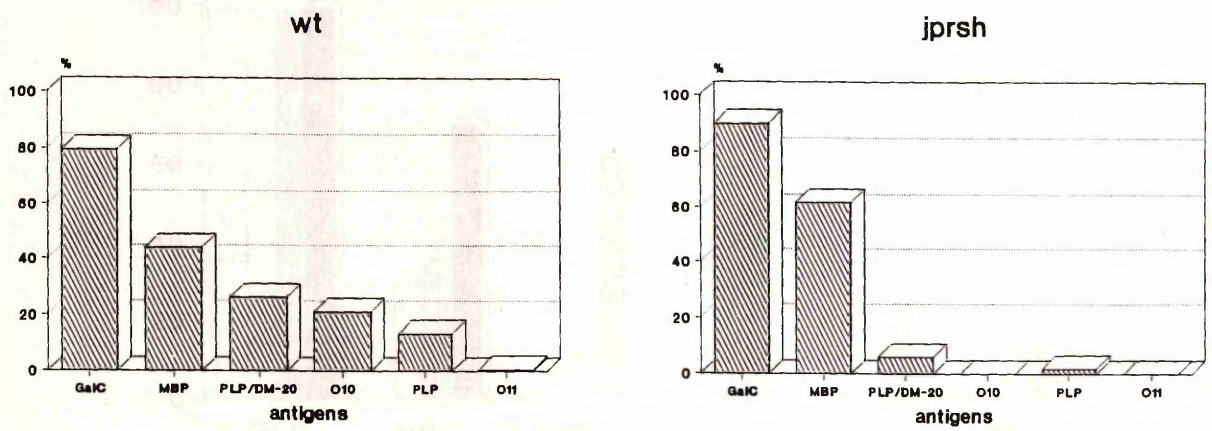

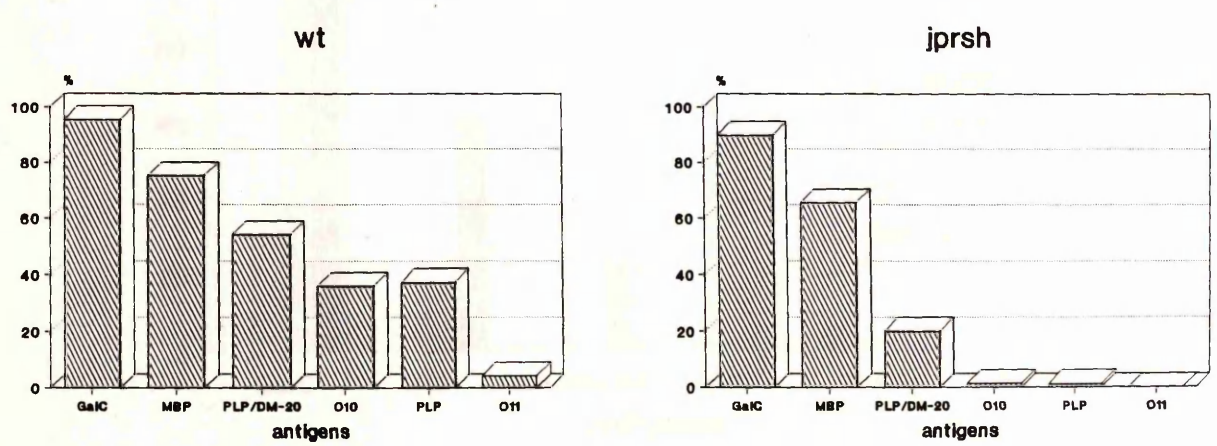

Figure 60: Antigenic profile of the oligodendrocytes obtained from 10 and 16-day-old wild type (WT) and jp^{rsh} mice spinal cords Values are the mean of a minimum of 2 experiments and refer to the percentage of the O4+ population expressing the represented antigens. The tissue was obtained from the ventral columns of the cervical cord, dissociated and immunostained 2 hours after plating.

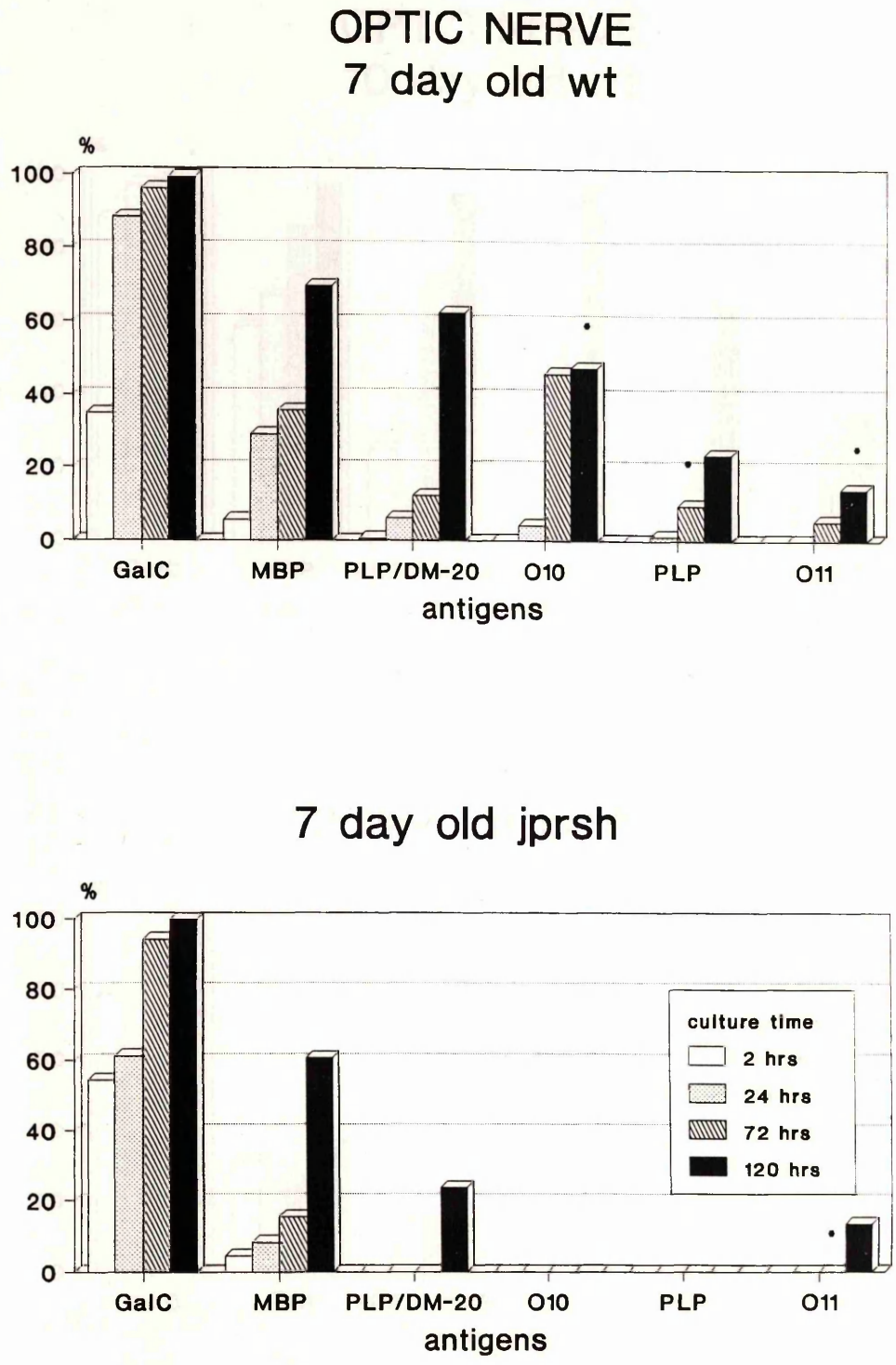

Figure 61: *In vitro* development of the antigenic profile of the oligodendrocytes obtained from 7-day-old wild type (WT) and *jp*^{rsh} mice optic nerves. Values are the mean of a minimum of 2 experiments and refer to the percentage of the O4+ population expressing the represented antigens. Asterisks have been placed where the result of a single experiment is shown. The tissue was obtained from the optic nerves, dissociated and left in culture for the indicated times.

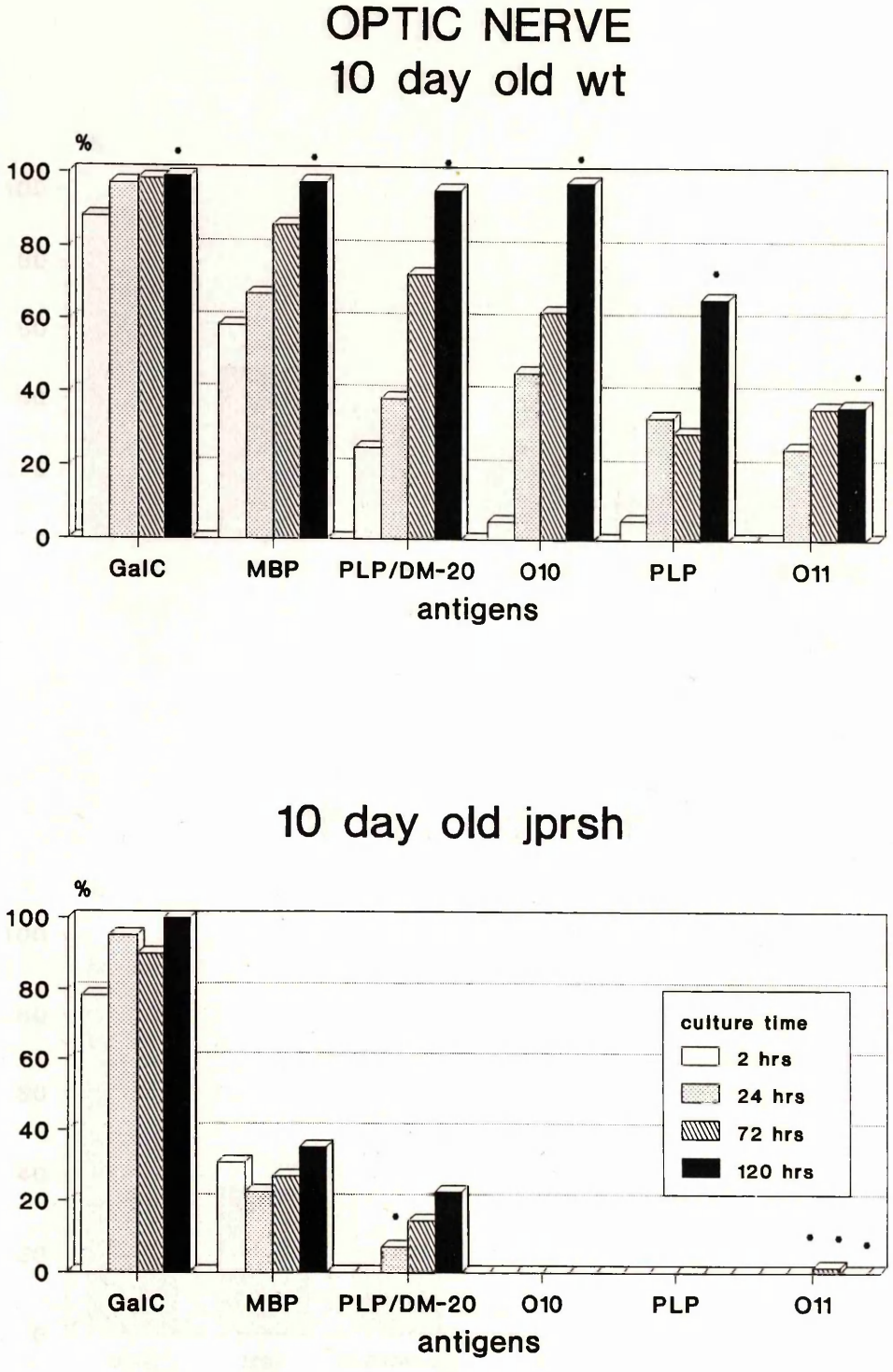

Figure 62: *In vitro* development of the antigenic profile of the oligodendrocytes obtained from 10-day-old wild type (WT) and jp^{rsh} mice optic nerves. Values are the mean of a minimum of 2 experiments and refer to the percentage of the O4+ population expressing the represented antigens. Asterisks have been placed where the result of a single experiment is shown. The tissue was obtained from the optic nerves, dissociated and left in culture for the indicated times.

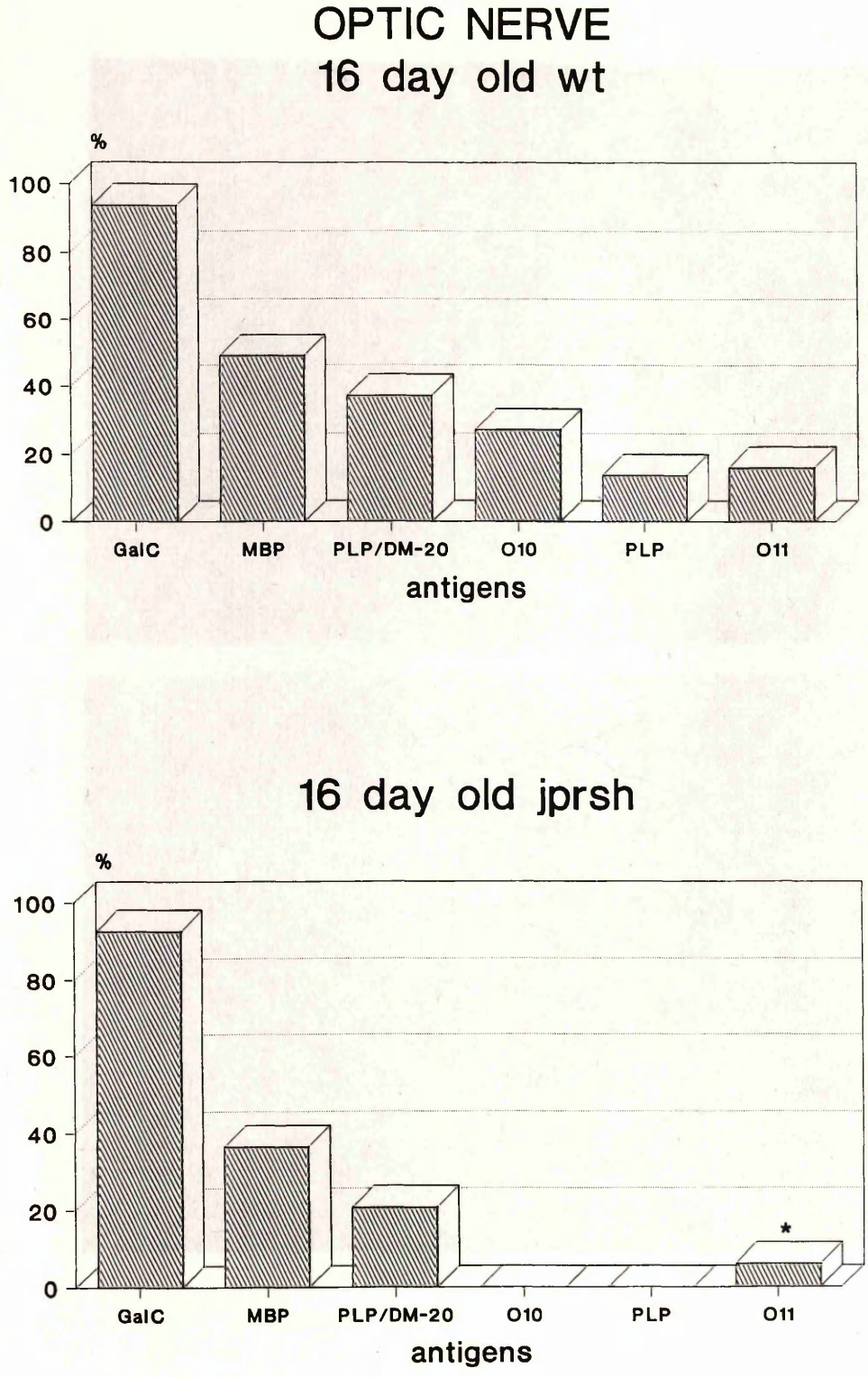

Figure 63: Antigenic profile of the oligodendrocytes obtained from 16-day-old wild type (WT) and *jp*^{rsh} mice optic nerve. Values are the mean of a minimum of 2 experiments and refer to the percentage of the O4+ population expressing the represented antigens. An asterisk has been placed where the result of a single experiment is shown. The tissue was obtained from the optic nerves, dissociated and immunostained 2 hours after plating.

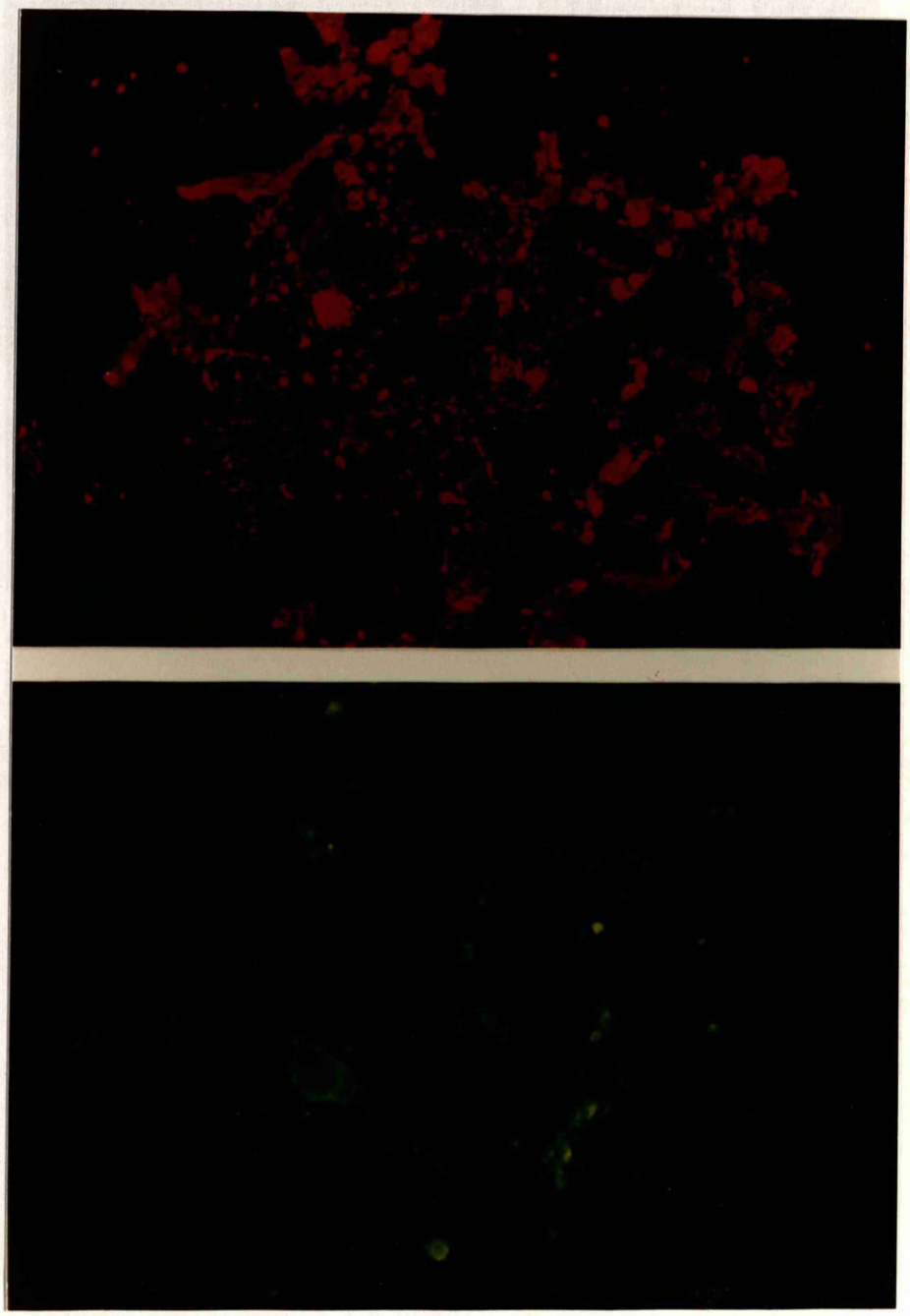

Figure 64: Double immunolabelling for GalC antigen and MBP in 120 hour-old cultures of spinal cord from 3-day-old *jp*^{rsh} mouse from the same experiment as in figures 55, 56, 74 and 75. GalC (upper panel) is visualized by rhodamine (goat-anti-mouse IgG_3 TRITC) and MBP (lower panel) protein by fluorescein (goat-anti-rabbit FITC) labels. GalC antibody was applied to live unfixed cultures. MBP was immunolabelled after cell permeabilization. *jp*^{rsh} oligodendrocytes achieve the MBP developmental stage, expressing normal amounts of MBP per cell. However, the percentages of MBP+ oligodendrocytes in the mutant are decreased as shown in figure 67. (Approx. magnification: x 450).

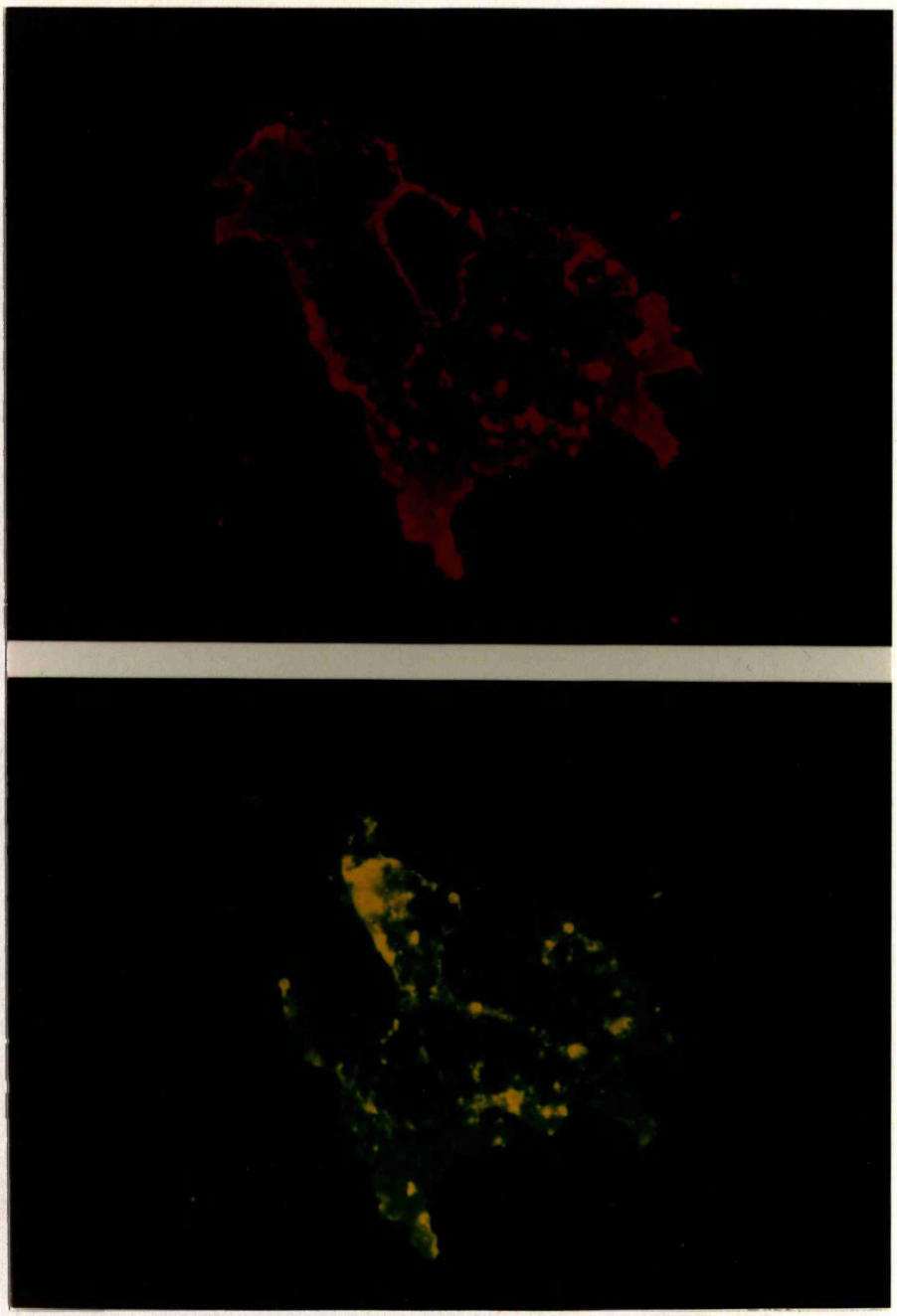

Figure 65: Double immunolabelling for GalC antigen and MBP in 120 hour-old cultures of optic nerve from 10-day-old *jp*^{rsh} mouse (same experiment as in figure 66). GalC (upper panel) is visualized by rhodamine (goat-anti-mouse IgG_3 TRITC) and MBP (lower panel) by fluorescein (goat-anti-rabbit FITC) labels. GalC antibody was applied to live unfixed cultures. MBP was immunolabelled after cell permeabilization. Optic nerve *jp*^{rsh} oligodendrocytes achieve the MBP stage expressing normal amounts of MBP per cell. Mutant optic nerve oligodendrocytes also produce myelin membranes. (Approx. magnification: x 450).

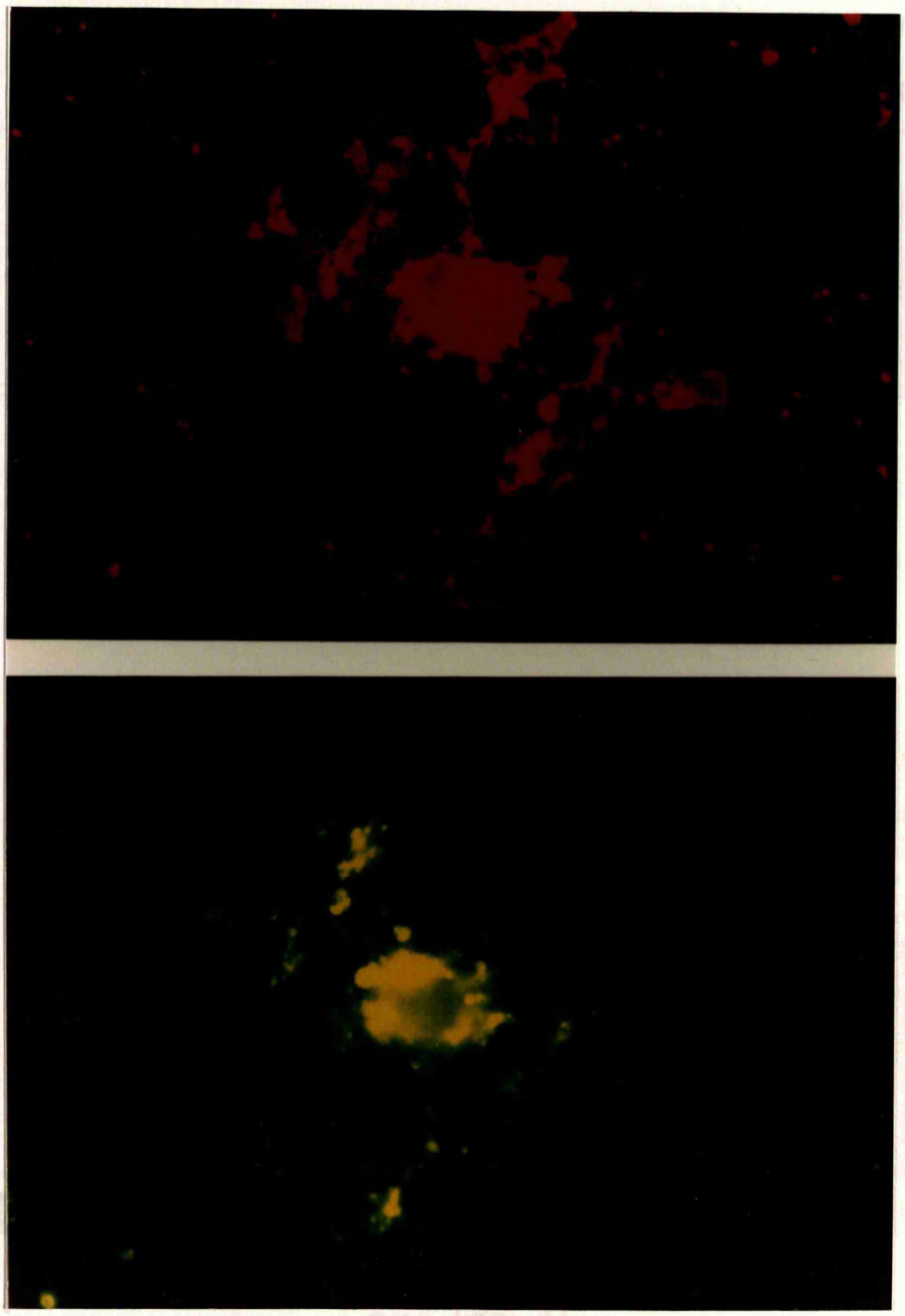

Figure 66: Double immunolabelling for GalC antigen and MBP in optic nerve cell dissociations of 120 hour-old cultures from 10-day-old *jp*^{rsh} mouse (same experiment as in the previous figure). GalC (upper panel) is visualized by rhodamine (goat-anti-mouse IgG_3 TRITC) and MBP (lower panel) protein by fluorescein (goat-anti-rabbit FITC) labels. GalC antibody was applied to live unfixed cultures. MBP was immunolabelled after cell permeabilization. Amounts of MBP equivalent to those in the wild type controls (not shown) are present in most mutant MBP+ oligodendrocytes. (Approx. magnification: x 450).

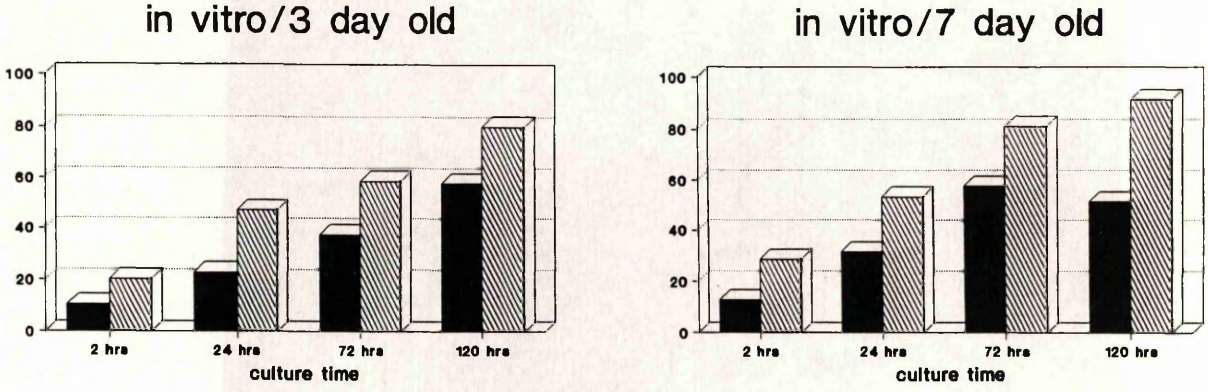

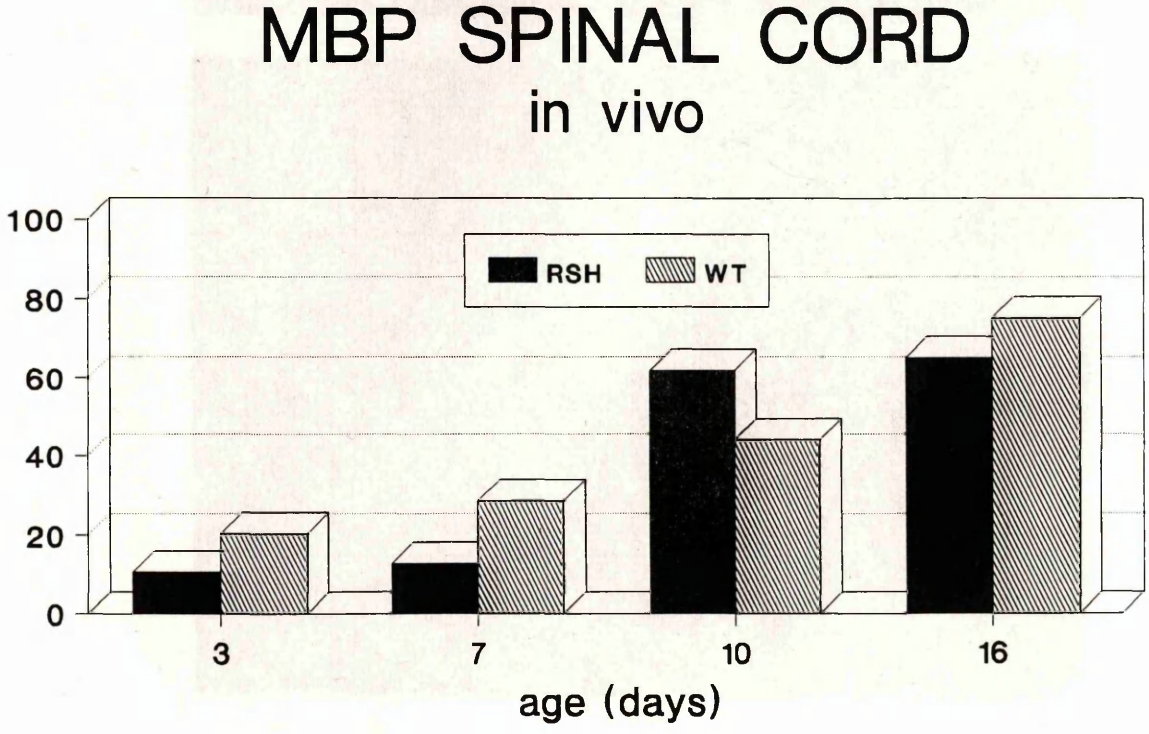

Figure 67: MBP *in vivo* and *in vitro* labelling on spinal cord cell dissociations from wild type and jp^{rsh} mice at different ages cultured for different times (as indicated). Comparison between the *in vivo* and the *in vitro* development. The results from 3 and 7-day-old mice cultures are represented. The *in vivo* situation improved the MBP expression in freshly dissociated cells as cultured oligodendrocytes never attained the same number of MBP positive cells as the wild type.

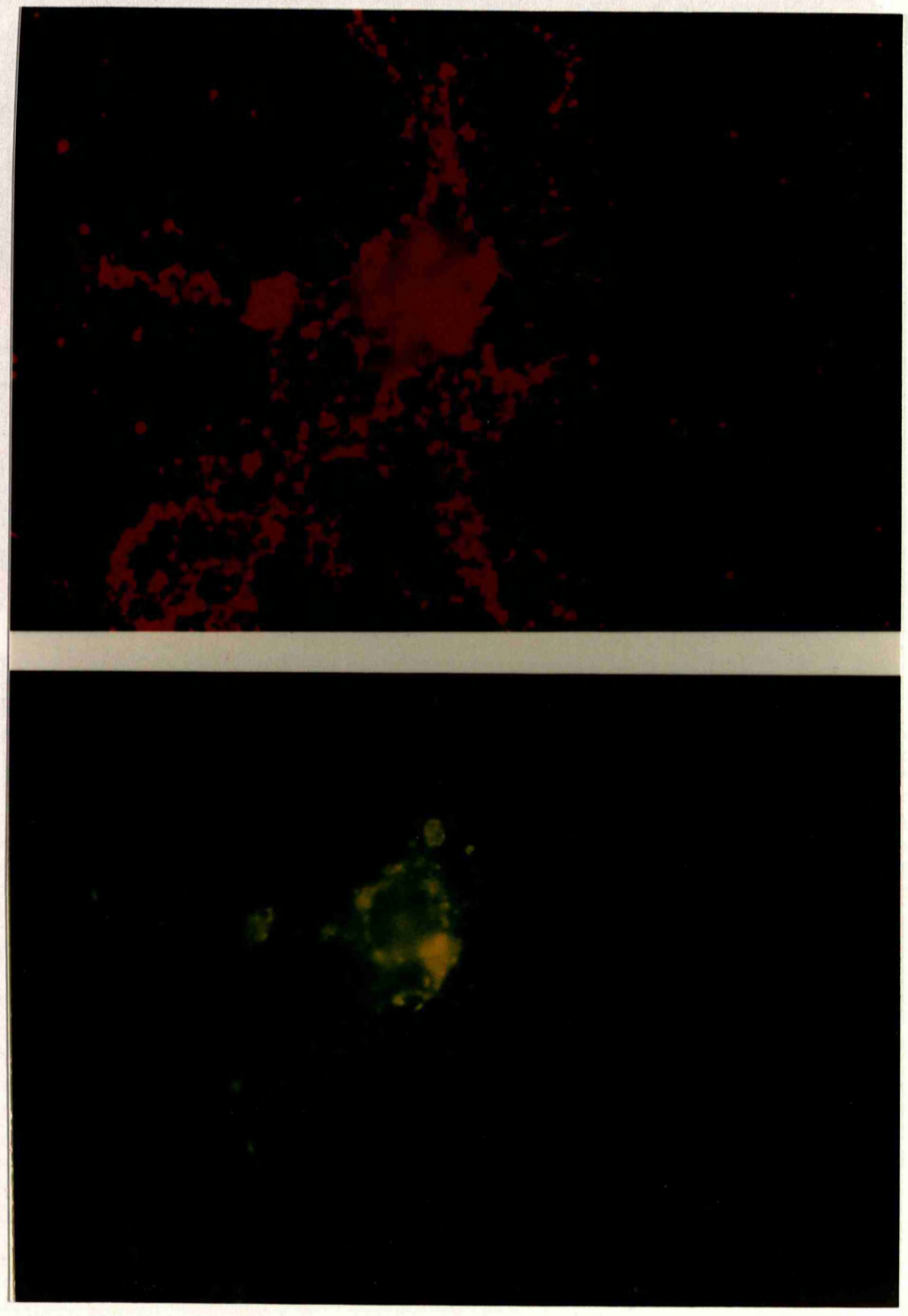

Figure 68: Double immunolabelling for O4 antigen and PLP/DM-20 proteins in cell dissociations from the spinal cord from 10-day-old wild type mouse cultured for 48 hours (same experiment as in figures 69 to 73). O4 (upper panel) is visualized by rhodamine (goat-anti-mouse IgM TRITC) and PLP/DM-20 (lower panel) by fluorescein (goat-anti-rabbit FITC) labels. O4 antibody was applied to live unfixed cultures. PLP/DM-20 was immunolabelled after cell permeabilization. (Approx. magnification: x 450).

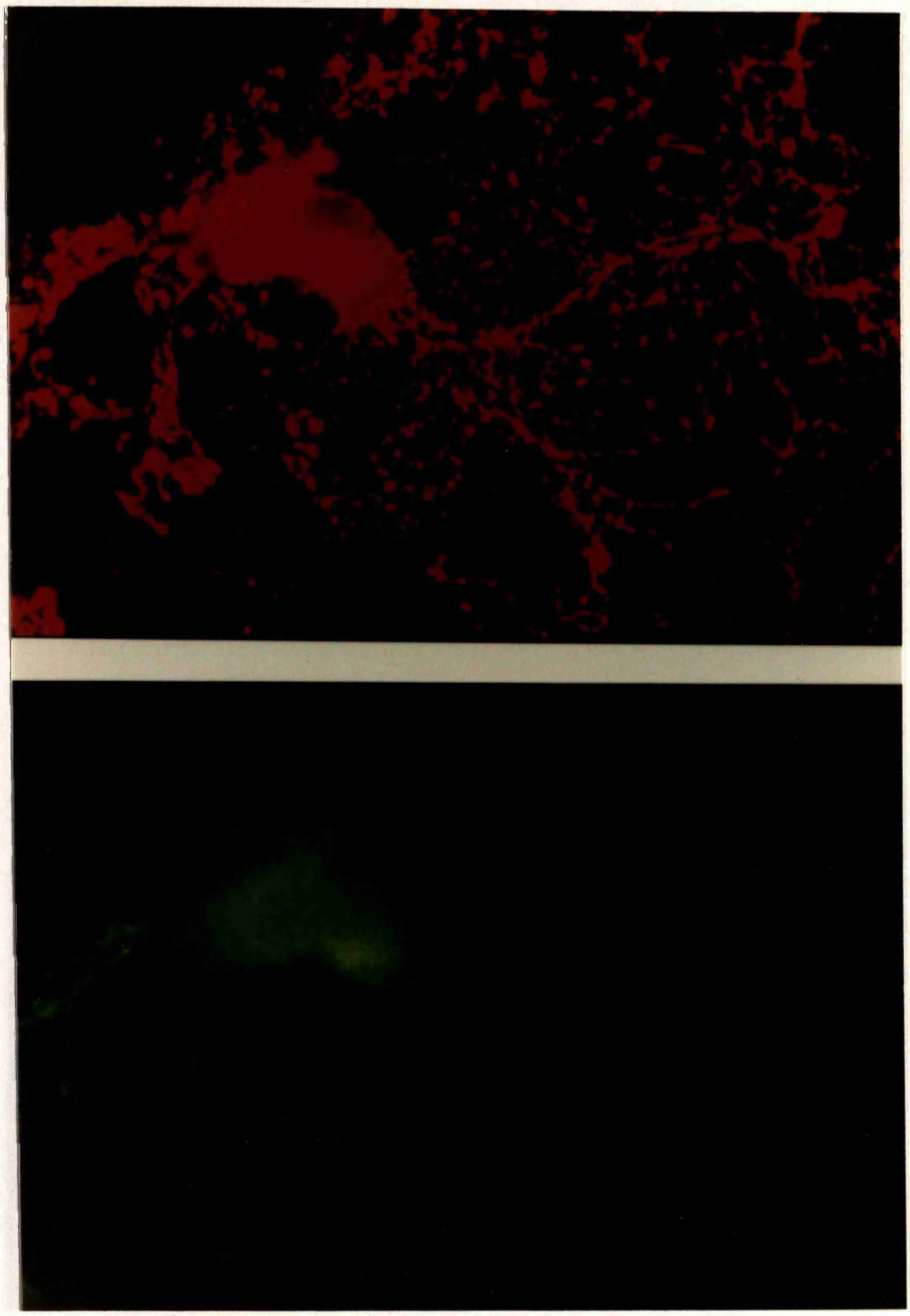

Figure 69: Double immunolabelling for O4 antigen and PLP/DM-20 proteins in cell dissociations from the spinal cord from 10-day-old jp^{rsh} cultured for 48 hours from the same experiment as in the previous figure. O4 (upper panel) is visualized by rhodamine and PLP/DM-20 (lower panel) by fluorescein labels. O4 antibody was applied to live unfixed cultures. PLP/DM-20 was immunolabelled after cell permeabilization. Most jp^{rsh} mutant oligodendrocytes immunostain for PLP/DM-20 although the immunoreactivity varies from cell to cell. This figure shows a jp^{rsh} mutant oligodendrocyte poorly immunostained for PLP/DM-20. (Approx. magnification: x 450).

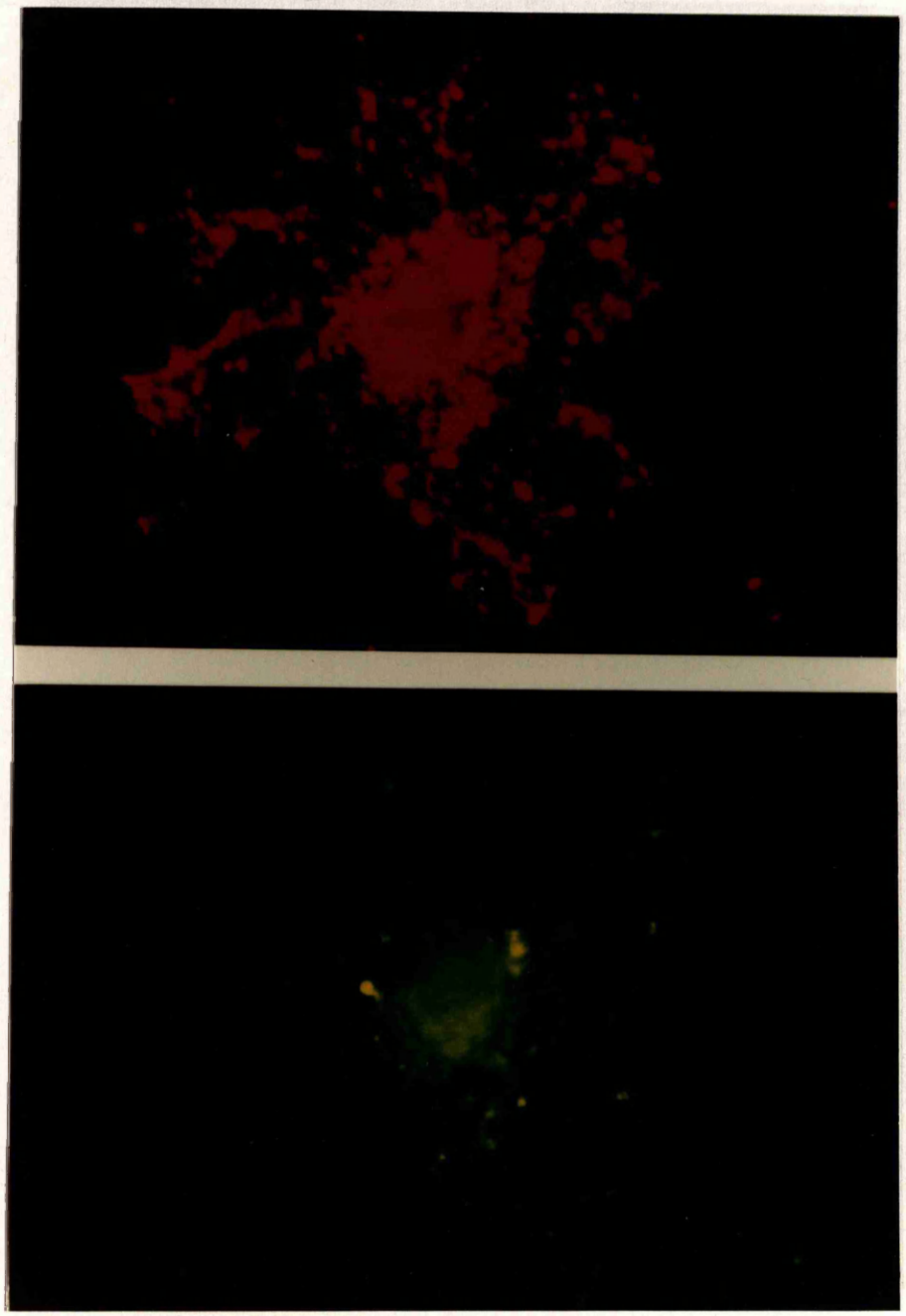

Figure 70: Double immunolabelling for O4 antigen and PLP/DM-20 proteins in cell dissociations from the spinal cord from 10-day-old jp^{rsh} cultured for 48 hour-old cultures of spinal cord from 10-day-old jp^{rsh} (same experiment as in figures 68 to 73). O4 (upper panel) is visualized by rhodamine and PLP/DM-20 (lower panel) by fluorescein labels. O4 antibody was applied to live unfixed cultures. PLP/DM-20 was immunolabelled after cell permeabilization. Many mutant oligodendrocytes exhibit almost normal amounts of PLP/DM-20. This figure shows the maximum degree of immunostain achieved by mutant oligodendrocytes in this experiment (see control wild type cell in figure 68). (Approx. magnification: x 450).

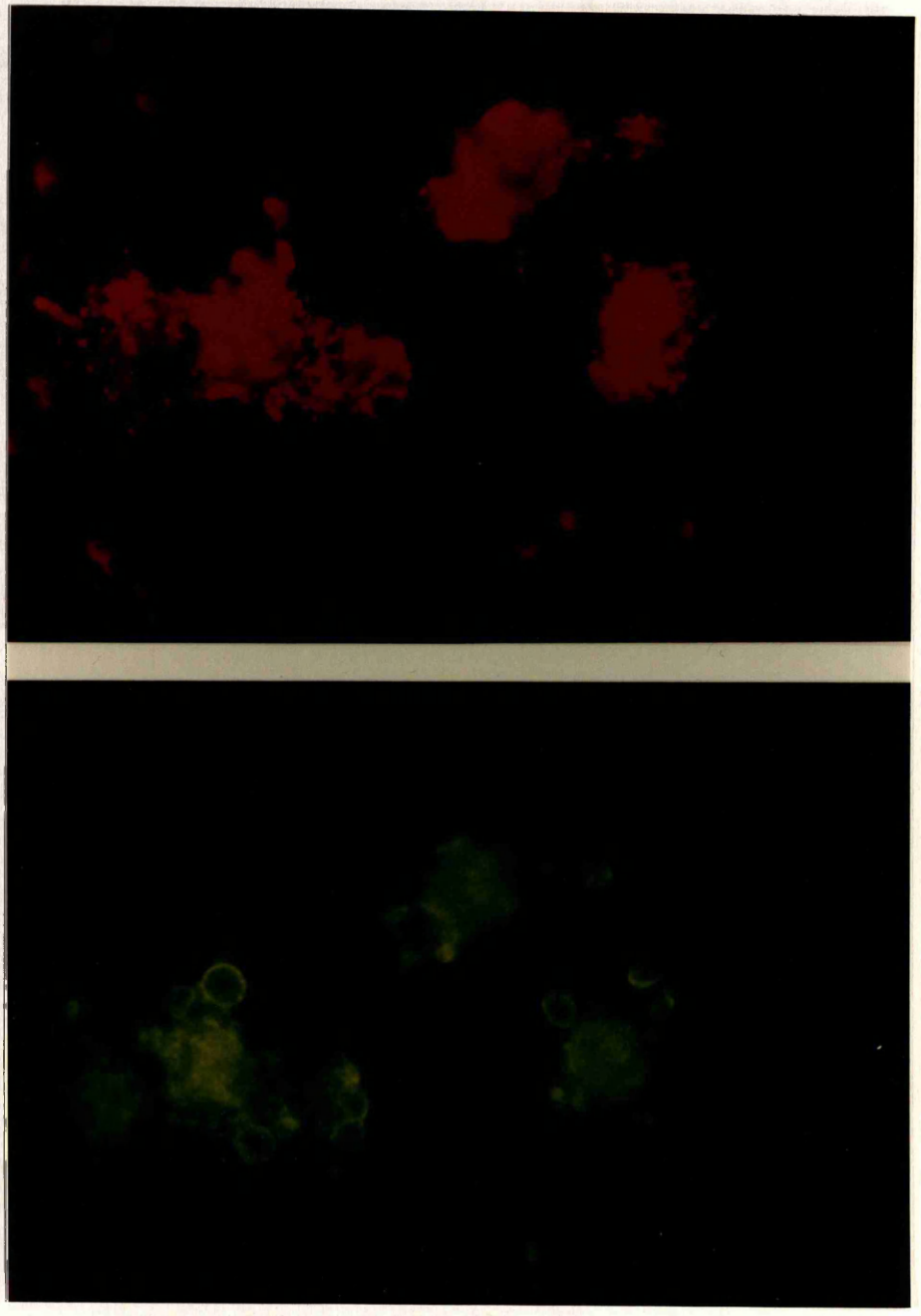

Figure 71: Double immunolabelling for O4 and PLP in cell dissociations from the spinal cord from 10-day-old wild type mice (same experiment as in figures 68 to 73). O4 (upper panel) is visualized by rhodamine (goat-anti-mouse IgM TRITC) and PLP (lower panel) by fluorescein (goat-anti-rabbit FITC) labels. O4 antibody was applied to live unfixed cultures. PLP was immunolabelled after cell permeabilization. These three wild type oligodendrocytes immunostain strongly with the antibody recognizing PLP which, at this stage of development labels circular structures in the cytoplasm around the nucleus. (Approx. magnification: x 450).

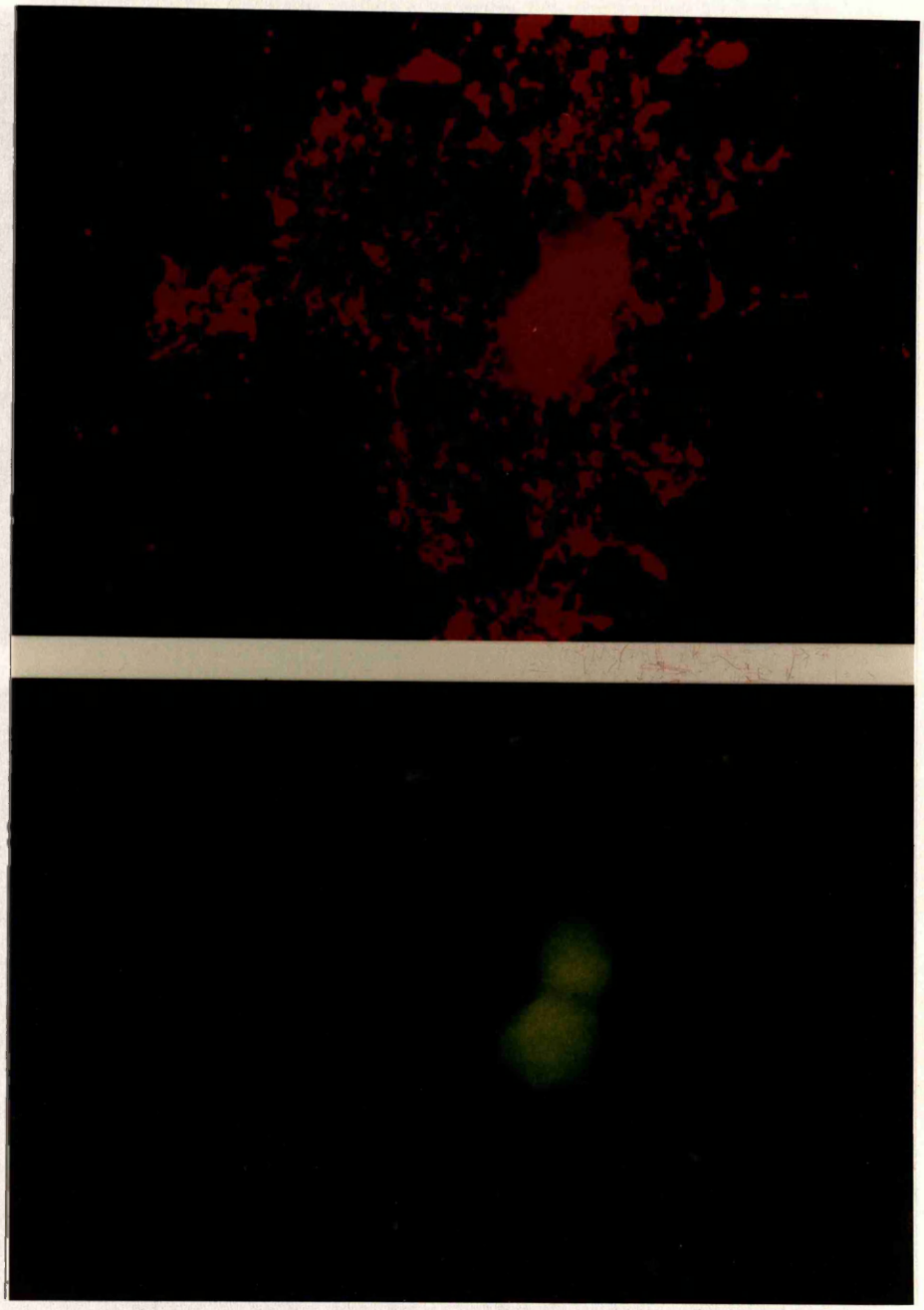

Figure 72: Double immunolabelling for O4 antigen and PLP in cell dissociations from the spinal cord from 10-day-old jp^{rsh} cultured for 48 hour-old cultures of spinal cord from 10-day-old jp^{rsh} (same experiment as in figures 68 to 73). O4 (upper panel) is visualized by rhodamine and PLP (lower panel) by fluorescein labels. O4 antibody was applied to live unfixed cultures. PLP was immunolabelled after cell permeabilization. The overall impression is that jp^{rsh} oligodendrocytes are negative when compared to wild type cells grown and immunostained under the same conditions (figure 71). However, detailed observation of some of these cells reveals small aggregations of the antibody at the processes. (Approx. magnification: x 450).

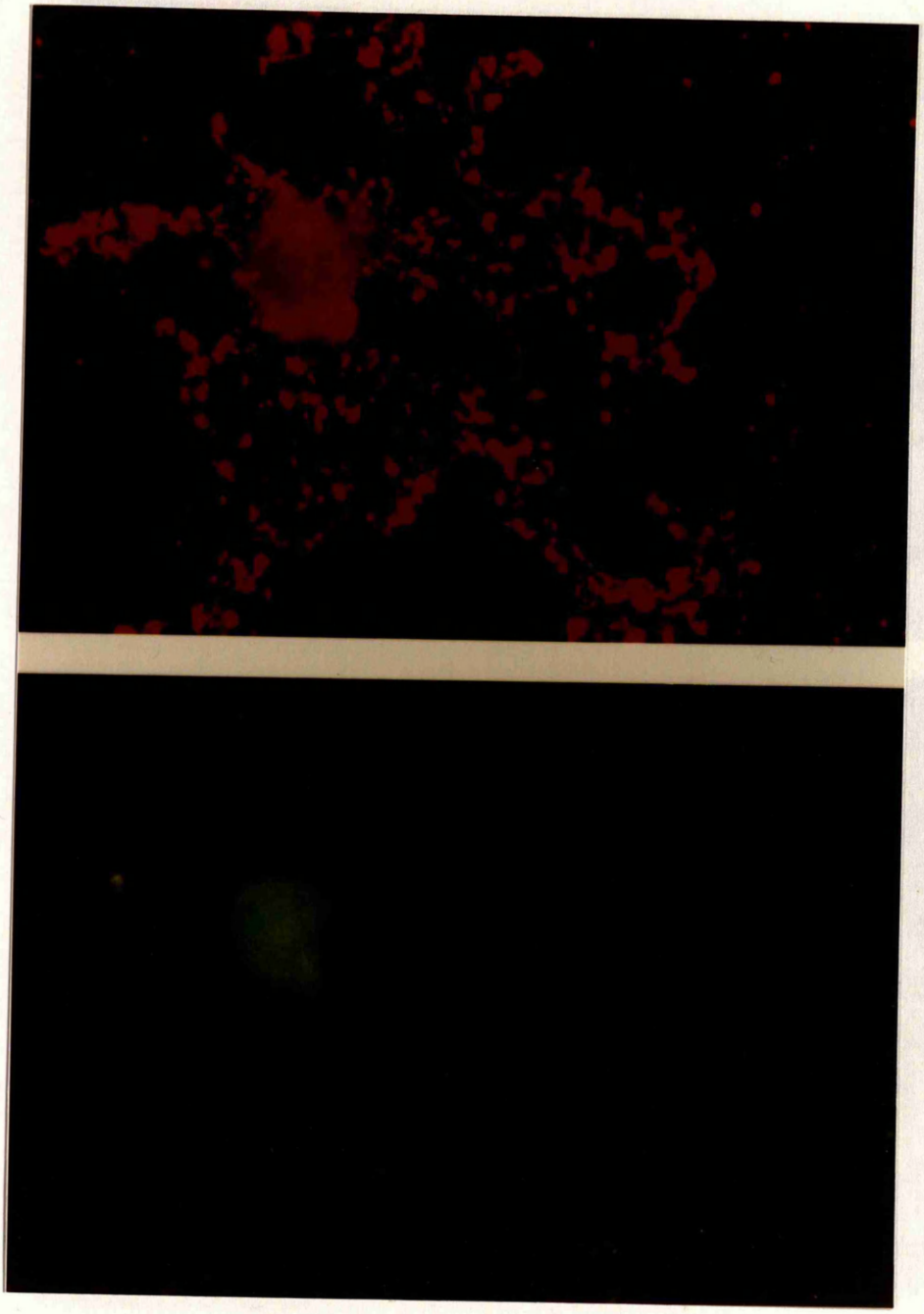

Figure 73: Double immunolabelling for O4 antigen and PLP; in cell dissociations from the spinal cord from 10-day-old *jp*^{rsh} mouse cultured for 48 hours (same experiment as in figures 69 to 73). O4 (upper panel) is visualized by rhodamine and PLP (lower panel) by fluorescein labels. O4 antibody was applied to live unfixed cultures. PLP was immunolabelled after cell permeabilization. Another example of a mutant oligodendrocyte showing only some PLP staining confined to small lumps at the processes. (Approx. magnification: x 450).

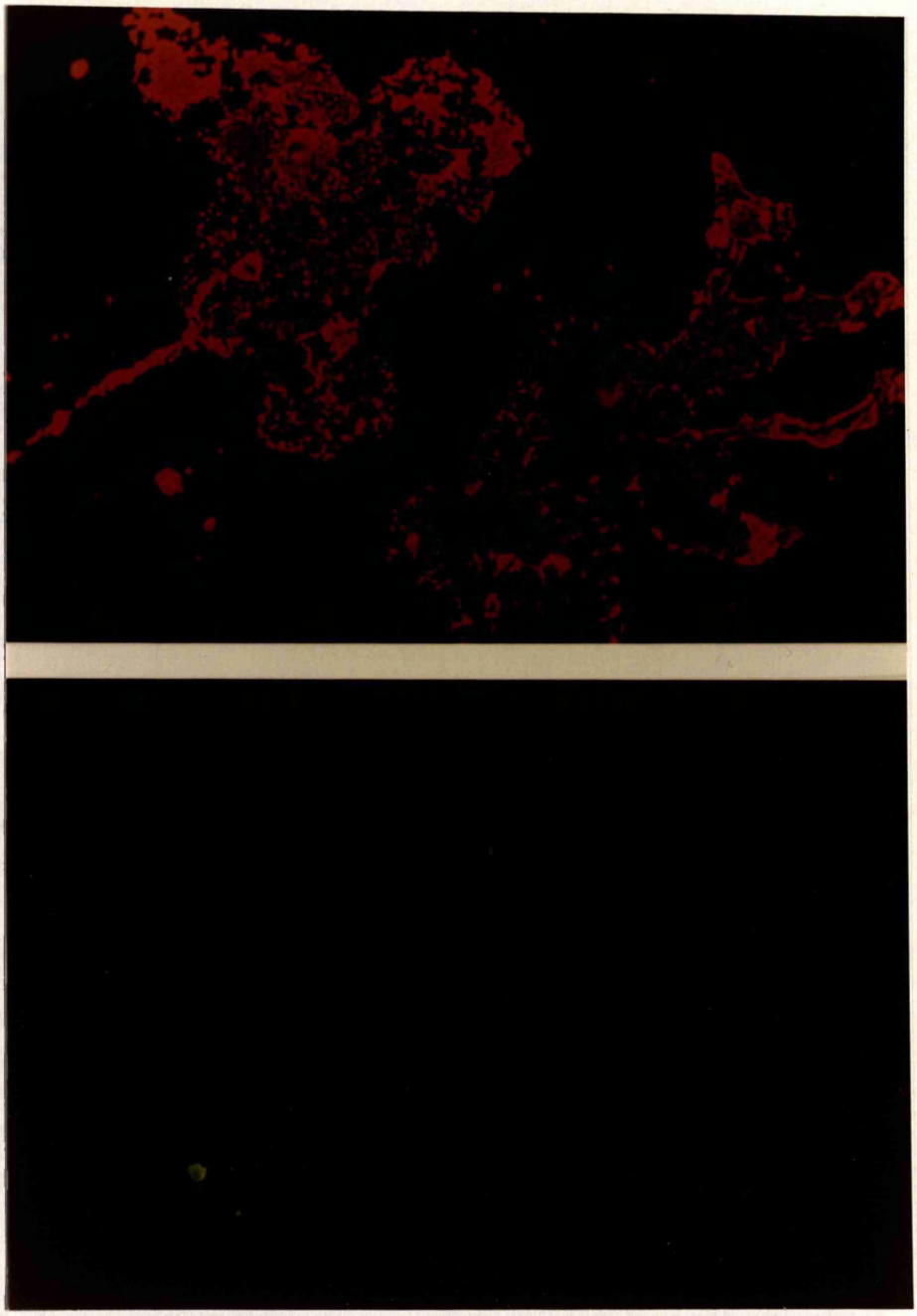

Figure 74: Double immunolabelling for GalC and O10 antigen in 120 hour-old cultures of spinal cord from 3-day-old jp^{rsh} mouse from the same experiment as in figures 55, 56, 64 and 75. GalC (upper panel) is visualized by rhodamine (goat-anti-mouse IgG_3 TRITC) and O10 (lower panel) by fluorescein (goat-anti-mouse IgM FITC) labels. Both antibodies were applied to live unfixed cultures. Most mutant oligodendrocytes do not achieve the O10+ stage. This picture shows two mutant oligodendrocytes one of which is positive for O10. However, the degree of O10 expression is very poor. (Approx. magnification: x 450).

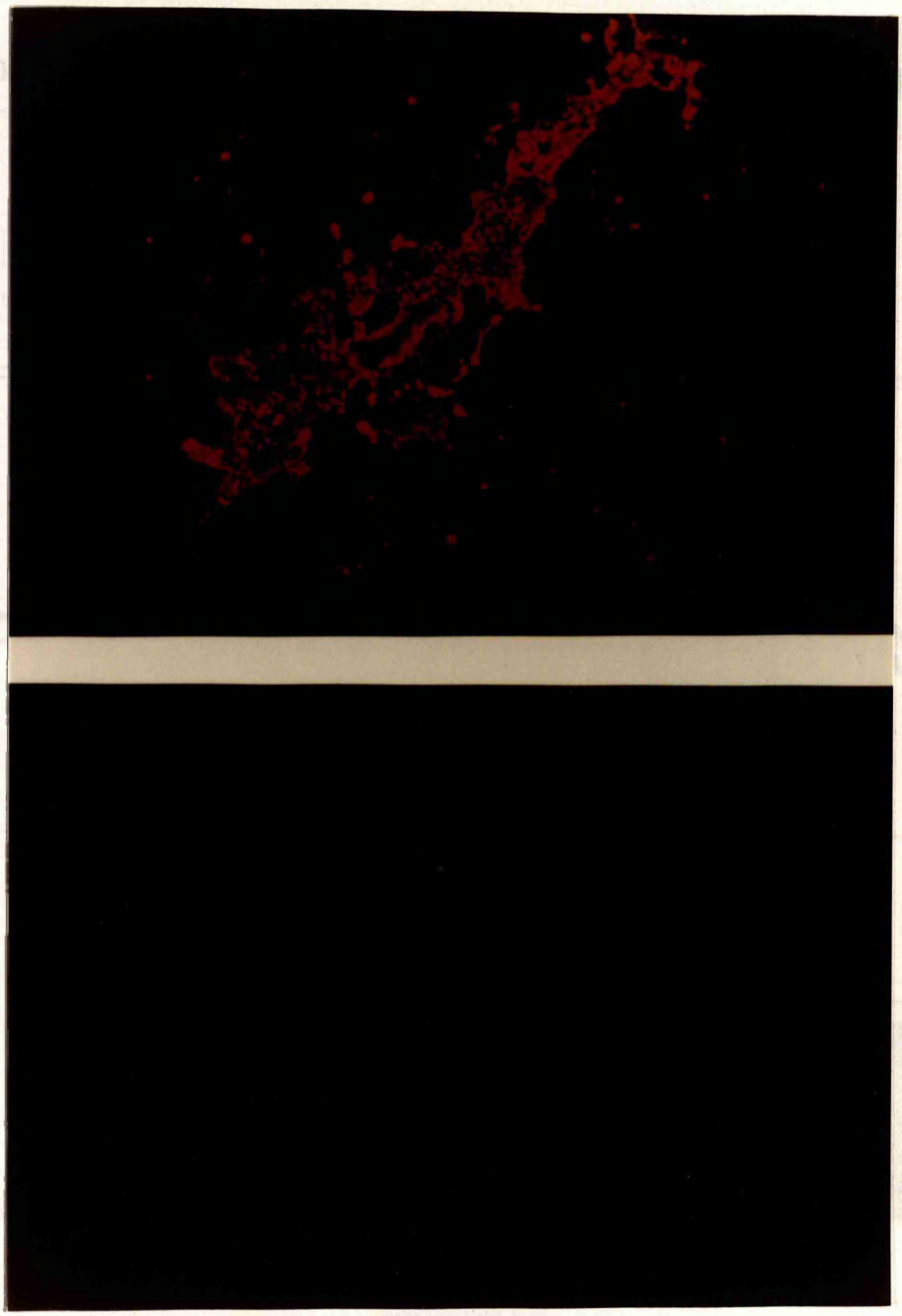

Figure 75: Double immunolabelling for GalC and O11 antigen in 120 hour-old cultures of spinal cord from 3-day-old *jp*^{rsh} mouse from the same experiment as in previous figures 55, 56, 64 and 74. GalC (upper panel) is visualized by rhodamine and O11 (lower panel) by fluorescein labels. Both antibodies were applied to live unfixed cultures. Most mutant oligodendrocytes do not achieve the O10+ stage. Picture of an O11 positive mutant oligodendrocytes. The degree of O11 expression in positive mutant oligodendrocytes is significantly reduced in intensity. (Approx. magnification: x 450).

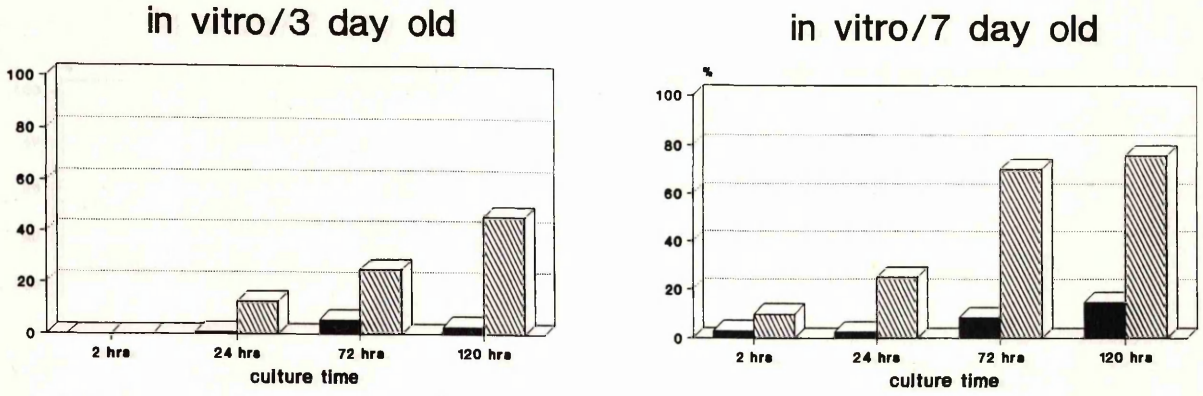

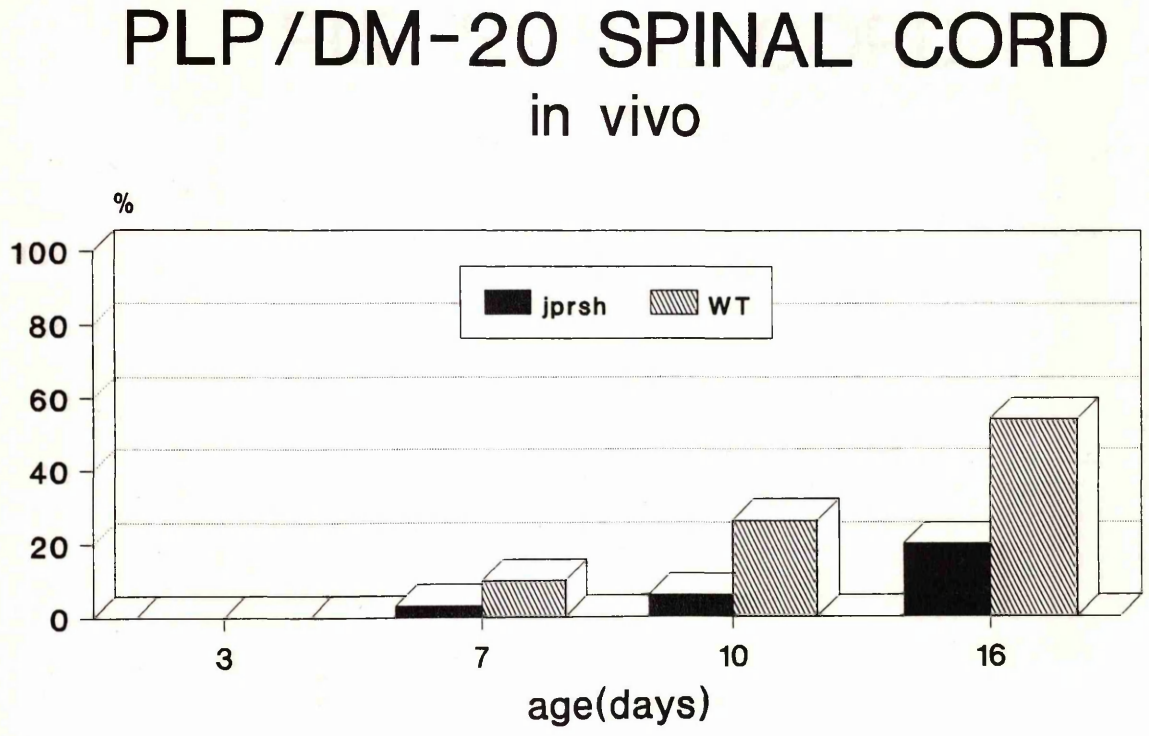

Figure 76: PLP/DM-20 *in vivo* and *in vitro* labelling. Spinal cord cell dissociations from wild type and jp^{rsh} mice at different ages cultured for different times (as indicated). Comparison between the *in vivo* and the *in vitro* development. The results from 3 and 7-day-old mice cultures are represented.

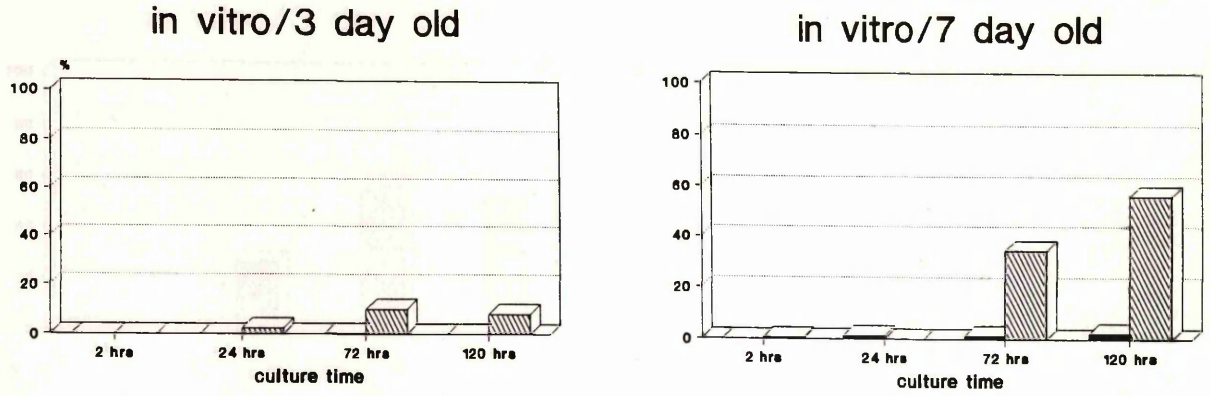

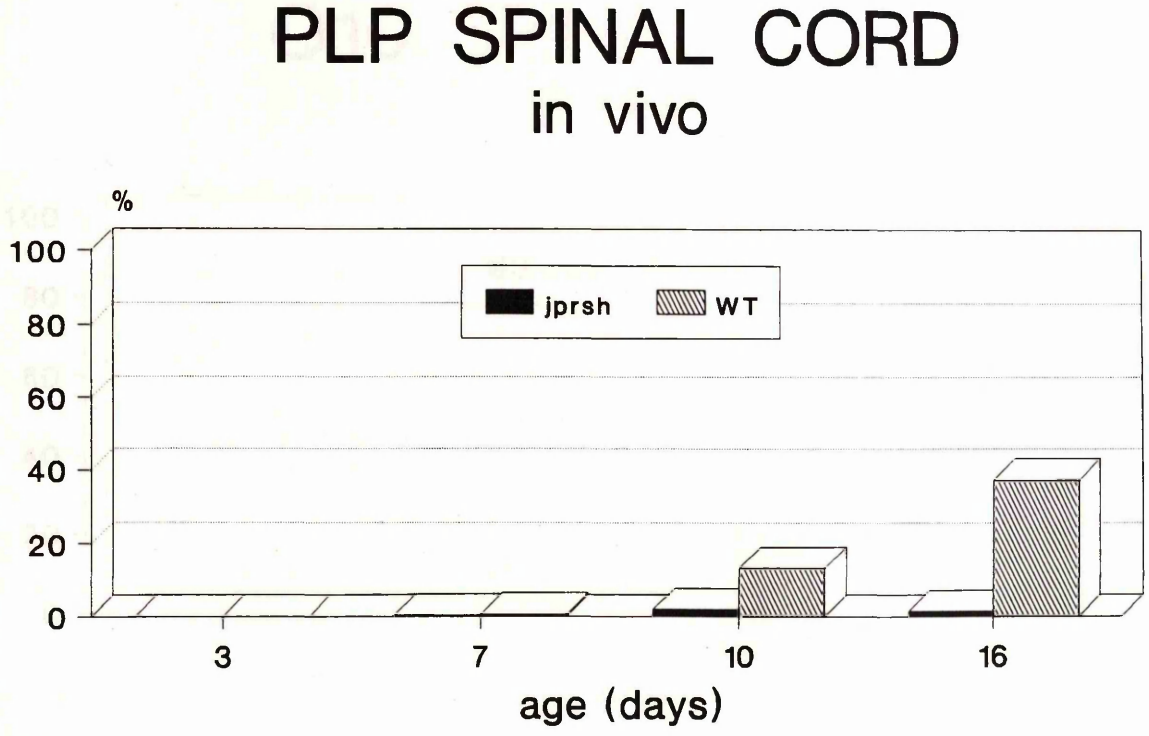

Figure 77: PLP *in vivo* and *in vitro* labelling. Spinal cord cell dissociations from wild type and jp^{rsh} mice at different ages cultured for different times (as indicated). Comparison between the *in vivo* and the *in vitro* development. The results from 3 and 7-day-old mice cultures are represented.

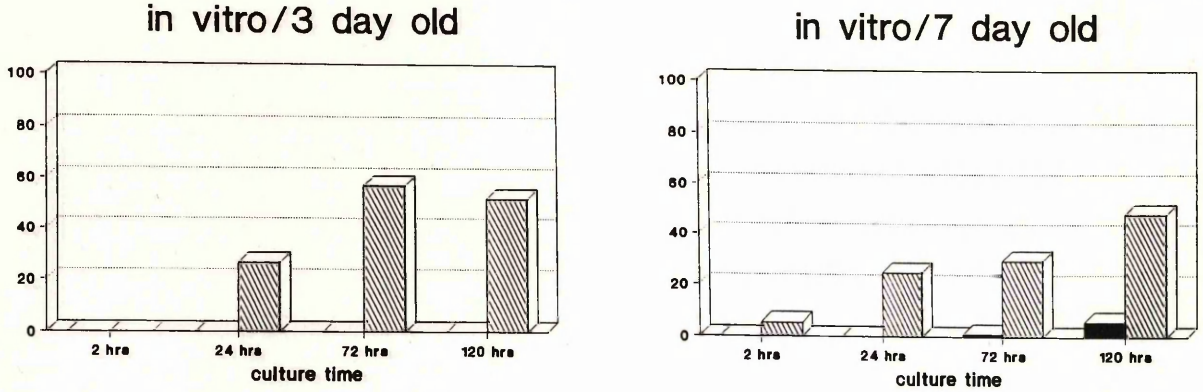

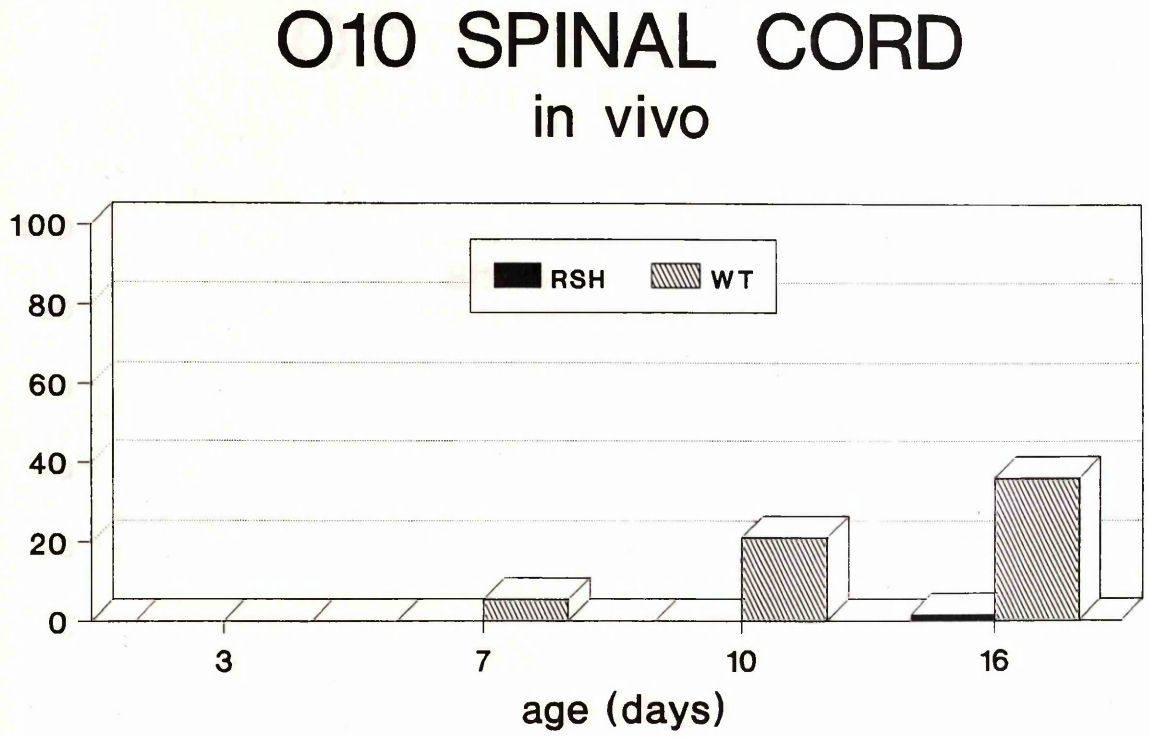

Figure 78: O10 antigen *in vivo* and *in vitro* labelling. Spinal cord cell dissociations from wild type and mutant jp^{rsh} at different ages cultured for different times (as indicated). Comparison between the *in vivo* and the *in vitro* development. The results from 3 and 7-day-old mice cultures are represented.

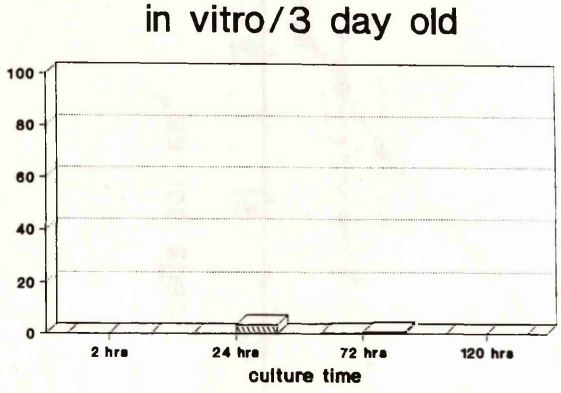

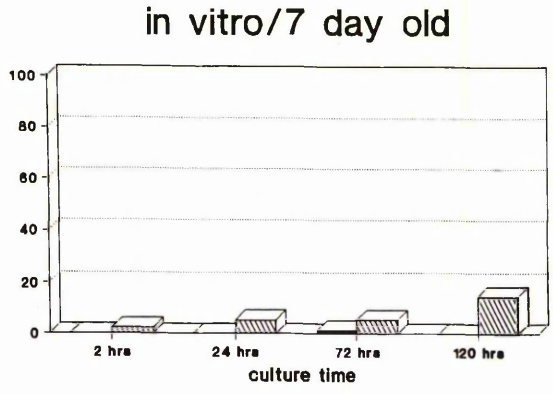

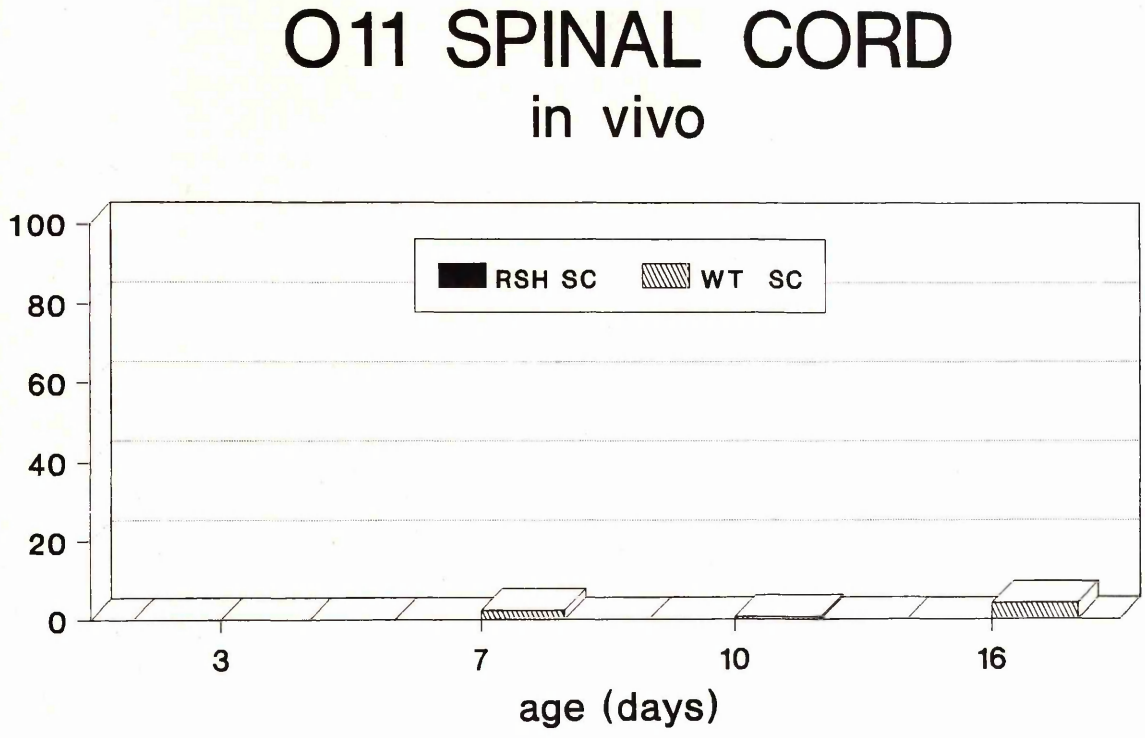

Figure 79: O11 antigen *in vivo* and *in vitro* labelling. Spinal cord cell dissociations from wild type and mutant mice at different ages cultured for different times (as indicated). Comparison between the *in vivo* and the *in vitro* development. The results from 3 and 7-day-old mice cultures are represented.

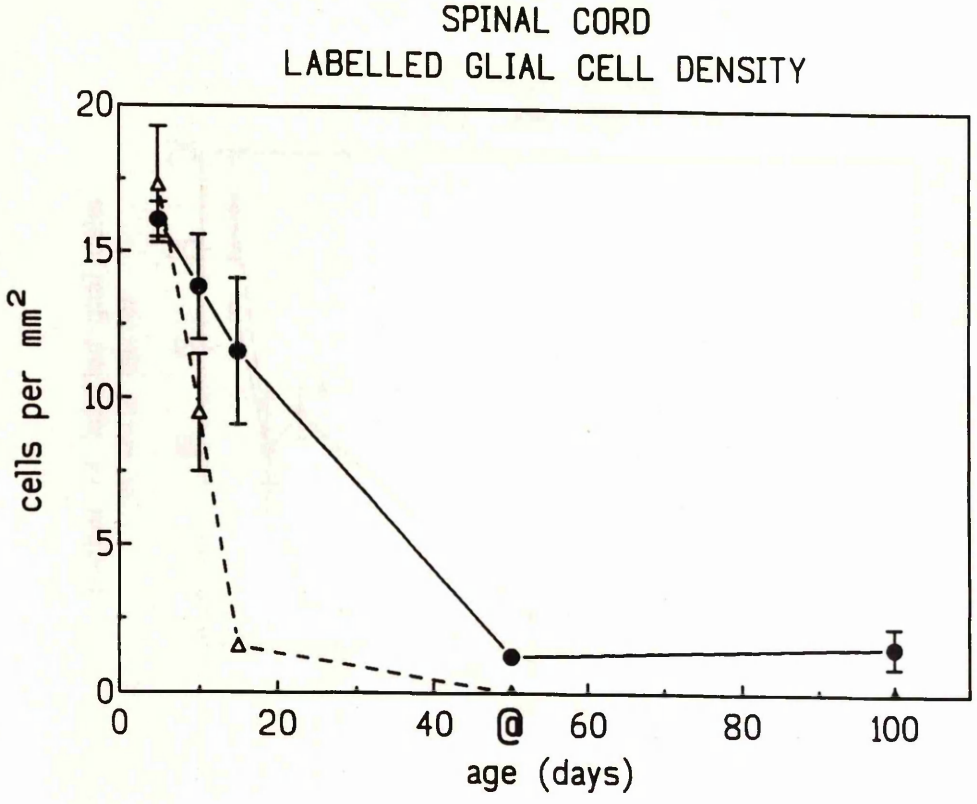

Figure 80: Cell mitosis in the ventral columns of the spinal cord. Thymidine-labelled glial cell density. Values from wild type (triangle) and jp^{rsh} mice (filled circle) white matter of the C2 segment of the spinal cord. All data represent mean ± SEM; where error bars are not seen they fall within the symbol. (@) Shows the result obtained from a single experiment. The spinal cord of jp^{rsh} shows an obviously increased labelled cell density indicating an increased cell proliferation. Dividing cells are probably oligodendrocytes or their immediate precursors as demonstrated by the morphological and the *in situ* hybridization results (figures 22, 23, 40). This finding is particularly outstanding in 100-day-old mutant labelled for 6 hours.

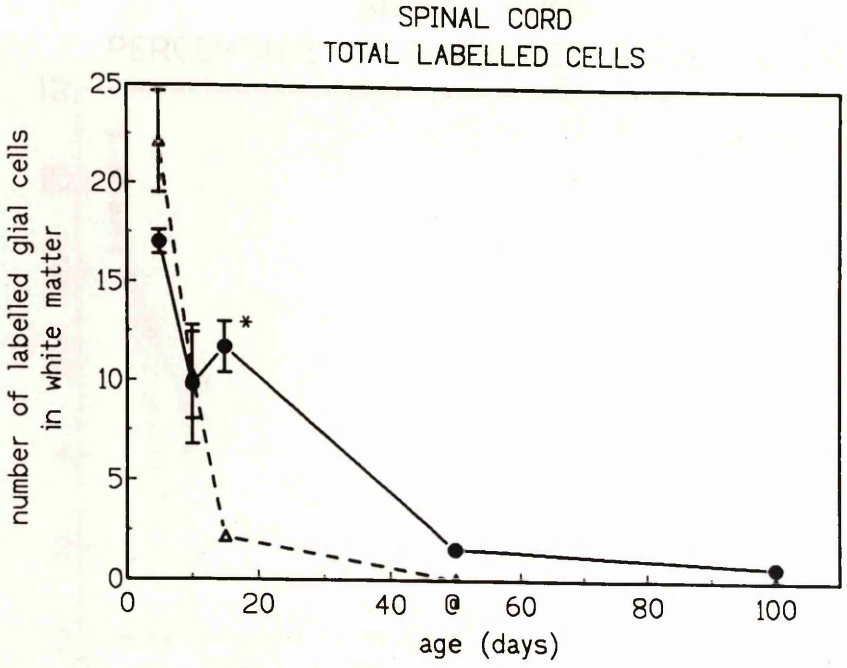

Figure 81: Total numbers of thymidine-labelled glial cells in the ventral columns of the C2 segment of the spinal cord from wild type (triangle) and *jp*^{rsh} mice (filled circle). All data represent mean ± SEM; where error bars are not seen they fall within the symbol. An asterisk has been placed beside the value that differs significatively from the wild type. (@) Shows the result obtained from a single experiment.

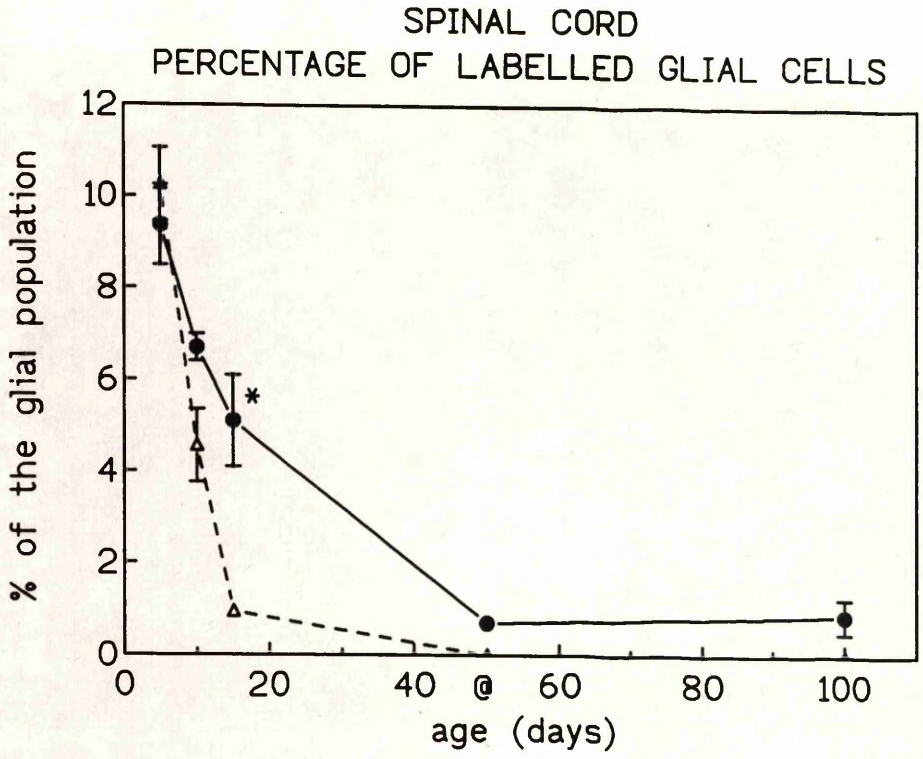

Figure 82: Percentage of thymidine-labelled glial cells in the ventral columns of the C2 segment of the spinal cord from the wild type (triangle) and *jp*^{rsh} mice (filled circle). All data represent mean ± SEM; where error bars are not seen they fall within the symbol. An asterisk has been placed beside the value that differs significatively from the wild type. (@) Shows the result obtained from a single experiment. The percentage of proliferating cells in the mutant spinal cord is noticeably increased after 16 days of age. 100-day-old mutant spinal cord shows a high proliferation percentage over 6 hours which may indicate a faster cell turnover in the mutant tissue. However, cell death was not conspicuous at this ages. Presumably, apoptosis of many cells must be taking place in this tissue (see figures 83 and 84).

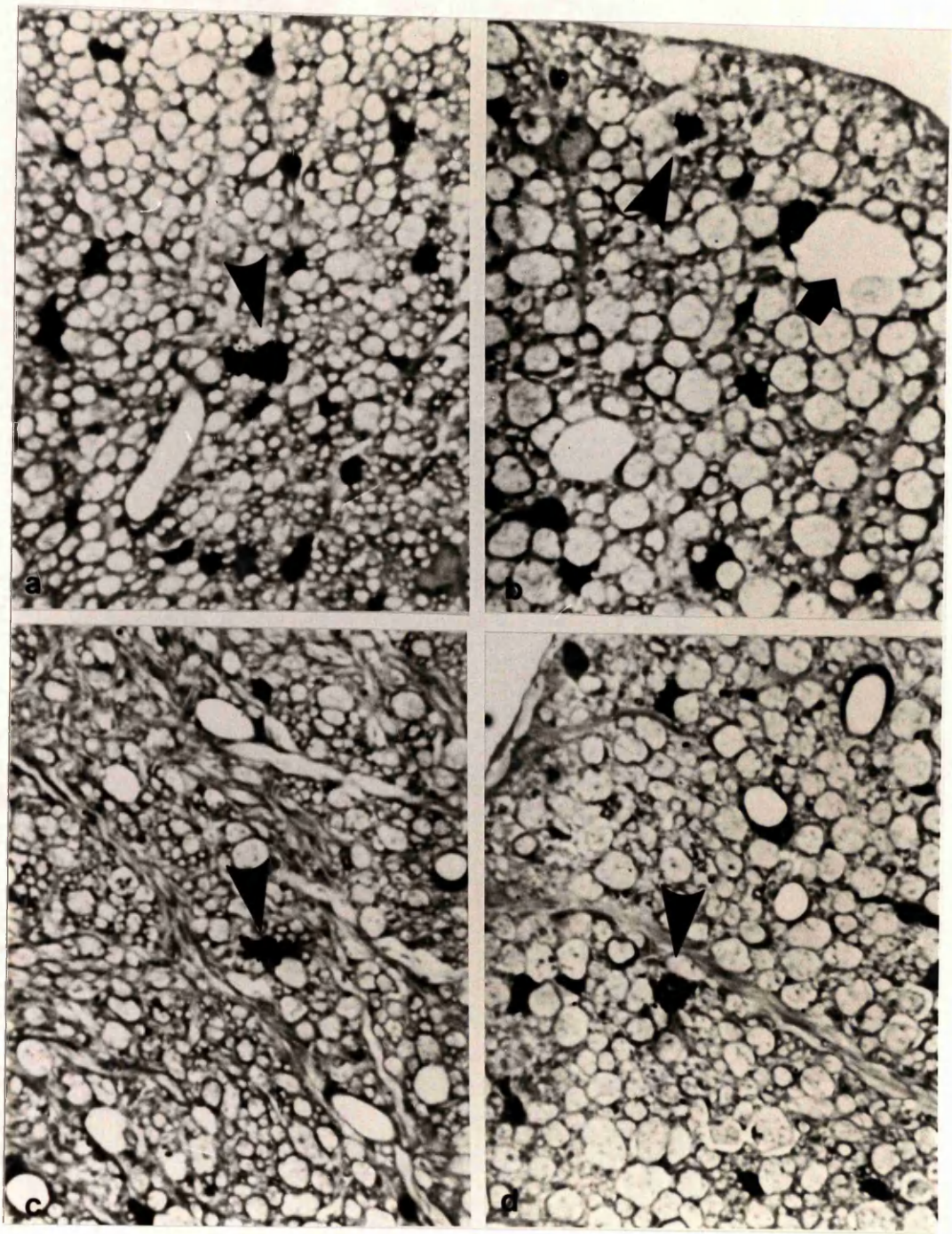

Figure 83: Autoradiography of 100-day-old *jp^{rsh}* spinal cord showing ^{3}H-thymidine labelled cells. Dorsal (a) and ventral columns (b, c, d) from a mutant mouse labelled over a period of 6 hours (3 injections). Arrow-heads point at cells morphologically resembling oligodendrocytes that have incorporated the isotope; therefore that were in the S-phase of the mitotic cycle during the labelling period (Knapp, 1992). (b) Vacuolation of a sheath is indicated (arrow). (Approx. magnification: x 1000).

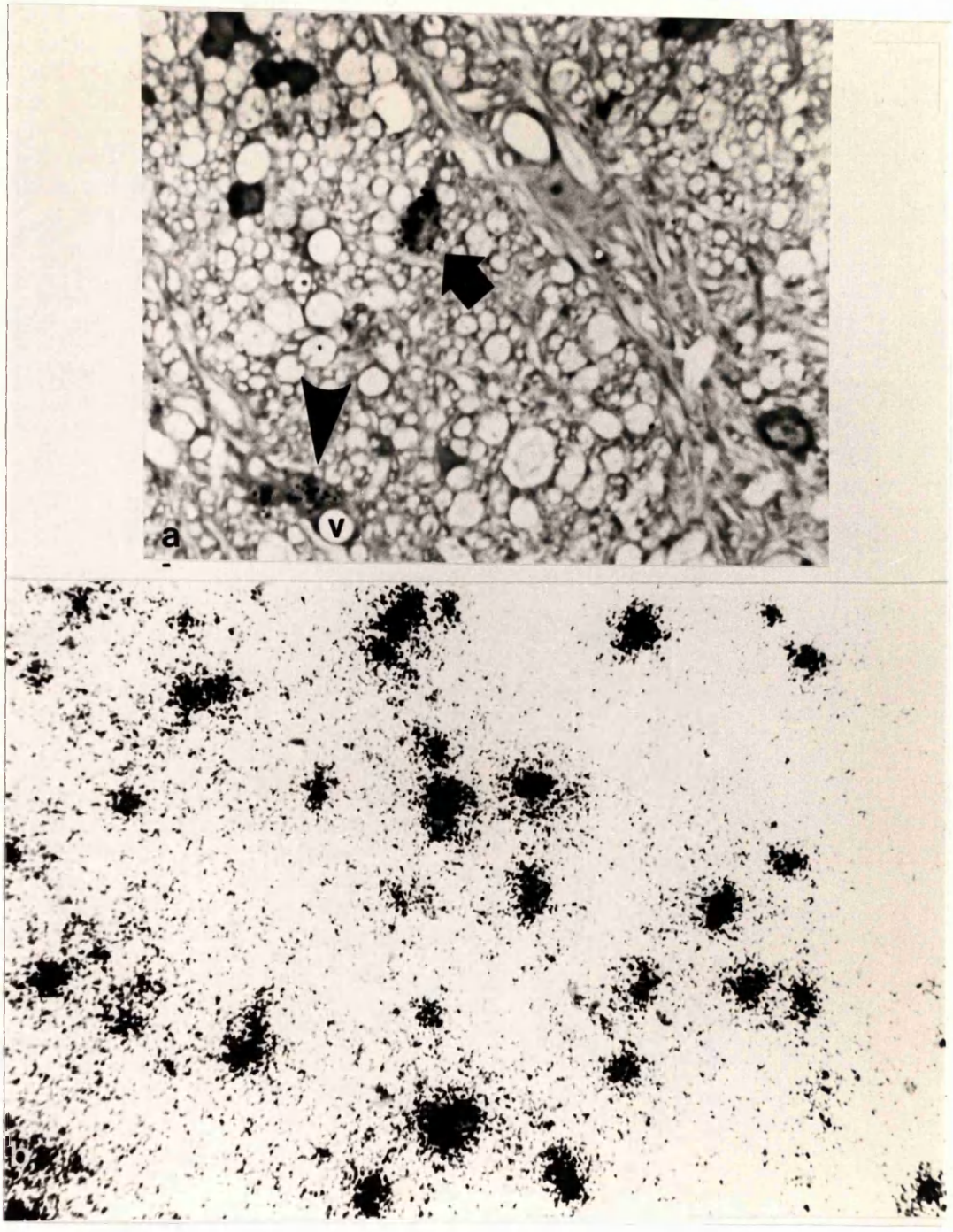

Figure 84: (a) Autoradiography of the 100-day-old jp^{rsh} spinal cord showing labelled cells. (b) *In situ* hybridization for PLP/DM-20 mRNA at the same age. (a) Section from the same mouse as in figure 83 showing other dividing cells in the mutant spinal cord such as an endothelial cell (arrow-head) and, possibly, an astrocyte (thick arrow); (v= blood vessel). (Approx. magnification: x 1000).
(b) In situ hybridization of the ventral columns from the spinal cord. Foci of silver grains signifying expressing oligodendrocytes. Nuclei of glial cells are not counterstained. The individual cell labelling indicates that most oligodendrocytes have increased their PLP/DM-20 mRNA levels with respect to younger ages (figures 46, 47). The density of PLP/DM-20 expressing cells is also increased (see figures 40, 41 for quantified data). (Approx. magnification: x 450).

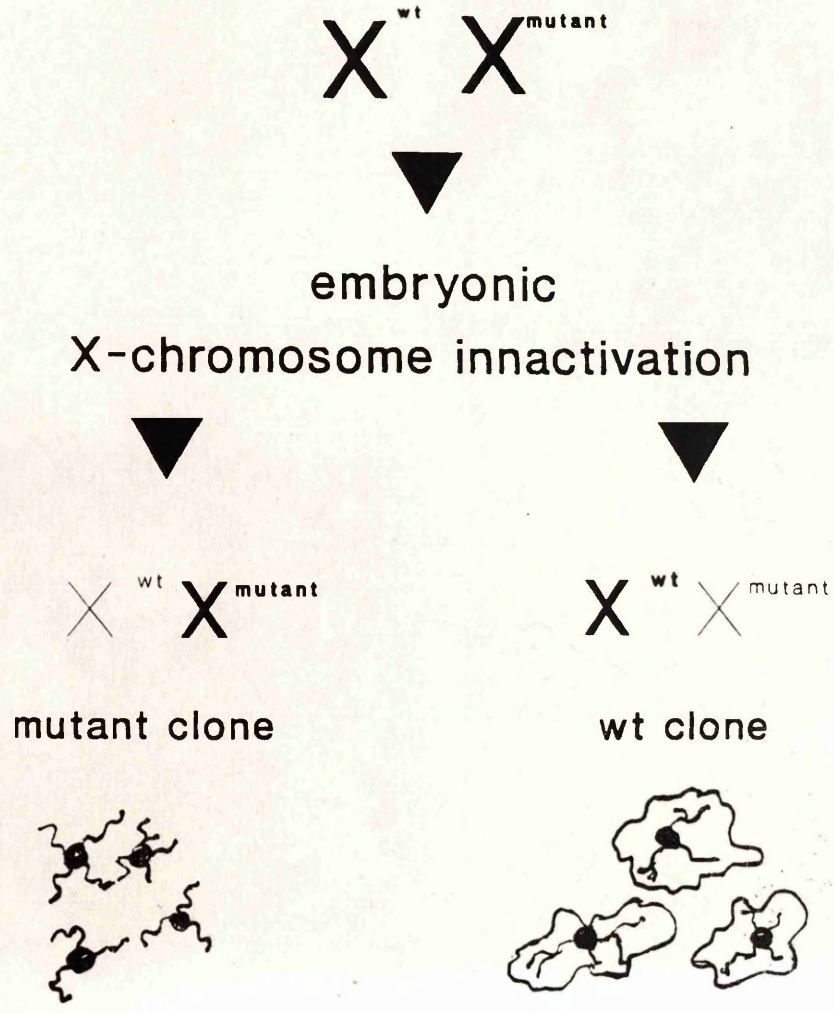

Figure 85: Outline of Lyon's hypothesis of X-chromosome inactivation (Lyon, 1972) during early embryonic development and oligodendrocyte clone formation (Nesbitt, 1971; Falconer and Avery, 1978; Nesbitt and Gartler, 1971).

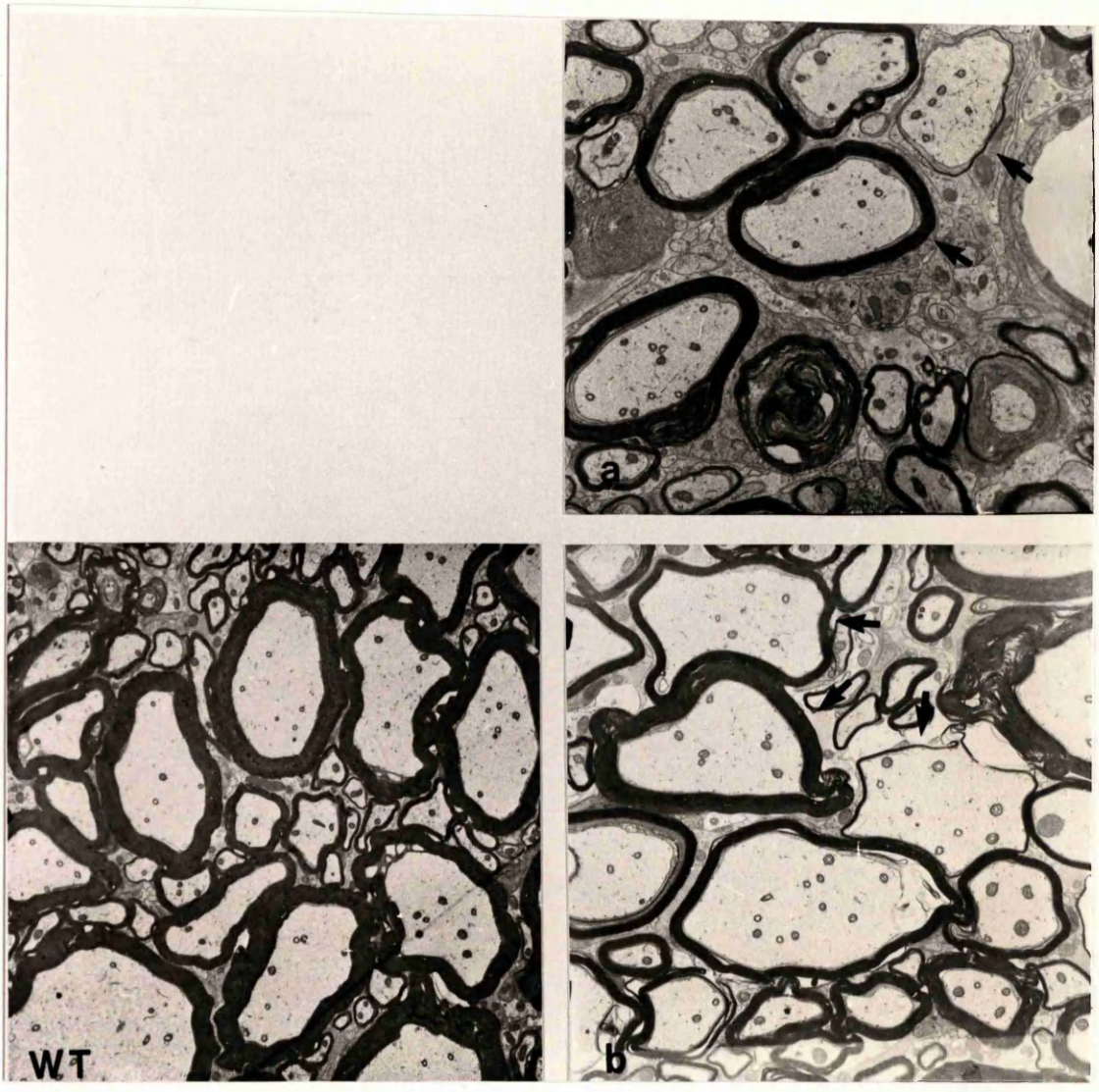

16 + 30 ?

Figure 86: Ultrastructure of 30-day-old wild type (WT), 16 (a) and 30 (b) *jp*^{rsh} heterozygote female ventral white matter of the spinal cord. The majority of axons in the female are myelinated although the thickness of myelin sheaths is not proportional to the axon diameter. Arrows point at axons with a similar diameter exhibiting myelin sheaths of different thickness. Redundant folds of myelin are a common finding in most female heterozygotes. No evidence of mosaicism was detected. (Approx. magnification: x 5000).

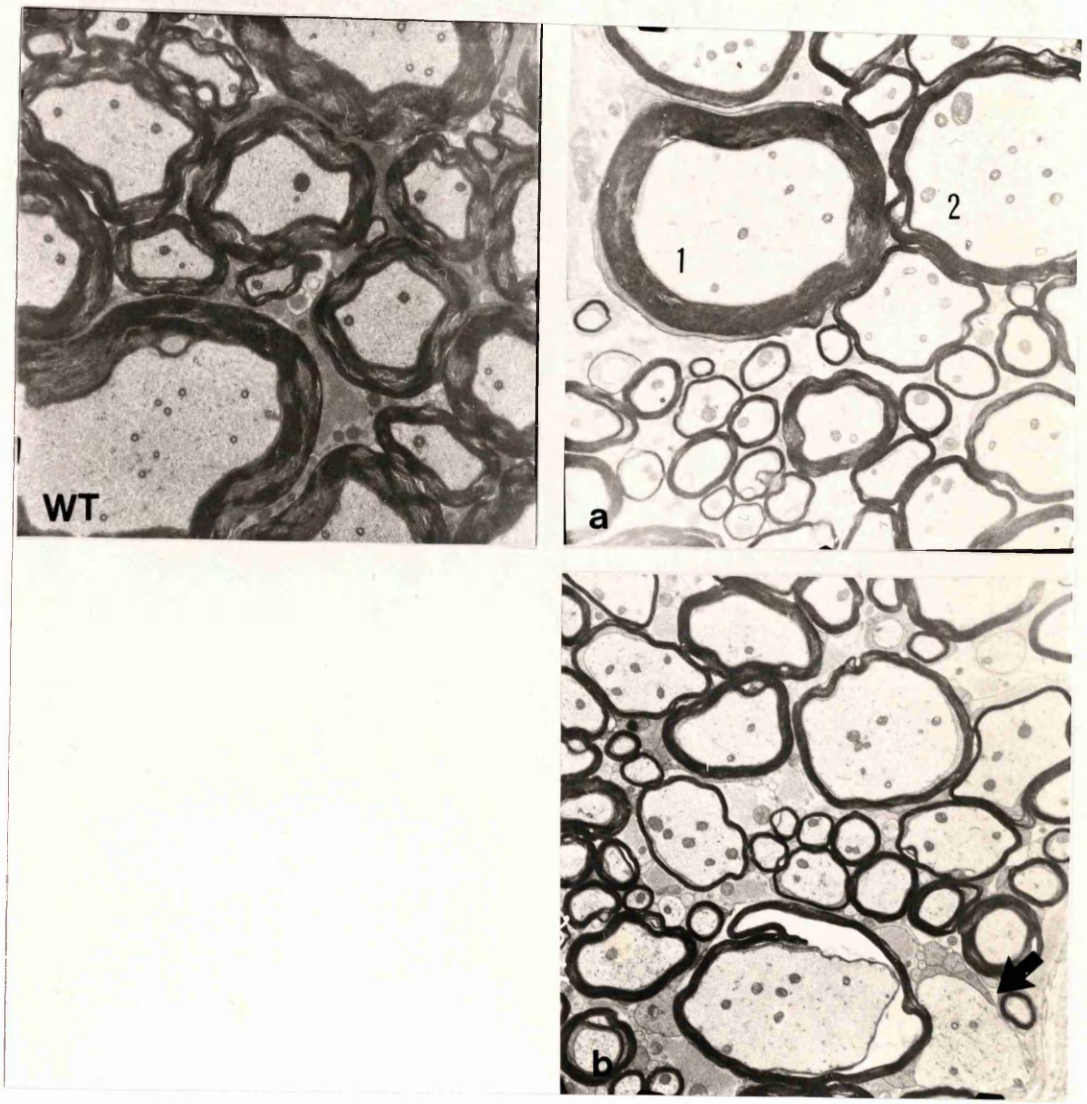

Figure 87: Ultrastructure of the ventral white matter of the spinal cord from 90-day-old *jp*^{rsh} heterozygote female and wild type sibling (WT). Hypomyelinated/amyelinated patches are not evident at this age. The majority of the axons are myelinated although the myelin sheaths are in many cases disproportionate with respect to the axonal diameter. (a) Axons of similar diameters exhibiting sheaths of different thickness (1, 2) are a common finding. (b) Vacuolation of some sheaths is still detectable in some myelin fibres at 90 days. No evidence of mosaicism is detected at this age. (Approx. magnification: x 5000).

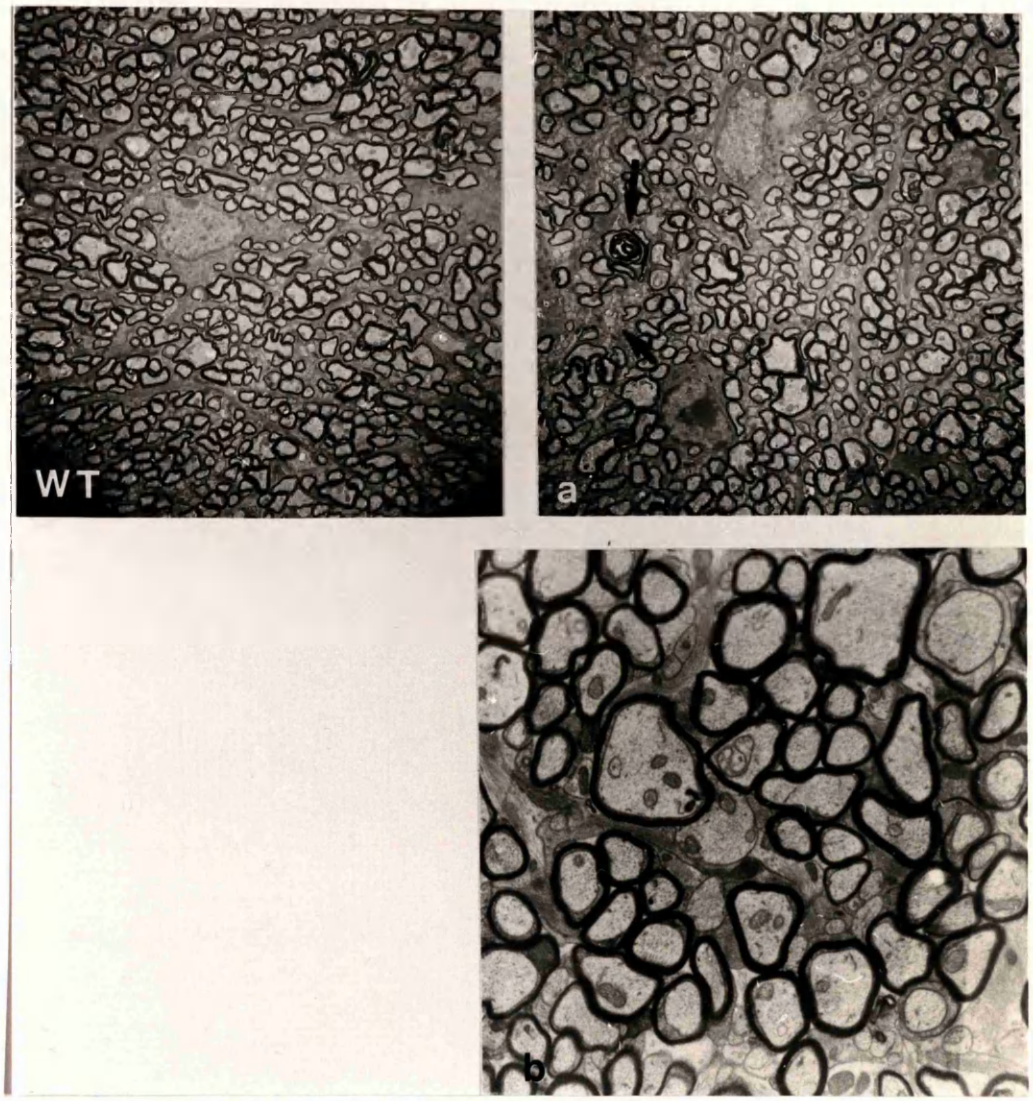

Figure 88: Ultrastructure of the optic nerves from 30-day-old jp^{rsh} heterozygote female (a, b) and wild type sibling (WT). No obvious mosaic changes in the optic nerve are detected at this age. A higher magnification (b) reveals occasional small bundles of naked fibres. Most myelinated axons exhibit a myelin sheath of normal characteristics. (Approx. magnification: upper panels: x 5000; b: x 7500).

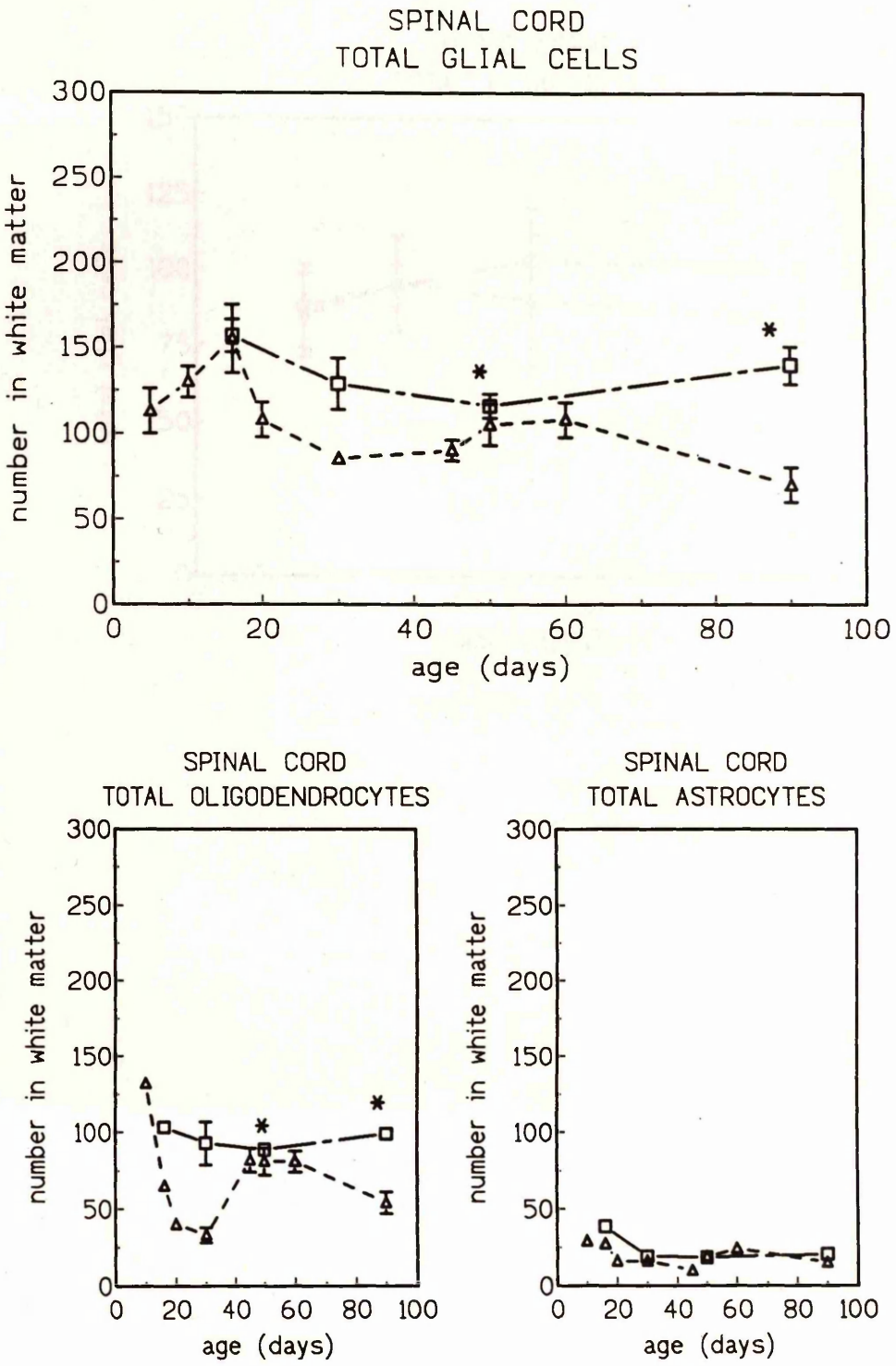

Figure 89: Total numbers of glial cells in white matter of C2 segment of spinal cord in *jp*^{rsh} heterozygote (square) and wild type siblings (triangle). Total numbers of oligodendrocytes and astrocytes in white matter are also shown individually. The growth in the total oligodendrocyte numbers is also supported by PLP/DM-20 expressing cell counts. All data represent mean ± SEM; where error bars are not seen they fall within the symbol. Asterisks have been placed in values that differ significatively from the wild type.

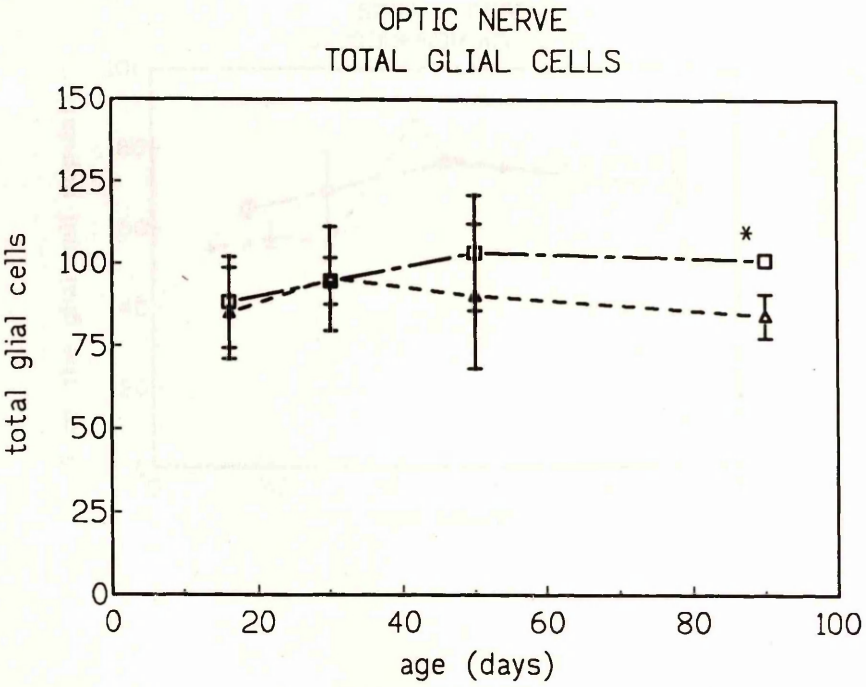

Figure 90: Total numbers of glial cells in the optic nerve of jp^{rsh} heterozygote (square) and wild type siblings (triangle). All data represent mean ± SEM; where error bars are not seen they fall within the symbol. An asterisk has been placed beside the value that differs significatively from the wild type.

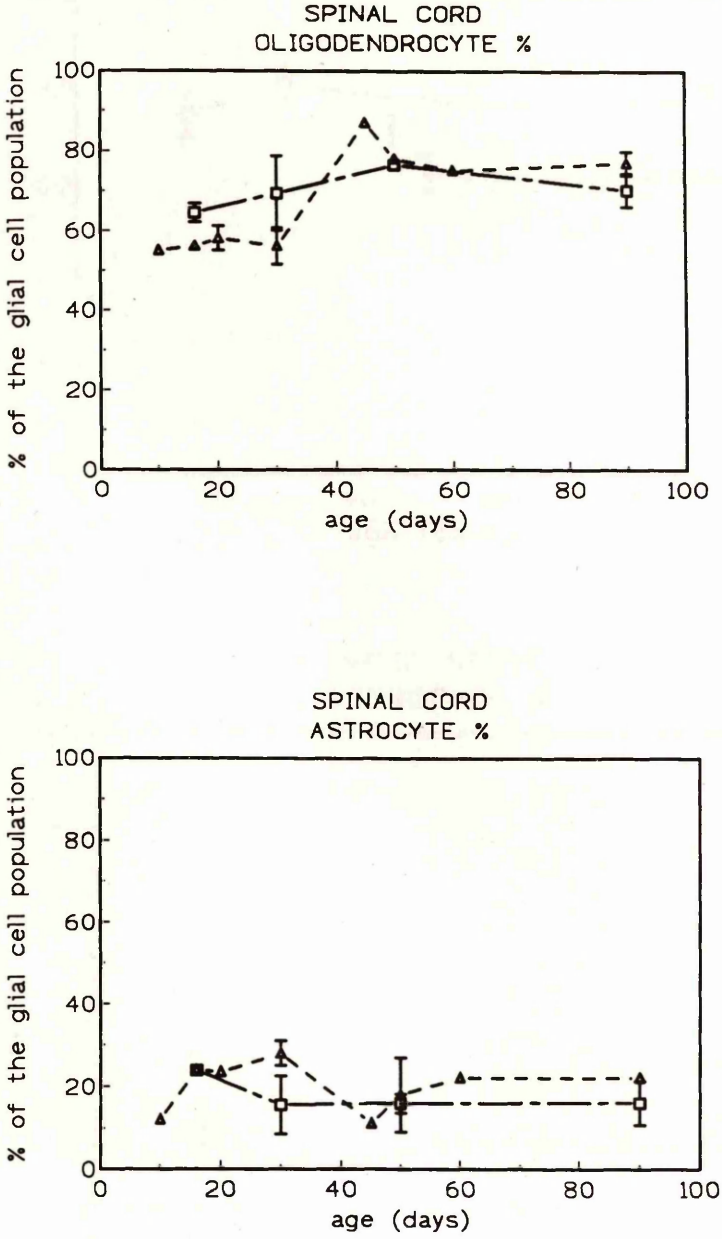

Figure 91: Percentages of oligodendrocytes and astrocytes in the white matter of the C2 segment of spinal cord of *jp*^{rsh} heterozygote (square) and wild type siblings (triangle). All data represent mean ± SEM; where error bars are not seen they fall within the symbol.

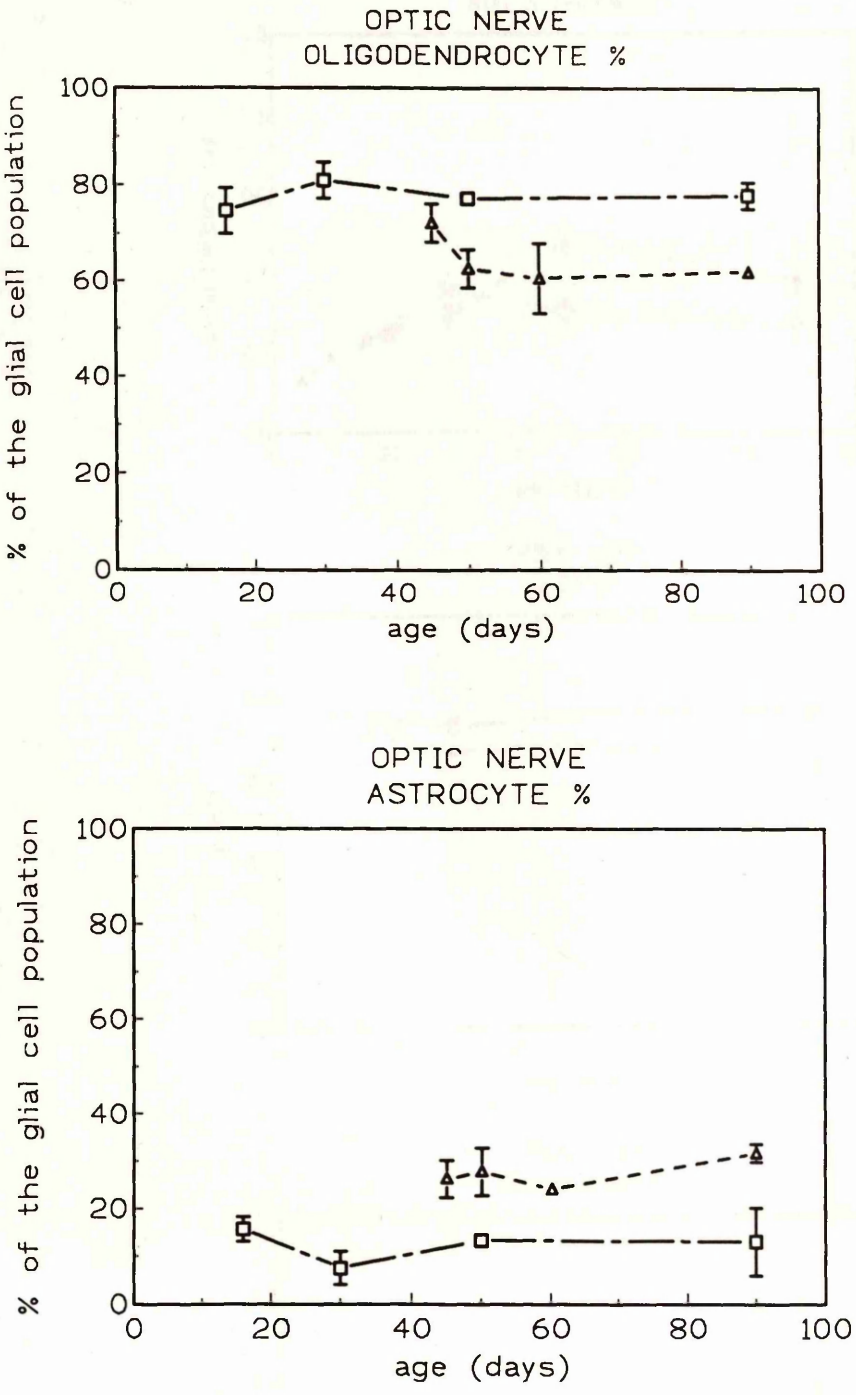

Figure 92: Percentages of oligodendrocytes and astrocytes in the optic nerves of jp^{rsh} heterozygote (square) and wild type siblings (triangle). All data represent mean ± SEM; where error bars are not seen they fall within the symbol.

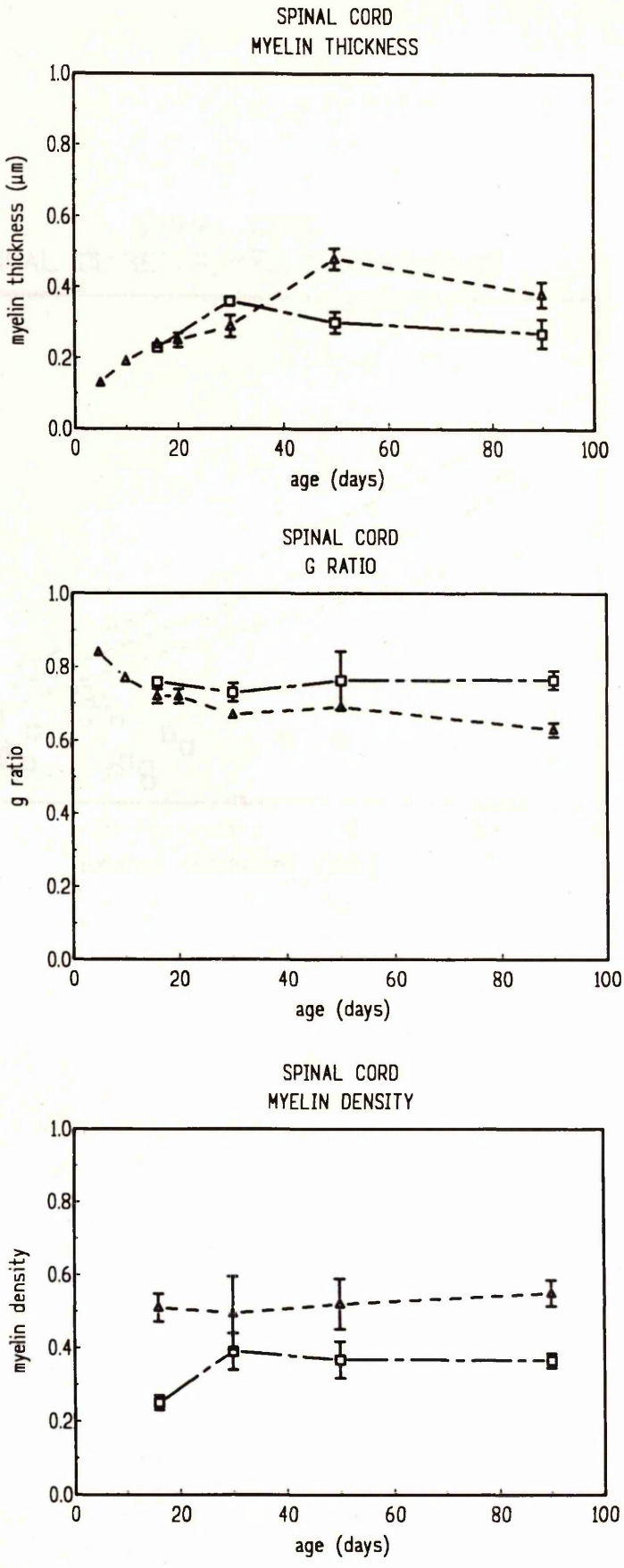

Figure 93: Morphometric analysis of the spinal cord of *jp*^{rsh} heterozygote (square) and wild type siblings (triangle). The values refer to the ventral columns of the spinal cord of the C2 segment of the spinal cord. All data represent mean ± SEM; where error bars are not seen they fall within the symbol. (upper panel) Myelin thickness. (centre) *g* ratio (*g* ratio defined as ratio of axon diameter to that of the axon plus myelin sheath). (lower panel) Myelin density (arbitrary units). Asterisks have been placed in values that differ significatively from the wild type.

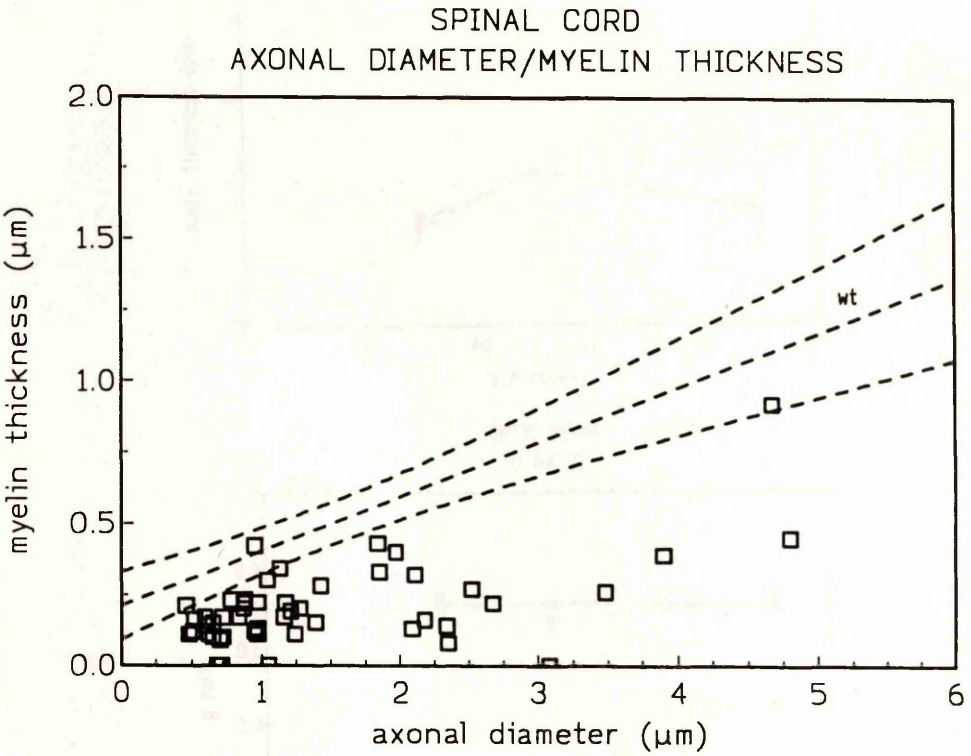

Figure 94: Scatter graph of the relationship between axon diameter and myelin thickness in *jp*^{rsh} heterozygote female spinal cord (square) at 90 days. The central line is the linear regression and the curved lines the prediction bands for similar data from 90-day-old wild type mice. Although the vast majority of values of *jp*^{rsh} female are lower than the wild type prediction area, a small proportion of myelin sheaths fall below much lower than the lower prediction band indicating a disproportionately thin myelin sheath or he absence of sheath.

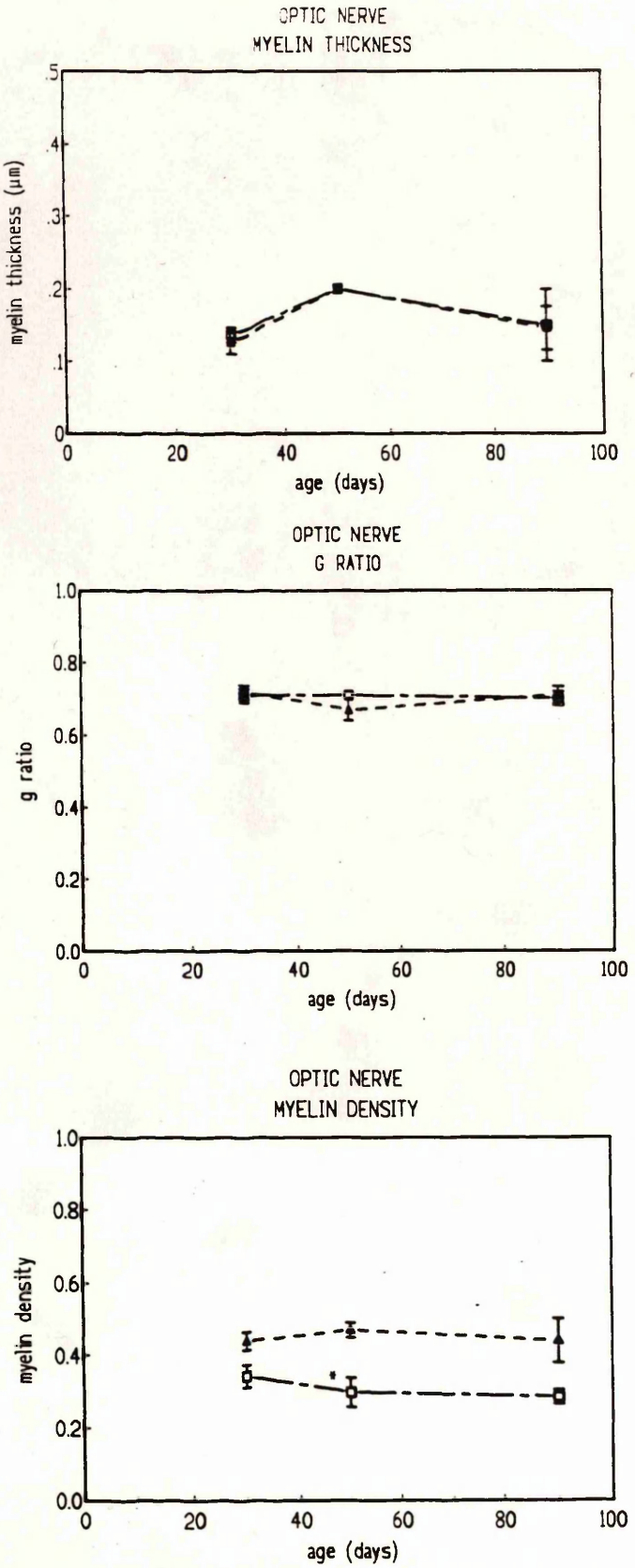

Figure 95: Morphometric analysis of the optic nerves of jp^{rsh} heterozygote (square) and wild type siblings (triangle). All data represent mean ± SEM; where error bars are not seen they fall within the symbol. (upper panel) Myelin thickness. (centre) *g* ratio (*g* ratio defined as ratio of axon diameter to that of the axon plus myelin sheath). (lower panel) Myelin density (arbitrary units). An asterisk has been placed beside the value that differs significatively from the wild type.

Figure 96: *In situ* hybridization for PLP/DM-20 mRNA in 30-day-old normal male (a) and jp^{rsh} heterozygote female (b) spinal cords. The intensity of signal per cell appears similar in both cords but quantification of cell numbers shows that the total number of expressing cells in the white matter is increased by approximately 36% in the heterozygote. The autoradiogram is counterstained with haematoxilin. Higher magnification of the same sections demonstrates that the number of expressing cells in the heterozygote female is increased and that the individual cell expression is not as affected as in jp^{rsh} mutants (figure 47). (Approx. magnification: upper panel x 65, lower panel x 450).

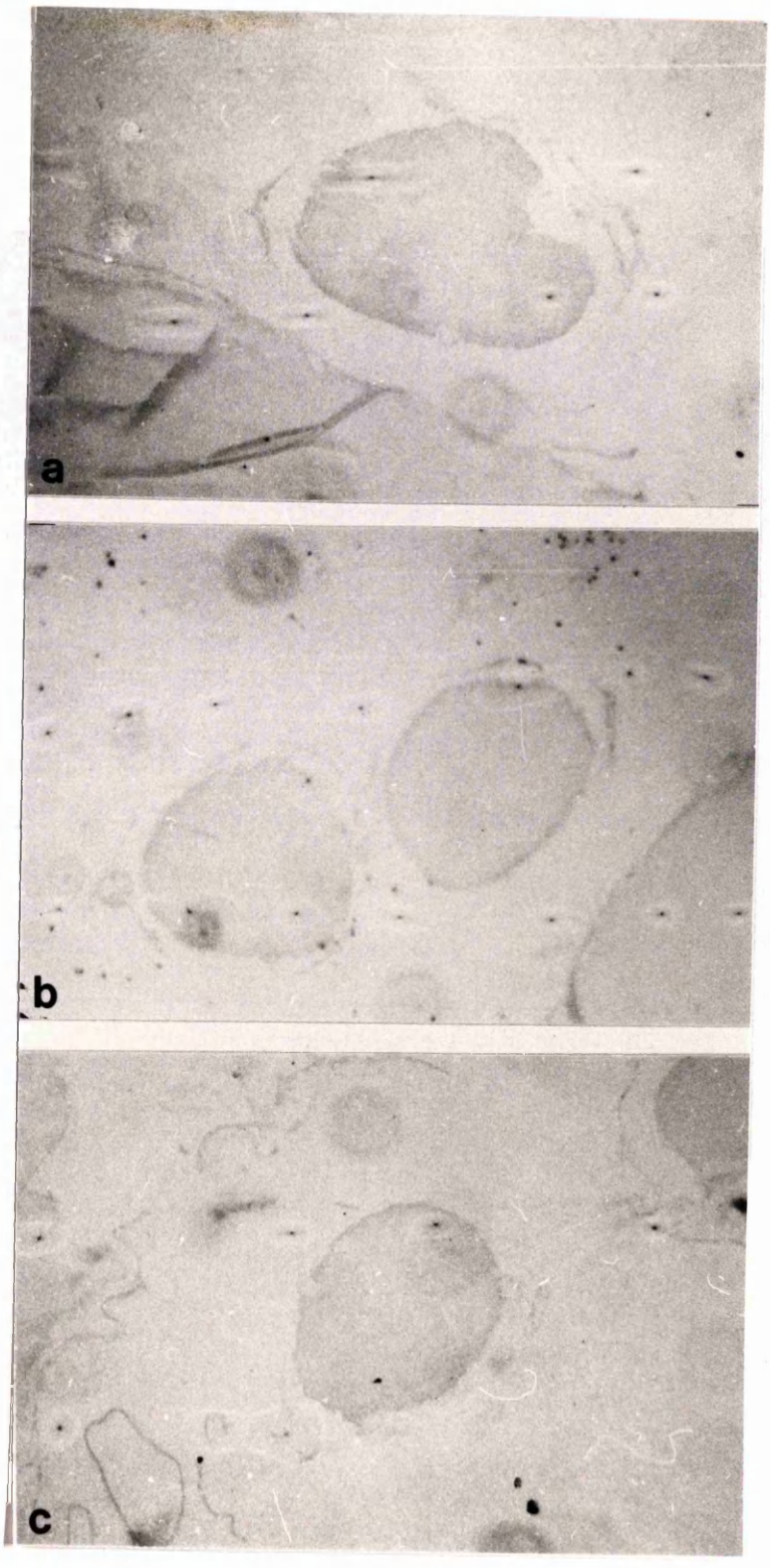

Figure 97: PAP control sections. Performed on paraffin-embedded sections of the optic nerves of wild type. In this experiment antibodies have been replaced by rabbit serum at the same concentrations; (a) 1:300 (b) 1:400 and (c) 1:1000. (Approx. magnification: x 90).

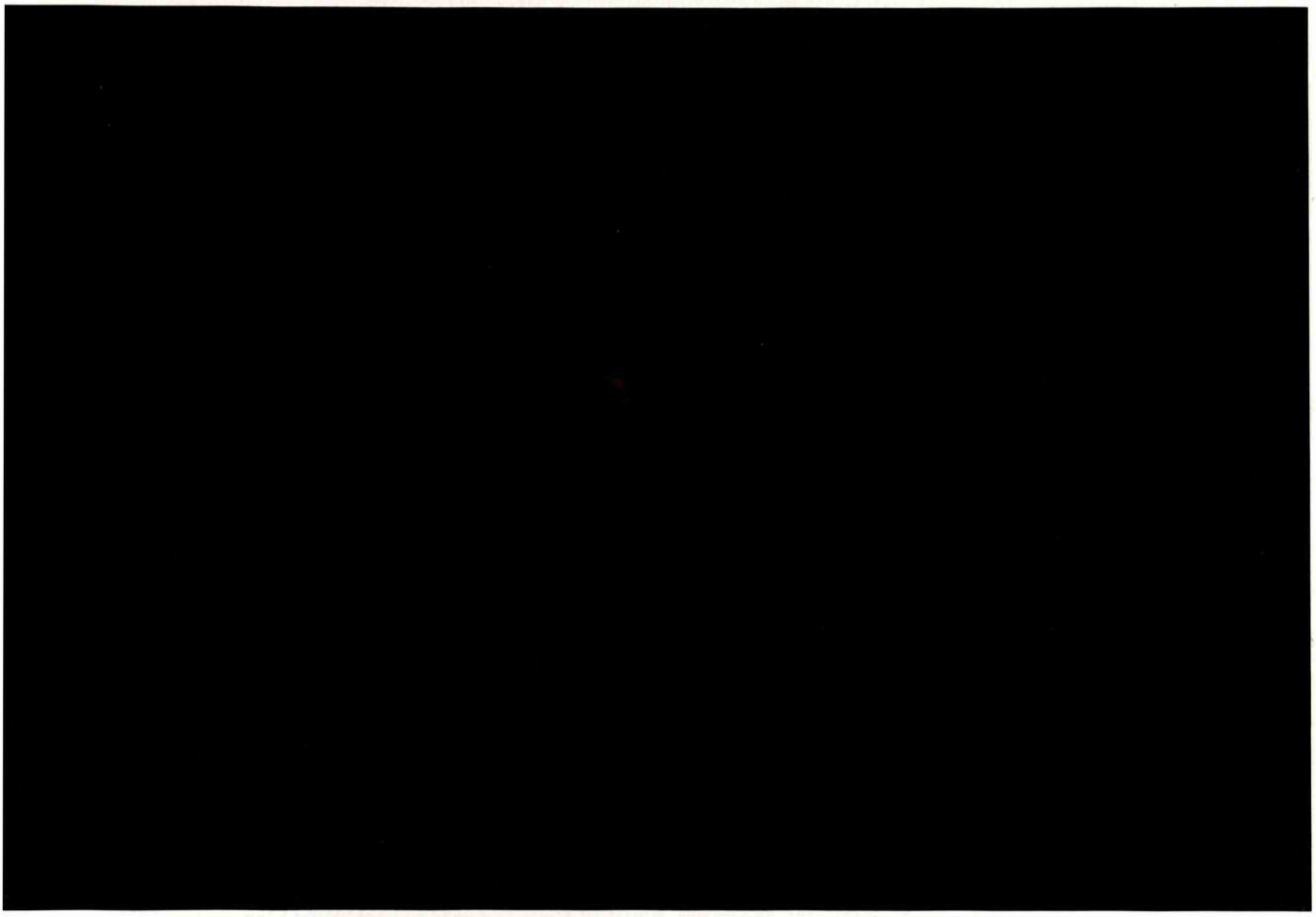

Figure 98: Immunofluorescence control. 1 week-old culture of spinal cord from 10-day-old wild type where rabbit Ig was substituted for the primary antibody. Other control experiments where the antibody was preincubated with the peptide recognized by the antibody or the primary antibody was replaced by BSA showed similar unspecific binding as in the present example (pictures not shown). (Approx. magnification: x 650).

ABBREVIATIONS

Bq= becquerel(s)

BrdU= bromo-deoxyuridine

CAII= carbonic anhydrase

CBAM= complement-binding and activating molecule

cm= centimetres

CNPase= 2',3',cyclic nucleotide 3'-phosphohydrolase

CNS= central nervous system

CNT= ciliary neurotrophic factor

Ci= curies

ddH2O= deionised-distilled water

DNA= deoxyribonucleic acid

EGF= epidermal growth factor

EM= electron microscopy

FCS= foetal calf serum

FGF= fibroblast growth factor

FITC= fluorescein isothiocyanate

μm= micrometers

g= grams

GalC= galactocerebroside

GFAP= glial fibrillary acidic protein

GPDH= glycerol phosphate dehydrogenase

HBSS= Hank's balanced salt solution

hr= hour(s)

IGF-1= insulin-like growth factor-1

IPL= intra-period line

ISH= *in situ* hybridization

jp= jimpy

jp^{msd}= jimpy myelin synthesis deficient

jp^{rsh}= jimpy rumpshaker

kDa= kiloDalton

l= litre(s)

L15= Liebowitz medium

LM= light microscopy

M= molar

MAG= myelin-associated glycoprotein

MBP= myelin basic protein

md rat= myelin deficient rat

MDL= major dense line

min= minute(s)

mm= millimetres

mM= millimolar

mRNA= messenger ribonucleic acid

NGF= nerve growth factor

O-2A= oligodendrocyte type-2 astrocyte

^{o}C= degrees centigrade

OD= optical density

PAP= peroxidase anti-peroxidase

PBS= phosphate buffered saline

PDGF= platelet-derived growth factor

PLP= proteolipid protein

PMD= Pelizaeus Merzbacher disease

PNS= peripheral nervous system

POA= pro-oligodendroblast antigen

qk= quaking

RER= rough endoplasmic reticulum

RNA= ribonucleic acid

RT = room temperature

sec = second(s)

sh pup = shaking pup

shi = shiverer

shi^{mld} = shiverer myelin deficient

tr = trembler

TRITC = tetramethyl rhodamine isothiocyanate

WT = wild type

REFERENCES

Amur-Umarjee, S.G., Hall, L. and Campagnoni, A.T. (1990) Spatial distribution of mRNAs for myelin proteins in primary cultures of mouse brain. *Dev.Neurosci.*, 12:263-272.

Arenella, L.S. and Herndon, R.M. (1984) Mature oligodendrocytes. Division following experimental demyelination in adult animals. *Arch.Neurol.*, 41:1162-1165.

Arquint, M., Roder, J., Chia, L-S., Down, J., Wilkinson, D., Bayley, H., Braun, P. and Dunn, R. (1987) Molecular cloning and primary structure of myelin-asociated glycoprotein. *Proc.Natl.Acad.Sci.USA*, 84:600-604.

Ayers, M.M. and Anderson, R.McD. (1973) Onion bulb neuropathy in the trembler mouse: a model of hypertrophic interstitial neuropathy (Dejerine-Sottas) in man. *Acta Neuropath.(Berl)*, 25:54-70.

Bansal, R., Warrington, A.E., Gard, A.L., Ranscht, B. and Pfeiffer, S.E. (1989) Multiple and novel specificities of monoclonal antibodies O1, O4 and R-mAb used in the analysis of oligodendrocyte development. *J.Neurosci.Res.*, 24:548-557.

Bansal, R., Stefansson, K. and Pfeiffer, S.E. (1992) Proligodendroblast antigen (POA), a developmental antigen expressed by A007/O4-positive oligodendrocyte progenitors prior to the appearance of sulfatide and galactocerebroside. *J.Neurochem.*, 58:2221-2229.

Barbarese, E., Carson, J.H. and Braun, P.E. (1978) Accumulation of the four myelin basic proteins in mouse brain during development. *J.Neurochem.*, 31:779-782.

Barbarese, E., Nielson, M.L. and Carson, J.H. (1983) The effect of the shiverer mutation on myelin basic protein expression in homozygous and heterozygous mouse brain. *J.Neurochem.*, 40:1680-1686.

Barnett, S.C., Hutchins, A.M. and Noble, M. (1993) Purification of olfactory nerve ensheathing cells from the olfactory bulb. *Dev.Biol.*, 155:in Press.

Barres, B.A., Hart, I.K., Coles, H.S.R., Burne, J.F., Voyvodic, J.T., Richardson, W.D. and Raff, M.C. (1992) Cell death and control of cell survival in the oligodendrocyte lineage. *Cell*, 70:31-46.

Bartlett, P.P., Noble, M., Pruss, R.M., Raff, M.C., Rattray, S. and Williams, C.A. (1981) Rat neural antigen-2 (Ran-2): a cell surface antigen on astrocytes, ependymal cells, Muller cells and leptomeninges defined by a monoclonal antibody. *Brain Res*, 204:339-351.

Bartlett, W.P., Knapp, P.E. and Skoff, R.P. (1988) Glial conditioned medium enables jimpy oligodendrocytes to express properties of normal oligodendrocytes: production of myelin antigens and membranes. *Glia*, 1:253-259.

Bartlett, W.P. and Skoff, R.P. (1986) Expression of the jimpy gene in the spinal cords of heterozygous female mice. I. An early myelin deficit followed by compensation. *J.Neurosci.*, 6:2802-2812.

Benjamins, J.A., Iwata, R. and Hazlett, J. (1978) Kinetics of entry of proteins into the myelin membrane. *J.Neurochem.*, 31:1077-1085.

Benjamins, J.A., Skoff, R.P. and Beyer, K. (1984) Biochemical expression of mosaicism in female mice heterozygous for the jimpy gene. *J.Neurochem.*, 42:487-492.

Benjamins, J.A., Studzinski, D.M., Skoff, R.P., Nedelkoka, L., Carrey, E.A. and Dyer, C.A. (1989) Recovery of proteolipid protein in mice heterozygous for the jimpy gene. *J.Neurochem.*, 53:279-286.

Berg, G. and Schachner, M. (1981) Immuno-electron-microscopic identification of O-antigen-bearing oligodendroglial cells in vitro. *Cell Tissue Res.*, 219:313-325.

Berg, G. and Schachner, M. (1982) Immunoelectron microscopic characterization of galactocerebroside and nervous system antigen-1 (ns-1) positive oligodendrocytes in culture. *Neurosci.Lett.*, 28:75-80.

Bernier, L., Alvarez, F., Norgard, E.M., Raible, D.W., Mentaberry, A., Schembri, J.G., Sabatini, D.D. and Colman, D.R. (1987) Molecular cloning of a 2',3'-cyclic nucleotide 3'-phosphodiesterase: mRNAs with different 5' ends encode the same set of proteins in nervous and lymphoid tissues. *J.Neurosci.*, 7:2703-2710.

Berry, M., Hall, S., Rees, L., Carlile, J. and Wyse, J.P.H. (1992) Regeneration of axons in the optic nerve of the adult Browman-Wyse (BW) mutant rat. *J.Neurocytol.*, 21:426-448.

Bignami, A., Eng, L.F. and Uyeda, C.T. (1972) Localization of the glial fibrillary acidic protein in astrocytes by immunofluorescence. *Brain Res*, 43:429-435.

Billings-Gagliardi, S., Adcock, L.H., Lamperti, E.D., Schwing-Stanhope, G. and Wolf, M.K. (1983) Myelination of *jp*, *jp^{msd}* and *qk* axons by normal glia in vitro: ultrastructural and autoradiographic evidence. *Brain Res*, 268:255-266.

Black, J.A., Foster, R.E. and Waxman, S.G. (1982) Rat optic nerve: freeze-fracture studies during development of myelinated axons. *Brain Res*, 250:1-20.

Blakemore, W.F., Harding, J.D.J. and Done, J.T. (1974) Ultrastructural observations on the spinal cord of a Landrace pig with congenital tremor type AIII. *Res.Vet.Sci.*, 17:174-178.

Blakemore, W.F. (1982) Myelination, demyelination and remyelination in the CNS. In *Recent Advances in Neuropathology. 2.* J.B. Cavanagh (ed): Churchill Livingstone, Edinburgh, pp. 53-81.

Boison, D. and Stoffel, W. (1989) Myelin-deficient rat: a point mutation in exon III (A→C, Thr75→Pro) of the myelin proteolipid protein causes dysmyelination and oligodendrocyte death. *EMBO J.*, 8:3295-3302.

Bologa-Sandru, L., Siegrist, H.P., Z'Graggen, A., Hofmann, K., Wiesmann, U., Dahl, D. and Herschkowitz, N. (1981) Expression of antigenic markers during the development of oligodendrocytes in mouse brain cell cultures. *Brain Res*, 210:217-229.

Bourre, J.M., Jacque, C., Delassalle, A., Nguyen-Legros, J., Dumont, O., Lachapelle, F., Raoul, M., Alvarez, C. and Baumann, N. (1980) Density profile and basic protein measurements in the myelin range of particulate material from normal developing mouse brain and from neurological mutants (jimpy; quaking; trembler;

shiverer and its *mld* allele) obtained by zonal centrifugation. *J.Neurochem.*, 35:458-464.

Bradel, E.J. and Prince, F.P. (1983) Cultured neonatal rat oligodendrocytes elaborate myelin membrane in the absence of neurons. *J.Neurosci.Res.*, 9:381-392.

Braun, P.E., Sandillon, F., Edwards, A., Matthieu, J.-M. and Privat, A. (1988) Immunocytochemical localization by electron microscopy of 2',3',-cyclic nucleotide 3'-phosphodiesterase in developing oligodendrocytes of normal and mutant brain. *J.Neurosci.*, 8:3057-3066.

Cammer, W., Sacchi, R., Kahn, S. and Sapirstein, V. (1985) Oligodendroglial structures and distribution shown by carbonic anhydrase immunostaining in the spinal cords of developing normal and shiverer mice. *J.Neurosci.Res.*, 14:303-316.

Campagnoni, A.T. (1988) Molecular biology of myelin proteins from the central nervous system. *J.Neurochem.*, 51:1-14.

Campagnoni, A.T. and Macklin, W.B. (1988) Cellular and molecular aspects of myelin protein gene expression. *Mol.Neurobiol.*, 2:41-89.

Campagnoni, C.W., Garbay, B., Micevych, P., Pribyl, T., Kampf, K., Handley, V.W. and Campagnoni, A.T. (1992) DM20 mRNA splice product of the myelin proteolipid protein gene is expressed in the murine heart. *J.Neurosci.Res.*, 33:148-155.

Cattanach, B.M. and Beechey, C.V. (1991) Evidence of allelism between rumpshaker and jimpy. *Mouse Genome*, 89:271.

Chan, D.S. and Lees, M.B. (1974) Gel electrophoresis studies of bovine brain white matter proteolipid and myelin proteins. *Biochem*, 13:2704-2711.

Chernoff, G.F. (1981) Shiverer: an autosomal recessive mutant mouse with myelin deficiency. *J.Hered.*, 72:128.

Climent, S. , and J.A. Bascuas (1982) *Cuadernos de anatomia y embriologia veterinaria. VI. Sistema nervioso central.* Libros Portico. Zaragoza.

Colman, D.R., Kreibich, G., Frey, A.B. and Sabatini, D.D. (1982) Synthesis and incorporation of myelin polypeptides into CNS myelin. *J.Cell Biol.*, 95:598-608.(Abstract)

Cox, K.H., DeLeon, D.V., Angerer, L.M. and Angerer, R.C. (1984) Detection of mRNAs in sea urchin embryos by *in situ* hybridization using asymmetric RNA probes. *Dev.Biol.*, 101:485-502.

Dautigny, A., Mattei, M-G., Morello, D., Alliel, P.M., Pham-Dinh, D., Amar, L., Arnaud, D., Simon, D., Mattei, J-F., Guenet, J-L., Jolles, P. and Avner, P. (1986) The structural gene coding for myelin-associated proteolipid protein is mutated in *jimpy* mice. *Nature*, 321:867-869.

Del Rio Hortega, P. (1921) Estudios sobre la neuroglia: La glia de escasas radiaciones (oligodendroglia). *Bol.R.Soc.Esp.Hist.Nat.*, 21:63-92.

Del Rio Hortega, P. (1922) Son homologables la glia de escasas radiaciones y la celula de Schwann? *Bol.R.Soc.Esp.Hist.Nat.*, 10:25-29.

Del Rio Hortega, P. (1924) La glie a radiations peu nombreuses et la cellule de Schwann sont elles homologables. *C.R.Soc.Biol.*, 91:818-820.

Dentinger, M.P., Barron, K.D. and Csiza, C.K. (1982) Ultrastructure of the central nervous system in a myelin deficient rat. *J.Neurocytol*, 11:671-691.

Diehl, H-J., Schaich, M., Budzinski, R-M. and Stoffel, W. (1986) Individual exons encode the integral membrane domains of human proteolipid protein. *Proc.Natl.Acad.Sci.USA*, 83:9807-9811.

Dubois-Dalcq, M., Behar, T., Hudson, L.D. and Lazzarini, R.A. (1986) Emergence of three myelin proteins in oligodendrocytes cultured without neurons. *J.Cell Biol.*, 102:384-392.

Dubois-Dalcq, M. (1987) Characterization of a slowly proliferative cell along the oligodendrocyte differentiation pathway. *EMBO J.*, 6:2587-2595.

Duncan, I.D., Griffiths, I.R. and Munz, M. (1983) "Shaking pup": a disorder of central myelination in the spaniel dog. III. Quantitative aspects of the glia and myelin in the spinal cord and optic nerve. *Neuropath.Appl.Neurobiol.*, 9:355-368.

Duncan, I.D., Hammang, J.P. and Jackson, K.F. (1986) Mosaicism in the CNS of two myelin mutants, the shaking pup and the myelin deficient (*md*) rat. *J.Neuropath.Exp.Neurol.*, 45:373.

Duncan, I.D., Hammang, J.P. and Jackson, K.F. (1987a) Myelin mosaicism in female heterozygotes of canine shaking pup and myelin-deficient rat mutants. *Brain Res*, 402:168-172.

Duncan, I.D., Hammang, J.P. and Trapp, B.D. (1987b) Abnormal compact myelin in the myelin-deficient rat: absence of proteolipid protein correlates with a defect in the intraperiod line. *Proc.Natl.Acad.Sci.USA*, 84:6287-6291.

Duncan, I.D., Hammang, J.P., Goda, S. and Quarles, R.H. (1989) Myelination in the jimpy mouse in the absence of proteolipid protein. *Glia*, 2:148-154.

Duncan, I.D. (1990) Dissection of the phenotype and genotype of the X-linked myelin mutants. *Ann.N.Y.Acad.Sci.*, 605:110-121.

Dupouey, P., Jacque, C., Bourre, J.M., Cesselin, F., Privat, A. and Baumann, N. (1979) Immunochemical studies of myelin basic protein in shiverer mouse devoid of major dense line of myelin. *Neurosci.Lett.*, 12:113-118.

Dyer, C.A. and Benjamins, J.A. (1989) Organization of oligodendroglial membrane sheets. II. Galactocerebroside: antibody interactions signal changes in cytoskeleton and myelin basic protein. *J.Neurosci.Res.*, 24:212-221.

Einsenbarth, G.S., Walsh, F.S. and Nirenberg, M. (1979) Monoclonal antibody to a plasma membrane antigen of neurons. *Proc.Natl.Acad.Sci.USA*, 76:4913-4917.

Espinosa de los Monteros, A., Roussel, G. and Nussbaum, J.L. (1986) A proceedure for long-term culture of oligodendrocytes. *Dev.Brain Res.*, 24:117-125.

Espinosa de los Monteros, A., Chiapelli, F., Fisher, R.S. and de Vellis, J. (1988) Transferrin: an early marker of oligodendrocytes in culture. *Int.J.Dev.Neuroscience*, 6:167-175.

Espinosa de los Monteros, A., Zhang, M., Gordon, M.N., Kumar, S., Scully, S.A. and de Vellis, J. (1990) The *myelin-deficient* rat mutant: partial recovery of oligodendrocyte maturation in vitro. *Dev.Neurosci.*, 12:326-339.

Espinosa de los Monteros, A. and Vellis, J. (1990) Oligodendrocyte differentiation: Developmental and functional subpopulations. *NATO ASI Series*, 43:33-45.

Falconer, D.S. and Avery, P.J. (1978) Variability of chimaeras and mosaics. *J.Embryol.Exp.Morph.*, 43:195-219.

Fanarraga, M., Griffiths, I.R., McCulloch, M.C., Barrie, J.A., Cattanach, B.M., Brophy, P.J. and Kennedy, P.G.E. (1991) Rumpshaker: an X-linked mutation affecting CNS myelination. A study of the female heterozygote. *Neuropath.Appl.Neurobiol.*, 17:289-297.

Fanarraga, M., Griffiths, I.R., McCulloch, M.C., Barrie, J.A., Kennedy, P.G.E. and Brophy, P.J. (1992a) Rumpshaker: an X-linked mutation causing hypomyelination. Developmental differences in myelination and glial cells between the optic nerve and spinal cord. *Glia*, 5:161-170.

Fanarraga, M., Montague, P., Griffiths, I.R. and Sommer, I. (1992b) Oligodendrocyte differentiation in the spinal cord of mice with the PLP mutation rumpshaker (rsh). *Neuropath.Appl.Neurobiol.*, 18:299.(Abstract)

Ferra, F.de., Engh, H., Hudson, L., Kamholz, J., Puckett, C., Molineaux, S. and Lazzarini, R.A. (1985) Alternative splicing accounts for the four forms of myelin basic protein. *Cell*, 43:721-727.

ffrench-Constant, C., Miller, R.H., Burne, J.F. and Raff, M.C. (1988) Evidence that migratory oligodendrocyte-type-2 astrocyte (O-2A) progenitor cells are kept out of the rat retina by a barrier at the eye-end of the optic nerve. *J.Neurocytol*, 17:13-25.

ffrench-Constant, C. and Raff, M.C. (1986) Proliferating bipotential glial progenitor cells in adult rat optic nerve. *Nature*, 319:499-502.

Fok-Seang, J. and Miller, R.H. (1992) Astrocyte precursors in neonatal rat spinal cord cultures. *J.Neurosci.*, 12:2751-2764.

Fraher, J.P. (1992) The CNS-PNS transitional zone of the rat. Morphometric studies at cranial and spinal levels. *Prog.Neurobiol.*, 38:261-316.

Fremeau, R.T.,Jr. and Popko, B. (1990) *In situ* analysis of myelin basic protein gene expression in myelin-deficient oligodendrocytes: antisense hnRNA and readthrough transcription. *EMBO J.*, 9:3533-3538.

Friedrich, V.L.,Jr. (1974) The myelin deficit in quaking mice. *Brain Res*, 82:168-172.

Friedrich, V.L.,Jr. (1975) Hyperplasia of oligodendrocytes in quaking mice. *Anat.Embryol.*, 147:259-271.

Fujita, N., Sato, S., Ishiguro, H., Inuzuka, T., Baba, H., Kurihara, T., Takahashi, Y. and Miyatake, T. (1990) The large isoform of myelin-associated glycoprotein is scacely expressed in the quaking mouse brain. *J.Neurochem.*, 55:1056-1059.

Gardinier, M.V., Macklin, W.B., Diniak, A.J. and Deininger, P.L. (1986) Characterization of myelin proteolipid mRNAs in normal and jimpy mice. *Mol.Cell.Biol.*, 6:3755-3762.

Gardinier, M.V. and Macklin, W. (1988) Myelin proteolipid protein gene expression in *jimpy* and *jimpy^{msd}* mice. *J.Neurochem.*, 51:360-369.

Gencic, S. and Hudson, L.D. (1990) Conservative amino acid substitution in the myelin proteolipid protein of *jimpy^{msd}* mice. *J.Neurosci.*, 10:117-124.

Ghandour, M.S. and Skoff, R.P. (1988) Expression of galactocerebroside in developing normal and *jimpy* oligodendrocytes *in situ*. *J.Neurocytol*, 17:485-498.

Gilmore, S.A. (1971) Neuroglial population in the spinal white matter of neonatal and early post-natal rats: an autoradiographic study of numbers of neuroglial and changes in their proliferative activity. *Anat.Rec*, 171:283-292.

Gordon, M.N., S. Kumar, A. Espinosa de los Monteros, S. Scully, M.S. Zhang, J. Huber, R.A. Cole , and J. de Vellis (1990) Developmental regulation of myelin-associated genes in the normal and the myelin deficient rat. In *Molecular Aspects of Development and Aging of the Nervous System*. J.M. Lauder (ed): Plenum Press, New York, pp. 11-22.

Greenfield, S., Brostoff, S.W. and Hogan, E.L. (1977) Evidence for defective incorporation of proteins in myelin of the quacking mutant mouse. *Brain Res.*, 120:507-515.

Griffiths, I.R., Duncan, I.D., McCulloch, M. and Harvey, M.J.A. (1981) Shaking pups: a disorder of central myelination in the spaniel dog. *J.Neurol.Sci.*, 50:423-433.

Griffiths, I.R., Mitchell, L.S., McPhilemy, K., Morrison, S., Kyriakides, E. and Barrie, J.A. (1989) Expression of myelin protein genes in Schwann cells. *J.Neurocytol*, 18:345-352.

Griffiths, I.R., Scott, I., McCulloch, M.C., Barrie, J.A., McPhilemy, K. and Cattanach, B.M. (1990) Rumpshaker mouse: a new X-linked mutation affecting myelination: evidence for a defect in PLP expression. *J.Neurocytol*, 19:273-283.

Guenet, J-L. (1980) Mutants of the mouse with abnormal myelination: a review for geneticists. In *Neurological Mutations Affecting Myelination*. N. Baumann (ed): Elsevier/North-Holland Biomedical Press, Amsterdam, pp. 11-21.

Hahn, A.F., Chan, Y. and Webster, H.deF. (1987) Development of myelinated nerve fibres in the sixth cranial nerve of the rat: A quantitative electron-microscopic study. *J.Comp.Neurol.*, 260:491-500.

Harding, J.D.J., Done, J.T., Harbourne, J.F. and Gilbert, F.R. (1973) Congenital tremor type AIII in pigs: An hereditary sex-linked cerebrospinal hypomyelinogenesis. *Vet.Rec.*, 92:527-529.

Hardy, R. and Reynolds, R. (1991) Proliferation and differentiation potential of rat forebrain oligodendroglial progenitors both *in vitro* and *in vivo*. *Development*, 111:1061-1080.

Hartman, B.K., Agrawal, H.C., Agrawal, D. and Kalmbach, S. (1982) Development and maturation of central nervous system myelin: comparison of immunohistochemical localization of proteolipid protein and basic protein in myelin and oligodendrocytes. *Proc.Natl.Acad.Sci.USA*, 79:4217-4220.

Hatfield, J.S. and Skoff, R.P. (1982) GFAP immunoreactivity reveals astrogliosis in females heterozygous for jimpy. *Brain Res*, 250:123-131.

Hayashi, S. (1978) Acetylation of chromosome squashes of Drosophilia melanogaster decreases the background in autorradiographs from hybridization with 125I-laballed RNA. *J.Histochem.Cytochem.*, 36:677-679.

Helynck, G., Luu, B., Nussbaum, J.L., Picken, D., Skalidis, G., Trifilieff, E., Van Dorsselaer, A., Seta, P., Sandeaux, R., Gavach, D., Heitz, F., Simon, D. and Spach, G. (1983) Brain proteolipids, isolation, purification and effects on ionic permeability of membranes. *Eur.J.Biochem.*, 133:689-695.

Hirano, M. and Goldman, J.E. (1988) Gliogenesis in rat spinal cord: evidence for origin of astrocytes and oligodendrocytes from radial precursors. *J.Neurosci.Res.*, 21:155-167.

Hogan, E.L. , and S. Greenfield (1984) *Myelin.* Plenum Press. New York and London, pp.489-524.

Houbre, D., Schindler, P., Trifilieff, E., Luu, B. and Duportail, G. (1990) Selectivity of lipid-protein interaction with myelin proteolipids PLP and DM-20. A fluorescence anisotropy study. *Biochim.Biophys.Acta Bio-Membr.*, 1029:136-142.

Hudson, L.D., Berndt, J., Puckett, C., Kozak, C.A. and Lazzarini, R.A. (1987) Aberrant splicing of proteolipid protein and mRNA in the dysmyelinating jimpy mutant mouse. *Proc.Natl.Acad.Sci.USA*, 84:1454-1458.

Hudson, L.D., Friedrich, V.L.,Jr., Behar, T., Dubois-Dalcq, M. and Lazzarini, R.A. (1989) The initial events in myelin synthesis: orientation of proteolipid protein in the plasma membrane of cultured oligodendrocytes. *J.Cell Biol.*, 109:717-727.

Hudson, L.D. (1990a) Molecular genetics of X-linked mutants. *Ann.N.Y.Acad.Sci.*, 605:155-165.

Hudson, L.D. (1990b) Molecular biology of myelin proteins in the central and peripheral nervous systems. *Sem.Neurosci.*, 2:483-496.

Ikenaka, K., Kagawa, T. and Mikoshiba, K. (1992) Selective expression of DM-20, an alternatively spliced myelin proteolipid protein gene product, in developing nervous system and in non-glial cells. *J.Neurochem.*, 58:2248-2253.

Ingraham, C.A. and McCarthy, K.D. (1989) Plasticity of process bearing glial cell cultures from neonatal rat cerebral cortical tissue. *J.Neurosci.*, 9:63-69.

Jackson, K.F., Duncan, I.D., Wells, M.R. and Worth, S.F. (1988) Observations on the CNS of the longer lived myelin deficient rats. *Soc.Neurosci.*, 14:829.(Abstract)

Jackson, K.F. and Duncan, I.D. (1988) Cell kinetics and cell death in the optic nerve of the myelin deficient rat. *J.Neurocytol*, 17:657-670.

Jordan, C., Friedrich, V.L.,Jr. and Dubois-Dalcq, M. (1989) In situ hybridization analysis of myelin gene transcripts in developing mouse spinal cord. *J.Neurosci.*, 9:248-257.

Jordan, C.A., Friedrich, V.L.,Jr. and Dubois-Dalcq, M. (1990) Proteolipid protein mRNA localization in PNS tissues. *Ann.N.Y.Acad.Sci.*, 605:371-373.

Kamholz, J., Sessa, M., Scherer, S., Vogelbacker, H., Mokuno, K., Baron, P., Wrabetz, L., Shy, M. and Pleasure, D. (1992) Structure and expression of proteolipid protein in the peripheral nervous system. *J.Neurosci.Res.*, 31:231-244.

Kerner, A.L. and Carson, J.H. (1984) Effect of the jimpy mutation on expression of myelin proteins in heterozygous and hemizygous mouse brain. *J.Neurochem.*, 43:1706-1715.

Knapp, P.E., Skoff, R.P. and Redstone, D.W. (1986) Oligodendroglial cell death in jimpy mice: an explanation for the myelin deficit. *J.Neurosci.*, 6:2813-2822.

Knapp, P.E., Bartlett, W.P. and Skoff, R.P. (1987) Cultured oligodendrocytes mimic *in vivo* phenotypic characteristics: cell shape, expression of myelin-specific antigens and membrane production. *Dev.Biol.*, 120:356-365.

Knapp, P.E., Dutta, S. and Skoff, R.P. (1990) Differences in levels of neuroglial cell death in jimpy male mice and carrier females. *Dev.Neurosci.*, 12:145-152.

Knapp, P.E. (1992) The cell cycle of glial cells grown in vitro: An immunocytochemical method of analysis. *J.Histochem.Cytochem.*, 40:1405-1411.

Konola, J.T., Tyler, B.M., Yamamura, T. and Lees, M.B. (1991) Distribution of proteolipid protein and myelin basic protein in cultured mouse oligodendrocytes: primary vs. secondary cultures. *J.Neurosci.Res.*, 28:49-64.

Konola, J.T., Yamamura, T., Tyler, B. and Lees, M.B. (1992) Orientation of the myelin proteolipid protein C-terminus in oligodendroglial membranes. *Glia*, 5:112-121.

Kronquist, K.E., Crandall, B.F., Macklin, W.B. and Campagnoni, A.T. (1987) Expression of myelin proteins in the developing human spinal cord: cloning and sequencing of human proteolipid protein cDNA. *J.Neurosci.Res.*, 18:395-401.

Kuhlmann-Krieg, S., Sommer, I. and Schachner, M. (1988) Ultrastructural features of cultured oligodendrocytes expressing stage-specific cell-surface antigens. *Dev.Brain Res.*, 39:269-280.

Kumar, S., Gordon, M.N., Espinosa de los Monteros, M.A. and Vellis, J. (1988) Developmental expression of neural cell type-specific mRNA markers in the myelin-deficient rat brain; inhibition of oligodendrocyte differenciation. *J.Neurosci.Res.*, 21:268-274.

Kurihara, T., Monoh, K., Takahashi, Y., Goto, K. and Kondo, H. (1992) 2',3'-Cyclic-nucleotide 3'-phosphodiesterase: Complementary DNA and gene cloning for mouse enzyme and *in situ* hybridization of the messenger RNA in mouse brain. *Adv.Second Messenger Phosphoprotein Res.*, 25:101-110.

Lai, C., Watson, J.B., Bloom, F.E., Sutcliffe, J.G. and Milner, R.J. (1987) Neural protein 1 B236/myelin-associated glycoprotein (MAG) defines a subgroup of the immunoglobulin superfamily. *Immunol.Rev.*, 100:129-151.

Langford, L.A. and Coggeshall, R.E. (1980) The use of potassium ferricyanide in neural fixation. *Anat.Rec.*, 197:297-303.

Lassmann, H., Ammerer, H.P. and Kulnig, W. (1978) Ultrastrucutal sequence of myelin degradation. I. Wallerian degeneration in the rat optic nerve. *Acta Neuropath.(Berl)*, 44:91-102.

Laursen, R.A., Samiullah, M. and Lees, M.B. (1984) The structure of bovine brain myelin proteolipid and its organization in myelin. *Proc.Natl.Acad.Sci.USA*, 81:2912-2916.

Lepage, P., Helynck, G., Chu, J-Y., Luu, B., Sorokine, O., Trifilieff, E. and Van Dorsselaer, A. (1986) Purification and characterization of minor brain proteolipids: use of fast atom bombardment-mass spectrometry for peptide sequencing. *Biochimie*, 68:669-686.

Levi, G., Gallo, V. and Ciotti, M.T. (1986a) Bipotential precursors of putative fibrous astrocytes and oligodendrocytes in rat cerebellar cultures express distinct surface features and "neuron-like" gamma-aminobutiric acid transport. *Proc.Natl.Acad.Sci.USA*, 83:1504-1508.

Levi, G., Gallo, V., Wilkin, G.P. and Cohen, J. (1986b) Astrocyte subpopulations and glial precursors in rat cerebellar cultures. *Adv.Biosci.*, 61:21-30.

Lyon, M.F. (1972) X-chromosome inactivation and developmental patterns in mammals. *Biol.Rev.*, 47:1-35.

Macklin, W.B., Campagnoni, A.T., Deininger, P.L. and Gardinier, M.V. (1987) Structure and expression of the mouse proteolipid protein gene. *J.Neurosci.Res.*, 18:383-394.

Macklin, W.B. (1988) The myelin proteolipid protein gene produces a non-oligodendrocyte mRNA. *Trans.Am.Soc.Neurochem.*, 19:132.(Abstract)

Macklin, W.B., Gardinier, M.V., Obeso, Z.O., King, K.D. and Wight, P.A. (1991) Mutations in the myelin proteolipid protein gene alter oligodendrocyte gene expression in jimpy and jimpy^{msd} mice. *J.Neurochem.*, 56:163-171.

Macklin, W.B. and Pfeiffer, S.E. (1983) Myelin proteolipid time course in primary cultures of fetal rat brain. *Trans.Am.Soc.Neurochem.*, 212.(Abstract)

Mattei, M-G., Alliel, P.M., Dautigny, A., Passage, E., Pham-Dinh, D., Mattei, J-F. and Jolles, P. (1986) The gene encoding for the major brain proteolipid (PLP) maps on the q-22 band of the human X chromosome. *Hum.Genet.*, 72:352-353.

McPhilemy, K., Griffiths, I.R. and Mitchell, L.S. (1989) Expression of glial-specific genes in Schwann cells. *Neuropath.Appl.Neurobiol.*, 15:268.(Abstract)

McQuarrie, I.G., Brady, S.T. and Lasek, R.J. (1986) Diversity in the axonal transport of structural proteins: major differences between optic and spinal axons in the rat. *J.Neurosci.*, 6:1593-1605.

Meier, C. and Bischoff, A. (1975) Oligodendroglial cell development in jimpy mice and controls. An electron microscopic study in the optic nerve. *J.Neurol.Sci.*, 26:517-528.

Meier, H. and MacPike, A.D. (1970) A neurological mutation (*msd*) of the mouse causing a deficiency of myelin synthesis. *Exp.Br.Res.*, 10:512-525.

Mikoshiba, K., Aoki, E. and Tsukada, Y. (1980) 2'-3'cyclic nucleotide 3'-phosphohydrolase activity in the central nervous system of a myelin deficient mutant (shiverer). *Brain Res*, 192:195-204.

Mikoshiba, K., Okano, H., Inoue, Y., Fujishiro, M., Takamatsu, K., Lachapelle, F., Baumann, N. and Tsukada, Y. (1987) Immunohistochemical, biochemical and electron microscopic analysis of myelin formation in the central nervous system of myelin deficient (*mld*) mutant mice. *Dev.Brain Res.*, 35:111-121.

Miller, R.H., David, S., Patel, R., Abney, E.R. and Raff, M.C. (1985) A quantitative immunohistochemical study of macroglial cell development in the rat optic nerve: *in vivo* evidence for two distinct astrocyte lineages. *Dev.Biol.*, 111:35-41.

Miller, R.H., Fulton, B.P. and Raff, M.C. (1989) A novel type of glial cell associated with nodes of Ranvier in the rat optic nerve. *Eur.J.Neurosci.*, 1:172-180.

Miller, R.H. and Raff, M.C. (1984) Fibrous and protoplasmic astrocytes are biochemically and developmentally distinct. *J.Neurosci.*, 4:585-592.

Miller, R.H. and Szigeti, V. (1991) Clonal analysis of astrocyte diversity in neonatal rat spinal cord cultures. *Development*, 113:353-362.

Milner, R.J., Lai, C., Nave, K-A., Lenoir, D., Ogata, J. and Sutcliffe, J.G. (1985) Nucleotide sequence of two mRNAs for rat brain myelin proteolipid protein. *Cell*, 42:931-939.

Mitchell, L.S., Griffiths, I.R. and Brophy, P.J. (1990) Rumpshaker mouse. A probable mutation of the PLP gene. *Ann.N.Y.Acad.Sci.*, 605:394-397.

Mitchell, L.S., Gillespie, C.S., McAllister, F., Fanarraga, M., Kirkham, D., Kelly, B., Brophy, P.J., Griffiths, I.R., Montague, P. and Kennedy, P.G.E. (1992) Developmental expression of the major myelin protein genes in the CNS of the X-linked hypomyelinating mutant rumpshaker. *J.Neurosci.Res.*, 33:205-217.

Mori, S. and Leblond, C.P. (1970) Electron microscopic identification of three classes of oligodendrocytes and a preliminary study of their proliferative activity in the corpus callosum of young rats. *J.Comp.Neurol.*, 139:1-30.

Nadon, N.L., Duncan, I.D. and Hudson, L.D. (1990) A point mutation in the proteolipid protein gene of the "shaking pup" interupts oligodendrocyte development. *Development*, 110:529-537.

Nave, K-A., Lai, C., Bloom, F.E. and Milner, R.J. (1986) Jimpy mutant mouse: A 74-base deletion in the mRNA for myelin proteolipid protein and evidence for a primary defect in RNA splicing. *Proc.Natl.Acad.Sci.USA*, 83:9264-9268.

Nave, K-A., Lai, C., Bloom, F.E. and Milner, R.J. (1987) Splice site selection in the proteolipid protein (PLP) gene transcript and primary structure of the DM-20 protein of central nervous system myelin. *Proc.Natl.Acad.Sci.USA*, 84:5665-5669.

Nave, K-A. and Milner, R.J. (1989) Proteolipid proteins: structure and genetic expression in normal and myelin-deficient mutant mice. *Crit.Rev.Neurobiol.*, 5:65-91.

Nesbitt, M.N. (1971) X chromosome inactivation mosaicism in the mouse. *Dev.Biol.*, 26:252-263.

Nesbitt, M.N. and Gartler, S.M. (1971) The applications of genetic mosaicism to developmental problems. *Ann.Rev.Genet.*, 5:143-162.

Noble, M., Wolswijk, G. and Wren, D. (1989) The complex relationship between cell division and the control of differentiation in oligodendrocyte-type-2 astrocyte progenitor cells isolated from perinatal and adult rat optic nerves. *Prog.Growth Fac.Res.*, 1:179-194.

Noble, M. and Murray, K. (1984) Purified astrocytes promote the division of a bipotential glial progenitor cell. *EMBO J.*, 3:2243-2247.

Norton, W.T. , and W. Cammer (1984) Isolation and characterization of myelin. In *Myelin*. P. Morell (ed): Plenum Press, New York and London, pp. 147-196.

Okano, H., Tamura, T., Miura, M., Aoyama, A., Ikenaka, K., Oshimura, M. and Mikoshiba, K. (1988) Gene organization and transcription of duplicated MBP genes of *myelin deficient (shi^{mld})* mutant mouse. *EMBO J.*, 7:77-83.

Omlin, F.X., Webster, H.deF., Palkovitz, C.G. and Cohen, S.R. (1982) Immunocytochemical localization of basic protein in major dense line regions of central and peripheral myelin. *J.Cell Biol.*, 95:242-248.

Omlin, F.X. and Anders, J.J. (1983) Abnormal cell relationships in jimpy mice: an electron microscopic and immunocytochemical findings. *J.Neurocytol*, 12:767-784.

Paterson, J.A., Privat, A., Ling, E.A. and Leblond, C.P. (1973) Investigation of glial cells in semithin sections. III. Transformation of subependymal cells into glial cells, as shown by radioautography after 3H-thymidine injection into the lateral ventricle of the brain of young rats. *J.Comp.Neurol.*, 149:83-102.

Pedraza, L., Frey, A.B., Hempstead, B.L., Colman, D.R. and Salzer, J.L. (1991) Differential expression of MAG isoforms during development. *J.Neurosci.Res.*, 29:141-148.

Peters, A., S.L. Palay , and H.deF. Webster (1976) *The fine structure of the nervous system*. W.B.Saunders. Philadelphia.

Pfeiffer, S.E., R. Bansal, A.L. Gard , and A.E. Warrington (1990) Regulation of oligodendrocyte progenitor development: antibody-perturbation sites. In *Cellular and Molecular Biology of Myelination*. G. Jeserich, H.A. Althaus, and T.V. Waehneldt (eds): Springer-Verlag, Berlin, pp. 19-31.

Phillips, D.E. (1973) An electron microscopic study of macroglia and microglia in the lateral funiculus of the developing spinal cord in the fetal monkey. *Z.Zellforsch.*, 140:145-167.

Popko, B., Puckett, C., Lai, E., Shine, H.D., Readhead, C., Hunt, S.W.,111., Sidman, R.L. and Hood, L. (1987) Myelin deficient mice: expression of myelin basic protein and generation of mice with varying levels of myelin. *Cell*, 48:713-721.

Popot, J.-L., Dinh, D.P. and Dautigny, A. (1991) Major myelin proteolipid: The 4-α-helix topology. *J.Membr.Biol.*, 120:233-246.

Privat, A., Jacque, C., Bourre, J.M., Dupouey, P. and Baumann, N. (1979) Absence of the major dense line in myelin of the mutant mouse shiverer. *Neurosci.Lett.*, 12:107-112.

Privat, A., Valat, J., Lachapelle, F., Baumann, N. and Fulcrand, J. (1982) Radioautographic evidence for the protacted proliferation of glial cells in the central nervous system of jimpy mice. *Dev.Brain Res.*, 2:411-416.

Puckett, C., Hudson, L.D., Ono, K., Benecke, J., Dubois-Dalcq, M. and Lazzarini, R.A. (1987) Myelin-specific proteolipid protein is expressed in myelinating Schwann cells but is not incorporated into myelin sheaths. *J.Neurosci.Res.*, 18:511-518.

Quarles, R.H., Barbarash, G.R. and MacIntosh, T.D. (1984) Methods for the identification and characterization of glycoproteins in central and peripheral myelin. *Rec.Methods Neurochem.*, 6:303-357.

Quarles, R.H. (1990) The biochemistry of myelin in X-linked mutants. *Ann.N.Y.Acad.Sci.*, 605:135-145.

Raff, M.C., Mirsky, R., Fields, K.L., Lisak, R.P., Dorfman, S.H., Silberberg, D.H., Gregson, N.A., Liebowitz, S. and Kennedy, M.C. (1978) Galactocerebroside is a specific marker for oligodendrocytes in culture. *Nature*, 274:813-816.

Raff, M.C., Miller, R.H. and Noble, M. (1983) A glial progenitor that develops *in vitro* into an astrocyte or an oligodendrocyte depending on culture medium. *Nature*, 303:390-396.

Raff, M.C., Abney, E.R. and Miller, R.H. (1984a) Two glial cell lineages diverge prenatelly in rat optic nerve. *Dev.Biol.*, 106:53-60.

Raff, M.C., Williams, B.P. and Miller, R.H. (1984b) The in vitro differentiation of a bipotential glial progenitor cell. *EMBO J.*, 3:1857-1864.

Raff, M.C. (1989) Glial cell diversification in the rat optic nerve. *Science*, 243:1450-1455.

Raff, M.C. (1992) Social controls on cell survival and cell death. *Nature*, 356:397-400.

Raskind, W.H., Williams, C.A., Hudson, L.D. and Bird, T.D. (1991) Complete deletion of the proteolipid protein gene (PLP) in a family with X-linked Pelizaeus-Merzbacher disease. *Am.J.Hum.Genet.*, 49:1355-1360.

Remahl, S. and Hildebrand, C. (1990) Relation between axons and oligodendroglial cells during initial myelination. I. The glial unit. *J.Neurocytol*, 19:313-328.

Richardson, W.D., Raff, M.C. and Noble, M. (1990) The oligodendrocyte-type-2-astrocyte lineage. *Sem.Neurosci.*, 2:445-454.

Roach, A., Takahashi, N., Pravtcheva, D., Ruddle, F. and Hood, L. (1985) Chromosomal mapping of mouse myelin basic protein gene and structure and transcription of the partially deleted gene in shiverer mutant mice. *Cell*, 42:149-155.

Rosenbluth, J. (1987) Abnormal axoglial junctions in the myelin-deficient rat. *J.Neurocytol*, 16:497-509.

Rosenfeld, J. and Friedrich, V.L.,Jr. (1984) Hypomyelination and recovery of the myelin deficit in heterozygous jimpy mice. *Int.J.Dev.Neuroscience*, 2:21-32.

Rosenfeld, J. and Friedrich, V.L.,Jr. (1986) Oligodendrocyte production and myelin recovery in heterozygous jimpy mice: An autoradiographic study. *Int.J.Dev.Neuroscience*, 4:179-187.

Roussel, G., Neskovic, N.M., Trifilieff, E., Artault, J-C. and Nussbaum, J.L. (1987) Arrest of proteolipid transport through the Golgi apparatus in jimpy brain. *J.Neurocytol*, 16:195-204.

Schindler, P., Luu, B., Sorokine, O., Trifilieff, E. and Van Dorsselaer, A. (1990) Developmental study of proteolipids in bovine brain: a novel proteolipid and DM-20 appear before proteolipid protein (PLP) during myelination. *J.Neurochem.*, 55:2079-2085.

Schneider, A., Montague, P., Griffiths, I.R., Fanarraga, M., Kennedy, P.G.E., Brophy, P.J. and Nave, K-A. (1992) Uncoupling of hypomyelination and glial cell death by a mutation in the proteolipid protein gene. *Nature*, 358:758-761.

Schnitzer, J. and Schachner, M. (1982) Cell type specificity of a neural cell surface antigen recognized by the monoclonal antibody A2B5. *Cell Tissue Res.*, 224:625-636.

Skoff, R.P. (1975) The fine structure of pulse labeled (^{3}H-thymidine cells) in degenerating rat optic nerve. *J.Comp.Neurol.*, 161:595-611.

Skoff, R.P. (1976) Myelin deficit in the jimpy mouse may be due to cellular abnormalities in astroglia. *Nature*, 264:560-562.

Skoff, R.P., Price, D.L. and Stocks, A. (1976a) Electron microscopic autoradiographic studies of gliogenesis in rat optic nerve. *J.Comp.Neurol.*, 169:291-312.

Skoff, R.P., Price, D.L. and Stocks, A. (1976b) Electron microscopic autoradiographic studies of gliogenesis in rat optic nerve. II. Time of origin. *J.Comp.Neurol.*, 169:313-334.

Skoff, R.P., Toland, D. and Nast, E. (1980) Pattern of myelination and distribution of neuroglial cells along the developing optic system of the rat and rabbit. *J.Comp.Neurol.*, 191:237-253.

Skoff, R.P. (1990) Gliogenesis in rat optic nerve: astrocytes are generated in a single wave before oligodendrocytes. *Dev.Biol.*, 139:149-168.

Skoff, R.P. and Knapp, P.E. (1990) Expression of the jimpy phenotype in relation to proteolipid protein appearance. *Ann.N.Y.Acad.Sci.*, 605:122-134.

Skoff, R.P. and Knapp, P.E. (1991) Division of astroblasts and oligodendroblasts in postnatal rodent brain: evidence for separate astrocyte and oligodendrocyte lineages. *Glia*, 4:165-174.

Skoff, R.P. and Montgomery, I.N. (1981) Expression of mosaicism in females heterozygous for jimpy. *Brain Res*, 212:175-181.

Small, R.K., Riddle, P. and Noble, M. (1987) Evidence for migration of oligodendrocyte-type-2 astrocyte progenitor cells into the developing rat optic nerve. *Nature*, 328:155-157.

Snipes, G.J., Suter, U., Welcher, A.A. and Shooter, E.M. (1992) Characterization of a novel peripheral nervous system myelin protein (PMP-22/SR13). *J.Cell Biol.*, 117:225-238.

Sommer, I., Lagenaur, C. and Schachner, M. (1982) Stage specific antigens O5 to O11 on oligodendrocyte cell surfaces detected by monoclonal antibodies. *Soc.Neurosci.Abstr.*, 8:246.(Abstract)

Sommer, I. and Schachner, M. (1981) Monoclonal antibodies (O1-O4) to oligodendrocyte cell surfaces: an immunocytological study in the central nervous system. *Dev.Biol.*, 83:311-327.

Sommer, I. , and M. Schachner (1984) Stage-specific antigens on oligodendrocyte cell surfaces. In *The Role of Cell Interactions in Early Neurogenesis*. A.-M. Dupret, A.C. Kato, and M. Weber (eds): Plenum Press, New York, pp. 201-205.

Sorg, B.A., Agrawal, D., Agrawal, H.C. and Campagnoni, A.T. (1986) Expression of myelin proteolipid protein and basic protein in normal and dysmyelinating mutant mice. *J.Neurochem.*, 46:379-387.

Sorg, B.A., Smith, M.M. and Campagnoni, A.T. (1987) Developmental expression of the myelin proteolipid protein and basic protein mRNA in normal and dysmyelinating mutant mice. *J.Neurochem.*, 49:1146-1154.

Sprinkle, T.J., Zarube, M.E. and McKhann, G.M. (1978) Activity of 2'3'-cyclic nucleotide 3'-phosphodiesterase in regions of rat brain during development: quantitative relationship to myelin basic protein. *J.Neurochem.*, 30:309-314.

Stensaas, L.J. and Stensaas, S.S. (1968) Astrocytic neuroglial cells, oligodendrocytes and microgliacytes in the spinal cord of the toad. II. Electron microscopy. *Z.Zellforsch.*, 86:184-213.

Sternberger, N.H., Itoyama, Y., Kies, M.W. and Webster, H.deF. (1978a) Immunocytochemical method to identify basic protein in myelin-forming oligodendrocytes of newborn rat C.N.S. *J.Neurocytol*, 7:251-263.

Sternberger, N.H., Itoyama, Y., Kies, M.W. and Webster, H.deF. (1978b) Myelin basic protein demonstrated immunocytochemically in oligodendroglia prior to myelin sheath formation. *Proc.Natl.Acad.Sci.USA*, 75:2521-2524.

Sternberger, N.H., Quarles, R.H., Itoyama, Y. and Webster, H.deF. (1979) Myelin-associated glycoprotein demonstrated immunocytochemically in myelin and myelin-forming cells of developing rat. *Proc.Natl.Acad.Sci.USA*, 76:1510-1514.

Stoffel, W., Hillen, H. and Giersiefen, H. (1984) Structure and molecular arrangement of proteolipid protein of central nervous system myelin. *Proc.Natl.Acad.Sci.USA*, 81:5012-5016.

Sturrock, R.R. (1976) Light microscopic identification of immature glial cells in semithin sections of the developing mouse corpus callosum. *J.Anat.*, 122:521-537.

Sturrock, R.R. (1983) *Problems of glial identification and quantification in the ageing central nervous system*. Raven press. New York.

Suter, U., Welcher, A.A., Özcelik, T., Snipes, G.J., Kosaras, B., Francke, U., Billings-Gagliardi, S., Sidman, R.L. and Shooter, E.M. (1992) *Trembler* mouse carries a point mutation in a myelin gene. *Nature*, 356:241-244.

Temple, S. and Raff, M.C. (1986) Clonal analysis of oligodendrocyte development in culture: evidence for a developmental clock that counts cell divisions. *Cell*, 44:773-779.

Timsit, S., Sinoway, M.P., Levy, L., Allinquant, B., Stempak, J., Staugaitis, S.M. and Colman, D.R. (1992) The DM20 protein of myelin: Intracellular and surface expression patterns in transfectants. *J.Neurochem.*, 58:1936-1942.

Timsit, S.G., Bally-Cuif, L., Colman, D.R. and Zalc, B. (1992) DM-20 mRNA is expressed during the embryonic development of the nervous system of the mouse. *J.Neurochem.*, 58:1172-1175.

Tosic, M., Roach, A., de Rivaz, J-C., Dolivo, M. and Matthieu, J-M. (1990) Post-transcriptional events are responsible for low expression of myelin basic protein in myelin deficient mice: role of antisense RNA. *EMBO J.*, 9:401-406.

Trapp, B.D., Itoyama, Y., MacIntosh, T.D. and Quarles, R.H. (1983) P2 protein in oligodendrocytes and myelin of the rabbit central nervous system. *J.Neurochem.*, 40:47-54.

Trapp, B.D., Moench, T., Pulley, M., Barbosa, E., Tennekoon, G.I. and Griffin, J.W. (1987) Spatial segregation of mRNA encoding myelin-specific proteins. *Proc.Natl.Acad.Sci.USA*, 84:7773-7777.

Trapp, B.D., Bernier, L., Andrews, B. and Colman, D.R. (1988) Cellular and subcellular distribution of 2',3'-cyclic nucleotide 3'-phosphodiesterase and its mRNA in the rat central nervous system. *J.Neurochem.*, 51:859-868.

Trapp, B.D., Andrews, S.B., Wong, A., O'Connell, M. and Griffin, J.W. (1989) Co-localization of the myelin-associated glycoprotein and the microfilament components F-actin and spectrin in Schwann cells of myelinated nerve fibres. *J.Neurocytol*, 18:47-60.

Trapp, B.D. (1990) Distribution of myelin protein gene products in actively-myelinating oligodendrocytes. In *Cellular and Molecular Biology of Myelination*. G. Jeserich, H.A. Althaus, and T.V. Waehneldt (eds): Springer-Verlag, Berlin, pp. 59-79.

Trotter, J. and Schachner, M. (1989) Cells positive for the O4 surface antigen isolated by cell sorting are able to differentiate into astrocytes or oligodendrocytes. *Dev.Brain Res.*, 46:115-122.

Ulrich, J., Matthieu, J.M., Herschkowitz, N., Kohler, R. and Heitz, U. (1983) Immunocytochemical investigations of murine leukodystrophies. A study of the mutants "jimpy" (jp) and "myelin deficient"(mld). *Brain Res*, 268:267-274.

Van Dorsselaer, A., Nebhl, R., Sorokine, O., Schindler, P. and Luu, B. (1987) The DM-20 proteolipid is a major brain protein. It is synthesised earlier in foetal life than the major myelin proteolipid (PLP). *C.R.Acad.Sci.Paris*, 305:555-560.

Vaughn, D.W. and Peters, A. (1974) Neuroglial cells in the cerebral cortex of rats from young adulthood to old age: an electron microscopic study. *J.Neurocytol.*, 3:405-429.

Vaughn, J.E., Hinds, P.L. and Skoff, R.P. (1970) Electron microscopic studies of Wallerian degeneration in rat optic nerves. I. The multipotential glia. *J.Comp.Neurol.*, 140:175-206.

Vaughn, J.E. and Peters, A. (1967) Electron microscopy of the early postnatal development of fibrous astrocytes. *Am.J.Anat.*, 121:131-152.

Vaysse, P.J-J. and Goldman, J.E. (1990) A clonal analysis of glial lineages in neonatal forebrain development in vitro. *Neuron*, 5:227-235.

Verity, A.N., Levine, M.S. and Campagnoni, A.T. (1990) Gene expression in the *jimpy* mutant: evidence for fewer oligodendrocytes expressing myelin protein genes and impaired translocation of myelin basic protein mRNA. *Dev.Neurosci.*, 12:359-372.

Vermeesch, M.K., Knapp, P.E., Skoff, R.P., Studzinski, D.M. and Benjamins, J.A. (1990) Death of individual oligodendrocytes in *jimpy* precedes expression of proteolipid protein. *Dev.Neurosci.*, 12:303-315.

Warf, B.C., Fok-Seang, J. and Miller, R.H. (1991) Evidence for the ventral origin of oligodendrocyte precursors in the rat spinal cord. *J.Neurosci.*, 11:2477-2488.

Warrington, A.E. and Pfeiffer, S.E. (1992) Proliferation and differentiation of O4$^+$ oligodendrocytes in postnatal rat cerebellum: Analysis in unfixed tissue slices using anti-glycolipid antibodies. *J.Neurosci.Res.*, 33:338-353.

Watanabe, I. and Bingle, G.J. (1972) Dysmyelination in "quaking" mouse. Electron microscopic study. *J.Neuropath.Exp.Neurol.*, 31:352-369.

Wilkinson, H.J., Bailes, J.A. and McMahon, A.P. (1987) Expression of the proto-oncogen interleukin-1 is restricted to specific neural cells in the developing mouse embryo. *Cell*, 50:79-88.

Williams, M.A. (1977) Stereological techniques. In *Practical Methods in Electron Microscopy. Vol. 6. Quantitative Methods in Biology*. A.M. Glauert (ed): North Holland, Amsterdam, pp. 5-84.

Wisniewski, H. and Morell, P. (1971) Quaking mouse: ultrastructural evidence for arrest of myelinogenesis. *Brain Res*, 29:63-73.

Wolswijk, G., Riddle, P.N. and Noble, M. (1991) Platelet-derived growth factor is mitogenic for O-2A^{adult} progenitor cells. *Glia*, 4:495-503.

Wolswijk, G. and Noble, M. (1989) Identification of an adult-specific glial progenitor cell. *Development*, 105:387-400.

Wolswijk, G. and Noble, M. (1992) Cooperation between PDGF and FGF converts slowly dividing O-2A^{adult} progenitor cells to rapidly dividing cells with characteristics of O-2A^{perinatal} progenitor cells. *J.Cell Biol.*, 118:889-900.

Wren, D., Wolswijk, G. and Noble, M. (1992) In vitro analysis of the origin and maintenance of O-2A^{adult} progenitor cells. *J.Cell Biol.*, 116:167-176.

Yanagisawa, K., Duncan, I.D., Hammang, J.P. and Quarles, R.H. (1986) Myelin-deficient rat: analysis of myelin proteins. *J.Neurochem.*, 47:1901-1907.

Yanagisawa, K., Möller, J.R., Duncan, I.D. and Quarles, R.H. (1987) Disproportional expression of proteolipid protein and DM-20 in the X-linked, dysmyelinating shaking pup mutant. *J.Neurochem.*, 49:1912-1917.

Zeller, N.K., Behar, T.N., Dubois-Dalcq, M. and Lazzarini, R.A. (1985) The timely expression of myelin basic protein gene in cultured rat brain oligodendrocytes is independent of continuous neuronal influences. *J.Neurosci.*, 5:2955-2962.